Investigation of a NKG2D-dependent tumor immune escape mechanism of head and neck squamous cell carcinoma and proof of concept of a clinical intervention strategy

Vom Fachbereich Biologie

der Technischen Univerisität Darmstadt

zur Erlangung des akademischen Grades

eines Doctor rerum naturalium (Dr. rer. nat.)

genehmigte Dissertation von

Diplom Biochemikerin Sandra Weil

aus Freudenstadt

1. Referentin:	Prof. Dr. Beatrix Süß
2. Referent:	Prof. Dr. Bodo Laube
3. Referent:	Prof. Dr. Joachim Koch

Tag der Einreichung: 30. September 2016

Tag der mündlichen Prüfung: 13. Dezember 2016

Darmstadt 2017

D17

TECHNISCHE
UNIVERSITÄT
DARMSTADT

GEORG SPEYER HAUS
INSTITUTE FOR TUMOR BIOLOGY
AND EXPERIMENTAL THERAPY

Die vorliegende Arbeit wurde unter der Leitung von Prof. Dr. Joachim Koch in der Arbeitsgruppe “NK Cell Biology” am Georg-Speyer-Haus, Institut für Tumorbiologie und experimentelle Therapie, Paul-Ehrlich-Straße 42-44, 60596 Frankfurt am Main und ab Mai 2016 in der Arbeitsgruppe “Immunobiology of Natural Killer Cells” am Institut für Medizinische Mikrobiologie und Hygiene, Universitätsmedizin Mainz, Obere Zahlbacher Str. 67, 55131 Mainz angefertigt.

Die Betreuung seitens der Technischen Universität Darmstadt erfolgte durch Prof. Dr. Beatrix Süß vom Fachbereich Biologie, Schnittspahnstraße 10, 64287 Darmstadt.

Index

List of Figures

List of Supplemental Figures

List of Tables

Summary

Natural killer cells are large granular lymphocytes of the innate immune system, which play an important role in the recognition and elimination of malignantly transformed and infected cells. The major activating NK cell receptor NKG2D, which is also expressed as co-stimulatory receptor on T cell subsets, is thereby a key modulator for tumor recognition and immune cell cytotoxicity. NKG2D recognizes several structurally related cellular ligands (MICA, MICB and ULBP1-6) commonly overexpressed on tumor cells. However, soluble NKG2D (sNKG2D) ligands released from malignant cells by proteolytical shedding, or on exosomes, can inhibit NKG2D-dependent NK and T cell cytotoxicity. Consequently, previous studies showed a correlation of elevated individual sNKG2D ligand plasma levels with impaired NK cell cytotoxicity in cancer patients. Moreover, in a phase I/II trial with high-risk neuroblastoma patients, sMICA was shown to inhibit not only autologous NK cells, but also adoptively transferred allogeneic NK cells after haploidentical stem cell transplantation.

Head and neck squamous cell carcinoma (HNSCC) is a highly heterogeneous and aggressive tumor of the upper aero-digestive tract accounting for 300,000 annual deaths worldwide due to failure of current therapies. In a previous study, sMICA in HNSCC patients' plasma was correlated with impaired NK cell function, indicating that NKG2D-dependent tumor immune escape might play a role for evasion of HNSCC from immunosurveillance. However, little is known about the cumulative role of all sNKG2D ligands and their impact during course of disease. Therefore, the aim of this thesis was the characterization of the NKG2D-dependent tumor immune escape in HNSCC to identify a patient cohort, which might benefit from restoration of NKG2D-dependent tumor immunosurveillance. In this respect, a proof of concept for the depletion of sNKG2D ligands from patients' plasma as future therapeutic intervention strategy to restore NKG2D-dependent antitumor immune cell function was established.

In this thesis, profiling of the plasma from 44 HNSCC patients in comparison to age-matched healthy donors revealed significantly elevated levels of sMICA, sMICB and sULBP1-3. The cumulative levels of sNKG2D ligands were patient specific and correlated with disease progression and tumor load. Moreover, these data suggested a prominent role of sULBP1 and sULBP3 in NKG2D-dependent tumor immune escape in HNSCC. In addition, the immunosuppressive state of HNSCC patients augments NKG2D-dependent escape especially through high plasma levels of TGF-β1.

In *in vitro* cytotoxicity assays, high levels of sNKG2D ligands and TGF-β1 in patients' plasma correlated with NK cell inhibition by blocking the NKG2D receptor. Importantly, the specific depletion of sNKG2D ligands by antibody-coupled magnetic beads successfully restored NK cell cytotoxicity of primary human NK cells against single tumor cell suspensions and in a 3D tumor spheroid model. Consequently, all sNKG2D ligands are indicative for NKG2D-dependent tumor immune escape in HNSCC and determine a time point at which malignant cells critically benefit from bypassing immunosurveillance. Based on tumor spheroids, it could be shown that inhibition of NKG2D-dependent cytotoxicity correlated with drastically reduced NK cell infiltration. These data were in accordance with low infiltration frequencies found in primary tumors of HNSCC patients. Therefore, interference with NKG2D-dependent tumor immune escape might boost both, NK cell cytotoxicity and redirect NK cells to infiltrate tumors.

As proof of concept, a biofunctionalized matrix for adsorption apheresis based on a monoclonal antibody for the representative ligand MICA was generated and showed high depletion capacity of soluble MICA allelic variants from human plasma *in vitro*. The data from HNSCC patients indicate that the simultaneous depletion of all sNKG2D ligands might be crucial for a clinical intervention strategy. Therefore, a pan-specific bioreactive surface using recombinant human IgG1-Fc fusion proteins of the NKG2D ectodomain was generated. *In vitro* depletion experiments demonstrated quantitative depletion of sMICA/B and sULBPs from human plasma. To validate adsorption apheresis of sNKG2D ligands, the anti-MICA antibody adsorber was used in a proof of concept study in rhesus monkeys (*Macaca mulatta*). The preclinical study in rhesus monkeys infused with soluble human MICA demonstrated that adsorption apheresis of sNKG2D ligands is technically feasible and that quantitative removal of sMICA can be achieved after three plasma volume exchanges.

In conclusion, the cumulative level of sNKG2D ligands and TGF-β1 might provide a novel diagnostic and/or prognostic marker combination to decipher a patient cohort, which benefits from restoration of NKG2D-dependent tumor immunosurveillance. Adsorption apheresis of sNKG2D ligands is proposed as therapeutic intervention strategy to improve the efficacy of autologous immune cells by restoration of tumor infiltration and cytotoxicity. Furthermore, adsorption apheresis as preconditioning strategy combined with cellular immunotherapies might help to improve the efficacy of therapeutically administered wildtype or engineered cytotoxic lymphocytes.

Summary (German)

Natürliche Killerzellen (NK-Zellen) des angeborenen Immunsystems sind große granuläre Lymphozyten die maßgeblich an der Immunabwehr von transformierten und infizierten Zellen beteiligt sind. Die Erkennung und Zerstörung dieser Zellen wird durch die relative Intensität von agonistischen und antagonistischen Signalen Keimbahn-kodierter aktivierender und inhibitorischer Rezeptoren reguliert. Für die Zerstörung von Tumorzellen durch NK-Zellen spielt dabei der aktivierende NKG2D-Rezeptor eine wichtige Rolle. Neben NK-Zellen exprimieren auch verschiedene T Zellsubtypen NKG2D als ko-stimulierenden Rezeptor. Die Liganden von NKG2D sind die strukturell verwandten Tumorantigene MICA, MICB und ULBP1-6, die auf der Oberfläche von Tumorzellen überexprimiert werden. Hochmaligne Tumore können jedoch die NKG2D-vermittelte Immunabwehr durch einen Tumor-Immun-*Escape*-Mechanismus basierend auf der Freisetzung löslicher NKG2D-Liganden durch proteolytische Spaltung (oder auf der Oberfläche von freigesetzten Exosomen) überwinden. Die molekularen Konsequenzen der Freisetzung von NKG2D-Liganden sind vielfältig: 1.) Die Zahl der Liganden auf der Zelloberfläche wird reduziert und somit die Anzahl der Interaktionsstellen für $NKG2D^+$ Immunzellen, und 2.) lösliche Liganden können an den NKG2D Rezeptor binden und führen zur Blockierung und Degradation des Rezeptors auf den Immunzellen. Somit vermindern lösliche NKG2D-Liganden maßgeblich die zytotoxische Aktivität von $NKG2D^+$ Immunzellen. Folglich zeigten verschiedene Studien einen Zusammenhang zwischen verringerter NK-Zellfunktionalität und erhöhten Plasmakonzentrationen einzelner NKG2D-Liganden bei Patienten mit verschiedenen Tumorentitäten. Dies betrifft neben den autologen Immunzellen aber auch die im Rahmen einer Zelltherapie transferierten $NKG2D^+$ Immunzellen wie bei einer NK-Zelltherapie nach haploidenter Stammzelltransplantation in einer klinischen Phase I/II Studie bei Patienten mit Hochrisiko-Neuroblastom im Zusammenhang mit löslichem MICA gezeigt wurde.

Das Plattenepithelkarzinom des Kopf-Hals-Bereiches (head and neck squamous cell carcinoma; HNSCC) ist ein solider und hochaggressiver Tumor, der aus den Epithelien des oberen Atemwegs- und Verdauungstraktes hervorgeht. HNSCC steht mittlerweile an sechster Stelle der Malignomerkrankungen mit jährlich über 650.000 neuen Fällen weltweit. Die 5-Jahres Überlebensrate liegt seit langem unverändert bei 40-50% und hat somit 300.000 Todesfälle pro Jahr zur Folge. Eine vorangegangene Studie konnte auch im Plasma von HNSCC Patien-

ten erhöhte Werte an sMICA nachweisen. Daher ist davon auszugehen, dass der NKG2D-vermittelte Tumor-Immun-*Escape* auch für diese Krebsart von Bedeutung ist.

Das Ziel der vorliegenden Arbeit war die Charakterisierung des NKG2D-abhängigen Tumor-Immune-*Escape*-Mechanismus bei Patienten mit HNSCC und die Etablierung eines Apherese-verfahrens als therapeutische Interventionsstrategie zur Entfernung der löslichen NKG2D-Liganden aus dem Patientenplasma.

Die Analyse der Plasmen von 44 HNSCC Patienten zeigte signifikant erhöhte Level der löslichen NKG2D-Liganden MICA/B und ULBP1-3 im Vergleich zu alterskorrelierten Gesundspendern. Dabei korrelierten die kumulativen Plasmalevel mit dem Krankheitsverlauf und der Tumorlast. Im Vergleich zu MICA/B konnten die löslichen Liganden ULBP1/3 als mögliche Hauptmediatoren des Tumor-Immun-*Escapes* bei HNSCC identifiziert werden. Die weitergehende Analyse von immunsuppressiven Faktoren zeigte zudem signifikant erhöhte TGF-β1 Plasmawerte, die zur Hemmung der NKG2D-vermittelten Immunabwehr beitragen.

In funktionalen *in vitro* Analysen wurde die Zytotoxizität von primären humanen NK-Zellen in Folge der Blockierung des NKG2D-Rezeptors durch lösliche NKG2D-Liganden und TGF-β1 im Patientenplasma deutlich inhibiert. In diesem Zusammenhang konnte gezeigt werden, dass eine spezifische Entfernung der löslichen NKG2D-Liganden, mit Hilfe von monoklonalen Antikörpern, die Zytotoxizität der NK-Zellen gegenüber Tumorzellen in Suspension und im 3D Tumorsphäroid-Modell nahezu vollständig wiederherstellen konnte. Folglich ist das Level an löslichen NKG2D-Liganden ein Indikator für das Ausmaß, in dem Tumore der NKG2D-vermittelten Immunabwehr entgehen. In Infiltrationsstudien im Tumorsphäroid-Modell konnte nachgewiesen werden, dass die Inhibition der NKG2D-vermittelten Zytotoxizität gegenüber den Tumorsphäroiden mit einer stark verminderten NK-Zellinfiltration korrelierte. Die Daten der Tumorsphäroide spiegeln die Situation in Patienten wieder. In weitergenden Studien an primären Tumoren von HNSCC Patienten, konnte ebenfalls eine strak verminderte oder abwesende NK-Zellinfiltration nachgewiesen werden. Daher ist davon auszugehen, dass die Intervention mit dem Tumor-Immun-*Escape* sowohl zytotoxische als auch Infiltrations-Eigenschaften von NK-Zellen deutlich verbessern kann.

Zur Entfernung von löslichen NKG2D-Liganden aus Patientenplasma wurde ein Plasmaphereseverfahren entwickelt. Hierzu wurde, als *proof of concept*, eine biofunktionalisierte Oberfläche basierend auf der Kopplung monoklonaler Antikörper gegen den repräsentativen Lig-

anden MICA generiert, die eine hohe Depletionseffizienz für verschiedene MICA Allele aus humanem Plasma *in vitro* aufwies. Bei der Untersuchung der löslichen NKG2D-Liganden im Patientenplasma zeigte sich jedoch eine individuelle Zusammensetzung der Plasmaspiegel. Für eine therapeutische Intervention könnte folglich die simultane Entfernung mehrerer löslicher NKG2D-Liganden aus Patientenplasma notwendig werden. Aus diesem Grund wurden in einem zweiten Ansatz Fusionsproteine aus einem humanen IgG1-Fc-Teil und der Ektodomäne des NKG2D-Rezeptors als panspezifischer Adsorber entwickelt. Dabei bindet der an die Matrix gekoppelte Rezeptor die löslichen NKG2D-Liganden mit der gleichen Effizienz wie der Rezeptor auf den NK-Zellen und verhindert somit die Auswirkungen des Tumor-Immun-*Escape*-Mechanismus. Die Apherese ist folglich unabhängig vom jeweiligen Patientenstatus bzw. dem Expressionslevel der Liganden effizient durchführbar. Die an eine Matrix gekoppelten NKG2D-Fusionsproteine konnten alle löslichen NKG2D-Liganden effizient aus humanem Plasma *in vitro* entfernen. Zur Validierung der Apherese wurde der Antikörper-basierte Adsorber als *proof of concept* in einem Rhesusaffen (*Macaca mulatta*) Modell mit injiziertem löslichen, humanem MICA getestet. Die präklinische Studie zeigte, dass die Apherese von löslichen NKG2D-Liganden aus dem Plasma eines Organismus technisch praktikabel ist und eine quantitative Entfernung des löslichen MICAs bereits nach dreimaligem Plasmaaustausch durch den Adsorber erfolgte.

Zusammenfassend konnten die löslichen NKG2D-Liganden und TGF-β1 als eine neue prognostische und/oder diagnostische Tumormarker-Kombination für HNSCC identifiziert werden. Die Tumormarker könnten zur Identifikation einer Patientengruppe dienen, die von einer Interventionsstrategie zur Überwindung des NKG2D-vermittelten Tumor-Immun-*Escape* zur Steigerung der anti-tumoralen Eigenschaften autologer Immunzellen profitieren kann. In diesem Zusammenhang stellt die Apherese löslicher NKG2D-Liganden ein vielversprechendes therapeutisches Konzept dar, das in Kombination mit Immunzelltherapien auch zur Steigerung der Effizienz allogener Immunzellen sowie genetisch modifizierter (autologer/allogener) Immunzellen beitragen kann.

1 Introduction

1.1 The Immune System

The human immune system is a complex network comprising cellular and humoral defense mechanisms to protect the host against infectious pathogens (e.g. viruses, bacteria, fungi and parasites) or degenerated self-cells[a]. It can be divided into two parts determined by the speed and specificity of reactions - namely the innate and adaptive immunity [2]. The innate immunity is the first line of defense including physical, chemical and microbiological barriers such as the epithelial and mucosiliary blankets. The immediate host defense is not antigen-specific and encoded in the hosts' germline genes. Innate immunity relies on a highly regulated interplay of cellular components such as leukocytes of the myeloid linage (e.g. neutrophils, eosinophils, mast cells, myeloid dentritic cells (DCs), monocytes and macrophages) or lymphoid linage (plasmacytoid DCs and natural killer (NK) cells) and humoral mediators such as chemokines and cytokines, the complement and acute-phase proteins. In contrast, the adaptive immunity is highly specific and develops during exposure against specific antigens by somatic rearrangement of gene elements encoding antigen-specific receptors expressed on T and B lymphocytes and the production of antibodies [3]. Due to the clonal expansion of antigen-specific cells, the adaptive immunity represents the late response encompassing immune memory leading to a rapid immune reaction after subsequent exposure to known antigens. The tightly regulated synergy between innate and adaptive immune response is essential for an intact and effective immunity [4].

Phagocytic macrophages and neutrophils along with the complement system are the first line of defense against intruding microorganisms. The complement cascade becomes activated by pathogenic surface structures leading directly to their osmotic lysis by assembly of the membrane-attack complex or to the opsonization of pathogens for the recognition by phagocytes [5]. Phagocytes recognize common pathogen-associated molecular patterns (PAMPs) expressed by many microbes, but not on host cells, or danger-associated molecular patterns (DAMPs) induced by infections, tissue injury or malignant cells via invariant pattern-recognition receptors (PRRs) such as mannose receptors, scavenger receptors and toll-like

[a] Unless otherwise denoted, "The Immune System" was reviewed in Janeway *et al.* (2005) [1].

receptors [6]. Engagement leads to the direct phagocytosis and to the activation of macrophages releasing cytokines and chemokines to recruit further immune cells to the site of inflammation [7, 8]. Furthermore, macrophages and mainly DCs initiate the adaptive immune response upon infection or cellular transformation to antigen-presenting cells (APCs). Internalized antigens are processed into peptide fragments, which are presented on major histocompatibility (MHC) complexes on the cell surface of APCs which then migrate through the lymphatics from the site of infection to the secondary lymphoid tissues (e.g. lymph nodes, spleen, tonsils or mucosa associated lymphoid tissue). There, naïve T and B cells, having undergone gene rearrangement and positive selection in the thymus or bone marrow, respectively, are located in lymphoid follicles. They become activated and further differentiate to gain antigen specificity upon stimulation by APCs and cytokines [9]. Mature naïve B cells express immunoglobulin B cell receptors (BCRs), which recognize native pathogenic antigen structures brought to the secondary lymphoid tissues. These antigens can be internalized and further processed leading to antigen presentation on MHC class II complexes for T cell activation. T cells in turn secrete cytokines for B cell differentiation and maturation to antibody producing plasma cells. Antibodies play a central role in boosting the innate and adaptive immunity by i) opsonization of pathogens, and infected or degenerated cells for the induction of antibody-dependent cellular cytotoxicity (ADCC) by killer cells, ii) neutralization of toxins and pathogens, and iii) the activation of the classical pathway of the complement cascade. During subsequent exposure to antigens, B cells can also be activated by follicular DCs in the germinal centers of lymph nodes.

The main T cell population is characterized by the surface expression of αβ T cell receptors (TCRs) with single specificity after somatic rearrangement. T cells undergo positive selection in the thymus and differentiate into two main subpopulations with distinct functions according to the expression of the co-receptors cluster of differentiation (CD) 4 (T helper (T_H) cells) or CD8 (cytotoxic T cells, CTLs). T cell activation is mediated through the recognition of linear antigen peptides (8-11 amino acids long) presented in the groove of MHC I complexes on APCs by the TCR and the co-receptor. The MHC molecule and co-receptor thereby determine the effector response. $CD4^+$ T cells recognize exogenous peptides on MHC class II complexes (mainly on B cells) resulting in cytokine secretion and activation/regulation of different cellular (T_H1 response) and humoral (T_H2 response) immune responses [10]. In contrast, $CD8^+$ CTLs become activated by endogenous peptides on MHC class I complexes upon viral infec-

tion or malignant cell transformation [11]. CTL activation leads to target cell lysis by release of cytotoxic granules containing perforin and granzymes or Fas/Fas-ligand induced apoptosis. To prevent tissue damage and autoimmune response, an effective T cell activation is dependent on further co-stimuli by molecules (e.g. CD80, CD86 and CD40) upregulated on APCs exposed to an inflammatory environment [12]. Some of the activated B and T cells remain within the body as long-lived memory cells mediating a fast immune response to subsequent antigen exposure.

Apart from the lymphocytes of the adaptive immunity, NK cells belonging to the innate immunity play a central role in immunosurveillance of viral infections and malignant cells [13-15]. They share many functional features of T cells such as an immune regulatory role by cytokine secretion or cytotoxic activity against target cells, therefore bridging the adaptive and innate immunity [16-18]. They contribute to a rapid initial immune response by recognition of microbial molecules after infections or stress-induced changes in autologous cells, thereby discriminating self from degenerated self. But unlike CTLs, NK cell activation does not need prior sensitization [19, 20].

1.2 Natural Killer Cells

NK cells were first described 1975 in mice as innate effector cells capable of killing target cells in the absence of antigen-specific priming [21, 22]. Like T and B cells, they arise from lymphatic progenitor ($CD34^+$ hematopoietic) cells in the bone marrow and were found to develop and differentiate in secondary lymphoid organs such as the liver, spleen, decidua and lymph nodes [23, 24]. Traditionally, NK cells are defined as large granular lymphocytes expressing the neural cell adhesion molecule (NCAM; CD56) and the FcγRIIIA receptor (CD16), but show absence of CD3 expression. More recently, they were grouped into the family of innate lymphoid cells (ILCs), which require the common γ (γc) chain of the interleukin-2 (IL-2) receptor and the transcriptional repressor Id2 for their development [25-27]. NK cells are therefor subsets of group 1 ILCs characterized based on the expression and requirement of eomesodermin (EOMES) and IL-15 for development, and the secretion of interferon γ (IFN-γ) and tumor necrosis factor α (TNF-α) upon IL-12 stimulation [28]. In humans, NK cells constitute 5-15% of peripheral blood mononuclear cells (PBMC) and have a life span of two weeks in circulation [29, 30]. Based on the expression levels of CD56, they can be subdivided into

two major subsets, the $CD56^{dim}CD16^{+}$ and $CD56^{bright}CD16^{-}$ population with distinct morphology, development, localization and function in the body [31]. $CD56^{dim}CD16^{+}$ cells are predominant in the peripheral blood, spleen and non-lymphoid tissues such as the lung and liver, and have a strong cytotoxic potential [32, 33]. In contrast, $CD56^{bright}CD16^{-}$ NK cells are enriched in lymphoid organs and display immune regulatory roles by cytokine secretion to enhance tissue inflammation, induce differentiation of T helper cells into T_H1 and T_H2 cells and ensure maturation of antigen presenting DCs [34-38]. The crosstalk of NK cells and other immune cells is a prerequisite for the regulation of an effective immune response. On the one hand, activated NK cells select for a functional DC population by killing of immature and tolerogenic DCs, further ensuring a T_H1-biased adaptive immune response [39-41]. On the other hand, they secrete cytokines as IFN-γ and TNF-α leading to the maturation of antigen-presenting DCs and their protection from killing [42]. In turn, resting NK cells become activated through type I interferons (IFN-α and IFN-β), IL-12, IL-18 and IL-15, or IL-2 produced by mature DCs and activated T_H cells, respectively [43-47]. NK cell activation leads to cell proliferation, secretion of high amounts of cytokines and a higher cytolytic potential [45, 48]. Besides their regulatory role to boost innate and adaptive immune responses, NK cells directly eradicate virus-infected and malignantly transformed cells. NK cell cytotoxicity is thereby tightly regulated by the integration of signals from a limited repertoire of invariant germ line-encoded inhibitory and activating receptors [49]. In general, NK cells are self-tolerant due to a prevalence of inhibitory signals upon engagement of MHC molecules expressed on healthy cells by inhibitory NK cell receptors (Figure 1A). NK cells become activated by degenerated cells with low or absent expression of MHC class I (‘missing-self hypothesis’, Figure 1B) and/or stress-induced expression of ligands for activating NK cell receptors that overcome inhibitory signals (‘induced-self hypothesis’, Figure 1C) [50-54]. Thus, NK cells recognize infected and transformed cells, which would normally evade antigen-specific CTL response, while protecting healthy tissues [55-58]. Furthermore, NK cells can recognize altered cells opsonized by antigen-specific antibodies via CD16 (FcγRIII) and induce ADCC (Figure 1D). Killing requires the formation of a complex immunological synapse between the target cell and the NK cell, which is highly organized in time and space [59-61]. Likewise to CTLs, lysis of target cells is mediated by the polarized release of cytotoxic granules containing perforin and granzymes into the synaptic cleft [62, 63], or by apoptosis induction through Fas ligand (Fas-L) and TNF-related apoptosis-inducing ligand (TRAIL) [64].

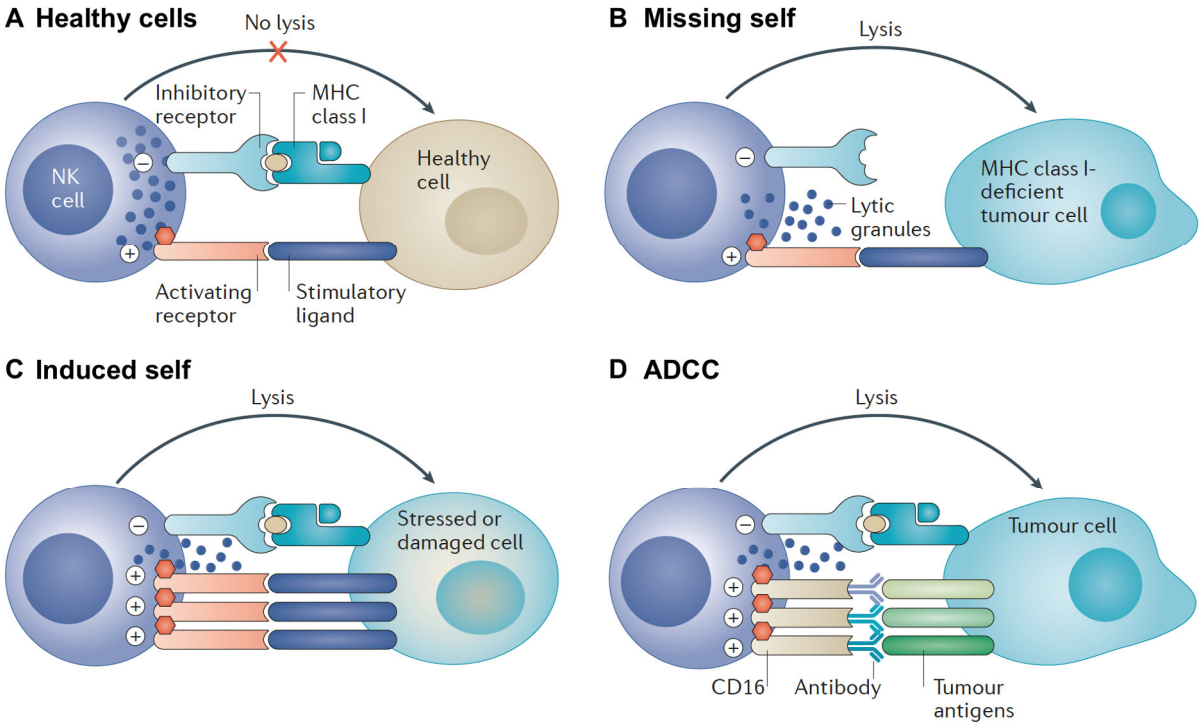

Figure 1: Schematic representation of physiological NK cell functions.
(A) A balance of signals delivered by activating and inhibitory receptors regulates the recognition of healthy cells by natural killer (NK) cells. (B) Tumor cells that downregulate major histocompatibility complex (MHC) class I molecules are detected as 'missing self' and are lysed by NK cells by the release of lytic granules containing perforin and granzyme. (C) Tumor cells can overexpress induced stress ligands recognized by activating NK cell receptors, which override the inhibitory signals and elicit target cell lysis. (D) Tumor antigen-specific antibodies bind to CD16 and elicit antibody-dependent NK cell-mediated cytotoxicity. The figure is reprinted from Morvan and Lanier 2016 [65].

The engagement of a variety of activating ligands mediates an immediate cytolytic response within minutes and can be repeated leading to serial killing of multiple target cells by one NK cell [66, 67]. Interestingly, NK cells were shown to exhibit also adaptive immune features upon activation in mice by a clonal-like expansion of long-lived memory NK cells, which reside in multiple organs for a fast and robust antigen-specific secondary immune response [68-70].

NK cells are known to contribute to the control of viral infections such as human cytomegalovirus (HCMV), herpes virus and human immunodeficiency virus (HIV) [71-73]. Several studies support the important role of NK cells in tumor recognition and elimination [74-76]. Along this line, high activity of peripheral blood NK cells was shown to be associated with a 10% lower incidence of tumors for men and 4% for women [77]. Moreover, NK cell infiltration into tumors represents a positive prognostic marker in several carcinomas [78-80]. The physiological importance of NK cell immunosureveillance is further illustrated by the finding

that patients with NK cell deficiency or impaired NK cell activity suffer from severe recurrent systemic and life-threatening infections mainly caused by HCMV or herpes virus [81-83] and have a higher incidence for various carcinomas [84-88]. Furthermore, viruses and tumor cells employed several escape mechanisms to evade immunosurveillance by NK cells [89-92].

1.3 NK cell Receptors and Function

NK cell recognition involves the consecutive steps of the initial binding to potential target cells, the formation of an immunological synapse, interactions between activating and inhibitory receptors with available ligands leading to the integration of signals transmitted by these receptors, which determines whether the NK cell detaches or responds by secretion of cytotoxic granules or pro-inflammatory cytokines [50, 93]. In contrast to T and B cell activation, which relies on exquisite antigen-specific receptors, NK cell activation is more complex and mediated by numerous receptors acting in synergy [50, 53, 94]. NK cell receptor families thereby achieved recognition flexibility through rapid genetic evolution and promiscuity of ligand binding instead of somatic rearrangement of gene clusters [95, 96].

NK cell receptors are highly conserved throughout species and are encoded in two main gene clusters. In humans, the NK C-type lectin receptor family members are encoded by the NK gene complex located on chromosome 12p12-p13 [97], and the Ig-like leukocyte receptor family cluster on chromosome 19q13.4 [98]. The mouse homologs receptor genes are found on syntenic regions on chromosome 6 and chromosome 7, respectively [99].

Inhibitory receptors mainly recognize classical and some “non-classical” MHC class I molecules, also named human leukocyte antigens (HLAs), expressed on all nucleated cells [100, 101]. Self-tolerance is thereby attained during maturation in the bone marrow by binding to cognate MHC class I molecules, a process termed licensing [102, 103]. NK cells must express at least one inhibitory receptor specific for an MHC molecule to become responsive to later encounters with target cells.

The two main inhibitory receptor families in humans are i) the inhibitory killer cell Ig-like receptors (KIRs) recognizing the different allelic groups HLA-A, -B and -C [104-107], and ii) the C-type lectin-like CD94/natural killer group 2 (NKG2)A heterodimer recognizing non-classical HLA-E molecules [108-110] (Figure 2). Inhibitory KIRs are type I transmembrane glycoproteins with two (KIR2DL) or three (KIR3DL) Ig-like domains and a long cytoplasmic

tail containing two immunoreceptor tyrosine-based inhibitory motifs (ITIMs) for signal transduction [111]. The KIR gene family is highly polymorphic and the repertoire of KIR genes expressed within an individual forms the KIR haplotype [112-114]. Moreover, the expression of KIR allelic variants can differ on NK cells within one individual and therefore each individual has different populations of NK cells that express an assortment of KIRs [115]. Interestingly, no KIR homologs are found in mouse, whereas CD94/NKG2 family members are conserved within the two species, with mouse CD94/NKG2A recognizing the mouse $Qa1^b$ [116]. In mouse, the major inhibitory receptor family comprises the polymorphic C-type lectin-like Ly49 receptors, which are structurally distinct from, but share the same functions as KIRs [117-119].

Upon engagement, inhibitory receptors rapidly accumulate in the inhibitory immunological synapse and mediate signal transduction [120-122]. The tyrosine within the ITIM consensus sequence (S/I/V/LxYxxI/V/L) (x represents any amino acid, slashes separate alternative amino acids occupying the given position) becomes thereby phosphorylated by a kinase of the Src (sarcoma) family, which leads to the recruitment of the Src homology 2 (SH2)-domain containing phosphatases SHP-1 or SHP-2 [121]. Subsequent dephosphorylation of molecules (e.g. Vav-1) involved in downstream signaling of activating receptors results in blocking of activating signal cascades and prevents actin-dependent processes, such as cell adhesion to target cells and cell polarization [123] (Figure 2).

Both receptor families moreover comprise molecules without ITIM motifs, namely the KIR2DS/KIR3DS (short cytosolic tail) and the NKG2C/E heterodimers. For signal transduction, they are associated with the adaptor DNAX-activation protein (DAP) 12 bearing immunoreceptor tyrosine-based activation motifs (ITAM) [124]. These receptors therefore transduce activating signals while recognizing the same HLA ligands as their inhibitory counterparts [125]. Several other activating or co-stimulatory receptors are known such as the signaling lymphocytic activation molecule (SLAM) receptor 2B4 [126], DNAX accessory molecule (DNAM)-1 [127], NKp80 [128], and NKp65 [129]. These receptors recognize non-MHC molecules upregulated on tumor cells.

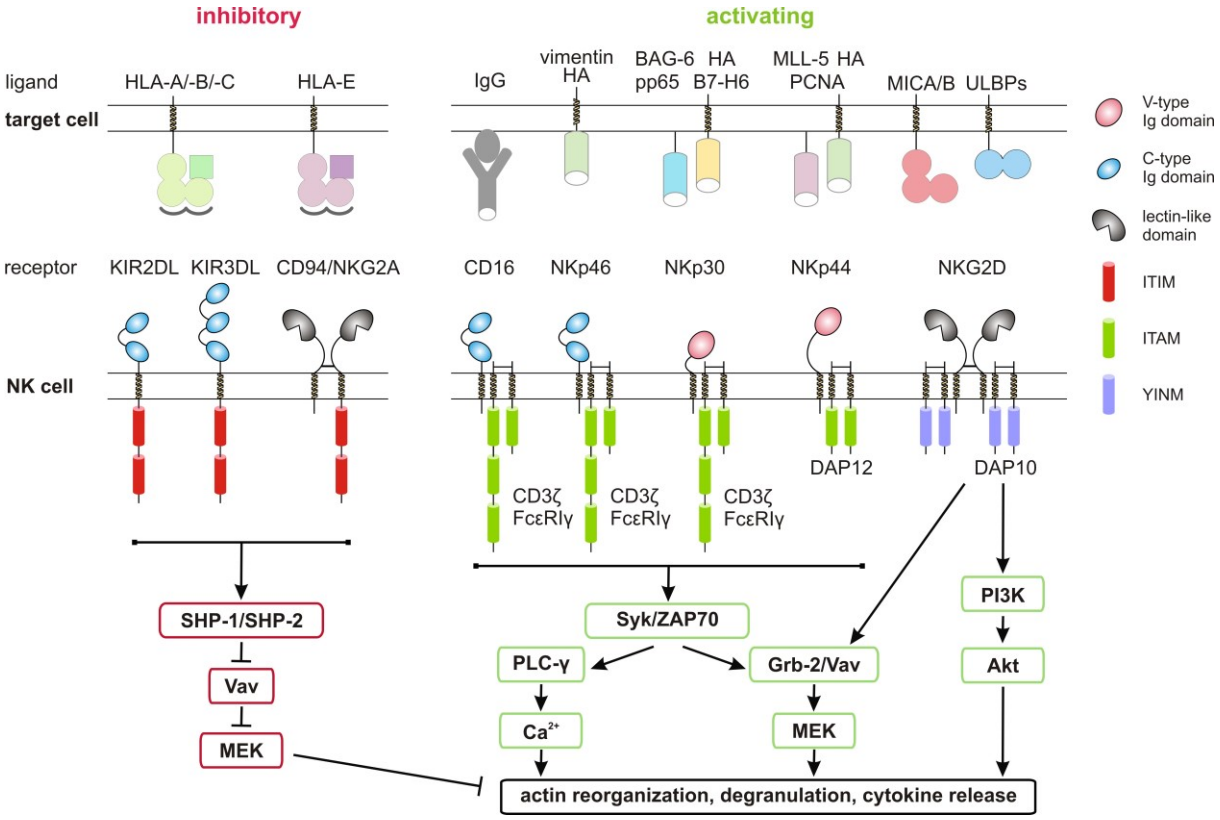

Figure 2: Human inhibitory and activating receptors.
Simplified overview of the major NK cell receptors and their identified ligands involved in regulation of NK cell functions. The major inhibitory receptors are the KIR family members KIR2DL and KIR3DL, and the heterodimer CD94/NKG2A. KIRs possess two (KIR2DL) or three (KIR3DL) Ig-like domains and bind their cognate ligands human leukocyte antigen (HLA)-A, -B or -C molecules. The heterodimer CD94/NKG2A containing two lectin-like domains recognizes HLA-E. All inhibitory receptors have two immunoreceptor tyrosine-based inhibitory motifs (ITIMs) within their cytoplasmic tail for signal transduction via the Src homology 2 (SH2)-domain containing phosphatases SHP-1/2 leading to subsequent dephosphorylation of Vav. The major activating receptors are CD16, NKG2D and the natural cytotoxicity receptor (NCR) family members NKp30, NKp44 and NKp46. CD16 and the NCRs contain either one (NKp30 and NKp44) or two (CD16 and NKp46) Ig-like domains. All of the NCRs bind to viral hemagglutinins (HA). Additionally, the human cytomegalovirus (HCMV) tegument protein pp65, the BCL2-associated anthanogene 6 (BAG-6) and a structural homolog of the B7 family (B7-H6) were described as ligands for NKp30. For NKp44 the proliferating cell nuclear antigen (PCNA) and the mixed-lineage leukemia-5 (MLL-5) protein, and for NKp46 vimentin were discovered. The disulfide-linked homodimer NKG2D contains two lectin-like domains and binds to the MHC class I chain-related proteins A/B (MICA/B) and to the UL16 binding proteins (ULBPs). The activating receptors associate with signaling adaptor molecules via oppositely charged amino acids in their transmembrane domains. CD16, NKp30 and NKp46 can associate with a CD3ζ homodimer or CD3ζ/FcεRIγ heterodimer, whereas NKp44 interacts with DNAX-activation protein (DAP) 12 and NKG2D with two DAP10 molecules. Signaling is mediated by phosphorylation of immunoreceptor tyrosine-based activating motifs (ITAMs) or in case of DAP10 the YINM motif leading to the recruitment of the spleen tyrosine kinase (Syk) or zeta chain-associated protein 70 (ZAP70) kinase pathways, mitogen-activated protein kinase (MAPK) cascade through growth factor receptor-bound protein-2 (Grb-2) and Vav, phosphoinositide 3-kinase (PI3K)/Akt pathway as well as phospholipase Cγ (PLCγ)-1/2. The figure is modified from Hartmann 2012 [130] and Vivier *et al.* (2004) [131].

The major activating receptors are represented by the natural cytotoxicity receptors (NCRs) NKp30 (NCR3, CD337) [132], NKp44 (NCR2, CD336) [133, 134] and NKp46 (NCR1, CD335) [135, 136], the NKG2 member NKG2D, and CD16 which are involved in recognition and killing of malignantly transformed or infected cells (Figure 2).

The NCRs are type I membrane glycoproteins comprised of an ectodomain with one (NKp30 and NKp44) or two (NKp46) Ig-like domains connected to a transmembrane-spanning α-helix via a short flexible stalk domain. The NCRs are primarily expressed on NK cells and cetrain ILC subsets [137-141]. While NKp44 is only expressed on activated NK cells, NKp30 and NKp46 are constitutively expressed [142, 143]. Interestingly, NKp46 is the only NCR that has a functional orthologue in mice [144, 145]. NKG2D is a type II transmembrane glycoprotein, which forms disulfide-linked homodimers containing two C-type lectin-like domains. All activating receptors have short cytoplasmic tails without signaling domains and associate with adaptor proteins via an opposing charge contact within the corresponding transmembrane segments [91]. CD16, NKp30 and NKp46 are associated either with ITAM-bearing CD3ζ disulfide-bonded homodimers or CD3ζ/FcεRIγ heterodimers [136, 146] and NKp44 with DAP12 homodimers [134, 147] (Figure 2). Ligation of ITAM-bearing receptor complexes leads to Src-family kinase (e.g. Lck, Fyn and Src) mediated tyrosin phosphorylation of the ITAM consensus sequence (YxxI/Lx_{6-12}YxxI/L) and subsequent recruitment of spleen tyrosine kinase (Syk) or zeta chain-associated protein 70 (ZAP70) kinase. Downstream signaling events include phospholipase Cγ (PLCγ)-1/2 mediated calcium signaling or activation of the mitogen-activated protein kinase (MAPK) cascade through recriutment of growth factor receptor-bound protein-2 (Grb-2) and Vav-1/2 (guanine nucleotide exchange factor) [131, 148]. In contrast, NKG2D associates with two DAP10 homodimers containing two YINM tyrosin-based motifs [149], which leads to Syk-independent signaling pathways by recruitment of Grb-2/Vav-1 and initiation of the MAPK cascade or the p85 regulatory subunit of the phosphoinositide 3-kinase (PI3K) and subsequent activation of the anti-apoptotic kinase (AKT)-dependent signaling pathway [150, 151] (Figure 2).

The NKG2D ligands including MHC class I chain-related proteins (MIC) A and B and the UL16 binding proteins (ULBPs) are structurally related and well characterized [152]. In contrast, a large number of structurally unrelated activating pathogen-associated ligands have been identified for the NCRs including viral hemagglutinins (HA) [153-155], or bacterial and fungal structures [156-159] and the HCMV tegument protein pp65 as inhibitory ligand for

NKp30 [160]. Several studies revealed that NCRs are triggered by self-molecules overexpressed by various primary tumors and cell lines [161-163]. However, the number of known cellular NCR ligands and knowledge about their mode of action is still scarce [91]. All NCRs were shown to bind heparin/heparan sulfate upregulated on tumor cells [164-168]. For NKp30 the tumor antigens B7-family member B7-H6 [169, 170] and B-cell lymphoma (BCL)2-associated athanogene 6 (BAG-6) released by stressed or transformed cells and immature DCs (iDCs) were identified as ligands [171, 172]. Recently galectin-3 was proposed as an inhibitory ligand for NKp30 [173]. NKp44 recognize the nuclear protein proliferating cell nuclear antigen (PCNA) [174] and the mixed lineage leukemia-5 (MLL-5) protein [175]. So far, only the intermediate filament protein vimentin was shown to contribute as cellular ligand to NKp46-mediated lysis of tuberculosis-infected monocytes and activated $CD4^+$ T cells [176, 177]. The importance of NCRs in tumor recognition is shown by association of reduced NCR expression with resistance to NK cell cytotoxicity in patients with acute myeloid leukemia (AML) [178-181], cervical cancer and precursor lesions [182], gastrointestinal stromal tumors [183, 184] as well as melanoma [185] or impaired NK cell function in HIV-1 infected patients [186].

1.4 The NKG2D/NKG2D Ligand System

The NKG2D receptor was first described as transcript encoding a 216 amino acid long type II transmembrane glycoprotein preferentially expressed by NK cells [187-189]. The *KLRK1* (killer cell lectin-like receptor subfamily K member 1) gene is evolutionary highly conserved throughout species and located in the NKG complex on human chromosome 12 and on the syntenic region on mouse chromosome 6 [190, 191]. Although grouped into the NKG2 C-type lectin receptor family, NKG2D differs markedly in sequence, receptor complex formation and ligand recognition from the CD94/NKG2A/C/E heterodimeric members [152]. In human, NKG2D is constitutively expressed on all NK cells, most NKT cells, $CD8^+$ T cells, peripheral γδ T cells and on a subset of intestinal intraepithelial γδ T cells [192-196]. However, in mice the expression pattern of NKG2D is more selective and found on all NK cells, only on activated or memory $CD8^+$ T cells, on 25% of splenic γδ T cells, and on a subset of peritoneal exudate macrophages upon lipopolysaccharide (LPS) or type I IFN stimulation [197, 198]. $CD4^+$ T cells normally lack NKG2D expression in human and mice, but can be found on

a small subset of human $CD4^+$ T cells that expand under certain pathophysiological conditions as seen in patients with rheumatoid arthritis or Crohn`s disease [192, 199, 200]. Like most activating receptors, NKG2D lacks a functional motif for signal transduction in its cytoplasmic tail and forms a multi-subunit immunoreceptor complex by association with specialized signaling adaptors also required for cell surface expression [201]. In humans, the disulfide-linked homodimeric NKG2D associates exclusively with two DAP10 homodimers to form a hexameric complex [149, 202] (see Figure 2). Formation of the non-covalent assembly is mediated by a conserved arginine residue in the transmembrane domain of each NKG2D monomer interacting with both transmembrane aspartic acids of DAP10 [202]. Engagement of the NKG2D-DAP10 complex triggers calcium-dependent granule release, cytotoxicity, and cytokine production via activation of the PI3K/Akt and Grb-2/Vav-1 pathways [150, 203, 204] (see Figure 2). In mouse a splice variant lacking 13 amino acids at the N-terminus of NKG2D can be expressed on activated NK cells, which can also associate with DAP12 homodimers indicating distinct functions of NKG2D in mice [205-209]. Furthermore, cytokine stimulation with IL-2, IL-12 or IL-15 leads to the upregulation of NKG2D-DAP10 complexes on NK and T cells and increases NKG2D-mediated killing of target cells [210-214]. Whereas NKG2D functions as primary activating receptor in NK cells, which is sufficient to overcome inhibitory signals [192, 197, 205], it rather acts as co-stimulatory receptor in T cells enhancing TCR-mediated activation [194, 215, 216]. However, NKG2D can also mediate TCR-independent T cell cytotoxicity as seen for some γδ T cells, or long-termed cultured or cloned human CTLs and chronically activated CTLs from patients with celiac disease [215, 217-219]. Thus, the mode of NKG2D activation can be regulated by additional signaling inputs and is dependent on the cellular activation status.

A variety of stress-induced cellular NKG2D ligands are known, which are structurally related to MHC class I molecules. In human, the non-classical MHC class I molecules MICA/B are encoded in the MHC gene complex on chromosome 6 and are highly polymorphic, with around 70 and 30 allelic variants described [220-222]. Similar to MHC class I, they are type I transmembrane glycoproteins comprising three Ig-like α-helical ectodomains (Figure 3A). In contrast, they do not associate with β2-micorglobulin and play no known role in antigen presentation [223-225]. In mice, no functional MIC homologs are found, whereas they are conserved in non-human primates, cattle and pig [222, 226-228]. The second group of human ligands comprises the ULBP protein family (also known as retinoic acid early transcript 1;

RAET1) with 6 functional (ULBP1-6) and four pseudogenes [229-234]. The ULBPs are located on the long arm of human chromosome 6 [235] and are homolog to the mouse NKG2D ligand family located on syntenic region on mouse chromosome 10, including the polymorphic RAE-1α-ε (retinoic acid early inducible-1) isoforms, histocompatibility antigen 60 (H60)a-c and mouse ULBP-like transcript 1 (MULT1) [236-242]. All of these ligands structurally share the MHC-like α1/α2 domains, but in contrast to the MICs lack the membrane-proximal α3 domain (Figure 3A). Moreover, human ULBP1–3/6, mouse RAE1α–ε and H60c are glycosylphosphatidylinositol (GPI)-linked, whereas human ULBP4/5, mouse MULT1 and H60a/b are transmembrane proteins.

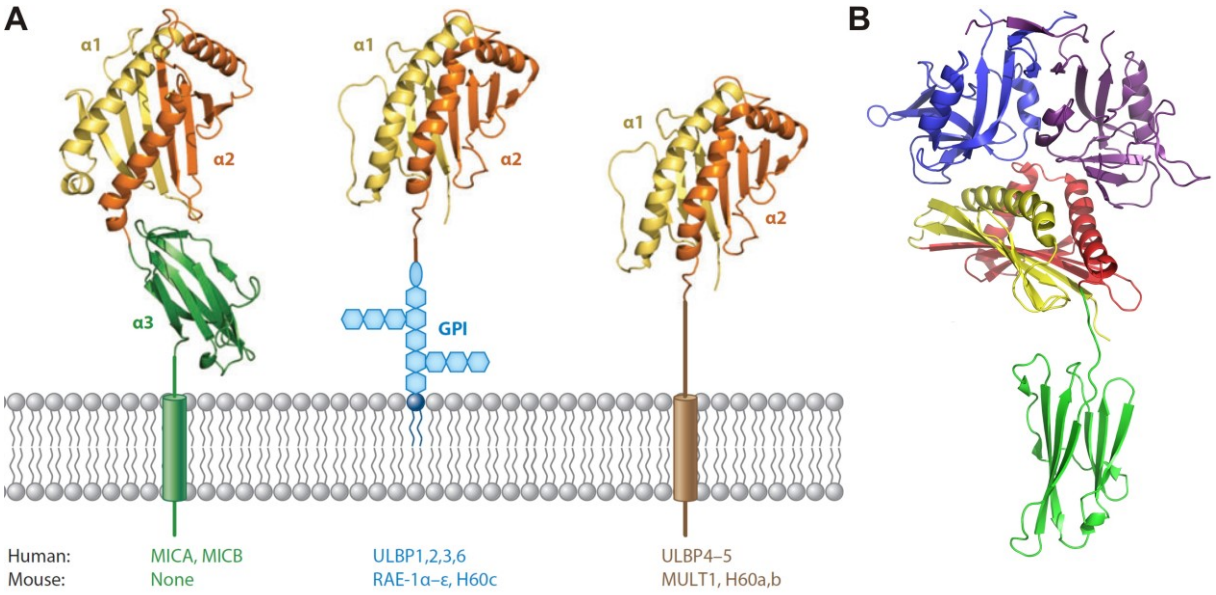

Figure 3: NKG2D ligands in humans and mice and the NKG2D-MICA complex.
(A) The human ligands MHC class I chain-related proteins MICA and MICB are transmembrane proteins with three domains analogous to the α1–α3 domains of MHC class I proteins (MICA structure shown on left; PDB 1HYR [243]). The remaining ligands contain two domains analogous to α1 and α2 of MHC class I proteins but no α3-like domain (the RAE-1β α1 and α2 domains are depicted in both the middle and right structures; PDB 1JFM [244]). Human ULBP1–3 and 6, mouse RAE1α–ε and H60c are glycosylphosphatidylinositol (GPI)-linked, whereas human ULBP4–5, mouse MULT1 and H60a/b are transmembrane proteins. In some cases (e.g. ULBP2 and possibly others), both GPI-linked and transmembrane forms of the protein are found on the same cell [245]. The image is reprinted from Raulet *et al.* (2013) [246]. (B) Crystal structure of the human NKG2D-MICA complex. The extracellular domain of the NKG2D homodimer binds diagonally to the asymmetric α1/α2 domains of MICA (PDB 1HYR). Color code: blue = NKG2D-A monomer; purple = NKG2D-B monomer; yellow = α1 domain; red = α2 domain; green = α3 domain.

Although the different NKG2D ligands vary considerably in sequence and different allelic variants exist, they are all recognized by the invariant NKG2D receptor. Structural studies of

different NKG2D-ligand complexes revealed that the NKG2D homodimer binds diagonally across the asymmetric α1/α2-helical surface of the different monomeric ligands (Figure 3B). Furthermore, most amino acid residues of the receptor that dominate binding to the ligands are conserved [243, 244, 247, 248]. In contrast, binding affinities vary significantly with dissociation binding constants ranging from $9x10^{-6}$ to $6x10^{-9}$ M for the interactions investigated, and studies suggest that the ligands might even compete for receptor binding [246, 249-252]. However, there is no evidence so far that the ligands induce qualitatively different effector responses, but maybe the different affinities account for quantitative differences by fine-tuning NK and T cell activation [152].

NKG2D ligands are generally absent or rarely expressed on normal cells, but upregulated by infected, transformed and/or stressed cells indicating a rational for NKG2D-mediated detection of pathological alterations in autologous cells [253]. In normal tissue, MICA/B are found only on gastrointestinal or bronchial epithelial cells, maybe due to stimulation by the neighboring microbial flora [223, 254], whereas the other ligands are found mainly on mRNA level in adult healthy tissues [235]. Consequently, inappropriate signaling through NKG2D and aberrant NKG2D ligand expression in healthy cells could lead to autoimmune diseases [255]. In contrast, overexpression of NKG2D ligands is commonly found on tumor cell lines and primary tumors of various epithelial and non-epithelial origins (e.g. carcinoma such as breast, lung, colon, ovary, and prostate, glioma, melanoma or leukemia) [193, 256-262], as well as upon viral infections [263-265]. Several studies showed that ectopic NKG2D ligand expression on cancer cells leads to tumor rejection by NK and T cells *in vitro* and *in vivo* irrespective of MHC class I expression, but in a perforin-dependent manner [192, 193, 218, 257, 258, 266-269]. The importance of the NKG2D/NKG2D ligand system in tumor immunosurveillance and prevention of tumor formation was further underlined by studies showing that NKG2D-deficient mice or *in vivo* blockade of NKG2D led to a higher incidence of spontaneous or carcinogen-induced cancer development [270, 271]. Moreover, in early stages of breast and colorectal cancer NKG2D ligand expression was shown to correlate with good prognosis [259, 272, 273]. However, differential expression patterns of the individual ligands in different tumor types and even throughout one tumor entity indicate that the ligands are not redundant in function and may have evolved as a consequence of evolutionary pressure due to tissue-specificity, malignant transformation or viral immunoevasins. Along this line, it was shown that apart from stress-induced expression via activation of the DNA damage pathway

[274] NKG2D ligands are differentially regulated on transcriptional and post-translational level during malignant transformation [246]. Furthermore, viruses have evolved strategies, which interfere with NKG2D ligand expression to escape NK cell recognition [275-277].

1.5 Cancer Immunoediting and NKG2D-dependent Tumor Immune Escape

Cancer immunoediting is a dynamic process of immunosurveillance and tumor progression comprising three phases - elimination, equilibrium and escape [278]. During elimination, transformed cells are destroyed by a competent immune system, whereby NKG2D plays a key role for tumor immunosurveillance by NK and T cells (Figure 4). In the equilibrium phase, tumor editing by immune selection occurs leading to less immunogenic tumor variants or impaired immune cell functions. These tumors evade the immune system, grow progressively, become clinically apparent and establish an immunosuppressive tumor microenvironment [279, 280]. Thereby, NKG2D-mediated cytotoxicity is impaired by cytokines, the cellular crosstalk with tumor-associated cells and specific tumor immune escape mechanisms [90, 278, 281-283] (Figure 4). Besides selection for low NKG2D ligand expressing tumor variants during cancer progression [284-286], also chronic stimulation of NKG2D can lead to impaired NKG2D-mediated functions of NK and T cells [287-289]. In addition, downregulation of NKG2D could be mediated by cytokines of the tumor microenvironment as shown for IFN-γ, which is secreted by activated immune cells in course of a negative regulation loop [290, 291]. In this respect, inhibition of antitumor functions could also be correlated to the major immunosuppressive cytokine transforming growth factor β1 (TGF-β1), which mediates NKG2D downregulation either through the direct interaction of $NKG2D^+$ immune cells with regulatory T cells (Tregs) or as soluble factor secreted by the tumor cells itself [292-295].

Moreover, a tumor immune escape mechanism evolved based on the release of NKG2D ligands from the plasma membrane of tumor cells. Thereby, members of the matrix metalloproteases (MMP-9 and MMP-14) and ADAMs (a disintegrin and metalloprotease; ADAM10/17) proteolytically shed NKG2D ligands [14, 296-302] leading to soluble NKG2D (sNKG2D) ligand ectodomains frequently found in the plasma of patients suffering from different types of cancer [303-309]. In the case of MICA, cleavage requires the association of MICA with the membrane-associated disulphide isomerase endoplasmic reticulum protein 5 (ERp5) [299].

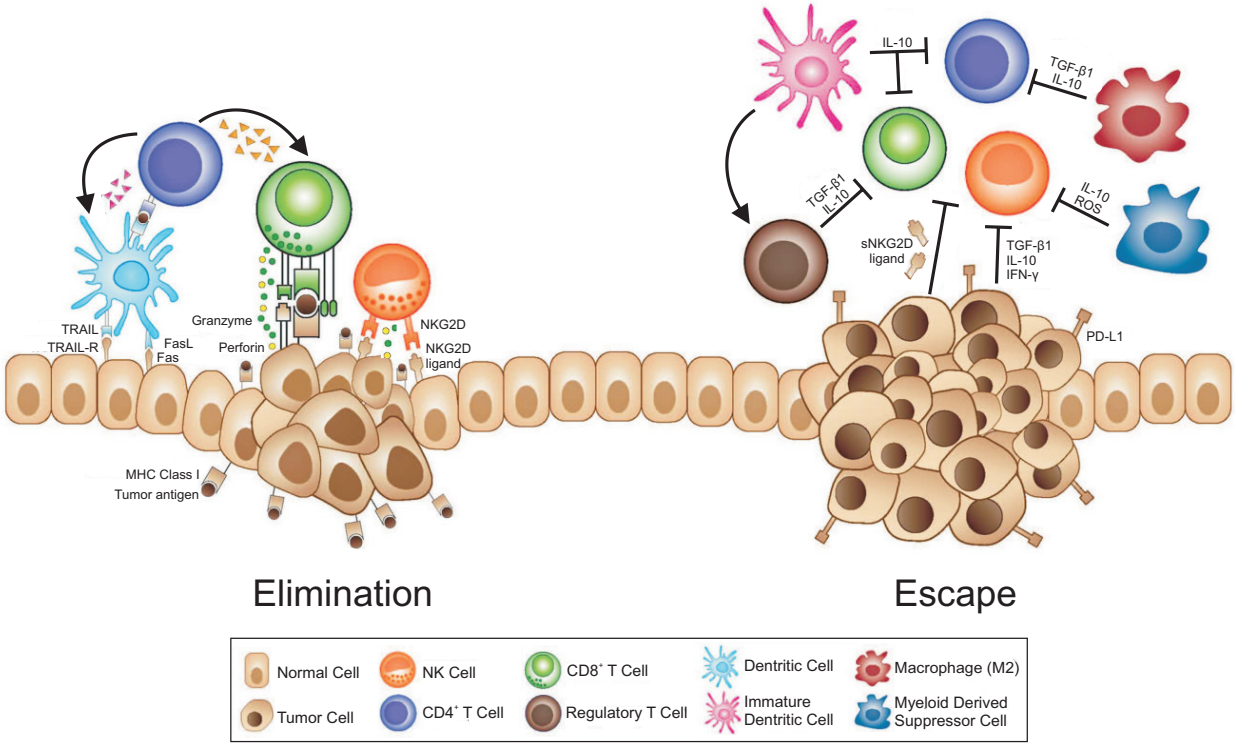

Figure 4: Immunosuppressive tumor microenvironment and tumor immune escape.
Simplified overview of the crosstalk between immune cells mediating tumor immunosurveillance, and tumor escape strategies. During the elimination phase immune effector cells such as $CD8^+$ T cells (CTLs) and NK cells with the help of dendritic and $CD4^+$ T cells are able to recognize and eliminate tumor cells. Tumor cell killing thereby mainly relies on the recognition of stress-induced ligands by the NKG2D receptor and recognition of MHC class I molecules by the TCR complex. As a result of tumor heterogeneity, tumor cells, which are less immunogenic or have upregulated immunosuppressive factors, are selected. These cells are able to subvert the immune response and escape immunosurveillance. On the one hand, tumor cells downregulate MHC molecules, loose expression of antigenic molecules and upregulate inhibitory molecules such as PD-L1 (programmed cell death protein ligand 1) to directly evade cytotoxic lymphocyte recognition. Moreover, the release of soluble NKG2D ligands leads to tumor escape by loss of surface antigens and subsequent blocking and downregulation of the NKG2D receptor on immune cells. On the other hand, tumor cells can secrete cytokines (e.g. TGF-β1 or IL-10) to generate an immunosuppressive tumor microenvironment and further recruit suppressive cells such as regulatory T (Treg) cells, immature myeloid cells (including immature dendritic cells (iDC) and myeloid-derived suppressor cells (MDSCs)), and M2 macrophages. iDC can cause T cell anergy due to lack of co-stimulatory molecules. M2 macrophages and MDSCs inhibit T cell responses through a variety of mechanisms, including reactive oxygen species (ROS) generation and secretion of immunosuppressive cytokines, which contribute to a microenvironment where immune responses are difficult to instigate an sustain. The figure is adapted and modified from Monjazeb *et al*. (2013) [310].

Besides proteolytical shedding, some NKG2D ligands are released on exosomes, as shown for the shedding resistant MICA allelic variant MICA*08 and for the GPI anchored ULBP3 [311,

312], or can be secreted as soluble forms due to alternative splicing as shown for ULBP4/5 [313, 314]. NKG2D ligand release results in impaired tumor immunosurveillance by $NKG2D^+$ immune cells due to i) reduced tumor recognition by the loss of antigenic NKG2D ligands on the tumor cell surface and ii) blocking and downregulation of the NKG2D receptor on cytotoxic immune cells by engagement of sNKG2D ligands [287, 315-317]. Consequently, previous studies with patients suffering from leukemia [256], neuroblastoma [305], cervical carcinoma [318, 319], multiple myeloma [303] or head and neck squamous cell carcinoma [304, 320, 321] demonstrated that elevated plasma levels of sMICA correlated with impaired NKG2D-dependent NK and T cell cytotoxicity.

The biological relevance of NKG2D ligand release in oncogenesis was further confirmed *in vivo* by implanting a mouse prostate cancer cell line overexpressing wildtype MICB, sMICB or a shedding-resistant MICB variant in severe combined immunodeficient (SCID) mice. Mice receiving the cancer cells expressing the shedding-resistant MICB variant did not develop prostate cancer, whereas sMICB promoted tumor growth [322]. Moreover, elevated sMICA/B levels could be correlated to severe disease progression in patients with malignant disease [323-325]. However, the diagnostic and prognostic value of individual sNKG2D ligand plasma levels is limited due to ligand polymorphism and heterogeneity.

1.6 Cancer Immunotherapies

Cancer remains the leading cause of death globally and the development of effective cancer therapies is still challenging. Besides standard cancer therapies comprising surgery, chemotherapy and radiotherapy, new combinatorial immunotherapies evolved to overcome tumor immune escape and enhance the antitumor functions of immune cells. These therapies including chemical compounds such as histone deacetlyase (HDAC) inhibitors [326] and protein tyrosine kinase inhibitors [327], which lead to inhibition of tumor cell proliferation and apoptosis induction, showed beneficial effects in several clinical trials with patients suffering from leukemia and some solid tumors. Moreover, anticancer therapies based on the use of monoclonal blocking antibodies as monotherapy or in combination with radio- or chemotherapy were invented. Antibodies targeting tumor antigens lead directly to tumor growth arrest, apoptosis, or induction of ADCC by cytotoxic immune cells. Consequently, clinical trials with antibodies against the tumor antigens epidermal growth factor receptor (EGFR) [328] or CD20

[329] demonstrated an improved survival of patients with colorectal cancer and head and neck squamous cell carcinoma, or B cell lymphoma, respectively. On the other hand, checkpoint blockade antibodies targeting the cytotoxic T lymphocyte-associated protein 4 (CTLA-4) [330, 331] or programmed cell death protein 1 (PD-1) [332], which are negative regulators of T cell activation, enhance antitumor functions of T cells and improved the clinical outcome of patients with different malignancies. Along this line, also bispecific proteins, which simultaneously bind to specific antigens on tumor cells and immunoreceptors on NK or T cells, are of great interest for immunotherapies. These molecules either combine antibody fragments (single-chain variable fragment, scFv) specific for a tumor antigen and an immunoreceptor, or ectodomains of an activating ligand or receptor (e.g. ULBP2-BB4 or NKG2D-CD3ζ scFv) leading to enhanced tumor recognition and immune cell cytotoxicity [333-336].

In recent years, cell-based cancer therapies (e.g. allogeneic hematopoietic stem cell transplantation (HSCT) or adoptive transfer of autologous and allogeneic T and NK cells) became more and more important. Adoptive cell therapies mainly rely on the transfer of clinical grade *ex vivo* IL-2 expanded autologous or allogeneic NK or T cells isolated from leukapheresis products. They are conducted either as monotherapy or in combination with HSCT or chemo-/immunotherapies. In the case of CTLs, further *ex vivo* antigen-stimulation is required to generate tumor-specific T cells or autologous tumor-specific T cells could be directly extracted from tumor samples (tumor-infiltrating T cells, TILs) of melanoma patients and showed promising effects in clinical trials [337-339]. However, the improvement of T cell therapies is still challenging due to the requirement for antigen-specificity, MHC-restriction, the availability of TILs extracted from tumor biopsies, tumor immune escape mechanisms and several occurring side effects [340]. In case of NK cells, several clinical trials showed the safety and feasibility of adoptive transfer of mainly *ex vivo* expanded allogeneic NK cells without or post-HSCT with improved graft vs. leukemia/tumor (GvL/T) but no graft vs. host disease (GvHD) effects in hematological disease and some solid tumors [341, 342].

Moreover, genetic engineering to redirect NK and T cells to tumor targets and enhance their cytotoxic functions is of great interest to further improve cellular therapies. In this respect, a main focus relies on NK and T cells modified to express recombinant chimeric antigen receptors (CARs), which are comprised of an extracellular antigen-specific scFv fused to intracellular signaling domains (mostly the CD3-derived ITAM signaling motif and a co-stimulatory molecule). Clinical trials using CD19-specific CAR T cells in hematological malignancies

were successful and induced even long-term remissions [343, 344] and several trials against different tumor antigens (e.g. CD138, HER2, ErB2 or EGFRvIII) expressed by solid tumors are ongoing [345]. Moreover, T cells equipped with NKG2D-CARs showed tumor elimination and activation of the host's immune response and even induced tumor-specific memory in pre-clinical studies [346-348]. However, genetically engineered T cells also increased severe side effects such as GvHD [340]. Therefore, CAR modified NK cells can represent a complementary therapeutic option as shown in pre-clinical studies with CD19-, CD20- or CD138-CAR expressing NK cells [349-352]. Furthermore, the transduction of an NKG2D-CAR markedly increased NKG2D surface expression in NK cells, which showed higher cytotoxicity against leukemia and solid tumor cell lines [353].

1.7 Head and Neck Squamous Cell Carcinoma

Head and neck squamous cell carcinoma (HNSCC) is a highly aggressive solid tumor originating from the epithelial lining of the upper aero-digestive tract, regularly involving the nasal and oral cavity, lip, pharynx, larynx, and paranasal sinuses. HNSCC is characterized by phenotypic, etiological, biological and clinical heterogeneity [354, 355]. The relative frequency of HNSCC correlates with tobacco and alcohol consumption, chewing betel nut (particularly in South Asia) as well as infection with high-risk human papillomavirus (HPV) subtypes [356-358]. With approximately 650,000 new patients and 300,000 deaths annually, HNSCC is the sixth most common cancer worldwide [356, 357, 359, 360]. Moreover, the incidence of HNSCC in younger adults (< 45 years) is increasing and can be correlated to rising HPV infections [361, 362]. Current therapeutic regimens for patients with HNSCC combine chemotherapy, radiotherapy and surgery with 5-year survival rates of 30–65% and 5–58% for the tumor stages T1–T4 and N0–N3, respectively [363]. Due to the broad range of epithelial malignant neoplasms of HNSCC, the identification of biomarkers for early diagnosis and therapeutic strategies to improve HNSCC treatment remains challenging. Prognosis remains poor due to (i) decreased leukocyte numbers, (ii) impaired proliferation of leukocytes, and (iii) increased numbers of $CD4^+CD25^+Foxp3^+$ regulatory T cells, which are immunosuppressive to T cells, NK and NKT cells [19, 364-369]. The impaired immune cell function is associated with the high secretion potential of cytokines and chemokines from HNSCC tumors, causing an immunosuppressive tumor microenvironment and aggressive nature of HNSCC [370-372].

1.8 Objectives

The NKG2D receptor recognizes several cellular NKG2D ligands overexpressed on tumor cells and is therefore important for tumor immunosurveillance. However, soluble NKG2D ligands released from malignant cells by proteolytical shedding or on exosomes can inhibit NKG2D-dependent NK and T cell cytotoxicity. Consequently, elevated individual sNKG2D ligand plasma levels correlated with impaired NK cell cytotoxicity in patients suffering from different cancers [373]. In this respect, a clinical phase I/II trail of adoptive transfer of allogeneic NK cells post-HSCT in patients with high-risk neuroblastoma showed inhibition of donors' NK cell cytotoxicity by blocking the NKG2D receptor through sMICA in patients' plasma [305]. Furthermore, previous studies on sMICA indicated a role of NKG2D-dependent tumor immune escape in HNSCC [320, 321], one of the most common cancers worldwide. So far, little is known about the role of cumulative plasma levels of all sNKG2D ligands and whether the impact of NKG2D-related escape strategies changes with course of disease. This knowledge is of particular importance to estimate the efficacy of NKG2D-dependent antitumor functions of autologous and adoptively transferred $NKG2D^+$ cytotoxic lymphocytes. Therefore, the aim of this thesis was the characterization of the NKG2D-dependent tumor immune escape in HNSCC patients and the development of an adsorption apheresis to deplete sNKG2D ligands from patients' plasma. Adsorption apheresis as therapeutic intervention strategy should improve NKG2D-dependent antitumor functions of autologous immune cells, and as preconditioning strategy, if combined with cellular immunotherapies, the efficacy of adoptively transferred immune cells. The following points should be investigated:

1. Evaluation of the levels of the sNKG2D ligands sMICA/B and sULBP1-3 in the plasma of HNSCC patients to elucidate the time course of sNKG2D ligand release during disease progression and to identify a patient cohort, which benefits from restoration of NKG2D-dependent tumor immunosurveillance. In this respect, also immunosuppressive factors should be monitored to further gain insights on additional mechanisms, which might influence tumor immune escape.

2. Determination of the impact of sNKG2D ligands on NK cell functions. The influence of sNKG2D ligands in patients' plasma on NK cell cytotoxicity should be addressed using *in vitro* cytotoxicity experiments with primary human NK cells. In order to study NK cell cytotoxicity and tumor infiltration, a 3D multicellular tumor spheroid model, which resembles

poorly vascularized and avascular regions of solid tumors and micrometastases, should be established based on HNSCC cell lines. The tumor spheroids should allow for the molecular determination of antitumor functions of NK cells in a well-defined *in vivo*-like system.

3. Generation of a bioreactive surface for adsorption apheresis of sNKG2D ligands from patients' plasma. As proof of concept, monoclonal anti-MICA antibodies should be screened to find a suitable candidate with high sMICA depletion efficacy. In a second approach, recombinant NKG2D proteins should be generated and characterized for the generation of a pan-specific adsorber matrix, which can deplete all sNKG2D ligands from patients' plasma simultaneously.

4. Pre-clinical validation of adsorption apheresis in a rhesus monkey (*Macaca mulatta*) model. As proof of concept, rhesus monkeys should be infused with recombinant, soluble human MICA to estimate the depletion kinetics and efficacy of the anti-MICA antibody-functionalized adsorber matrix to remove sMICA from plasma *in vivo*.

2 Materials and Methods

2.1 Materials

2.1.1 Chemicals, Consumables and Instruments

Unless otherwise denoted, all chemicals for laboratory use and cell culture were obtained in p.a. quality from the companies AppliChem (Darmstadt, Germany), Carl Roth GmbH (Karlsruhe, Germany), GE Healthcare (Buckinghamshire, UK), Miltenyi Biotec GmbH (Bergisch-Gladbach, Germany), PAA (Cölbe, Germany), PAN Biotech GmbH (Aidenbach, Germany), Roche (Mannheim, Germany), Sigma-Aldrich GmbH (Saint Louis, USA) and Thermo Fisher Scientific Inc. (Waltham, USA). Consumables for cell culture, molecular biology and protein biochemistry were obtained from BioRad Laboratories (Hercules, USA), Greiner Bio-One (Kremsmünster, Austria), Merck Millipore (Darmstadt, Germany), Lonza (Basel, Switzerland), Sarstedt AG & Co (Nümbrecht, Germany) or Whatman (Dassel, Germany). Unless otherwise mentioned, all instruments were common lab equipment.

2.1.2 Enzymes, Inhibitors, Antibiotics, Additives and Cytokines

Enzymes	**Supplier**
Fast Digest® restriction endonucleases	Thermo Fisher Scientific
*Fast*AP™ thermo sensitive alkaline phosphatase	Thermo Fisher Scientific
DreamTag™ polymerase	Thermo Fisher Scientific
Phusion® polymerase	Thermo Fisher Scientific
Pfu polymerase	Thermo Fisher Scientific
T4 DNA ligase	Thermo Fisher Scientific

Inhibitor	**Supplier**
cOmplete™ protease inhibitor cocktail	Roche

Antibiotic	**Supplier**
Ampicillin	AppliChem
Gentamycin	Gibco
Geneticin	Gibco

Antibiotic	Supplier
Penicillin/Streptomycin	Gibco
Puromycin	Gibco
Zeocin	Invivogen

Cytokine	Supplier
Interleukin-2 (IL-2)	PromoKine

Additive	Supplier
L-Glutamine	Gibco
NEAA (non essential amino acids)	Gibco
Sodium Pyruvate	Gibco
Human AB Serum	PAA
Fetal calf serum (FCS)	PAA / PAN Biotech
IPTG	AppliChem

2.1.3 Antibodies, Isotype controls and Cell Staining Reagents

Antibodies are indicated with respective clone number and IgG-isotype. Antibodies were used in different applications as indicated: CA = cytotoxicity assay, ELISA = enzyme linked immunosorbent assay, FC = fluorescence cytometry, IB = immunoblotting, IP = immunoprecipitation, IHC = immunohistochemistry, PS = peptide spot array.

Primary Antibody, conjugate	Subtype / Clone	Application	Supplier
anti-human NKG2D (CD314), APC	mouse IgG1; BAT221	FC	Miltenyi Biotec
anti-human NKG2D (CD314), PE	mouse IgG1; BAT221	FC	Miltenyi Biotec
anti-human NKG2D (CD314)	mouse IgG1; MAB139	FC, CA	R&D Systems
anti-human MICA	mouse IgG2b; MAB1300	ELISA	R&D Systems
anti-human MICA	mouse IgG1; AMO1	ELISA, FC, IP	A. Steinle[b]

[b] The antibodies were kindly provided by A. Steinle, Institute for Molecular Medicine, Goethe-University, Frankfurt am Main, Germany.

Primary Antibody, conjugate	Subtype / Clone	Application	Supplier
anti-human MICA	goat (polyclonal);AF1300	ELISA, IB	R&D Systems
anti-human MICA/B	mouse IgG2a; BAMO3	ELISA, FC, IP	A. Steinle[b]
anti-human MICA/B	mouse IgG2a; BMO2	ELISA	A. Steinle[b]
anti-human MICB	mouse IgG1; BAMO1	ELISA, FC	A. Steinle[b]
anti-human MICB	mouse IgG2b; MAB1599	ELISA, IP	R&D Systems
anti-human MICB	goat (polyclonal); AF1599	ELISA, IB	R&D Systems
anti-human ULBP1	mouse IgG2a; MAB1380	ELISA, IP	R&D Systems
anti-human ULBP1	goat (polyclonal); AF1380	ELISA, IB, IP	R&D Systems
anti-human ULBP1	mouse IgG2a; AUMO2	ELISA	A. Steinle[b]
anti-human ULBP1	mouse IgG1; AUMO5	ELISA	A. Steinle[b]
anti-human ULBP2/5/6	mouse IgG2a; MAB1298	ELISA, IB, IP	R&D Systems
anti-human ULBP2/5/6	goat (polyclonal); AF1298	ELISA, IB	R&D Systems
anti-human ULBP2	mouse IgG1; BUMO1	ELISA	A. Steinle[b]
anti-human ULBP2	rabbit IgG; 27080002	IHC	Novus biologicals
anti-human ULBP3	mouse IgG2a; MAB1517	ELISA, IB, IP	R&D Systems
anti-human ULBP3	goat (polyclonal); AF1517	ELISA, IB	R&D Systems
anti-human ULBP3	mouse IgG1; CUMO3	ELISA	A. Steinle[b]
anti-human CD45, APC	mouse IgG2a; 5B1	FC, CA	Miltenyi Biotec
anti-human CD45, PE eFluor610	mouse IgG1; HI30	FC	eBioscience
anti-human CD45	mouse IgG; 2B11+PD7126	IHC	Dako
anti-human CD56	mouse IgG1; 123C3	IHC	Invitrogen
anti-human CD56, PeCy7/APC	mouse IgG1; HCD56	FC	BioLegend
anti-human CD16, FITC/PE	mouse IgG1; 3G8	FC	BioLegend
anti-human CD3, PE	mouse IgG1; SP34.2	FC	BD Pharmingen

Primary Antibody, conjugate	Subtype / Clone	Application	Supplier
anti-human CD3	rabbit (polyclonal); SP7	IHC	Thermo Scientific
anti-human CD3, APC-Cy7	mouse IgG2a; HIT3a	FC	BioLegend
anti-human CD4, PacificBlue	mouse IgG2b; OKT4	FC	BioLegend
anti-human CD8a, AlexaFluor700	mouse IgG1; HIT8a	FC	BioLegend
anti-human CD8	mouse IgG1; C8/144B	IHC	Dako
anti-human CD14, PerCP Cy5.5	mouse IgG2a; M5E2	FC	BD Pharmingen
anti-human CD20, FITC	mouse IgG2b; 2H7	FC	BioLegend
anti-human CD20	mouse IgG2a; L26	IHC	Dako
anti-human CD68	mouse IgG3; PG-M1	IHC	Dako
anti-human CD163	mouse IgG1; MRQ-26	IHC	Cell Marque
anti-human p16	mouse IgG2a; E6H4	IHC	Ventana-Roche
anti-human cleaved caspase 3	rabbit (polyclonal); SA1E	IHC	Cell Signaling Technologies
anti-His, HRP	mouse IgG2a; HIS-1	ELISA, IB	Sigma-Aldrich
anti-Biotin, HRP	goat (polyclonal)	ELISA, IB	Sigma-Aldrich

Secondary Antibody / Reagent, conjugate	Clone		Supplier
anti-goat IgG, HRP	rabbit (polyclonal)	IB	Sigma-Aldrich
anti-mouse IgG, HRP	goat (polyclonal)	IB, PS	Sigma-Aldrich
anti-mouse IgG1, FITC	rat IgG1; X-56	FC	Miltenyi Biotec
anti-mouse IgG1, PE	rat IgG1; X-56	FC	Miltenyi Biotec
anti-mouse IgG1, APC	rat IgG1; X-56	FC	Miltenyi Biotec
anti-mouse IgG1, HRP	goat (polyclonal)	ELISA	Southern Biotech
anti-mouse IgG2a/b, APC	rat IgG1; X-57	FC	Miltenyi Biotec
anti-mouse IgG2a/b, PE	rat IgG1; X-57	FC	Miltenyi Biotec
anti-mouse IgG2a, HRP	goat (polyclonal)	ELISA	Southern Biotech
anti-human IgG-Fc, HRP	goat (polyclonal)	IB, ELISA	Sigma-Aldrich
anti-human IgG-Fc, DyLight649	goat (polyclonal)	FC	Dianova
anti-monkey IgG, HRP	goat (polyclonal)	ELISA	Sigma-Aldrich

Secondary Antibody / Reagent, conjugate	Clone		Supplier
anti-monkey IgM, HRP	goat (polyclonal)	ELISA	Sigma-Aldrich
Streptavidin, HRP	31334288	ELISA	Immunotools
Streptavidin, HRP	streptavidin polymer	IB	Sigma-Aldrich

Isotype control		Supplier
mouse IgG1, APC	κ-isotype; MOPC-21	BioLegend
mouse IgG1, PE	κ-isotype; MOPC-21	BioLegend
mouse IgG1, APC	130-092-214	Miltenyi Biotec
mouse IgG2a, APC	130-098-850	Miltenyi Biotec
mouse IgG2b, APC	130-098-890	Miltenyi Biotec

Cell Stains / Counting beads	Supplier
CellTrace™ CFSE Cell Proliferation Kit	Thermo Fisher Scientific
Sytox® Blue Dead Cell Stain	Thermo Fisher Scientific
LIVE/DEAD® Fixable Aqua Dead Cell Stain	Thermo Fisher Scientific
CountBright™ Absolute Counting Beads	Thermo Fisher Scientific

2.1.4 Kits

Kit	Supplier
BD™ CBA Human Soluble Protein Master Buffer Kit	BD Bioscience
BD™ CBA Human IFN-γ Flex Set	BD Bioscience
BD™ CBA Human TNF Flex Set	BD Bioscience
BD™ CBA Human IL-1β Flex Set	BD Bioscience
BD™ CBA Human IL-6 Flex Set	BD Bioscience
BD™ CBA Human IL-8 Flex Set	BD Bioscience
BD™ CBA Human IL-10 Flex Set	BD Bioscience
BD™ CBA Human MCP-1 Flex Set	BD Bioscience
BD™ CBA Human MIP-1α Flex Set	BD Bioscience

Kit	Supplier
BD™ CBA Human MIP-1β Flex Set	BD Bioscience
BD™ CBA Human RANTES Flex Set	BD Bioscience
BD™ CBA Human TGF-β1 Single Plex Flex Set	BD Bioscience
CD45 MicroBeads, human	Miltenyi Biotec
EnVision+ HRP.Mouse (AEC+)	Dako
EnVision+ HRP.Rabbit (DAB+)	Dako
EnVision G/2 Doublestain System Rabbit/Mouse (DAB+/Permanent Red)	Dako
GeneJET™ Plasmid Miniprep Kit	Thermo Fisher Scientific
GeneJET™ Gel Extraction Kit	Thermo Fisher Scientific
Human MICB DuoSet ELISA	R&D Systems
Human ULBP-1 DuoSet ELISA	R&D Systems
Human ULBP-2 DuoSet ELISA	R&D Systems
Human ULBP-3 DuoSet ELISA	R&D Systems
INNOTEST® HIV Antigen mAb	INNOGENETICS
NucleoBond Xtra Midi / Maxi Kit	Macherey-Nagel
NK Cell Isolation Kit, human	Miltenyi Biotec
NK Cell Activation/Expansion Kit, human	Miltenyi Biotec
Pierce™ LAL Chromogenic Endotoxin Quantitation Kit	Thermo Fisher Scientific
Rapid ELISA Mouse mAb Isotyping Kit	Thermo Fisher Scientific
ToxinSensor™ Chromogenic LAL Endotoxin Assay Kit	Genscript

2.1.5 Bacterial strains and Culture media

Strain	Genotype	Supplier
DH5α	K-12 strain derivative: *F-* θ*80lac ZΔ* M15 *lac* ZYA-*)* Δ*(arg*F U169 *rec*A1 *and* A1 *hsd*R17 *(rK -mK+) pho*A *sup*E44 *λ - thi -1 gyr*A96 *rel*A1	Thermo Fisher Scientific
BL21(DE3)	B strain derivative: F- *omp*T *hsdS*$_B$ (r_B-m_B-) gal dcm (DE3)	Thermo Fisher Scientific

For the cultivation of bacteria, lysogeny broth (LB) medium [374] and agar with the low salt-formulation of Lennox [375] were purchased from Carl Roth.

2.1.6 Cell lines and Culture media

2.1.6.1 Unmodified Mammalian Cell Lines

Unless otherwise noted, all cell lines were purchased from the American Type Culture Collection (ATCC).

Cell Line	Characterization	Supplier
CAL-27	human tongue squamous cell carcinoma cells (CRL-2095)	ATCC
Detroit562	human pharyngeal carcinoma cells (CCL-138)	ATCC
FaDu	human pharynx squamous cell carcinoma cells (HTB-43)	ATCC
SiHa	grade II, human cervix squamous cell carcinoma cells (HTB-35)	A. Cerwenka[c]
UKF-NB3	human neuroblastoma cells	J. Cinatl[d] [376]
C1R	human B cell lymphoma (CRL-2369)	ATCC

2.1.6.2 Genetically Modified Cell Lines

Cells	Insertion	Supplier
HEK 293T/17	human embryonic kidney cells expressing large T antigen (CRL-11268)	ATCC
C1R-neo	Neomycin resistance; mock transduced	A. Steinle[e]
C1R-MICA01	MICA*01 ligand	A. Steinle[e]
C1R-MICA04	MICA*04 ligand	A. Steinle[e]
C1R-MICA07	MICA*07 ligand	A. Steinle[e]
C1R-MICA08	MICA*08 ligand	A. Steinle[e]
C1R-MICB	MICB ligand	A. Steinle[e]
C1R-ULBP1	ULBP1 ligand	A. Steinle[e]
C1R-ULBP2	ULBP2 ligand	A. Steinle[e]
C1R-ULBP3	ULBP3 ligand	A. Steinle[e]
C1R-MICA01-His	MICA*01 ligand with N-terminal hexahistidine tag	this thesis

[c] The cell line was kindly provided by A. Cerwenka, Innate Immunity, German Cancer Research Center, Heidelberg, Germany.
[d] The cell line was kindly provided by J. Cinatl, Institute for Medical Virology, Goethe-University, Frankfurt am Main, Germany.
[e] The cell lines were kindly provided by A. Steinle, Institute for Molecular Medicine, Goethe-University, Frankfurt am Main, Germany.

Cells	Insertion	Supplier
C1R-MICA04-His	MICA*04 ligand with N-terminal hexahistidine tag	this thesis
C1R-MICA07-His	MICA*04 ligand with N-terminal hexahistidine tag	this thesis
C1R-MICA08-His	MICA*04 ligand with N-terminal hexahistidine tag	this thesis
C1R-MICB-His	MICB ligand with N-terminal hexahistidine tag	this thesis
C1R-ULBP1-His	ULBP1 ligand with N-terminal hexahistidine tag	this thesis
C1R-ULBP2-His	ULBP2 ligand with N-terminal hexahistidine tag	this thesis
C1R-ULBP3-His	ULBP3 ligand with N-terminal hexahistidine tag	this thesis
UKF-NB3-iMICA	doxycycline MICA01 with N-terminal decahistidine tag	this thesis

2.1.6.3 Culture Media

DMEM compl.

Dulbecco's modified Eagle medium (DMEM, Gibco) supplemented with 2 mM L-glutamine (Gibco), 100 U/ml penicillin, 100 µg/ml streptomycin (Gibco), 10% fetal calf serum (FCS, PAA or PAN Biotec) for culturing 293T/17 and SiHa cells.

HNSCC medium

Minimum Essential Medium (MEM, Gibco) supplemented with 2 mM L-glutamine, 100 U/ml penicillin, 100 µg/ml streptomycin, 10% FCS and 1 mM sodium pyruvate (Gibco) for HNSCC cell lines FaDu, CAL27 and Detroit562.

UKF-NB3 medium

Iscove's modified Dulbecco's medium (IMDM, Gibco) supplemented with 100 U/ml penicillin, 100 µg/ml streptomycin and 10% FCS for UKF-NB3 cells.

C1R medium

RPMI 1640 medium supplemented with 2 mM L-glutamine, 100 U/ml penicillin, 100 µg/ml streptomycin, 10% FCS was used for culturing C1R cells. For C1R transfectants 1.8 mg/ml gentamicin (G418, Gibco) were added to the media.

pNK medium

X-Vivo10 medium (Lonza) supplemented with 5% human AB serum (PAA) and 1000 U/ml IL-2 for culturing of primary human NK cells.

2.1.7 Buffers

Unless otherwise denoted, all buffers were prepared in deionized water and the pH was adjusted with HCl or NaOH.

Buffer / Solution		Formulation
Agarose Gel Electrophoresis		
TAE buffer	0.04 M	TRIS
	0.01 M	EDTA
	1.14% (v/v)	acetic acid
EtBr stain	0.01% (v/v)	EtBr in TAE buffer
Biotinylation of proteins *in vitro*		
Biotin assay buffer	0.001 M	$MgCl_2$
	0.001 M	ATP
	100 µM	D-biotin
	0.1 M	Tris
	0.025 M	NaCl
		adjust to pH 8.0
Competent Bacteria		
TFB I	0.03 M	potassium acetate
	0.01 M	$CaCl_2$
	0.05 M	$MnCl_2$
	0.1 M	RbCl
	15% (v/v)	glycerol
		adjust to pH 5.8 with acetic acid
TFB II	0.01 M	MOPS
	0.075 M	$CaCl_2$
	0.01 M	RbCl
	15% (v/v)	glycerol
		adjust to pH 6.8 with KOH

Buffer / Solution		Formulation
ELISA		
Coating Buffer mAb	0.05 M 0.05 M	Na_2CO_3 $NaHCO_3$ adjust to pH 9.6
Blocking Buffer mAb	0.2% (w/v) 0.1% (v/v)	gelatin NaN_3 in PBS
Sample Buffer	1% (w/v)	albumin fraction V (BSA) in PBS
PBS-T	0.05% (v/v)	Tween20 in PBS
Flow Cytometry / Cytotoxicity Assays		
FACS buffer	2% (v/v)	FCS in PBS
FACS fix	1% (v/v)	formaldehyde in PBS
Cytotoxicity medium	5% (v/v)	human AB serum in X-Vivo10
CFSE stain	1:1000	CFSE solution in PBS
Dead stain solution	1:1000	Sytox® Blue in PBS
Immunoblotting / Peptide Spot Arrays		
Transfer buffer	0.192 M 0.025 M 20% (v/v)	M glycin TRIS EtOH (≥ 99.8%, p.a.)
TBS-T	0.05 M 0.15 M 0.1% (v/v)	TRIS NaCl Tween20
WB blocking buffer	2% (w/v)	skim milk powder in TBS-T
Spot blocking buffer	5% (w/v) 5% (w/v)	skim milk powder albumin fraction V in TBS-T
Spot buffer	10% (v/v)	Spot blocking buffer in TBS-T
Coumarin solution	0.09 M	*p*-coumaric acid in DMSO
Luminol solution	0.25 M	luminol in DMSO
ECL I solution	0.1 M 396 µM 0.005 M	Tris pH 8.5 coumarin luminol

Buffer / Solution		Formulation
ECL II solution	0.1 M	Tris pH 8.5
	0.2% (v/v)	H_2O_2
Regeneration buffer A	8 M	urea
	1% (w/v)	SDS
	0.1% (v/v)	β-mercaptoethanol
Regeneration buffer B	50% (v/v)	EtOH
	10% (v/v)	acetic acid
Immunoprecipitation		
PBS-T	0.05% (v/v)	Tween20 in PBS
IP buffer	0.02% (v/v)	Tween20 in PBS
Elution buffer I	0.06 M	TRIS pH 6.8
	2% (v/v)	SDS
	10% (v/v)	10% glycerol
	0.001% (w/v)	bromphenol blue
	5% (v/v)	β-mercaptoethanol
	0.3 mM	DTT
Elution buffer II	0.1 M	glycin pH 2.7
Isolation of pNK cells		
PBS/EDTA	0.002 M	EDTA in PBS
Protein Purification / Refolding		
Resuspension buffer (*E. coli*)	0.02 M	$MgCl_2$
	10 µg/ml	DNAse
	0.001 M	PMSF
		in PBS, adjust to pH 8.0 at 4 °C
Solubilization buffer (*E. coli*)	0.05 M	glycin
	0.1 M	Tris
		adjust to pH 8.0 at RT
Wash buffer (IMAC, denat.)	8 M	urea
	0.05 M	glycin
	0.1 M	Tris
	0.02 M	imidazole
		adjust to pH 8.0 at RT

Buffer / Solution		Formulation
Elution buffer (IMAC, denat.)	8 M	urea
	0.05 M	glycin
	0.1 M	Tris
	0.25 M	imidazole
		adjust to pH 8.0 at RT
Wash buffer (IMAC, sMICA)	0.05 M	Tris
	0.5 M	NaCl
	0.02 M	imidazole
		adjust to pH 7.5 at 4 °C
Elution buffer (IMAC, sMICA)	0.05 M	Tris
	0.5 M	NaCl
	0.25 M	imidazole
		adjust to pH 7.5 at 4 °C
Regeneration buffer (IMAC)	0.5 M	NaCl
	0.1 M	EDTA pH 8.0
Ni^{2+} solution (IMAC)	0.1 M	$NiSO_4$
Dialysis buffer A (sMICA)	0.05 M	Tris
	0.5 M	NaCl
		adjust to pH 7.5 at 4 °C
Dialysis buffer I (*E. coli*)	4 M	urea
	0.1 M	Tris
	0.4 M	L-arginine
	0.01 M	EDTA
		adjust to pH 8.0 at 4 °C
Dialysis buffer II (*E. coli*)	2 M	urea
	0.1 M	Tris
	0.4 M	L-arginine
	0.01 M	EDTA
		adjust to pH 8.0 at 4 °C
Dialysis buffer III (*E. coli*)	1 M	urea
	0.1 M	Tris
	0.4 M	L-arginine
	0.01 M	EDTA
		adjust to pH 8.0 at 4 °C

Buffer / Solution		Formulation
Dialysis buffer IV (*E. coli*)	0.1 M	Tris
	0.4 M	L-arginine
	0.01 M	EDTA
		adjust to pH 8.0 at 4 °C
Dialysis buffer V (*E. coli*)	0.025 M	Tris
	0.1 M	L-arginine
	0.0025 M	EDTA
		adjust to pH 8.0 at 4 °C
TBS (*E. coli*)	0.15 M	NaCl
	0.01 M	Tris
		adjust pH 8.0 at 4 °C
Collection buffer (Protein A/G))	1 M	TRIS pH 8.8
Elution buffer II (Protein A/G)	0.1 M	glycin pH 2.7
Regeneration buffer (Protein A/G)	0.02 M	NaH_2PO_4
	0.05% (w/v)	NaN_3
	0.02 M	Na_2HPO_4 to adjust pH 7.4
Storage buffer	0.01% (v/v)	NaN_3
Size exclusion chromatography		
TBS	0.05 M	Tris
	0.025 M	NaCl
		adjust to pH 7.4 at 4 °C
SDS-PAGE		
SDS running buffer	0.025 M	Tris
	0.192 M	glycin
	0.1% (w/v)	SDS
5x SDS sample buffer (non-reducing)	0.3 M	TRIS pH 6.8
	10% (w/v)	SDS
	50% (v/v)	glycerol
	0.005% (w/v)	bromphenolblue
5x SDS sample buffer (reducing)	5x	SDS sample buffer (non-reducing)
	25% (v/v)	β-mercaptoethanol

Buffer / Solution		Formulation
Transfection of Mammalian Cells		
TA-Trans	0.018 M	polyethylenimine, branched in cell culture grade H_2O
TA-glucose	5% (w/v)	glucose in cell culture grade H_2O
DMEM/Gln	2 mM	L-glutamine in DMEM
DMEM/FCS	5% (v/v)	FCS in DMEM/Gln
DMEM/Biotin	5% (v/v) 0.02 M	PanexinNTA D-Biotin in DMEM/Gln

2.1.8 Oligonucleotides and Plasmids

2.1.8.1 Oligonucleotides

All oligonucleotides (primers) were synthesized by Sigma-Aldrich. Sequences and calculated melting temperatures are indicated (T_M), numbers correspond to an intralaboratory database.

No.	Name	Sequence (5' → 3')	T_M [°C]
38	pET16b_seq_for	AGCCAACTCAGCTTCCTTTC	62.4
39	pEET16b_Colony_rev	GGGAATTGTGAGCGGATAAC	63.1
45	pFUSE_hIgG1_Fc2_seq_for	TGCGCCGTTACAGATCCAAG	68.2
46	pFUSE_hIgG1_Fc2_seq_rev	ACCGTCAGTCTTCCTCTTCC	62.2
47	pFUSE_hIgG1_Fc2_seq_rev_2	CGGGAGATCATGAGGGTGTC	66.9
72	pET_upstream_for	ATGCGTCCGGCGTAGA	64.3
256	pFUSE_seq_rev	TGTGGTTTGTCCAAACTCATC	62.4
328	BglII_MICA_for	CTCAGATCTTTTCCCAGAGGGCAC	56.0
332	OE_pET20b_for	CAGCAGCCAACTCAGCTTCC	67.5
333	OE_NKG2D_K150M_rev	CTTAAACTGGTGATGTCATATCATTGG	65.0
334	OE_NKG2D_K150M_for	CCAATGATATGACATCACCAGTTTAAG	65.0
335	OE_NKG2D_K150R_rev	CTTAAACTGGTGCGGTCATATCATTGG	70.2
336	OE_NKG2D_K150R_for	CCAATGATATGACCGCACCAGTTTAAG	70.2

No.	Name	Sequence (5' → 3')	T_M [°C]
337	OE_NKG2D_K150W_rev	CTTAAACTGGTGTGGTCATATCATTGG	66.8
338	OE_NKG2D_K150W_for	CCAATGATATGACCACACCAGTTTAAG	66.8
339	OE_NKG2D_I182R_rev	CCTACTAACAATACGTGAAATGCAGAAGG	67.7
340	OE_NKG2D_I182R_for	CCTTCTGCATTTCACGTATTGTTAGTAGG	67.7
341	OE_NKG2D_I182W_rev	CCTACTAACAATATGGGAAATGCAGAAGG	68.3
342	OE_NKG2D_I182W_for	CCTTCTGCATTTCCCATATTGTTAGTAGG	68.3
343	OE_NKG2D_K186M_rev	CAATAATTGAAATGCAGATGGGAGACTGTGCACTC TATG	77.3
344	OE_NKG2D_K186M_for	CATAGAGTGCACAGTCTCCCATCTGCATTTCAATTA TTG	77.3
345	OE_NKG2D_S117E_rev	CAATTTTTTGATGAGGAGAAAAACTGGTATGAG	70.3
346	OE_NKG2D_S117E_for	CTCATACCAGTTTTTCTCCTCATCAAAAAATTG	70.3
347	OE_NKG2D_S151D_rev	TAAACTGGTGAAGGACTATCATTGGATGG	69.7
348	OE_NKG2D_S151D_for	CCATCCAATGATAGTCCTTCACCAGTTTA	69.7
350	BglII_MICA_His_STOP_for	CTCAGATCTCTAATGGTGGTGATGATGGTGTTTCC	76.2
351	sMICA_His_rev	GGAGCCCCACAGTCTTCGTTATAACC	68.0
409	NcoI_hIgG1-FcEQ_for	CGATATCGGCCATGGTTAGATCTGAC	66.0
410	hIgG1-FcEQ-ΔSTOP_BamHI_NheI_rev	CTAGCTAGCGCCATATACAGGATCCTTTACCCGGA GACAGGGAGAGG	68.0
411	BamHI_GS_NKG2D_EC_for	TATAGGATCCTCCGGAAACTCATTATTCAACCAAG AAG	64.0
412	NKG2D_EC_NheI_rev	CGTGCTAGCTTACACAGTCCTTTGCATGC	56.0
438	RSV.5neo_seq_for	CGCCATTTGACCATTCACC	66.3
439	RSV.5neo_seq_rev	CATTCTAGTTGTGGTTTGTC	54.5
480	SacII_His6_ULBP1_for	GCCGCCGCGGACCATCACCATCACCATCACGACA CACACTGTCTTTGCTATGACTTCATC	94.0
481	SacII_His6_ULBP2_for	GCCGCCGCGGACCATCACCATCACCATCACGACC CTCACTCTCTTTGCTATGACATCAC	94.5
482	SacII_His6_ULBP3_for	GCCGCCGCGGACCATCACCATCACCATCACGACG CTCACTCTCTCTGGTATAACTTCAC	93.2
483	SacII_His6_MICB_for	GCCGCCGCGGACCATCACCATCACCATCACGAGC CCCACAGTCTTCGTTAC	94.8
484	SacII_His6_MICA_for	GCCGCCGCGGACCATCACCATCACCATCACGAGC CCCACAGTCTTCGTTAT	94.3

No.	Name	Sequence (5' → 3')	T_M [°C]
485	XhoI_ULBP1_rev	CCGATATCTCGAGTCATCTG	59.8
486	XhoI_ULBP2/3_rev	CCGATATCTCGAGTCAGATG	59.8
487	XhoI_MICA/B_rev	CGATATCTCGAGCTAGGCGCCCTCAGTG	77.1

2.1.8.2 Plasmids

All plasmids used in this thesis were amplified in the *E. coli* DH5α strain. Plasmid numbers correspond to an intralaboratory database. Corresponding plasmid maps are listed in the appendix.

No.	Expression Plasmid (*E. coli*)	Resistance	Supplier
1901	pET16b-His_{10}-NKG2D-EC	Amp^R	J. Havenstein[f]
5802	pET20b-Avi-NKG2D-Flag/His	Amp^R	A. Steinle[g]
5701	pET11a-sMICA01-His	Amp^R	A. Steinle[g]
5801	pET20b-sMICA04-His	Amp^R	A. Steinle[g]
5901	pDEST26_HisMICA01	Neo^R/Kan^R	imaGenes
130	pUC57-Avi-hIgG1-FcEQ-NKG2D	Amp^R	Genscript
3601	pCMV-SPORT6-NKG2D-EC	Amp^R	imaGenes

No.	Expression Plasmid (mammalian cells)	Resistance	Supplier
24	pFUSE-hIgG1-Fc2	Zeo^R	Invitrogen
68	pFUSE-hIgG1-FcEQ	Zeo^R	J. Hartmann[h] [377]
6834	pFUSE-hIgG1-FcEQ-MICA01	Zeo^R	this thesis
6835	pFUSE-hIgG1-FcEQ-MICA04	Zeo^R	this thesis
8502	pFUSE-MICA01-His	Zeo^R	this thesis
8504	pFUSE-MICA04-His	Zeo^R	this thesis

[f] The plasmid was kindly provided by J. Havenstein in the lab of J. Koch, Georg-Speyer-Haus, Frankfurt am Main, Germany.
[g] The plasmids were kindly provided by A. Steinle, Institute for Molecular Medicine, Goethe-University, Frankfurt am Main, Germany.
[h] The plasmid was kindly provided by J. Hartmann in the lab of J. Koch, Georg-Speyer-Haus, Frankfurt am Main, Germany.

No.	Expression Plasmid (mammalian cells)	Resistance	Supplier
6837a	pFUSE-hIgG1-FcEQ-ΔStop	Zeo^R	this thesis
6837	pFUSE-hIgG1-FcEQ-GS-NKG2D	Zeo^R	this thesis
6838	pFUSE-hIgG1-FcEQ-NKG2D-K150M	Zeo^R	this thesis
6839	pFUSE-hIgG1-FcEQ-NKG2D-K150R	Zeo^R	this thesis
6840	pFUSE-hIgG1-FcEQ-NKG2D-K150W	Zeo^R	this thesis
6841	pFUSE-hIgG1-FcEQ-NKG2D-I182R	Zeo^R	this thesis
6842	pFUSE-hIgG1-FcEQ-NKG2D-I182W	Zeo^R	this thesis
6843	pFUSE-hIgG1-FcEQ-NKG2D-K182M	Zeo^R	this thesis
6844	pFUSE-hIgG1-FcEQ-NKG2D-S117E	Zeo^R	this thesis
6845	pFUSE-hIgG1-FcEQ-NKG2D-S151D	Zeo^R	this thesis
91	RSV.5neo	Amp^R	A. Steinle[g]
9101	RSV.5neo-MICA01	Amp^R	A. Steinle[g]
9102	RSV.5neo-His_6-MICA01	Amp^R	this thesis
9103	RSV.5neo-MICA04	Amp^R	A. Steinle[g]
9104	RSV.5neo-His_6-MICA04	Amp^R	this thesis
9105	RSV.5neo-MICA07	Amp^R	A. Steinle[g]
9106	RSV.5neo-His_6-MICA07	Amp^R	this thesis
9107	RSV.5neo-MICA08	Amp^R	A. Steinle[g]
9108	RSV.5neo-His_6-MICA08	Amp^R	this thesis
9109	RSV.5neo-MICB	Amp^R	A. Steinle[g]
9110	RSV.5neo-His_6-MICB	Amp^R	this thesis
9111	RSV.5neo-ULBP1	Amp^R	A. Steinle[g]
9112	RSV.5neo-His_6-ULBP1	Amp^R	this thesis
9113	RSV.5neo-ULBP2	Amp^R	A. Steinle[g]
9114	RSV.5neo-His_6-ULBP2	Amp^R	this thesis
9115	RSV.5neo-ULBP3	Amp^R	A. Steinle[g]
9116	RSV.5neo-His_6-ULBP3	Amp^R	this thesis

No.	Expression Plasmid (mammalian cells)	Resistance	Supplier
6846	pFUSE-Avi-hIgG1-FcEQ-NKG2D	Zeo^R	this thesis
6902	pDisplay-BirA-ER	Amp^R	J. Hartmann[i]
6903	pDisplay-sBirA	Amp^R	J. Hartmann[i]
9201	pES.1-2(M2N) (M2, rtTA)	Amp^R	A. Kinner[j]
9202	pES.1-T6-PGKPuro-MICA01	Amp^R	A. Giannattasio[k]

2.1.9 Recombinant proteins

Recombinant proteins are indicated with the plasmid number encoding for the corresponding DNA sequence and the theoretical molecular weigh (MW) calculated for monomeric proteins without posttranslational modifications. Corresponding protein sequences are listed in the appendix.

Proteins expressed in *E. coli*	No.	MW [kDa]	Supplier
rNKG2D-His (N-terminal His-tag)	1901	18.3	this thesis
rMICA*01-His (C-terminal His-tag)	5701	32.7	this thesis
rMICA*04-His (C-terminal His-tag)	5801	32.7	this thesis
rNKG2D-Biotin (N-terminal Avi-tag)	5802	20.2	this thesis
BAG-$6_{686-936}$		28.6	J. Binici[l] [378]

Proteins expressed in HEK293T/17 or UKF-NB3	No.	MW [kDa]	Supplier
sMICA*01-His (C-terminal His-tag)	8502	32.7	this thesis
sMICA*04-His (C-terminal His-tag)	8504	34.9	this thesis
MICA*01::hIgG1-FcEQ	6834	57.7	this thesis

[i] The plasmid was kindly provided by J. Hartmann in the lab of C. Buchholz, Paul-Ehrlich-Institut, Langen, Germany.
[j] The plasmid was kindly provided by A. Kinner in the lab of M. Grez, Georg-Speyer-Haus, Frankfurt am Main, Germany.
[k] The plasmid was kindly provided by A. Giannattasio in the lab of J. Koch, Georg-Speyer-Haus, Frankfurt am Main, Germany.
[l] The protein was kindly provided by J. Binici in the lab of J. Koch, Georg-Speyer-Haus, Frankfurt am Main, Germany.

Proteins expressed in HEK293T/17 or UKF-NB3	No.	MW [kDa]	Supplier
MICA*04::hIgG1-FcEQ	6835	57.8	this thesis
NKG2D::hIgG1-FcEQ	6837	44.7	this thesis
NKG2D::hIgG1-FcEQ-K150M	6838	44.7	this thesis
NKG2D::hIgG1-FcEQ-K150R	6839	44.7	this thesis
NKG2D::hIgG1-FcEQ-K150W	6840	44.7	this thesis
NKG2D::hIgG1-FcEQ-I182R	6841	44.7	this thesis
NKG2D::hIgG1-FcEQ-I182W	6842	44.7	this thesis
NKG2D::hIgG1-FcEQ-K186M	6843	44.7	this thesis
NKG2D::hIgG1-FcEQ-S117E	6844	44.7	this thesis
NKG2D::hIgG1-FcEQ-S151D	6845	44.7	this thesis
NKG2D::hIgG1-FcEQ-Biotin	6846	47.0	this thesis
NKp30::hIgG1-FcEQ		39.8	J. Hartmann[m]
NKp46::hIgG1-FcEQ		52.7	J. Hartmann[n]
B7H6::hIgG1-Fc		52.9	J. Hartmann[m] [377]
shedMICA*01 (UKF-NB3; N-terminal His-tag)	9202	~35	this thesis

2.2 Methods of Microbiology

2.2.1 Cultivation of Bacteria

For the amplification of DNA or production of recombinant proteins, *E. coli* derivatives of the K12 strain or B strain, respectively, were cultured in LB medium overnight at 37 °C and 200 rpm in a bacteria shaker. For the selection of single clone colonies, bacteria cultures were cultivated on LB-plates overnight at 37 °C in an incubator. Culture medium or LB-plates were supplemented with either 100 µg/ml ampicillin or zeocin for selection of bacterial clones carrying an antibiotic resistant gene.

[m] The proteins were kindly provided by J. Hartmann in the lab of J. Koch, Georg-Speyer-Haus, Frankfurt am Main, Germany.
[n] The proteins were kindly provided by J. Hartmann in the lab of J. Koch, Georg-Speyer-Haus, Frankfurt am Main, Germany.

2.2.2 Generation and Transformation of Competent Bacteria

Chemically competent bacteria were generated by the $CaCl_2$/RbCl method [379] for the transformation of DNA following subsequent amplification via cellular replication. Therefor, an *E. coli* culture in 100 ml of LB medium was incubated at 37 °C and 200 rpm until reaching an OD_{600} = 0.4 - 0.6. The bacteria culture was cooled down on ice for 10 min following centrifugation at 2,000xg for 10 min at 0 °C. The bacteria pellet was resuspended in 7.5 ml of ice cold TFB I buffer and incubated for 1 h on ice. After centrifugation at 3,000xg for 10 min at 0 °C, the bacteria pellet was resuspended in 2 ml of ice cold TBF II buffer and aliquoted in 50 µl stocks. The aliquots were shock frozen in liquid nitrogen and stored at -80 °C.
Rb-competent bacteria were transformed with either 50 - 100 ng of plasmid DNA, for plasmid DNA amplification, or 10 µl of ligation reaction (2.3.2.3) and incubated on ice for 20 min following a heat shock for 90 s at 42 °C and cooling down for 3 min on ice. After pre-incubation of the transformation reaction in 500 µl of LB medium at 37 °C and 600 rpm for 1 h, the bacteria suspension was either used for inoculation of 1 - 500 ml of LB medium cultures or plated on LB agar supplemented with the respective antibiotic and incubated overnight at 37 °C. Bacteria cultures were pelleted by centrifugation (9000xg, 5 min, 4 °C) and used for plasmid DNA purification (2.3.4.2).

2.3 Methods of Molecular Biology

2.3.1 Polymerase Chain Reaction (PCR)

For the exponentially amplification of specific gene fragments from genomic or plasmid DNA *in vitro* the polymerase chain reaction (PCR) [380, 381] was used. PCR can further be used to introduce genetically modifications into the gene fragment (i.e. endonuclease restriction sites or point mutations) by primer engineering or to quickly verify the existence of a specific gene after transformation in bacterial colonies (termed Colony PCR).

In this thesis, the thermostable polymerases *DreamTag*™ (no proof-reading activity) or *Phusion*® (3' - 5' exonuclease activity) (both Thermo Fisher Scientific) were used for analytical (Colony PCR) or preparative (for subsequent cloning or site directed mutagenesis) DNA amplification. For PCR protocols, the annealing temperature and elongation time was calculated individually, depending on the melting temperature (T_M) of primers used, the length of DNA fragment to be amplified, and the elongation time of the polymerase. Standard sample

preparation and PCR reaction protocols for analytical (Table 1) and preparative PCR (Table 2) are depicted. All reagents and buffers were obtained from Thermo Fisher Scientific.

Table 1: Standard reaction mixture and PCR protocol for analytical PCR (Colony PCR).

Reaction mixture		PCR protocol			
1	bacterial colony	98 °C	30 s		initial denaturation
1 µM	forward primer	98 °C	10 s		denaturation
1 µM	reverse primer	55 °C	15 s	25x	annealing
0.2 mM	dNTP mix (2 mM each)	72 °C	30 s		elongation (<0.5 kb)
2.5% (v/v)	DMSO	72 °C	5min		final elongation
1x	*DreamTag*™ green buffer	4 °C	∞		
0.025 U/µl	*DreamTag*™ polymerase				
to 25 µl	with H_2O				

Table 2: Standard reaction mixture and PCR protocol for preparative PCR.

Reaction mixture		PCR protocol			
20 ng	template DNA	98 °C	30 s		initial denaturation
0.5 µM	forward primer	98 °C	10 s		denaturation
0.5 µM	reverse primer	55 °C	15 s	25x	annealing
0.2 mM	dNTP mix (2 mM each)	72 °C	30 s		elongation (1 kb/15-30 s)
3% (v/v)	DMSO	72 °C	5 min		final elongation
1x	*Phusion*® GC buffer	4 °C	∞		
0.02 U/µl	*Phusion*® polymerase				
to 100 µl	with H_2O				

The introduction of single amino acid exchanges (point mutations) in a gene segment results from overlap extension PCR (OE-PCR) [382]. Thereby, two overlapping DNA fragments covering the whole gene sequence are generated using a mutagenic primer (OE-primer) and the respective forward (OE-PCR 1) or reverse (OE-PCR 2) primer flanking the sequence at

the 5' end and 3' end, respectively. The mutagenic primers introduce the point mutation in the overlapping complementary region of the two PCR constructs generated. In a third round of PCR (OE-PCR 3) the whole gene sequence containing the mutation is amplified by the use of the two PCR fragments as templates, and the two flanking primers. In this thesis, the thermostable *Pfu* Polymerase (Thermo Fisher Scientific) was used and standard reaction mixture and PCR protocol for the OE-PCR 1 - 3 are listed in Table 3.

Table 3: Standard reaction mixture and PCR protocol for overlap extension PCR.

Reaction mixture OE-PCR 1/2	
50 ng	template DNA
0.5 µM	flanking primer forward/reverse
0.5 µM	OE-primer reverse/forward
0.2 mM	dNTP mix (2 mM each)
2.5% (v/v)	DMSO
1x	*Pfu* buffer + $MgSO_4$
0.025 U/µl	*Pfu* polymerase
to 100 µl	with H_2O

PCR protocol			
95 °C	3 min		initial denaturation
95 °C	30 s		denaturation
50 °C	30 s	30x	annealing
72 °C	60 s		elongation (1 kb/2 min)
72 °C	5 min		final elongation
4 °C	∞		

Reaction mixture OE-PCR 3	
25 ng	product OE-PCR 1
25 ng	product OE-PCR 2
0.5 µM	flanking primer forward
0.5 µM	flanking primer reverse
0.2 mM	dNTP mix (2 mM each)
2.5% (v/v)	DMSO
1x	*Pfu* buffer + $MgSO_4$
0.025 U/µl	*Pfu* polymerase
to 100 µl	with H_2O

PCR protocol			
95 °C	3 min		initial denaturation
95 °C	30 s		denaturation
50 °C	30 s	35x	annealing
72 °C	90 s		elongation (1 kb/2 min)
72 °C	5 min		final elongation
4 °C	∞		

PCR reactions were analyzed by agarose gel electrophoresis (2.3.3) and amplified DNA fragments from preparative PCR were purified (2.3.4) and used for subsequent cloning.

2.3.2 Restriction, Dephosphorylation and Ligation of DNA

2.3.2.1 Enzymatic Restriction

All restriction type II endonucleases used were *FastDigest*® enzymes (Thermo Fisher Scientific) and are listed with corresponding restriction sites in Table 4. A standard restriction mixture using two enzymes for double restriction is listed in Table 5. Unless otherwise noted, DNA restrictions were performed according to the manufacturer's instructions using supplied *10x FastDigest*® buffer or *10x FastDigest*® green buffer and incubation for 15 min at 37 °C and subsequent enzyme inactivation at 80 °C for 10 min. Restriction samples were either analyzed by agarose gel electrophoresis (2.3.3) or directly purified (2.3.4).

Table 4: Type II restriction endonucleases and corresponding restriction sites.

Enzyme	Restriction site	Enzyme	Restriction site	Enzyme	Restriction site
BamHI	5'…G|GATCC...3' 3'...CCTAG|G…5'	EcoRV	5'...GAT|ATC…3' 3'...CTA|TAG…5'	XbaI	5'…T|CTAGA…3' 3'…AGATC|T…5'
BglII	5'…A|GATCT…3' 3'...TCTAG|A...5'	NcoI	5'…C|CATGG…3' 3'…GGTAC|C…5'		
EcoRI	5'…G|AATTC...3' 3'…CTTAA|G…5'	NheI	5'...G|CTAGC…3' 3'...CGATC|G…5'		

Table 5: Reaction mixtures for preparative and analytical restriction.

	preparative restriction	analytical restriction
DNA	1-5 µg	0.5-1 µg
10x FastDigest® buffer	5 µl	2 µl
FastDigest® enzyme I	2.5 µl	0.5 µl
FastDigest® enzyme II	2.5 µl	0.5 µl
adjust with H_2O	to 50 µl	to 20 µl

2.3.2.2 Enzymatic Dephosphorylation

To enhance ligation specificity of DNA fragments and plasmid DNA by preventing recirculation of the plasmid backbone, the phosphorylated 5'end of the linearized plasmid DNA was enzymatically dephosphorylated. Therefor, 1 - 5 µg of linearized plasmid DNA were mixed with 5 µl of 10x FastAP buffer (supplied with the enzyme) and 1 µl of FastAP alkaline phosphatase (Thermo Fisher Scientific) in a total volume of 50 µl in H_2O and incubated for 10 min

at 37 °C. After enzyme inactivation for 5 min at 75 °C, dephosphorylated DNA was purified (2.3.4) and used for enzymatic ligation (2.3.2.3).

2.3.2.3 Enzymatic Ligation

For ligation of linearized DNA fragments generally 50 ng of vector DNA (maximal DNA amount of 100 ng) was used and the amount of insert DNA in a molar excess of 3:1 to vector DNA was calculated by the following equation:

$$insert\ DNA\ [ng] = \frac{molar\ excess\ \times\ insert\ DNA\ [bp]\ \times\ plasmid\ DNA\ [ng]}{plasmid\ DNA\ [bp]}$$

The calculated insert DNA and 50 ng of vector DNA were mixed with 5 U T4 DNA ligase (Thermo Fisher Scientific) and 2 µl of the supplied T4 buffer in a total volume of 20 µl aqueous solution and incubated 1 h at 22 °C or overnight at 16 °C. After enzyme inactivation for 10 min at 65 °C, the ligated DNA was used for transformation (2.2.2) or stored at -20 °C.

2.3.3 Agarose Gel Electrophoresis

DNA molecules were separated according to their size using agarose gel electrophoresis. Depending on the DNA size, agarose gels consisting of 0.8% or 1.2% (w/v) agarose in TAE buffer for DNA fragments > 1 kb or smaller were used, respectively. DNA samples were supplemented with 6x DNA loading dye (Thermo Fisher Scientific) or already contained *DreamTag*™ green buffer (2.3.1) or *FastDigest*® green buffer (2.3.2.1). Samples were loaded together with GeneRuler 1kb Plus DNA ladder (Thermo Fisher Scientific) in the agarose gels and separated at 160 V for approximately 45 min in a WIDE MINI-SUB cell GT chamber (Bio-Rad) with TAE buffer. For visualization of DNA fragments, agarose gels were incubated for 15 min in EtBr stain and analyzed under UV light (254 nm) using a Gel Doc 2000 gel documentation system (BioRad).

2.3.4 Isolation of DNA from Agarose Gels and DNA Purification

2.3.4.1 Isolation of DNA from Agarose Gels

Specific DNA fragments separated by agarose gel electrophoresis (2.3.3) can be isolated from the gel matrix and used for subsequent cloning. Therefor, gel slices containing the respective

DNA fragment were cut out under low intensity UV light (302 nm), to prevent DNA damage, and DNA was isolated using the GenJET™ Gel Extraction Kit (Thermo Science) according to the manufacturer's instructions. The DNA was eluted from the silica membrane with 50 µl of pre-warmed H_2O (50 °C) and DNA concentration was determined (2.3.5).

2.3.4.2 Purification of DNA

Plasmid DNA from 1 - 5 ml bacteria cultures was purified using the GeneJET™ Plasmid Miniprep kit (Thermo Fisher Scientific) according to the manufacturer's instruction. Plasmid DNA from 100 - 1000 ml bacteria cultures was purified with the NucleoBond Xtra Midi/Maxi kit (Macherey-Nagel) according to the manufacturer's protocol for high copy plasmid amplification.

DNA fragments of PCR (2.3.1), restriction or dephosphorylation reactions (2.3.2) were purified using the GeneJET™ Gel Extraction kit according to the manufacturer's instructions, to remove disturbing buffer components and enzymes for further applications. After purification, the DNA molecules were reconstituted in an appropriate volume (0.02 - 1 ml) of pre-warmed H_2O (50 °C) and DNA concentration was determined (2.3.5).

2.3.5 Determination of DNA Concentration

For the spectrophotometric determination of the DNA concentrations 1 - 2 µl of DNA aqueous solution was measured at the UV absorbance spectrum between 220 nm and 300 nm using a NanoDrop 1000 device against H_2O as blank. The purity of the DNA solution was determined by the absorbance ratio of 260/280 nm (260 nm = absorbance of purine and pyrimidin bases; 280 nm = absorbance of aromatic amino acids), with a value of approximately 1.8 accounting for pure DNA.

2.3.6 Nucleic Acid Sequencing

Sequencing samples were prepared by mixing 0.5 µg of DNA (100 ng/µl) with 25 pmol of the respective primer in a total volume of 10 µl. Sequencing of DNA fragments or plasmid DNA was performed by the sequencing service of GATC Biotech.

2.3.7 Cloning Strategies

All used oligonucleotides for PCR amplification and generated plasmids are listed with their corresponding numbers (2.1.8.1 and 2.1.8.2). After each cloning step, the DNA was purified according to the protocols in 2.3.4. All constructs were verified by nucleotide sequencing (2.3.6) and corresponding protein sequences are listed in the appendix (6.2).

For the generation of soluble human IgG1-Fc (hIgG1-Fc) fusion proteins, the pFUSE-hIgG1-Fc2 (no.24) expression plasmid system (Invitrogen) was used. The plasmid contains an N-terminal IL-2 secretion signal and a C-terminal hIgG1-Fc tag under the control of the hEF1-HTLV promoter allowing for the long lasting expression of soluble bivalent hIgG1-Fc fusion proteins in mammalian cell lines. In this thesis, the plasmid pFUSE-hIgG1-FcEQ (no. 68, kindly provided by J. Hartmann) was used for transgene expression, containing a modified Fc variant incapable of Fc receptor binding due to the two point mutations L118E/N180Q [377].

2.3.7.1 Generation of soluble MICA Variants for Production in Mammalian Cell Lines

The MICA ligand is a highly polymorphic and glycosylated protein. To ensure high affinity binding of the ligand to the NKG2D receptor, the allelic MICA variants MICA*01 and MICA*04 were generated for the production as soluble MICA (resembling the naturally shed MICA) or full-length proteins in mammalian cell lines.

For the generation of soluble MICA variants, the gene sequence encoding the extracellular domain of MICA*01 or MICA*04 was amplified via PCR (2.3.1) using the plasmids 5701 or 5801 as templates, respectively. For the generation of soluble MICA-His variants, a C-terminal histidine (His) tag followed by a STOP codon as well as the restriction sites *EcoRV* and *BglII* were introduced using the primer pair 350/351. Prior to ligation (2.3.2.3), the PCR products and the plasmid 68 were enzymatically digested with *EcoRV/BglII* (2.3.2.1), following plasmid dephosphorylation (2.3.2.2). The DNA sequences of the newly generated plasmids 8502 and 8504 were verified using the primers 45, 46 and 256.

For the generation of MICA::hIgG1-FcEQ fusion proteins, the sequences of MICA*01 and MICA*04 ectodomains were amplified (2.3.1) using the primer pair 328/351 introducing the restriction sites *EcoRV/BglII* without histidine tag or STOP codon to allow for the fusion of

the MICA ectodomain to the hIgG1-FcEQ part. The PCR products were enzymatically restricted and ligated into the plasmid 68 as described earlier, generating the plasmids 6834 and 6835.

2.3.7.2 Generation of NKG2D::hIgG1-FcEQ Fusion Proteins

The NKG2D receptor is a type II transmembrane protein forming functional active homodimers. To generate functional bivalent human Fc fusion proteins, the NKG2D ectodomain must therefor be fused to the C-terminal region of the hIgG1-Fc part. For this purpose, the STOP codon of the human IgG1-FcEQ gene segment was removed while additional *BamHI/NheI* restriction sites were introduced at the 3' end via PCR amplification (2.3.1) using plasmid 68 as template and the primer pair 409/410. The PCR fragment and the plasmid 24 (pFUSE-hIgG1-Fc2) were enzymatically digested (2.3.2.1) with the enzymes *NcoI* and *NheI*, removing the original hIgG1-Fc2 gene sequence from the plasmid. After dephosphorylation (2.3.2.2) of the linearized plasmid DNA it was enzymatically ligated (2.3.2.3) with the PCR fragment. Positive clones were identified using colony PCR (2.3.1) with the primer combination 45/47 and DNA sequence of the generated pFUSE-hIgG1-FcEQ-ΔSTOP (no. 6837a) was verified (2.3.6).

For the introduction of the human NKG2D ectodomain into the newly generated plasmid 6837a, the gene fragment was amplified (2.3.1) using the plasmid 3601 as template. Additionally, the restriction sites *BamHI* and *NheI* as well as an N-terminal GSSG linker sequence was introduced by the primer pair 411/412. The PCR fragment and plasmid were enzymatically digested (2.3.2.1) with *BamHI/NheI* and after dephosphorylation (2.3.2.2) of the linearized plasmid both DNA molecules were enzymatically ligated (2.3.2.3). The DNA sequence of the generated plasmid 6837 and positive clones were again verified using the primer pair 45/256.

To ensure directed immobilization of the hIgG1-Fc part of NKG2D::hIgG1-FcEQ fusion proteins an additional Avi-tag sequence was introduced at the N-terminal region of the Fc part. Using the Avi-tag technology, the proteins can be biotinylated *in vivo* during protein production. The whole gene sequence of the Avi-hIgG1-FcEQ-NKG2D construct was synthesized by the company GenScript and delivered in the pUC57 plasmid (130). For ligation (2.3.2.3) of the Avi-hIgG1-FcEQ-NKG2D DNA fragment into the pFUSE expression plasmid, the pUC57 plasmid 130 and pFUSE plasmid 24 were enzymatically digested (2.3.2.1) using *EcoRV* and

NheI enzymes, following plasmid dephosphorylation (2.3.2.2) of the pFUSE plasmid prior to ligation. The DNA sequence of the generated plasmid 6846 was verified using primers 45/256.

2.3.7.3 Generation of NKG2D mutant Proteins (MICA Affinity Maturation)

To improve the binding affinity of the NKG2D receptor to its ligand MICA, mutant proteins were generated introducing single mutations in the binding interface of NKG2D. The single amino acid mutations showing higher binding affinities were calculated bioinformatically by A. Metz in the group of H. Gohlke (Computational Pharmaceutical Chemistry and Molecular Bioinformatics, Heinrich-Heine University, Düsseldorf, Germany).

In this thesis eight single amino acid mutations (K150M, K150R, K150W, I182R, I182W, K186M, S117E and S151D) were introduced into the human NKG2D ectodomain for protein production of NKG2D::hIgG1-FcEQ fusion proteins using OE-PCR (2.3.1) with the template pCMV-SPORT6-NKG2D (no. 3601). For the introduction of the single point mutations, two overlapping DNA fragments were amplified using the respective OE-primer 333-348 (introduced mutations depicted in primer name (2.1.8.1)) and the flanking primer 412 (in combination with OE-primers with even numbers for OE-PCR 1) and 411 (in combination with OE-primers with odd numbers for OE-PCR 2). The generated PCR fragments containing the mutation from the respective OE-PCR 1 and 2 reactions were further used as templates for the OE-PCR 3 with the flanking primer pairs 411/412. The PCR products comprising the whole gene sequence and expression plasmids were enzymatically digested (2.3.1.1) with the combination *BamHI/NheI* for ligation into plasmid 6847a. Sequences were analyzed using primers 45/256. The generated plasmids 6838-6845 are listed in 2.1.8.2.

2.4 Methods of Cell Biology

2.4.1 Protein Production in *Escherichia Coli*

E. coli are a well-established expression system for the production of high amounts of pure proteins. In this study, recombinant human NKG2D or rMICA proteins were produced in BL21 (DE3) strains. An aliquot of BL21 (DE3) were transformed (2.2.1.2) with the respective pET plasmid (proteins and corresponding plasmid numbers denoted in table 2.1.9) to generate

an overnight culture in 10 ml of LB medium supplemented with ampicillin. The pre-cultured bacteria were used to inoculate 1 L of LB medium. Bacteria were cultivated at 37 °C and 200 rpm until the culture reached an OD_{600} = 0.6. Next, protein expression was initiated by adding 0.5 mM isopropyl-β-D-1-thiogalactopyranoside (IPTG) to the culture. Bacteria cultures were harvested after 4 h incubation at 37 °C and 200 rpm by centrifugation (6000xg, 10 min, 4 °C). Cell pellets were either stored at -20 °C or directly used for protein purification (2.2.4.2).

2.4.2 Cultivation of Cell Lines

All cell lines were cultivated in the appropriate medium (2.1.6.3) at 37 °C and 5% CO_2 in saturated water atmosphere under sterile conditions in a cell culture incubator. Cells were split on a regular basis every two to three days, depending on cell growth, to maintain optimal growth conditions. Adherent cells were washed in PBS and detached using TrypLE™ Express (Thermo Fisher Scientific) or Accutase (PAA) treatment and an appropriate amount of cells was seeded in a new culture flask and fresh medium. For suspension cultures, cells were counted in a Neubauer counting chamber (Carl Roth), pelleted and resuspended in fresh medium in the appropriate cell density. For cryo-preservation, cells were frozen in FCS containing 10% DMSO at -80 °C and stored in liquid nitrogen or remained at -80 °C. Cells were thawed on a regular basis.

2.4.3 Transfection of Mammalian Cell Lines

2.4.3.1 Transient Transfection

For the transient expression of proteins, mammalian cell lines were chemically transfected using polyethylenimine (PEI) [383, 384]. Therefor, HEK293T/17 cells were seeded at a density of $1x10^7$ cells per flask into T175 culture flask with 20 ml of pre-warmed DMEM compl. medium 24 h prior transfection. Two PEI transfection protocols were used for the generation of soluble proteins or for co-transfection to produce proteins with *in vivo* biotinylation. On day of transfection, the medium was exchanged with 13 ml (for soluble proteins) or 11 ml (for biotinylated proteins) of pre-warmed DMEM/Gln. Next the transfection solutions A and B were prepared (Table 6). Both solutions were mixed for 1 min at maximum speed on a Vortex

Genie 2 (Scientific Industry) and incubated for 10 min at RT. After incubation, both solutions were combined, mixed again for 1 min following incubation for 10 min at RT. Directly before application to the cells, 1 ml of pre-warmed DMEM/Gln medium was added to the transfection mixture. After 4 - 6 h incubation at 37 °C, the transfection medium was exchanged with 25 ml of DMEM/FCS or 25 ml of DMEM/Biotin for *in vivo* biotinylation of proteins and cells were further cultivated.

Table 6: Formulation of transformation solutions for the production of secreted proteins.

Ingredient	soluble (Fc fusion) proteins		biotinylated proteins	
	Solution A	**Solution B**	**Solution A**	**Solution B**
pFUSE	65 µg		7 µg	
pDisplay-BirA-ER			14 µg	
pDisplay-sBirA			14 µg	
TA-trans		65 µl		140 µl
TA-glucose	310 µl	310 µl		
DMEM/Gln			2.3 ml	2.2 ml

2.4.3.2 Electroporation

For the stable integration of full-length MICA*01, UKF-NB3 cells were electroporated using the Neon Transfection System (Thermo Fisher Scientific). Therefor, $1x10^6$ cells were co-transfected with 2.5 µg of pES.1-T6-PGKPuro-MICA01 and 2.5 µg of pES1-2(M2N) (M2, rtTA) in 100 µl of resuspension buffer R (Neon® Kit 100 µl, Thermo Fisher Scientific) and electroporated using protocol 16 (including electroporation parameters: voltage: 1400 V; pulse width: 20, pulse numbers: 2). Directly after electroporation, cells were transferred in 900 µl of pre-warmed UKF-NB3 medium and cultured in T25 flasks coated with fibronectin (5 $\mu g/cm^2$). Two days after electroporation UKF-NB3-indMICA cells were selected by addition of 0.25 mg/ml G418 and 1 µg/ml puromycin (Life Technologies) to the culture medium.

For the generation of C1R cells expressing full-length NKG2D ligands containing an N-terminal hexahistidine tag, $1x10^6$ cells were electroporated with 2 µg of the respective RSV.5neo plasmids (plasmid 9102-9116 even numbers; see table 1.6.8.2) using the Amaxa® Nucleofector® device (program D-023) with Nucleofector Kit V (both Lonza) according to the manufacturer's protocol. Two days after electroporation cells were selected in C1R medium

containing G418. Two weeks after selection, cells were stained with respective anti-NKG2D ligand antibodies and cells were further selected on a FACSAria II cell sorter (BD Bioscience) for high NKG2D ligand expression.

2.4.4 Protein Production in Mammalian Cell Lines

For the production of soluble MICA*01, MICA*04 or the NKG2D- or MICA::hIgG1-Fc fusion protein variants, 20 - 100 T175 culture flasks of HEK293T/17 cells were transfected with the respective pFUSE plasmid (proteins and corresponding plasmid numbers see table 2.1.9) using the PEI method described in 2.4.4.1. For the production of *in vivo* biotinylated NKG2D::hIgG1-FcEQ the pFUSE plasmid no.6846 was used for transfection. Three days after transfection, cell culture supernatants were collected and cell debris was removed by centrifugation (5,000xg, 5 min, 4 °C) following sterile filtration (0.22 µm). Filtered supernatants were supplemented with 0.01% (v/v) sodium azide and protease inhibitor (Roche) and directly used for protein purification (2.5.2.2 for His-tagged MICA*01/04; 2.5.2.3 for hIgG1-Fc fusion proteins).

To generate shedMICA*01 from UKF-NB3-indMICA cells, MICA expression was induced by addition of 2 µg/ml doxycycline (Sigma-Aldrich) to the cell culture medium. Cells were stressed by serum starvation for 72 h to induce MICA shedding. sMICA was purified as described in 2.5.2.2 from cell culture supernatant.

Cell culture supernatants containing shed NKG2D ligands were generated from CAL27 cells or C1R transfectants (2.1.6.2) expressing the NKG2D ligands MICA allelic variants, MICB or ULBP1-3. Therefor, 100 - 300 ml of C1R suspension cultures at a density of 1 - 2x10^6 cells/ml or CAL27 tumor spheroids and confluent monolayer cultures were stressed by serum starvation for 72 h to induce shedding. Cell culture supernatants were collected, centrifuged (5,000xg, 5 min, 4 °C) and sterile filtered (0.22µm). Cell culture supernatants were 10x concentrated using amicon centrifugal filter units with a MWCO of 10 kDa (Merck Millipore) at 4 °C.

2.4.5 Isolation and Expansion of primary human NK cells

Primary human NK cells were isolated from peripheral blood mononuclear cells (PBMCs) by negative selection at high purity and pre-activated and expanded under IL-2 as described previously for clinical applications [385]. Buffy coats, derived from whole blood donations of healthy volunteers were kindly provided by the German Red Cross Blood Service (Institute for Transfusion Medicine and Immunohematology, Goethe-University Frankfurt am Main, Germany). They were used in an anonymized fashion with written donor approval and approval by the Ethics Committee of the Goethe-University Frankfurt (Frankfurt am Main, Germany, permit #329/10). First, PBMCs were isolated via density gradient centrifugation (400xg, 1 h, RT) using Biocoll reagent (Biozol) following subsequent washing steps in PBS/EDTA (300xg, 15 min, RT). NK cells were purified from $2x10^8$ PBMCs via indirect magnetic immunoselection using the human NK Cell Isolation Kit (Miltenyi Biotec) according to the manufacturer's protocol. NK cells were cultured in pNK medium at a cell density of 1 - $2x10^6$ cells/ml for up to 10 days. For pNK cell activation and expansion the NK Cell Activation and Expansion Kit (Miltenyi Biotec) was used. For maintenance of optimal growth and activation conditions, cell density was adjusted every two days by adding medium with 1000 IU/ml IL-2. At day 7 of culture, cells were used for cytotoxicity assays (2.4.8).

2.4.6 Tumor Spheroid Formation

Multicellular tumor spheroids were generated from the HNSCC cell lines FaDu, CAL27 and Detroit562 or the cervical carcinoma cell line SiHa. Cells were washed with PBS dissociated from cell culture flasks by TrypLE™ Express (Life Technologies) and cell number was determined. For fluorescent labeling, $1x10^6$ cells were stained with Cell Trace CFSE Proliferation kit (Life Technologies) according to the manufacturer's protocol. Afterwards, $5x10^3$ cells/well were seeded in a volume of 150µl/well respective culture medium in 96-well plates coated with 1.5% agarose in basal MEM or DMEM medium, respectively. Solid tumor spheroids formed within approximately 24 - 48 h after initial seeding (d0) and were used in functional assays. Growth was monitored by transmission and fluorescence microscopy. For tumor spheroid growth curves, phase contrast pictures of independent solid spheroids were analyzed by ImageJ software [386].

2.4.7 Flow Cytometry

For detection of NKG2D ligands, 1 - 5x10^5 cells of single-cell suspensions or TrypLE™ Express-treated (Life Technologies) tumor spheroids were stained with mouse monoclonal antibodies (2.1.3: AMO1, MAB1599, MAB1380, MAB1298, MAB1517; at 0.25 µg/10^6 cells in FACS-buffer) or NKG2D proteins (2.4.5: 50 µg/ml in FACS-buffer) for 45 min at 4 °C, washed three times in FACS-buffer (centrifugation 300xg, 3 min, 4 °C) and probed with respective fluorochrome-conjugated secondary antibodies (2.1.3) for 30 min at 4 °C under light protection. For the detection of primary human NK cells 1x10^4 - 5x10^5 NK cells were stained with anti-human CD45-APC and/or anti-human NKGD-PE antibodies (both Miltenyi Biotec) in FACS-buffer for 30 min at 4 °C. Viability of cells was determined by SytoxBlue (Life Technologies) stain according to the manufacturer's protocol. As negative control, samples incubated with secondary antibodies only or respective isotype controls were used. Cells were resuspended in FACS-buffer and measured on a FACS Canto II instrument (BD Bioscience) equipped with a 96-well plate high throughput sampler (HTS) and analyzed with FlowJo software. 10.000 events of viable cells were analyzed of individual experiments to calculate the median fluorescence intensity (MFI) over background.

For infiltration studies (2.4.8.3), primary human NK cells were stained with anti-human CD56 and anti-human CD16 on day 7 of cultivation and 1x10^7 cells were sorted according to the expression levels for the $CD56^{bright}/CD16^{dim/-}$ or $CD56^{dim}/CD16^{+}$ population on a FACSAria II cell sorter (BD Bioscience).

For the staining of rhesus macaque PBMCs, 100 µl of whole blood samples were incubated with an antibody cocktail (2.1.3: anti-human CD3-PE, anti-human CD14-PerCp Cy5.5, anti-human CD20-FITC, anti-human NKG2D-APC) in PBS for 30 min at RT under light protection. Afterwards, erythrocytes were lysed using ACK Lysis Buffer (Thermo Fisher Scientific) according to the manufacturer's instructions for 30 - 60 min at RT. Cells were washed three times in PBS (centrifugation 400xg, 4 min, 4 °C), resuspended in FACS fix and measured on a FACS Canto II or LSRII instrument (BD Bioscience). Cells were analyzed with FlowJo software of 50.000 events to calculate MFI over background.

Cryo-preserved PBMCs of healthy volunteers or HNSCC patients and corresponding disintegrated primary tumor samples were stained with an antibody cocktail (2.1.3: anti-human CD3-APC-Cy7, anti-human CD4-PacificBlue, anti-human CD8a-AlexaFluor700, anti-human

CD16-FITC, anti-human CD56-PE-Cy7, anti-human CD45-Pe-Flour610 and anti-human NKG2D-PE). For cell viability Aqua Dead Cells stain (Thermo Fisher Scientific) was used. Cellular events were measured on a Gallios cytometer and analyzed using Kaluza software (both Beckmann Coulter). Percentage of NK cell subsets and MFI ratios for NKG2D expression were calculated from $CD45^+$ lymphocyte fraction. The analyses were kindly performed by A. Lechner (Department of Otorhinolaryngology, Head and Neck Surgery, University Cologne, Medical Faculty, Cologne, Germany).

2.4.8 Cytotoxicity Assay

2.4.8.1 Cytotoxicity Assay of Single Cell Suspension

For monolayer cell cytotoxicity assays, FaDu, CAL27, Detroit562 or SiHa cells were washed with PBS, dissociated from cell culture flasks using TrypLE™ Express (Life Technologies), and $1x10^6$ cells were fluorescently labeled with CFSE (Life Technologies) according to the manufacturer's instructions. After staining, 10,000 target cells were co-cultured overnight (FaDu, CAL27 and Detroit562 cells) or for 2 h (SiHa cells) at 37 °C with primary human NK cells at appropriate effector-to-target (E:T) ratios in NK cell medium without IL-2.

For blocking experiments, primary human NK cells were pre-incubated for 30 min with anti-human NKG2D antibodies (MAB139). For NK cell inhibition experiments, primary human NK cells were pre-incubated overnight with plasma of HNSCC patients or healthy donors before and after depletion of sNKG2D ligands prior to co-culturing with SiHa target cells for 2 h. At the endpoint of the cytotoxicity assay, NK cells were labeled with anti-human CD45-APC antibody (clone 5B1). Live/dead cell discrimination was achieved by staining with SytoxBlue (Life Technologies). 10,000 events of target cells were analyzed on a FACS Canto II instrument (BD Bioscience) equipped with a 96-well plate HTS. The percentage of target cell lysis was calculated by gating on target cells ($CFSE^+$) and analysis of $SytoxBlue^+$ and $SytoxBlue^-$ cells.

2.4.8.2 Cytotoxicity Assay of Tumor Spheroids

Cytotoxicity experiments in tumor spheroids were performed, as previously described [387]. After tumor spheroid formation (2.4.6), FaDu, CAL27, Detroit562 and SiHa tumor spheroids

at solid spheroidal state (d0) were co-cultured with primary human NK cells at appropriate E:T ratios in NK cell medium without IL-2. For NK cell inhibition experiments, primary human NK cells were pre-incubated overnight with 10x concentrated non- and sNKG2D ligand-depleted CAL27 culture supernatant (2.4.5). Cytotoxicity and spheroid destruction was measured after 24 - 48 h of single tumor spheroids dissociated with TrypLE^{TM} Express (Life Technologies). NK cells in these single-cell suspensions were labeled with anti-human CD45-APC antibody. Live/dead cell discrimination was achieved by staining with SytoxBlue (Life Technologies). The percentage of viable cells was calculated with FlowJo software by evaluation of the gates for NK cells ($CD45^+$/$SytoxBlue^-$) and target cells ($CFSE^+$/$SytoxBlue^-$) from complete samples measured on a FACS Canto II instrument (BD Bioscience) equipped with a 96-well plate HTS.

2.4.8.3 Tumor Spheroid Infiltration and MACS-based NK cell Isolation

For infiltration studies under inhibitory conditions, NK cells were pre-treated overnight with CAL27 supernatant or shed MICA*01 (2.4.4) and seeded with HNSCC or SiHa cells at an E:T ratio of 1:1 into 96-well plates coated with 1.5% agarose in medium. For infiltration studies of NK cell sub-populations, FaDu tumor spheroids were co-cultured with pre-sorted (2.4.7) primary human NK cells ($CD56^{bright}$/$CD16^{dim/-}$ or $CD56^{dim}$/$CD16^+$ populations) at an E:T ratio of 1:1. Tumor spheroid formation was monitored for 48 h by light microscopy. Cryosections were stained for cleaved caspase 3 and/or for human CD45 by standard histology techniques (2.5.11). The number of infiltrated NK cells was calculated by counting $CD45^+$ NK cells of cryosections from single tumor spheroids and by calculating the percentage of NK cells from whole cell numbers using ImageJ software.

Isolation of tumor spheroid infiltrated NK cells was performed after the previously published protocol [387]. In brief, tumor spheroids of CFSE-labeled SiHa cells were co-cultured with primary human NK cells at an E:T ratio of 3:1 for 24 h. Tumor spheroids were harvested with a cut 1000 µl-tip, pooled, and separated from the supernatant containing peripheral NK cells by mild centrifugation at 300xg for 10 s. Following two washing steps in 50 ml of FACS buffer, tumor spheroids were dissociated by TrypLE^{TM} Express-treatment for 5 min. The single cell suspension was washed again and subjected to CD45 MACS-bead isolation according to the manufacturer's instructions. Cells from the periphery, MACS flow through and elution

fractions were analyzed by flow cytometry. Tumor spheroids without NK cells served as controls and were treated with the same procedure. NK cells were labeled with anti-human CD45-APC antibody prior to addition of counting beads to calculate cell numbers according to the manufacturer's instructions. Cell suspensions were analyzed for viable target cells and NK cells as described in 2.4.8.2.

2.5 Methods of Protein Biochemistry

2.5.1 Determination of Protein Concentration

Protein concentrations were determined using UV absorbance-based quantification at 280 nm or fluorometric quantification, depending on the protein characteristics and buffer composition (i.e. pH, ionic strength and additives). For spectrophotometric quantification, 2 µl of protein solution were measured at 280 nm on a NanoDrop ND1000 (PeqLab Biotechnology) using the corresponding buffer solution as blank. For fluorometric quantification, the Qubit Protein Assay Kit (Thermo Fisher Scientific) was used according to the manufacture's instructions and protein concentration was determined on a corresponding Qubit® Fluorometer (Thermo Fisher Scientific).

2.5.2 Protein Purification from Inclusion Bodies or Cell Culture Supernatants

2.5.2.1 IMAC and Refolding of Proteins produced in E. coli

Proteins produced in *E. coli* (2.4.1) containing either an N- or C-terminal histidine tag were purified via immobilized metal ion affinity chromatography (IMAC) under denaturating conditions. Therefor, bacterial cell pellets were thawed on ice and resuspended in 50 ml of resuspension buffer. To isolate inclusion bodies, cells were sonified on ice (duty cycle 90%, output control 5, pulse 5x 1 min, 30 s pause) and centrifuged (9000xg, 20 min, 4 °C). The pellet, containing the inclusion bodies was resuspended in 100 ml of solubilization buffer and incubated for 1 h at 50 °C while shaking and insoluble fragments were removed by centrifugation (9000xg, 20 min, RT). For IMAC purification, the protein solution was supplemented with 5 mM imidazole and incubated with wash buffer equilibrated Ni-NTA agarose (Macherey-Nagel) for 1 h at RT on a roller shaker. After incubation, the Ni-NTA slurry was subjected

onto an Econo-Pac gravity flow column (Bio-Rad) including a bed support frit (30 µm polyethylene), washed with 5 column volumes (CV) of wash buffer and bound proteins were eluted with 150 ml of elution buffer. Afterwards, the Ni-NTA agarose was regenerated with 5 CV of regeneration buffer and 2 CV of Ni^{2+}-solution. The agarose was stored in 20% ethanol at 4 °C until re-use.

To initiate refolding of the purified proteins, the solution was incubated with 0.5 mM oxidized glutathione (GSSG) and 5 mM reduced glutathione (GSH) overnight at 4 °C under rotation. For refolding using dialysis steps against buffers containing descending urea concentrations, the protein solution was filled in dialysis membranes with a molecular weight cut-off of 3 - 4 kDa (Carl Roth) and dialyzed against a 1:100 volume of dialysis buffer I - V. Buffers were exchanged every 24 h. In the last step, dialysis buffer V was exchanged through 2 steps of dialysis for 12 h in TBS. Refolded proteins were collected and precipitates containing unfolded and aggregated proteins were removed via centrifugation (18000xg, 30 min at 4 °C). Protein concentration was measured as described (2.5.1). Protein concentration was adjusted to 1 mg/ml by centrifugal concentration steps (5000xg, at 4 °C) using amicon centrifugal filter units (Merck Millipore) with MWCO of 10 kDa.

The refolded rNKG2D protein containing an Avi-tag was *in vitro* biotinylated. The protein was diluted in biotin assay buffer to a final protein concentration of 40 - 100 µM, incubated for 16 h at 27 °C and centrifuged for 5 min at 3200xg and 4 °C. For further purification and removal of excess biotin, proteins were subjected to size exclusion chromatography (2.5.3).

2.5.2.2 IMAC of Protein Produced in Mammalian Cell Lines

Soluble or shed proteins containing an N- or C-terminal histidine tag (2.4.5) were purified from mammalian cell culture supernatants using IMAC under native conditions. To ensure integrity of the proteins, all steps were carried out at 4 °C with ice-cold buffers. Cell culture supernatants were dialyzed for 24 h in dialysis buffer A to remove disturbing medium additives. Afterwards, the protein solution was supplemented with 5 mM imidazole and Ni-NTA agarose and incubated for 1 h at 4 °C. The Ni-NTA slurry was subjected to an Econo-Pac gravity flow column (Bio-Rad) including a bed support frit (30 µm polyethylene), washed with 5 CV of wash buffer and bound proteins were eluted in elution buffer. Finally, the elution buffer was exchanged to TBS or PBS during protein concentration using amicon centrifugal

filter units (Merck Millipore) with a molecular weight cut off (MWCO) of 10 kDa (5000xg, steps of 10 min, 4 °C). Protein concentration was determined as described in 2.5.1 and proteins were used for flow cytometry and ELISA measurements. For the use of sMICA*04 in the *in vivo* apheresis study (2.6.2), the protein was further subjected to size exclusion chromatography (2.5.3) and tested for endotoxin levels with the Pierce™ LAL Chromogenic Endotoxin Quantification Kit and ToxinSensor™ Chromogenic LAL Endotoxin Assay Kit according to the manufacturer's protocols. Additionally, viral contents were excluded using the INNOTEST® HIV Antigen mAb ELISA according to the manufacturer's instructions.

2.5.2.3 Protein A Purification

All human IgG1-Fc fusion proteins produced in HEK293T/17 cells (2.4.5) were purified from cell culture supernatants via rec-Protein A-Sepharose® 4B Conjugate (Thermo Fisher Scientific). Protein A binds with high affinity to the constant human IgG1-Fc-part. All steps were performed at 4 °C with ice-cold buffers. In brief, cell culture supernatants were supplemented with 20 µl of sepharose slurry per 25 ml of supernatant and incubated for 2 - 4 h at 4 °C on a tilt/roller mixer. After collecting the sepharose matrix in an Econo-Pac gravity flow column (Bio-Rad) including a bed support frit (30 µm polyethylene), the matrix was washed with 10 CV of PBS. Bound proteins were eluted from the matrix using 10 ml of elution buffer II. Eluates were collected in conical tubes containing 1 ml (1:10 of elution volume) of collection buffer for pH neutralization. Protein A-sepharose was regenerated using regeneration buffer and stored in PBS containing 0.01% azide at 4 °C. Directly after purification, the buffer was exchanged to PBS using amicon centrifugal filter units (Merck Millipore) with a MWCO of 50 kDa and subsequent centrifugation steps (5000xg, 10 min, 4 °C) following determination of protein concentration (2.5.1).

2.5.3 Size Exclusion Chromatography (SEC)

Size exclusion chromatography was used for further purification of proteins [388]. In this thesis, a HiLoad 16/600 Superdex® 200 pg or Superdex® 200 10/300 GL column (fractionation range: $1x10^4$ - $6x10^5$ kDa) was used for protein fractionation on an Äkta Prime FPLC System (all GE Healthcare). For separation of hIgG1-Fc fusion proteins and sMICA from mammalian cells SEC was performed in PBS, for proteins produced in *E. coli* TBS was used.

All buffers were prepared at 4 °C and sterile filtered (filter size 0.22 µm). The columns were washed and equilibrated with 1.5 CV of deionized water and TBS or PBS, respectively. The protein samples were injected into an appropriate sample loop and chromatography was performed with flow rates of 0.3 or 0.5 ml/min. Elution fractions of 1 ml were collected and retention volume (V_r), molecular weight and void volume (V_0) determinations form recorded UV absorption spectrum at 280 nm were carried out according to the manufacturer's instructions using the Gel Filtration LMW Calibration Kit (GE Healthcare) as standard. For long-term storage, the columns were washed with 1.5 CV of deionized water and stored in 20% (v/v) EtOH at 4 °C.

2.5.4 Circular Dichroism (CD) Spectroscopy

Circular dichroism (CD) spectroscopy is a quick method for analysis of secondary structure and protein folding properties based on the differential absorption of circularly polarized light by optically active molecules according to the Beer's law [389]. The change in polarization is expressed as degrees of ellipticity θ. Secondary structure motives show characteristic ellipticity patterns. Predominant α-helical proteins have minima of ellipticity at 222 nm and 207 nm and a maximum at 192 nm. In contrast, proteins with antiparallel β-sheets have a minimum at 215 - 220 nm and a maximum at 195 nm. Disordered proteins have very low ellipticity above 210 nm and negative values near 195 nm. For the CD measurement, refolded rNKG2D-His protein was re-buffered in 20 mM sodium phosphate buffer (pH 8) using amicon centrifugal filter units with a MWCO of 10 kDA, filtered through a 22 µM filter (Merck Millipore) and 10 µl of protein solution (2 mg/ml) were mounted into a CaF_2 cuvette with a path length of 50 µm. The far-UV spectra of 10 scans were collected from 180 to 250 nm on a J-720 spectrometer (Jasco) with a resolution of 0.1 nm. The sample holder was temperature controlled by an external water bath, allowing analyzing protein stability with time at different temperatures. The experiments were kindly performed in the group of W. Mäntele (Institute of Biophysics, Goethe-University, Frankfurt am Main, Germany).

2.5.5 Immunoprecipitation and *ex vivo* Depletion of sMICA

2.5.5.1 Depletion of sNKG2D Ligands using monoclonal Antibodies

To test the depletion efficacy of monoclonal mouse anti-MICA antibodies (AMO1, BAMO3) with different epitopes, 1 µg of the respective antibodies in IP buffer was coupled to 20 µl/sample Protein A/G PLUS-Agarose beads (Santa Cruz) for 2 h at 4 °C and 5 rpm. After three washing steps with PBS-T and subsequent centrifugation (1,000xg, 5 min, 4 °C) the antibody-coupled beads were incubated overnight at 4 °C with 5 rpm rotation in either cell culture supernatants containing sMICA variants or human plasma supplemented with sMICA*01/sMICA*04 proteins. Beads were removed from supernatants by centrifugation (1,000xg, 7 min, 4 °C). Levels of sMICA in non-depleted and depleted supernatants were measured by Sandwich ELISA (2.5.9.1).

In order to deplete sNKG2D ligands from plasma of HNSCC patients, healthy donors or cell culture supernatants, Protein A Dynabeads (20 µg/sample; Thermo Scinetific) were pre-coated with 3 µg of the respective antibodies (anti-human MICB (MAB1599), anti-human ULBP1 (MAB1380), anti-human ULBP2 (MAB1298) or anti-human ULBP3 (MAB1517)) in IP buffer for 2 h at 4 °C with 5 rpm. Beads were removed and washed three times in PBS-T. Coated Dynabeads were resuspended in 20 µl of PBS. Depletion of sMICA was performed using anti-human MICA (AMO1) covalently coupled to magnetic MACSxpress beads (3 µg AMO1 per 20 µl beads; especially produced for this project by Miltenyi Biotec). The respective antibody coated beads were mixed in equal amounts, transferred to the samples and incubated overnight at 4 °C with 5 rpm. Magnetic beads containing bound ligands were removed from plasma samples by magnetic separation on a MACSxpress Seperator (Miltenyi Biotec). Residual beads were washed three times with 1 ml of PBS-T and bound ligands were eluted either with elution buffer I for subsequent immunoblot analysis (2.5.7) of ligands or in elution buffer II for ELISA measurements (2.5.9.1). For further use of depleted cell culture supernatants or plasma in cytotoxicity assays (2.4.8), a final centrifugation step (1000xg, 10 min, 4 °C) was applied to ensure the complete removal of magnetic beads. The levels of NKG2D ligands in depleted and non-depleted samples were analyzed by Sandwich ELISA (2.5.9.1).

2.5.5.2 Depletion of sNKG2D Ligands using NKG2D Proteins

In a second approach, the depletion capacity of the pan-specific human NKG2D proteins was tested. Therefor, 10 µg of biotinylated NKG2D produced in *E. coli* (2.4.1) or NKG2D::hIgG1-Fc-Biotin (2.4.5) were coupled to 20 µl Dynabeads M-280 Streptavidin (Thermo Fisher Scientific) or rNKG2D-His to anti-His Dynabeads, respectively, for 2 h at 4 °C and 5 rpm. For the simultaneous depletion of different NKG2D ligands, human plasma samples supplemented with recombinant NKG2D ligands (soluble His-tagged or hIgG1-Fc fusion proteins), patients' plasma or cell culture supernatants were used. Immunoprecipitation was performed as described earlier (2.5.4.1) and samples were analyzed accordingly.

2.5.5.3 Ex vivo Depletion of sMICA under Apheresis-like Conditions

For the *in vitro* depletion of sNKG2D ligands under apheresis-like conditions, an adsorber cartridge containing the anti-MICA antibody functionalized sepharose matrix was generated. The anti-MICA antibody (AMO1) was covalently coupled to sepharose Cl-4B at 0.95 mg AMO1/g sepharose (Miltenyi Biotec). To test the depletion efficacy, 200 ml of human plasma (kindly provided by the German Red Cross Blood Service Frankfurt am Main, Germany) was supplemented with 100 µg of sMICA*04 (500 ng/ml). The plasma reservoir and the adsorber cartridge were connected to an Äkta Prime System (GE Healthcare) and the plasma volume was exchanged six times through the cartridge with a flow rate of 25 ml/min. The plasma levels of sMICA, before and after each plasma volume exchange, were analyzed by Sandwich ELISA (2.5.9.1). After PBS wash, bound sMICA was eluted from the sepharose matrix with elution buffer II and the regenerated cartridge was stored in PBS supplemented with 15% EtOH and 0.01% azide at 4 °C.

2.5.6 Sodium Dodecyl Sulfate-Polyacrylamide Gel Electrophoresis (SDS-PAGE)

To separate proteins with a molecular mass of 5 to 250 kDa discontinuous SDS-PAGE was used at reducing or non-reducing conditions [390]. Protein samples (i.e. IP eluates, 2 µg of purified proteins or cell culture supernatants) were mixed with an appropriate amount of either reducing or non-reducing 5x SDS sample buffer to a final concentration of 1x SDS sam-

ple buffer. For analysis of samples at reducing conditions, SDS sample buffers were further supplemented with 300 mM DTT and samples were heated for 5 min at 95 °C and centrifuged to remove precipitates (20,000xg, 5 min). Polyacrylamide gels were prepared as depicted in Table 7 and 20 - 30 µl samples were loaded into the gel together with a PageRuler Protein Ladder (Thermo Fisher Scientific) as size standard. The electrophoresis was performed at 200 V for 45 - 60 min (depending on pore size) in a Mini-PROTEAN II electrophoresis cell (BioRad) filled with SDS running buffer.

For visualization of separated proteins, polyacrylamide gels were stained with InstantBlue protein staining solution (Expedeon) for 1 h according to the manufacturer's protocol. For the specific detection of proteins, polyacrylamide gels were further used for immunoblotting (2.5.7).

Table 7: Polyacrylamide gel composition.
The formulation is for the preparation of 2 polyacrylamide gels (100 x 100 x 1 mm).

Ingredients		Resolving Gel		Stacking Gel
		12%	10%	5%
30%	acrylamide	4.0 ml	3.3 ml	1 ml
	H_2O	3.3 ml	4.0 ml	4.0 ml
1.5 M	Tris pH 8.8	2.5 ml	2.5 ml	--
1.5 M	Tris pH 6.8	--	--	0.75 ml
20%	SDS	50 µl	50 µl	30 µl
10%	ammonium persulfate (APS)	100 µl	100 µl	60 µl
	TEMED	4 µl	4 µl	6 µl

2.5.7 Immunoblotting

For immunodetection, separated proteins were transferred from SDS polyacrylamide gels onto a nitrocellulose membrane using a Trans-Blot SD Semi-Dry transfer cell (BioRad) according to the manufacturer's instructions [391]. A stack consisting of transfer buffer pre-soaked blotting paper, nitrocellulose membrane, polyacrylamide gel and blotting paper were prepared on the transfer cell and blotted for 15 min at 15 V. After blotting, the membrane was incubated in blocking buffer for 30 min at RT following incubation with the appropriate primary antibody diluted in blocking buffer for 2 h at RT or overnight at 4 °C. Membranes were washed three times in TBS-T for 5 min at RT. For the specific detection of unconjugated primary antibod-

ies, membranes were further incubated with the appropriate horseradish peroxidase (HRP) conjugated secondary antibodies for 2 - 4 h at RT. Membranes were washed again three times in TBS-T prior to incubation with Novex ECL HRP-Chemiluminescent detection kit after the manufacturer's protocol. Chemiluminescence signals were detected using Super RX medical x-ray film 100NIC (Fuji Film Europe GmbH) on a XR 24 NDT Automatic x-ray Film Processor (Dürr NDT) or using the Fusion FX7 system (Peqlab).

2.5.8 Peptide Spot Array

In this study, peptide arrays were used for antibody epitope mapping of the monoclonal anti-MICA antibodies AMO1 and BAMO3. Therefor, the human MICA sequence (UniProtKB ref. no. Q29983; aa23 - aa308; spots: 18 amino acids with off-set by four amino acid) was synthesized on cellulose membranes using Fmoc chemistry at activated PEG spacers by automated parallel peptide synthesis on a MultiPep RS instrument (Intavis) [392, 393]. For epitope mapping, synthesized membranes were placed in pure ethanol and then rehydrated by stepwise substitution with deionized water. Membranes were washed three times in TBS-T for 5 min and subsequently incubated for 1 h at RT in spot blocking buffer. Afterwards, antibody incubation (antibodies and dilutions Table 8) and ECL detection were performed as described for immunoblotting (2.5.7).

Membranes were regenerated by three washing steps of 10 min in regeneration buffer A, following three washing steps for 10 min in regeneration buffer B and a final flush in pure ethanol. After complete drying, the membranes were stored at -20 °C and reused after rehydration.

Table 8: Antibodies and dilutions for Peptide Spot Arrays.
All antibodies were diluted in spot buffer.

Antibody	concentration/dilution
anti-MICA (AMO1)	5 µg/ml
anti-MICA/B (BAMO3)	5 µg/ml
anti-mouse IgG, HRP conjugated (for detection)	1:20,000

2.5.9 Enzyme Linked Immunosorbent Assay (ELISA)

2.5.9.1 Sandwich ELISA for Detection of individual sNKG2D Ligands

To analyze the levels of sNKG2D ligands in the plasma of HNSCC patients and healthy donors, samples were diluted 1:2 for analysis and measured in duplicates. To analyze shedding of NKG2D ligands, supernatants of 96 solid tumor spheroids or monolayer cultures were collected at different time points within 72 h (d0, d1, d2) and concentrated 10-fold using amicon centrifugal filter units with a molecular weight cut-off of 10 kDa (Merck Millipore).

Soluble MICA was analyzed as described [296] with slight modifications. Soluble MICB, ULBP1, ULBP2 and ULBP3 were detected with a similar protocol [256, 298, 394]. All antibody combinations and protein standards for the detection of the respective NKG2D ligands are listed in Table 9. Briefly, 96 well MICROLON600 plates (Greiner Bio-One) were coated with 100 µl/well of the respective capture antibody diluted in PBS overnight at 4 °C. After saturation with 200 µl/well of BSA blocking solution (Candor) for 1 h at RT, the plates were washed three times with 200 µl/well of PBS-T. For sampling, 100 µl/well of the respective plasma diluted 1:2 in 1% BSA-PBS or cell culture supernatants and standard proteins were incubated for 2 h at 37 °C following three washing steps with PBS-T. For detection and quantification of soluble ligands, 100 µl/well of sandwich antibodies were incubated for additional 2 h at 37 °C following subsequent washing steps and incubation with 100 µl/well of respective detection antibodies for 1 h at 37 °C. After plate washing, visualization was performed with 100 µl/well of TMB substrate (KPL) and 50 µl/well of 1 N H_2SO_4 and signals were measured in a microtiter plate reader (Anthos) at $\lambda = 450$ nm (reference filter 650 nm) and analyzed with Prism 6 software (GraphPad). Data for tumor spheroids or monolayer cultures were calculated as mean ± SEM per 10.000 cells (per spheroid) of three independent experiments (n = 3), measured in duplicates. Data for plasma levels were calculated as mean ± SEM of duplicates.

Table 9: **Antibodies and standard proteins for respective NKG2D ligand ELISA.**
Standard 1:2 dilution series (8 dilutions starting at 20 ng/ml) were used. All Fc fusion proteins were purchased from R&D Systems, sMICA*04 was produced as described in 2.4.5. Capture antibodies were diluted in PBS, all other reagents in 1% BSA-PBS.

NKG2D ligand	standard protein	capture antibody	sandwich antibody	detection antibody
MICA	sMICA*04	AMO1 [5 µg/ml]	BAMO3 [1 µg/ml]	anti-mouse IgG_{2a}-HRP 1:10,000
MICB	MICB-Fc	BAMO1 [2 µg/ml]	BMO2 [1 µg/ml]	
ULBP1	ULBP1-Fc	AUMO5 [2 µg/ml]	AUMO2 [4 µg/ml]	
ULBP2	ULBP2-Fc	BUMO1 [2 µg/ml]	MAB1298 [1 µg/ml]	anti-mouse IgG_1-HRP 1:10,000
ULBP3	ULBP3-Fc	AF1517 [2 µg/ml]	CUMO3 [2 µg/ml]	

2.5.9.2 Determination of Binding Affinities for NKG2D Proteins

Binding affinities of NKG2D proteins to the individual NKG2D ligands were determined by ELISA. Therefor, 96 well MICROCOLON600 plates (Greiner Bio-One) were coated over-night at 4 °C with sMICA*01/04, MICA*01/04::hIgG1-Fc (2.4.4) or the hIgG1-Fc fusion proteins of MICB and ULBP1-3 (R&D Systems) at 10 µg/ml in PBS with 100 µl/well. The plates were blocked with 200 µl/well of BSA Blocking Solution (Candor) for 1 h at RT and washed three times with 200 µl/well of PBS-T. Plates were incubated for 1 h at RT with serial dilutions strating from 2 nM of either rNKG2D-His, rNKG2D-Biotin or NKG2D::hIgG1-FcEQ proteins in PBS. After three washing steps with 200 µl/well of PBS-T, NKG2D proteins were detected using anti-His-HRP, Streptavidin-HRP or anti-humanIgG-Fc-HRP, respectively, for 1 h at RT. Plates were washed again three times and incubated with 100 µl/well of TMB substrate (KPL) followed by 50 µl/well of 1 N H_2SO_4. Signals were measured at 450 nm with a microtiterplate reader. Data were represented as mean ± SEM of duplicates.

2.5.9.3 Detection of Rhesus Monkey anti-MICA IgG and IgM Antibodies

For the analysis of anti-MICA rhesus macaque IgG/IgM antibodies MICROCOLON600 plates (Greiner Bio-One) were coated with 10 µg/ml of sMICA*04 in PBS overnight and blocked for 1 h at RT with 200 µl/well of BSA blocking solution (Candor). After three washing steps with 200 µl/well of PBS-T, plates were incubated with rhesus macaque plasma (prior and three weeks after sMICA*04 injection) in different dilutions (1:2; 1:10; 1:50; 1:100; 1:500; 1:1000 in PBS). After three washing steps with PBS-T, bound antibodies were detected with either anti-monkey-IgG or anti-monkey-IgM HRP-conjugated antibodies for 1 h at RT. Plates were washed again three times and incubated with 100 µl/well of TMB substrate (KPL) followed by 50 µl/well of 1 N H_2SO_4. Signals were measured at 450 nm with a microtiter plate reader. Data were represented as mean ± SEM of duplicates.

2.5.10 Cytometric Bead Array (CBA)

The cytometric bead array (CBA) is a highly sensitive flow cytometry-based assay to quantify various soluble factors in low amounts of human plasma or culture supernatants. The concentrations of IFNγ, TNFα, IL-1, IL-6, IL-8, IL-10, MCP-1, RANTES, MIP-1α, MIP-1β and TGF-β1 in plasma of HNSCC patients and healthy donors were determined using the BD™ CBA Flex Set System (BD Bioscience). Each BD™ CBA Flex Set contained a one-bead population with distinct fluorescence intensity and the appropriate phycoerythrin (PE) detection reagent and standard. The tests were performed according to the manufacturer's instructions and samples were diluted 1:30 for TGF-β1 Flex set or 1:4 for all other Flex sets and measured in duplicates. Samples were measured with the BD FACS Array™ (BD Bioscience) and analyzed with FCAP Array Software (BD Bioscience). Cytokine levels of HNSCC patient samples were normalized to healthy controls and data are represented as x-times median control. CBA measurements were kindly performed by P. Schön in the group of R. Schubert (Division of Allergology, Pneumology and Cystic Fibrosis, Department of Children and Adolscents, University Hospital Frankfurt, Goethe-University, Frankfurt am Main, Germany).

2.5.11 Immunohistochemistry

Individual spheroids (n > 8) were collected and embedded into OCT compound (Sakura). Cryosections (7 µm) of solid tumor spheroids were analyzed by standard two-step polymer methods with Envision kits (DAKO). 3,3'-Diaminobenzidine (DAB) and Permanent Red or 3-Amino-9-Ethylcarbazol (AEC) were used as chromogen. Tumor spheroid cryosections were stained with anti-human cleaved caspase 3 and anti-human CD45 diluted in Ab-Diluent (Dako). For counterstaining, Mayer's Hematoxylin (Lillie's Modification) (DAKO) was used according to the manufacturer's instructions. Immunohistological stainings were kindly performed by A. Giannattasio in the lab of J. Koch (Georg-Speyer-Haus, Frankfurt am Main, Germany).

Paraffin-embedded primary tumor tissues were stained with anti-human CD3 (1:50 in citrate buffer pH 6), anti-human CD8 (1:200 in citrate buffer pH 6), anti-human CD20 (1:250 in citrate buffer pH 6) and anti-human CD56 (1:500 in citrate buffer pH 6) antibodies (2.1.3) for the lymphocyte markers as well as anti-human CD68 (1:400 in 1 mM EDTA pH 8) and anti-human CD163 (1:100 in 1 mM EDTA pH 8) antibodies for the macrophage markers using the BOND-MAX automated IHC-stainer (Leica Biosystems) according to the manufacturer's instructions. For evaluation of the HPV status, tumor tissues were stained with anti-human p16 antibodies (CINtec® p16 Histology kit) and HPV type 16-DNA was detected via PCR. Immunohistochemical stainings were kindly performed in the group of A. Quaas (Institute of Pathology, University of Cologne, Cologne, Germany).

2.6 *In vivo* Experiments and primary human Samples

2.6.1 HNSCC Patients and healthy Volunteer Samples

Plasma samples from 39 male and 5 female HNSCC patients (Department of Otorhinolaryngology, Head and Neck Surgery, University of Cologne, Medical Faculty, Cologne, Germany) were analyzed (2.5.9.1) and used for experiments in this thesis. Patients' age ranged from 39 to 88 years with most patients in their 60 - 80s. HNSCC patient demographics and tumor characteristics are summarized in Table 10. Tumor staging was assigned according to the TNM classification of the International Union Against Cancer. A random patient cohort was included in this study with treatment naïve patients at initial diagnosis, recurrent disease and

patients under palliative treatment at time of sample collection. Sample collection of HNSCC patients (blood samples and paraffin sections of primary tumors) was in accordance and approved by the Ethics Committee of the University Clinic Cologne (Immuncan study 11-116, 2011). Plasma samples of 12 age-matched healthy volunteers (mean age: 55 years) were used with informed consent.

2.6.2 Adsorption Apheresis in an *in vivo* Rhesus Macaque Model

Three male rhesus macaque animals (age 6 years) from the German Primate Center breeding colony (German Primate Center, Göttingen) were used for the *in vivo* experiments with the approval by the *Niedersächsisches Landesamt für Verbraucherschutz und Lebensmittelsicherheit* (33.19-42502-04-14/1715). All experimental and medical procedures were done under narcosis initiated with ketamine, (Dex-) medetomidine, Robinul and during the experimental procedures with isoflurane for inhalation anesthesia with 1 l O_2/min. The blood volume was calculated in ml as 7% of total body weight in kg according to the GV-SOLAS table. For calculation of the plasma volume the individual hematocrit of the animals was used. For the pilot study and apheresis experiments, the animals were intravenously (i.v.) injected with 100 µg of sMICA*04 (2.5.2.2) per liter of blood volume. In the pilot study the body distribution and renal clearance of the administered sMICA*04 was determined. Three animals were monitored over three to six hours and 1 ml blood samples were taken from a catheter in the *vena saphena* every 15 min. Moreover, urine samples were taken from a bladder catheter. Three weeks after the experiment, blood samples were taken for the detection of anti-MICA monkey IgG/IgM antibodies (2.5.8.4).

For the apheresis experiment, two animals were connected to a Life18™ apheresis unit equipped with an anti-MICA adsorber cartridge (anti-MICA antibody covalently coupled to sepharose Cl-4B at 0.95 mg AMO1/g sepharose) via a double lumen catheter in the *vena femoralis*. During the experiment, animals got heparin (50 U/kg) i.v. injection as anticoagulant. Apheresis was started 15 min post-injection of sMICA*04 with a flow-rate of 25 - 30 ml/min over a time period of 90/120 min (until three complete plasma volume exchanges through the apheresis unit were reached). Blood samples were taken every 15 min during the apheresis. The sMICA*04 plasma and urine levels of all samples were determined by Sandwich ELISA (2.5.8.1).

3 Results

The NKG2D/NKG2D ligand system is important for tumor immunosurveillance by NK cells and other NKG2D$^+$ cytotoxic lymphocytes. Therefore, the aim of the current study was the characterization of a NKG2D-dependent tumor immune escape in head and neck squamous cell carcinoma and the establishment of an adsorption apheresis for depletion of soluble NKG2D ligands from patients' plasma. For this purpose, primary samples of HNSCC patients were analyzed for sNKG2D ligand levels showing a correlation with disease progression as well as NK cell inhibition. Moreover, multicellular tumor spheroids were used to determine the impact of sNKG2D ligands on NK cell cytotoxicity and infiltration. As proof of concept, an adsorption apheresis based on monoclonal anti-MICA antibodies was established and further, a pan-specific approach for the simultaneous depletion of all sNKG2D ligands was developed using NKG2D fusion proteins. The successful depletion of sNKG2D ligands *in vitro* could be validated in a pre-clinical study using a rhesus macaque model. The generation of recombinant protein variants of sMICA and the NKG2D receptor ectodomain is described in detail in "Cloning Strategies" (2.3.7) and not further mentioned in the "Results" section (protein sequences depicted in 5.2). Parts of this thesis are published in Giannattasio *et al.* 2015 and Weil *et al.* (submitted).

3.1 The NKG2D/NKG2D ligand system in HNSCC

3.1.1 HNSCC Patients have elevated sNKG2D Ligand Plasma Levels

Previous studies revealed an NKG2D-dependent tumor immune escape mechanism in various types of cancers mediated by proteolytical shedding of NKG2D ligands [256, 303, 305, 318]. Recently, elevated sMICA plasma levels were correlated to disease progression and NK cell dysfunction in HNSCC [304, 320, 321]. Although many studies investigated tumor escape from immunosurveillance by NKG2D-expressing cells in different tumor entities, little is known about the impact of all sNKG2D ligands and their cumulative role as diagnostic and/or prognostic marker in cancer progression. This is partly due to the lack of reliable commercially available assays for the detection of ligands in plasma samples and the high polymorphism and heterogeneous expression of the different ligands [395]. To identify the levels of the shed NKG2D ligands sMICA, sMICB and sULBP1-3, the plasma of 44 HNSCC patients was ana-

lyzed. A random patient cohort was included in the study with primary neoplasms mainly in the oral cavity (22.7%), oropharynx (20.5%), hypopharynx (27.3%) and larynx (15.9%). Seventy-seven percent of patients were diagnosed with primary tumors compared to 23% with recurrent disease. The majority of patients was diagnosed with stage IVA HNSCC (43.2%), while the other patients were classified as stage I (6.8%), stage II (9.1%), stage III (15.9%), stage IVB (4.5%) and stage IVC (13.6%) exhibiting distant metastases. Four patients (9.1%) were tested positive for human papillomavirus infection. Whereas 68% of patients were treatment naïve at the time of sample collection, 32% got standard treatment with most of the patients in palliative radio- or chemotherapy. Case history and patients' characteristics are summarized in Table 10.

Table 10. Clinical parameters and frequencies of HNSCC patients.

n.d. = not defined; T = primary tumor size, N = spread to regional lymph nodes, M = distant metastasis, RTx = radiotherapy, CTx = chemotherapy, RCTx = radio-chemotherapy, HPV = human papillomavirus

Parameter	Absolute numbers and frequency (%)	Parameter	Absolute numbers and frequency (%)	Parameter	Absolute numbers and frequency (%)	Parameter	Absolute numbers and frequency (%)
Age (Ø 65 years)		**TNM classification**		**Status**		**HPV status**	
20 - 40	1 (2.3)	**T**		**primary**	34 (77.3)	**positive**	4 (9.1)
40 - 60	15 (34.1)	**1**	5 (11.4)	**relapse**	10 (22.7)	**negative**	34 (77.3)
60 - 80	24 (54.5)	**2**	8 (18.2)	**Disease stage**		**n.d.**	6 (13.6)
> 80	4 (9.1)	**3**	9 (20.5)	**I**	3 (6.8)		
Sex		**3 - 4 / 4**	17 (38.6)	**II**	4 (9.1)		
male	39 (88.6)	**n.d.**	5 (11.4)	**III**	7 (15.9)		
female	5 (11.4)	**N**		**IVA**	19 (43.2)		
Therapy		**0**	16 (36.4)	**IVB**	2 (4.5)		
no therapy	30 (68.2)	**1**	6 (13.6)	**IVC**	6 (13.6)		
post surgery	2 (4.5)	**2**	1 (2.3)	**other**	3 (6.8)		
post surgery and RCTx	2 (4.5)	**2b**	9 (20.5)	**Localization**			
palliative RTx/CTx	10 (22.7)	**2c**	7 (15.9)	**Oral cavity**	10 (22.7)		
Noxa		**3**	3 (6.8)	**Oropharynx**	9 (20.5)		
none	11 (25.0)	**n.d.**	2 (4.5)	**Hypopharynx**	12 (27.3)		
Smoking	16 (36.4)	**M**		**Larynx**	7 (15.9)		
Alcohol	1 (2.3)	**0**	38 (86.4)	**Larynx/ Hypopharynx**	3 (6.8)		
Smoking and alcohol	16 (36.4)	**1**	6 (13.6)	**other**	3 (6.8)		

For the determination of sNKG2D ligand levels, different commercially available ELISA kits were tested for the detection of the sNKG2D ligands sMICA/B and sULBP1-3 in plasma. Whereas most of the ELISA kits provided reproducible results analyzing ligand levels in cell culture supernatants, high detection variances could be seen especially for the sULBPs in human plasma (data not shown). Therefore, sandwich ELISAs using ligand-specific antibody pairs were optimized for the stable and reproducible detection in human plasma after previously published protocols [256, 296, 298, 394]. For reference, plasma of 12 age-matched healthy volunteers (mean age 55 years) was analyzed and the plasma levels of HNSCC patients were correlated (Figure 5).

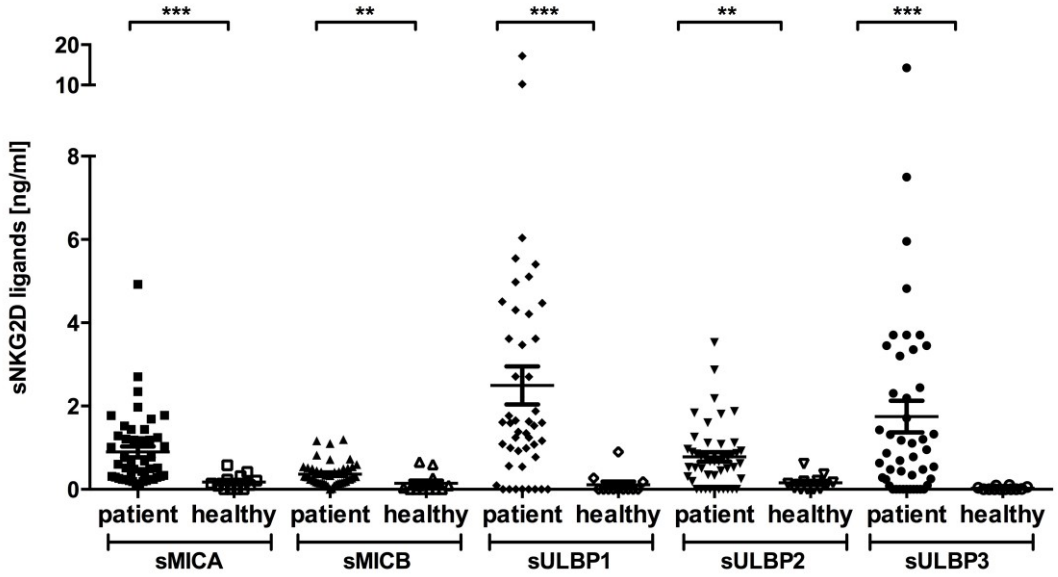

Figure 5: Elevated sNKG2D ligand plasma levels in HNSCC patients.
Quantification of the sNKG2D ligands sMICA, sMICB and sULBP1-3 in HNSCC patients' plasma (n = 44) compared to age-matched healthy plasma (n = 12) by respective Sandwich ELISAs. Each dot represents one plasma sample as mean of duplicates. Statistical significance was determined by Student's t-test for $p < 0.05$. ** $p < 0.005$, *** $p < 0.0001$.

Compared to healthy donors, significantly elevated levels of all sNKG2D ligands were detected in patients' plasma. Interestingly, levels of sMICA (0.899 ± 0.130 ng/ml vs. 0.175 ± 0.054 ng/ml), sMICB (0.365 ± 0.041 ng/ml vs. 0.144 ± 0.069 ng/ml) and sULBP2 (0.778 ± 0.113 ng/ml vs. 0.186 ± 0.059 ng/ml) showed a 2.5 - 5-fold increase compared to healthy plasma, whereas the most prominent sNKG2D ligands in HNSCC were sULBP1 (2.500 ± 0.454 ng/ml vs. 0.112 ± 0.076 ng/ml) and sULBP3 (1.750 ± 0.379 ng/ml vs. 0.025 ± 0.011 ng/ml) with over 20-fold increase (Figure 5). Importantly, sNKG2D ligand plasma levels showed high patient-to-patient variation suggesting that the composition and

total level of sNKG2D ligands represents an important patient-specific clinical parameter (Figure S1).

3.1.2 sNKG2D Ligand Levels correlate with HNSCC Disease Staging

To further elucidate the role of NKG2D ligand release in the course of disease, the total burden of sNKG2D ligands was correlated with relapsed or primary tumor diagnosis as well as tumor staging (Figure 6).

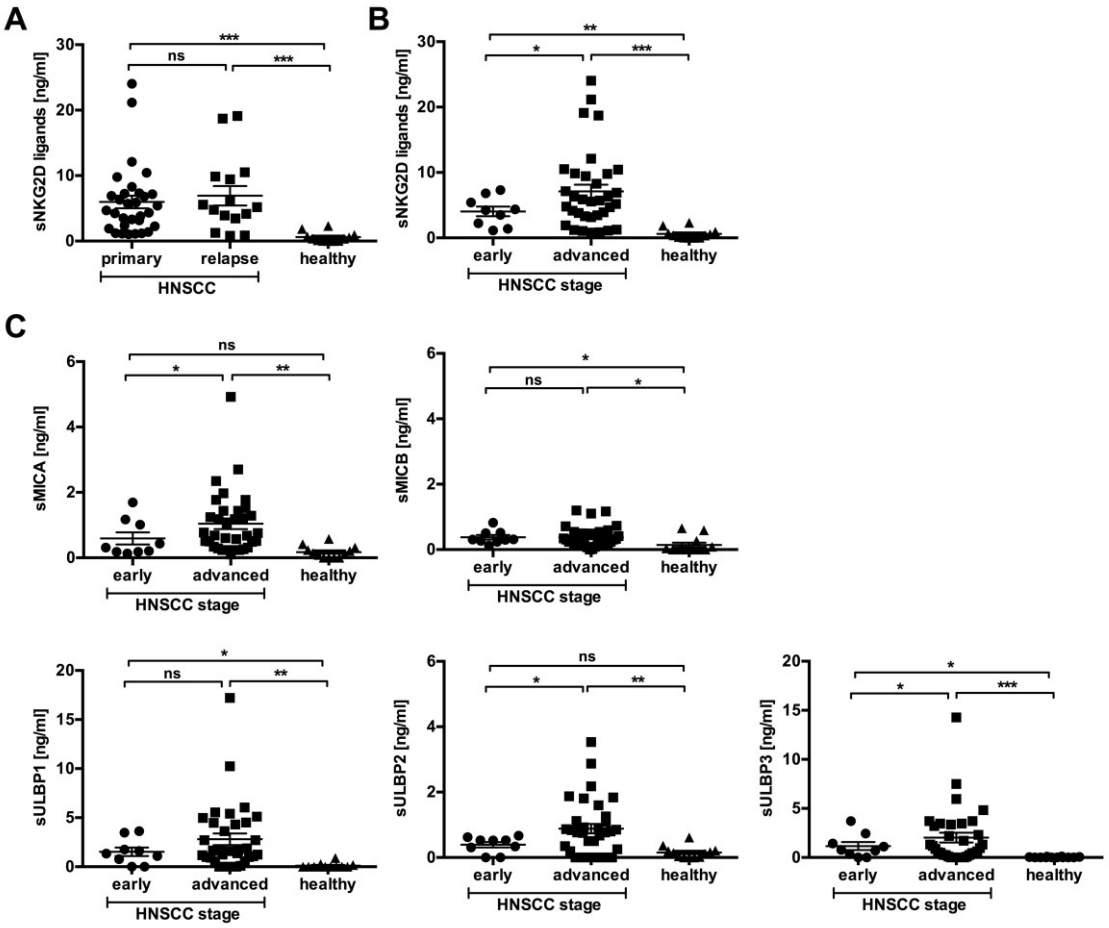

Figure 6: sNKG2D ligand plasma levels correlate with HNSCC disease stage.
(A/B) Cumulative sNKG2DL levels (sum of sMICA/B, sULBP1-3) grouped according to primary vs. relapsed tumors or disease stage (early = stage I+II; advanced = III+IV). (C) sMICA/B, sULBP1-3 plasma levels grouped according to disease stage (early = stage I+II; advanced = III+IV). Data are presented as mean ± SEM of representative experiments. Analysis of significance was performed by one-way ANOVA. * p = 0.01 - 0.05, ** p = 0.001 - 0.01, *** p < 0.001.

Whereas no significant alterations in sNKG2D ligand levels between patients with primary and relapsed tumors (Figure 6A) could be detected, sNKG2D ligands were found to peak in the plasma of patients with advanced disease (stage III+IV; Figure 6B). This stage dependency was also seen for the individual sNKG2D ligands, which increased until the pre-metastatic stage III (Figure 6C). The further subdivision of treatment naïve patients at initial diagnosis or recurrent disease confirmed that patients with relapsed disease and in advanced stages showed overall high sNKG2D ligand levels (Figure 7). In contrast, patients with relapsed disease currently under palliative chemo- or radiotherapy had lower sNKG2D levels. Interestingly, patients after tumor resection without indication of disease had sNKG2D levels similiar to those of patients at early disease stage with low tumor burden.

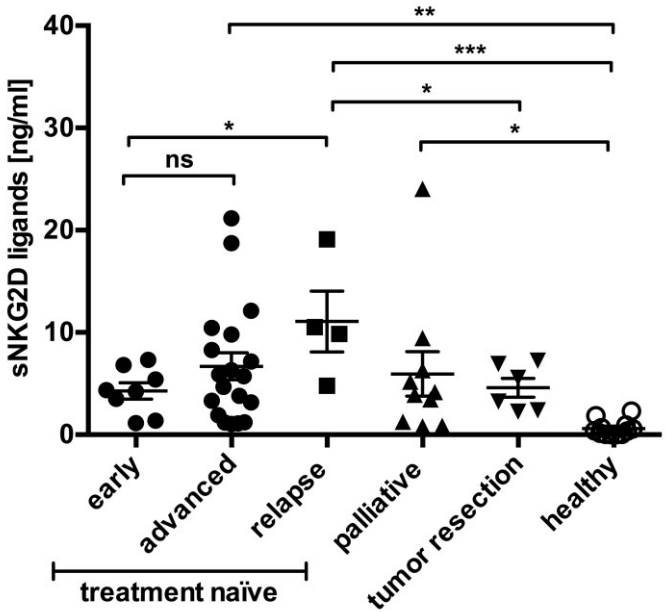

Figure 7: Impact of therapeutic treatment on sNKG2D ligand levels.
Comparison of sNKG2D ligand levels of treatment naïve patients, patients under treatment at time of plasma sample collection and healthy controls. Treatment naïve patients were grouped according to early and advanced disease at initial diagnosis and recurrent disease (relapse). Patients with treatment were grouped according to palliative therapy (radio- and/or chemotherapy) in comparison to patients after tumor resection without indication of tumor burden. Statistical significance was analyzed using one-way ANOVA, * $p < 0.05$, ** $p < 0.005$, *** $p < 0.001$.

These results are in accordance with the studies of Tamaki *et al.* [304] and Kloess *et al.* [320] analyzing sMICA, showing that NKG2D-depenent tumor immune escape is not an early event during tumor formation but rather is correlated to the tumor burden and disease progression.

Furthermore, radio- and chemotherapy might show a beneficial effect but could not lead to total clearance of sNKG2D ligands or tumor burden. Moreover, patients without primary tumor had in fact lower sNKG2D ligand levels, but tumor resection did not lead to a complete decrease comparable to ligand levels of healthy patients. This might be due to additional factors favoring expression and release of sNKG2D ligands like cytokine release and cellular stress induced by the treatments.

3.1.3 Immunosuppressive Cytokines contribute to HNSCC Immune Escape

HNSCC is characterized as a highly heterogeneous cancer including different neoplasms with a highly immunosuppressive tumor microenvironment [396, 397]. Beside cancer cells themselves, which promote an inflammatory milieu by production of proinflammatory and/or immunosuppressive factors (e.g. TGF-β1, IL-6, IL-8, IL-10, IL-1β, MCP-1, TNF-α), also tumor-residing immune cells, like tumor-associated macrophages (TAMs) and myeloid-derived suppressor cells (MDSCs), directly contribute to tumor growth, angiogenesis and invasion [398]. Moreover, immunosuppressive factors impair the antitumor functions of cytotoxic T and NK cells [281, 399]. To further understand the mechanism of tumor immune escape in HNSCC patients, plasma levels of the cytokines TGF-β1, IL-6, IL-8, IL-10, IL-1β, IFN-γ, TNF-α and the chemokines MIP-1α, MIP-1β, RANTES and MCP-1 were analyzed using cytometric bead array (CBA). Compared to healthy controls, markedly elevated levels could be detected for TGF-β1 (3890 ± 289.8 pg/ml vs. 187.8 ± 106.9 pg/ml), MIP-1β (1112.4 ± 21.95 pg/ml vs. 5.15 ± 2.43 pg/ml), RANTES (23720 ± 2683 pg/ml vs. 2204 ± 218.6 pg/ml), IL-8 (286.6 ± 126.4 pg/ml vs. 10.38 ± 0.99 pg/ml), MCP-1 (208.5 ± 29.86 pg/ml vs. 65.62 ± 6.95 pg/ml), and IL-6 (34.45 ± 4.91 pg/ml vs. 12.15 ± 1.02 pg/ml). Interestingly, plasma of HNSCC patients showed no significant differences in the levels of IFN-γ, TNF-α, IL-10, IL-1β and MIP-1α when compared to healthy controls (Figure 8A). Notably, a high variability in plasma levels between patients could be seen (Figure 8B). Due to the heterogeneity the expression patterns of most of the cytokines and chemokines could not be directly correlated to disease progression or therapeutic treatment. Moreover, no correlation of the individual immune factors and sNKG2D ligand release could be seen.

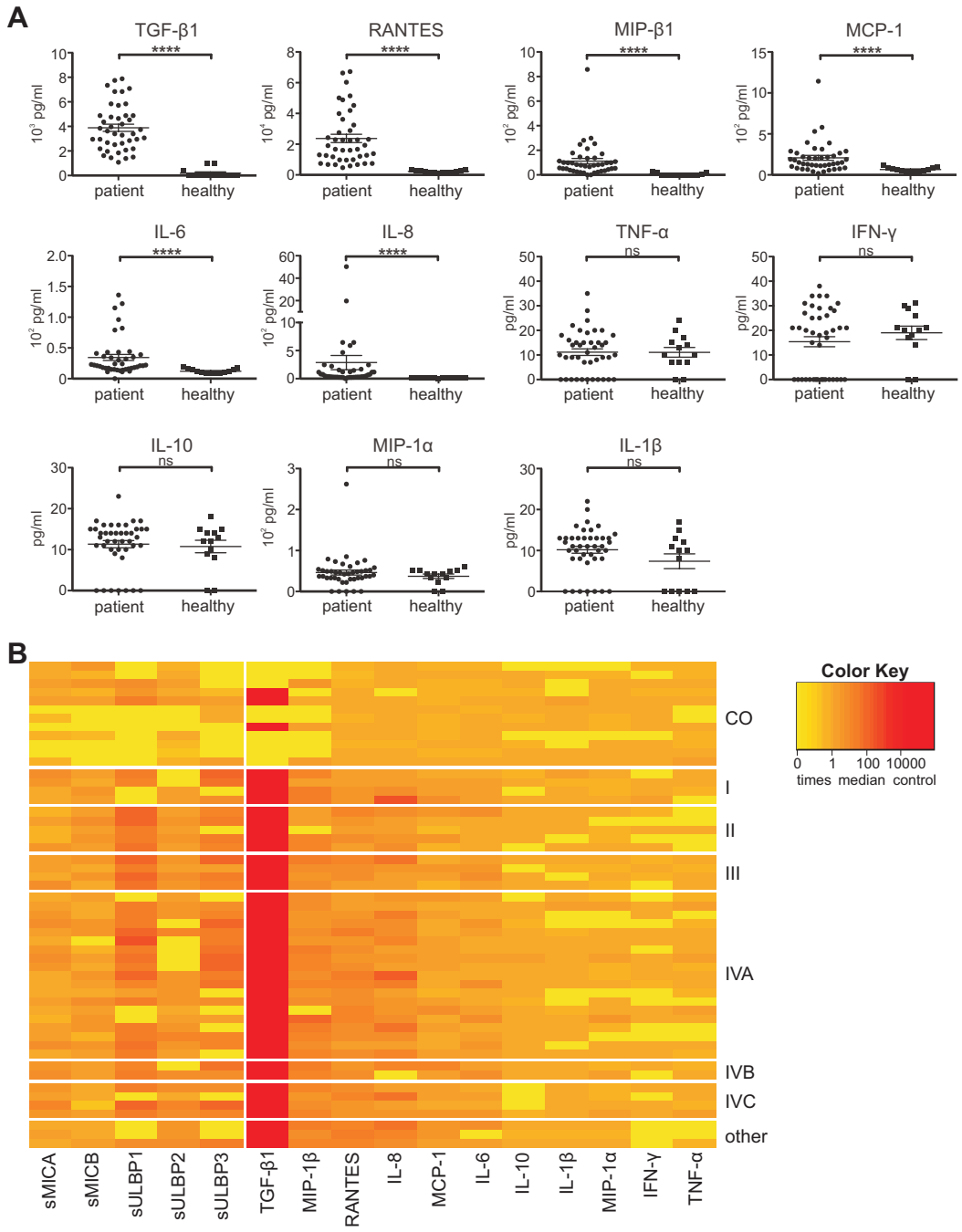

Figure 8: Elevated immunosuppressive factors in HNSCC patients.
Patients' plasma was analyzed for the levels of the cytokines TGF-β1, IL-6, IL-8, IL-10, IL-1β, IFN-γ, TNF-α and chemokines MIP-1α, MIP-1β, RANTES and MCP-1 by cytometric bead array (CBA). (A) Quantification of chemokine and cytokine levels compared to healthy controls. Each dot represents one plasma sample as mean of duplicates. Statistical significance was determined by Student's t-test for $p < 0.05$, **** $p < 0.0001$. (B) Heat-map representation of sNKG2DL levels (see also Figure 5), cytokine and chemokine levels as x-times median control (CO; of 12 healthy donors) grouped according to disease stage (I - IVC). Color code: yellow = normal; orange = elevated; and red = highly elevated.

Interestingly, TGF-β1 plasma levels were highly upregulated throughout all patients analyzed and showed an increase during advanced disease from 2677 pg/ml to 5358 pg/ml between disease stage I - IV (Figure 9A). In contrast, no differences between primary and relapsed tumors could be observed (Figure 9B).

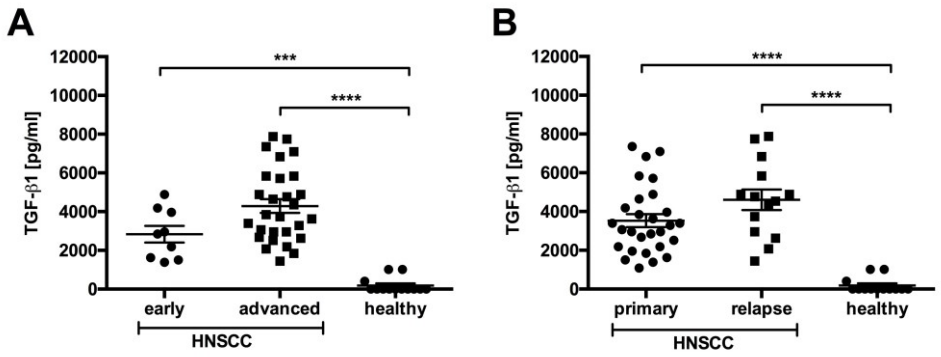

Figure 9: TGF-β1 plasma levels correlate with disease progression.
TGF-β1 plasma levels of HNSCC patients and healthy volunteers determined by cytometric bead array (CBA) were grouped according to (A) disease stage (early = stage I+II; advanced = III+IV) and (B) primary vs. relapsed tumor and compared to healthy controls. Statistical significance was determined by one-way ANOVA. *** $p < 0.001$, **** $p < 0.0001$

These data demonstrate the high complexity of the immune system and tumor microenvironment. The aberrant cytokine and chemokine levels, especially regarding TGF-β1, are indicative for an imbalanced immune system and thus impaired tumor surveillance. Due to the individual immune status of the patients no comprehensive correlations of individual soluble factors to disease progression or direct contribution to NKG2D-dependent tumor immune escape could be seen for the patient cohort analyzed.

3.1.4 Inhibition of NK Cell Cytotoxicity by sNKG2D Ligands in HNSCC Patients' Plasma

NKG2D ligand expression on tumor cells leads to NKG2D engagement and subsequent NK cell activation. In contrast, binding of shed NKG2D ligands inhibits NKG2D and thus augments tumor escape from immunosurveillance by NKG2D-expressing cells [315, 400]. In order to investigate the inhibitory potential of sNKG2D ligands in the plasma of HNSCC patients, flow cytometry-based cytotoxicity assays were performed using IL-2 activated primary human NK cells after pre-incubation with plasma from HNSCC patients, healthy donors or

anti-NKG2D blocking antibodies (gating strategy Figure S2). As target cells, the human cervix squamous cell carcinoma cell line (SiHa) was used whose killing is strongly dependent on NKG2D as shown by blocking experiments with anti-NKG2D antibodies (see Figure 18). For the relative quantification of tumor cell lysis, the mean lysis of NK cells pre-incubated with different healthy donor plasma was used for normalization of NK cell lysis with HNSCC plasma or blocking antibody incubation.

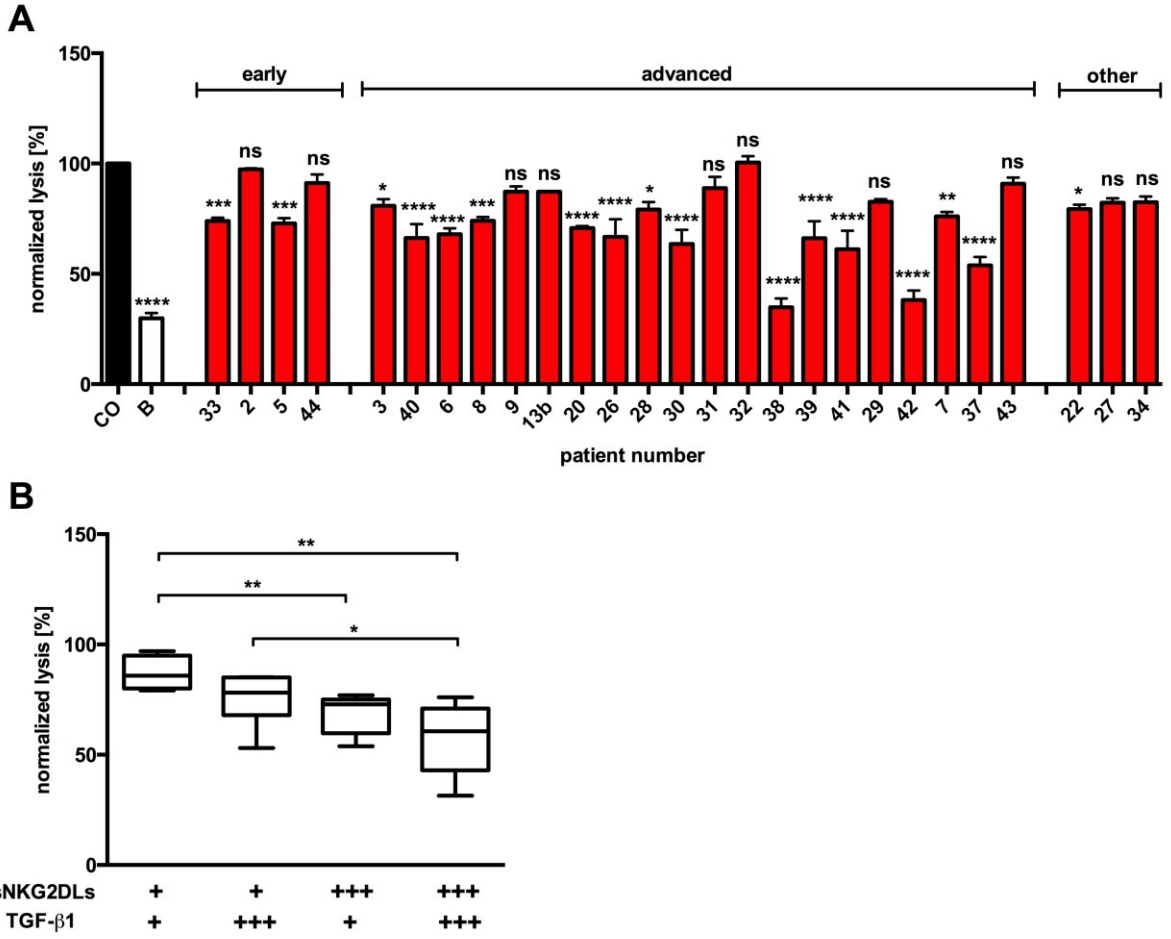

Figure 10: sNKG2D ligand-dependent inhibition of NK cell cytotoxicity.
(A) Cytotoxicity assay of NK cells with CFSE-labeled target cells (E:T = 15:1; 2 h). NK cells were pre-incubated overnight with HNSCC plasma prior to the assay. NK cells pre-incubated with healthy plasma (CO) or NKG2D blocking antibodies (B) served as controls. Target cell lysis was calculated by flow cytometry and analysis of dead ($CFSE^+/SytoxBlue^+$) and viable ($CFSE^+/SytoxBlue^-$) cells. Data were normalized to CO (mean of six samples) and are represented as mean ± SEM of triplicates of an independent experiment. (B) Lysis of target cells (see A) grouped according to sNKG2DL (+ low = 0 - 2.5 ng/ml and +++ high > 2.5 ng/ml) and TGF-β1 (+ low = 0 - 3000 pg/ml and ++ high > 3000 pg/ml) plasma levels. Statistical significance was analyzed using one-way ANOVA. ns = non-significant for $p > 0.05$, * $p = 0.01 - 0.05$, ** $p = 0.001 - 0.01$, *** $p < 0.001$ and **** $p < 0.0001$.

Most of the HNSCC plasma samples significantly inhibited target cell killing compared to plasma of age-matched healthy donors (Figure 10A). Incubation with NKG2D blocking antibodies showed the high degree of NKG2D-dependent tumor cell lysis. To further elucidate the impact of NKG2D-depedent NK cell inhibition in HNSCC plasma, tumor cell lysis was correlated to plasma contents. Since patients' plasma contained high levels of TGF-β1, which is known to contribute to NKG2D downregulation [295, 401], the lytic capacity of NK cells preincubated with patients' plasma was correlated to the plasma levels of sNKG2D ligands and TGF-β1. Patients' plasma containing high levels of both, sNKG2D ligands (> 2.5 ng/ml; median: 7.6 ng/ml) and TGF-β1 (> 3000 pg/ml; median: 5319 pg/ml) showed lower NK cell cytotoxicity when compared to patients' plasma with low sNKG2D ligands (< 2.5 ng/ml; median: 1.4 ng/ml) and TGF-β1 (< 3000 pg/ml; median: 2045 pg/ml) levels (Figure 10B). Interestingly, sNKG2D ligands and TGF-β1 had an additive effect on NK cell inhibition compared to plasma containing only high amounts of only one factor.

Human plasma is a complex protein mixture containing various soluble factors, which could contribute to impaired NK cell function. To verify the impact of the sNKG2D ligands in patients' plasma on NK cell cytotoxicity, sNKG2D ligands were removed by selective depletion of sMICA, sMICB, sULBP1, sULBP2 and sULBP3 with a cocktail of anti-NKG2D ligand antibody-coupled beads. The depletion efficiencies were verified by ELISA and ranged between 61.9% and 93.2% for the cumulative ligand plasma levels (Figure 11A). To ensure no disturbing effects on cytotoxicity assays due to bead incubation and removal of other soluble factors or residual antibodies, healthy plasma samples were incubated with antibody-coupled beads as controls. Cytotoxicity assays with depleted and non-depleted plasma showed that the removal of sNKG2D ligands from patients' plasma efficiently restored NK cell cytotoxicity compared to healthy plasma controls (Figure 11B), whereas depletion of healthy plasma containing no/low levels of sNKG2D ligands had no effect on NK cell cytotoxicity. Collectively, these *in vitro* experiments demonstrate that the sole depletion of sNKG2D ligands was sufficient to restore NK cell cytotoxicity, assuming shedding of ligands as a key mechanism of NKG2D-dependent tumor immune escape.

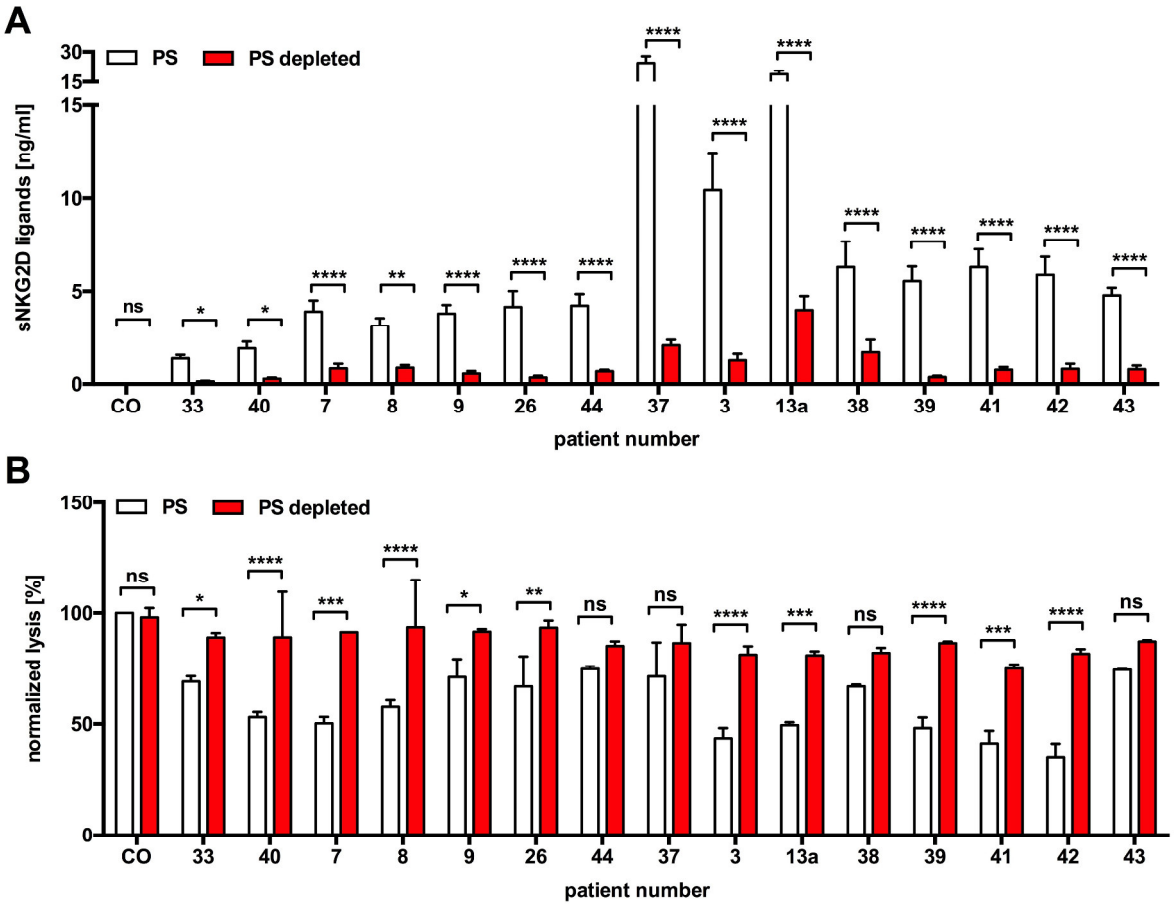

Figure 11: Restoration of NK cell cytotoxicity by sNKG2D ligand depletion.
(A) NKG2D ligands were depleted from patients' plasma using antibody-coupled magnetic beads. Depletion of healthy plasma served as control. Plasma levels pre-/post depletion were determined by respective NKG2D ligand ELISAs and are depicted as sum of sNKG2D ligands of individual patients presented as mean ± SEM of duplicates. (B) NK cells were incubated overnight with patients' plasma (PS; high sNKG2DL levels) or sNKG2D ligand-depleted plasma (PS depleted) prior to cytotoxicity assays. NK cells incubated with healthy/healthy-depleted plasma (CO) served as controls. Data were normalized to CO and are presented as mean ± SEM, measured in triplicates of an independent experiment. Statistical significance was analyzed using one-way ANOVA. ns = non-significant for $p > 0.05$, * $p = 0.01 - 0.05$, ** $p = 0.001 - 0.01$, *** $p < 0.001$ and **** $p < 0.0001$.

To further verify the direct effect of the soluble ligands on NKG2D-dependent NK cell cytotoxicity, the NKG2D expression levels on plasma-treated NK cells were analyzed by flow cytometry. Compared to the expression levels of NK cells treated with healthy plasma, a reduction of NKG2D expression was observed for patients' plasma-treated NK cells or NK cells incubated with anti-NKG2D blocking antibodies (Figure 12). Moreover, the degree of NKG2D downregulation was correlated with the amount of sNKG2D ligands in the plasma as shown exemplarily for two plasma samples (patient 13a and 43, see Figure 11A and 12B). In

contrast, NKG2D expression on NK cells incubated with NKG2D ligand-depleted plasma was not reduced.

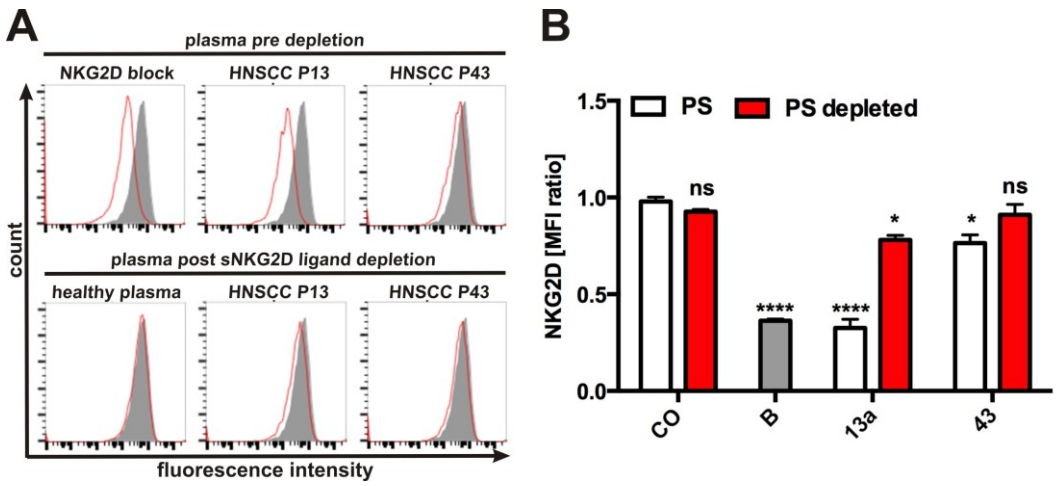

Figure 12: NKG2D-dependent NK cell inhibition in HNSCC plasma.
(A) Flow cytometric analysis of NKG2D surface expression on primary human NK cells treated with HNSCC plasma or healthy plasma samples pre-/or post sNKG2D ligand depletion. Grey = healthy control plasma, red = as indicated: NKG2D blocking antibody, patient plasma or depleted patient/healthy plasma. One representative experiment of three is shown. (B) NKG2D surface expression on NK cells treated with non-depleted or sNKG2D ligand-depleted healthy plasma (CO), patient plasma (PS) or NKG2D blocking antibody (B). Data are represented as MFI ratio normalized to healthy plasma (CO) as mean ± SEM of duplicates of a representative experiment. Statistical significance was analyzed by Student's t-test with * $p < 0.05$, **** $p < 0.0001$.

In these studies, a direct correlation of the cumulative sNKG2D ligands in HNSCC patients' plasma to impaired antitumor NK cell function due to NKG2D receptor blocking and down-regulation upon sNKG2D ligand engagement could be shown. Moreover, NK cell cytotoxic activity could be efficiently restored by sNKG2D ligand depletion.

3.1.5 sNKG2D Ligand and TGF-β1 Plasma Levels correlate with Tumor Burden

In a single case study of one representative patient, plasma samples were taken directly before and after surgery of the primary tumor. Determination of sNKG2D ligand and TGF-β1 levels showed reduced load of soluble molecules after surgery (Figure 13A). As expected, incubation of primary NK cells with plasma containing lower levels of sNKG2D ligands showed a higher cytotoxic activity compared to the plasma sample with higher sNKG2D ligand titers (Figure 13C). Furthermore, a patient with high sNKG2D ligand and TGF-β1 levels at initial

diagnosis had reduced but reappearing levels of sNKG2D ligands and TGF-β1 with relapsed disease after tumor resection and palliative chemotherapy (Figure 13B/D).

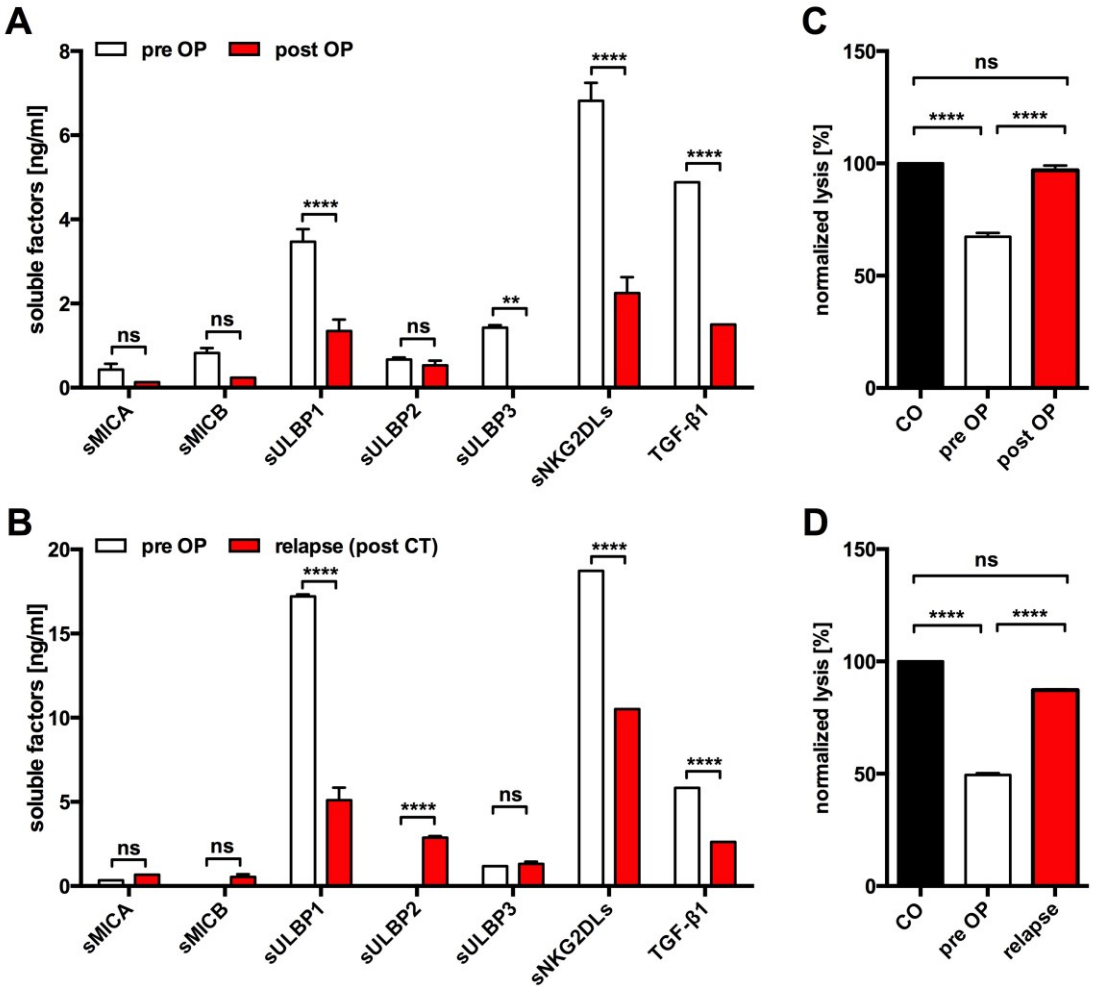

Figure 13: sNKG2D ligands and TGF-β1 plasma level correlate with tumor burden.
(A/B) Individual and cumulative plasma levels of sNKG2D ligands and TGF-β1 analyzed by ELISA or CBA of one representative patient pre- and post surgery (A) and one patient at initial diagnosis and after relapse diagnosis after chemotherapy (post CT) (B) presented as mean ± SEM of duplicates. (C/D) NK cell cytotoxicity against SiHa target cells measured by flow cytometry of NK cells pre-treated with HNSCC plasma pre- and post-surgery (C) or at initial and relapse diagnosis (D). Data was normalized to healthy control (CO) and bars correspond to mean ± SEM of triplicates. Statistical significance was analyzed using one-way ANOVA. ns = non-significant for $p > 0.05$, * $p < 0.05$, ** $p = 0.005$, *** $p = 0.0001$ and **** $p < 0.0001$.

These findings demonstrate a direct link between tumor burden, NKG2D ligand shedding and TGF-β1 release in HNSCC and confirm the importance of the cumulative sNKG2D ligand

levels as a diagnostic and/or prognostic marker for tumor immune escape from NK cell immunosurveillance.

3.1.6 Low Lymphocyte Infiltration in primary HNSCC Tumors

The tumor microenvironment (TME) is a highly dynamic network of tumor cells and non-malignant cells, which can comprise 50% of the primary tumor mass [402]. Tumor infiltrating lymphocytes (TILs) including cytotoxic $CD8^+$ T cells, $CD4^+$ T helper cells, B cells and NK cells are frequently found in tumors mediating tumor immunogenicity, as well as tumor associated macrophages (TAMs), which can either have pro- or antitumor functions [398, 403]. Moreover, NK cell antitumor activity can coincide with their tumor infiltrating potential which is associated with a better prognosis in several cancer entities such as colorectal cancer, non-small cell lung cancer, and clear cell renal cell carcinoma [404-406]. To evaluate lymphocyte infiltration, primary tumor sections of eleven HNSCC patients were stained according to the expression markers for $CD20^+$ B cells, $CD3^+$ T cells, $CD8^+$ cytotoxic T cells and $CD56^+$ NK cells (and NKT cells). Additionally, TAMs were stained for the linage marker CD68, recognizing activated and resting macrophages, and the M2 phenotype-specific macrophage marker CD163 (Figure 14A). The primary tumor samples were randomly selected including different epithelial origins, tumor stages and HPV status. Infiltrating cells were analyzed separately for the invasive margin (IM) or tumor core (TC) by counting the cells in high power fields (HPF) of the tumor samples (Figure 14B). In all tumor samples, moderate T cell numbers were found in the invasive margin ($CD3^+$ T cells: mean 71 cells/HPF; $CD8^+$ T cells: mean 50 cells/HPF). In contrast, only a small number of lymphocytes could infiltrate into the tumor core ($CD3^+$ T cells: mean 17 cells/HPF; $CD8^+$ T cells: mean 20 cells/HPF). The cytotoxic $CD8^+$ T cells showed a similar distribution as the whole $CD3^+$ T cell population, with only weak infiltration into the tumor core. Whereas high numbers of $CD20^+$ B cells ($CD20^+$ B cells: 200 cells/HPF) were located in the invasive margin, very low B cells infiltrated into the tumor core ($CD20^+$ B cells: 4 cells/HPF). Interestingly, only very low numbers or a complete absence of NK cells could be found in the tumor tissues (IM/TC: mean 2 cells/HPF). Moreover, TAMs could be found throughout the tissue showing an equal distribution between the invasive margin and tumor core without correlation to the lymphocyte infiltration potential. Interestingly, most TAMs were of the M2 phenotype, which is characterized by its pro-

tumoral functions. The low infiltration potential of the different lymphocyte populations and the presence of M2 macrophages are indicative for the insufficient tumor rejection and immunosuppressive TME of primary tumors in HNSCC patients.

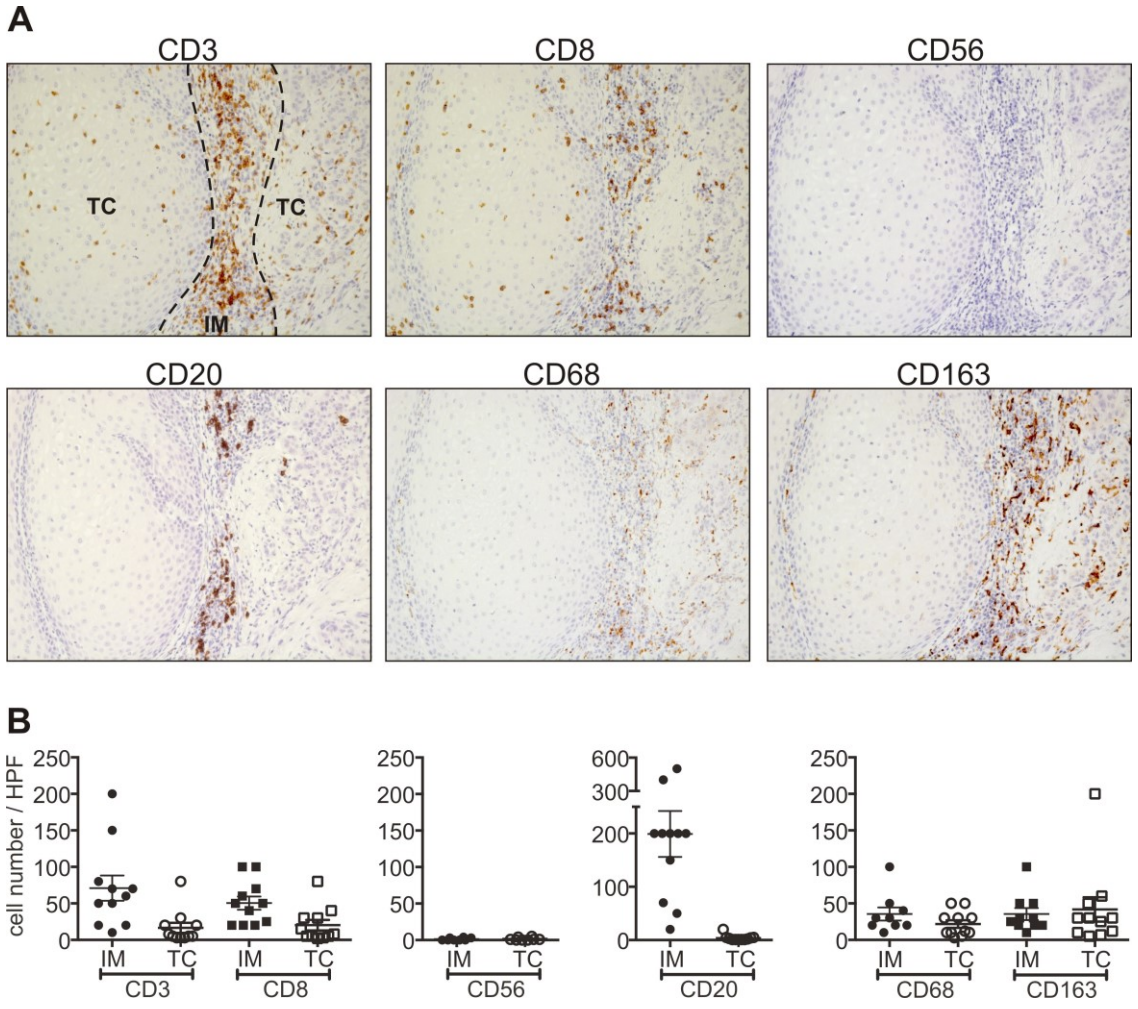

Figure 14: Low lymphocyte infiltration in primary HNSCC tumors.
Paraffin sections of primary tumors were stained for $CD3^+$, $CD8^+$, $CD20^+$ and $CD56^+$ lymphocytes or $CD68^+/CD163^+$ macrophages. (A) Consecutive sections of a representative patient are shown at 200x magnification. Dotted line represents the border between tumor core (TC) and invasive margin (IM). (B) Number of infiltrated lymphocytes and macrophages quantified by counting infiltrating cells in the tumor core (TC) and invasive margin (IM) in high power fields (HPF) of the tumor slides. Total cell numbers/HPF of 11 patients are plotted with mean ± SEM.

For further analysis, HNSCC patients' peripheral blood mononuclear cells (PBMCs) and corresponding dissociated tumor samples were subjected to flow cytometry experiments. Analysis of the $CD45^+$ lymphocyte population showed that the total number of circulating $CD3^+$ T cells was unaltered compared to the lymphocytes of healthy controls (Figure 15A). No chang-

es in the ratio of $CD4^+$ and the $CD8^+$ T cell subpopulations could be detected within the $CD3^+$ T cells. Analysis of the tumor infiltrating cells confirmed the data from immunohistochemical stainings showing that roughly 60% of the $CD45^+$ TILs correspond to T cell populations. Interestingly, the $CD4^+/CD8^+$ ratio in the tumor samples correlated with the ratio of the circulating T cells in the blood. Moreover, as expected $CD4^+$ T cells showed low NKG2D surface expression compared to the $CD8^+$ cytotoxic T cells (Figure 15B).

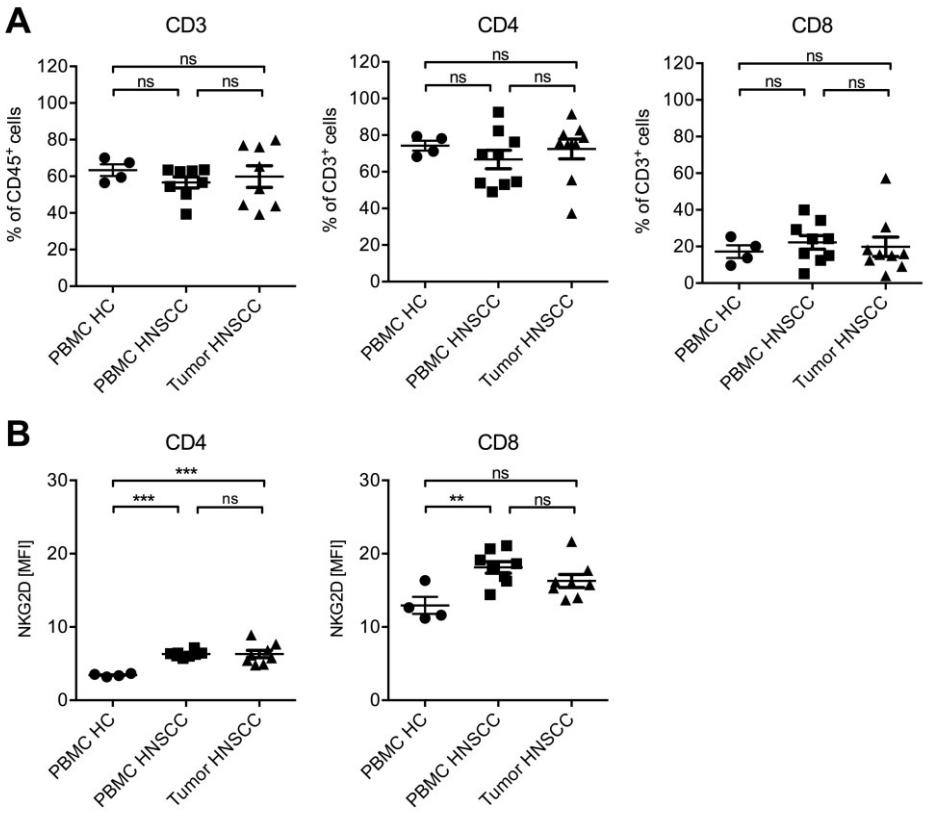

Figure 15: Analysis of T cells in PBMCs and tumor samples of HNSCC patients.
(A) Flow cytometric analysis of $CD3^+$ T cells and T cell subpopulations ($CD4^+$ T-helper cells and $CD8^+$ cytotoxic T cells) of patients' PBMCs and corresponding tumor tissues. Healthy PBMCs served as control. $CD3^+$ T cell numbers were calculated and plotted as % of $CD45^+$ lymphocytes and subpopulations as % of $CD3^+$ cells (n = 9 patients; n = 4 healthy controls). (B) Corresponding NKG2D expression levels of T cell subpopulations plotted as MFI over background with mean ± SEM (n = 9 patients; n = 4 healthy controls). Statistical significance was analyzed using one-way ANOVA, ns = non-significant for $p > 0.05$, ** $p = 0.001$ - 0.01, *** $p < 0.001$.

Compared to healthy controls, only a 0.5-fold increase in NKG2D expression levels could be observed for the $CD8^+$ cytotoxic T cells. Furthermore, NK cell subpopulations within the PBMCs and tumor samples of the HNSCC patients were analyzed. The total number of circu-

lating NK cells in the CD45$^+$ lymphocyte population of PBMCs was nearly unchanged compared to healthy controls (Figure 16A).

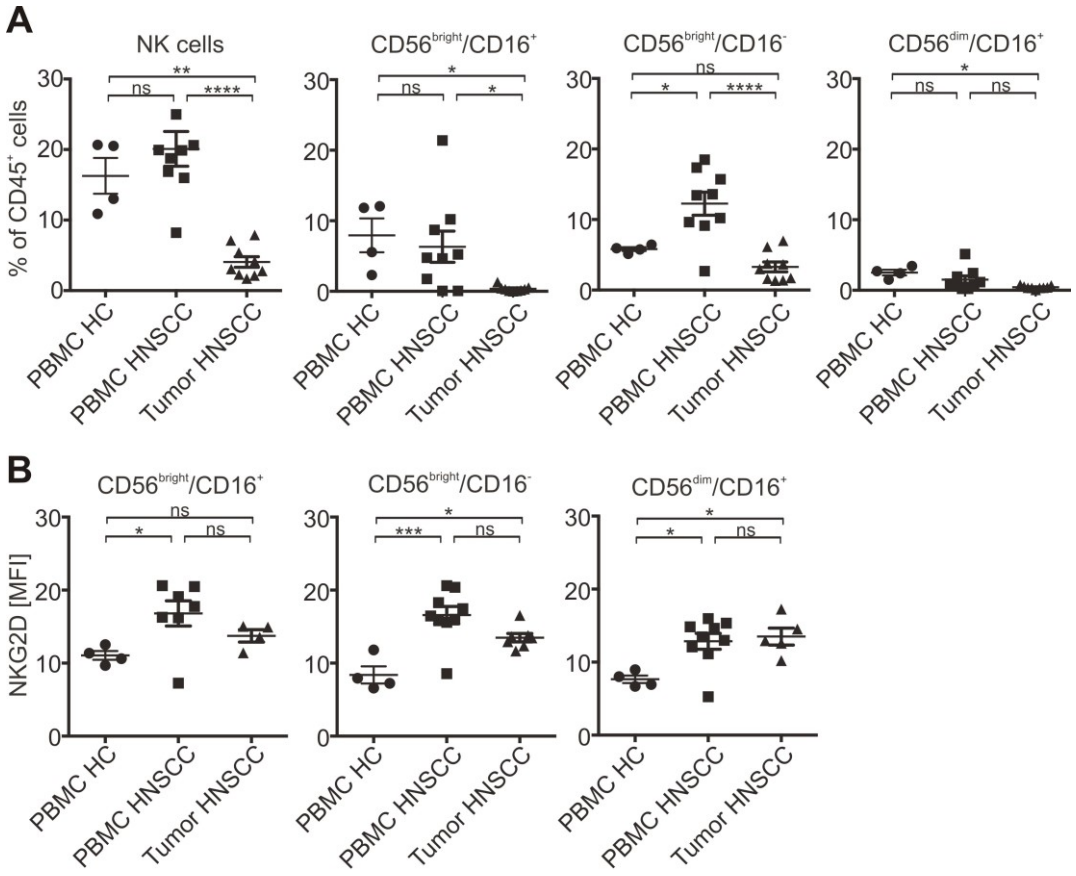

Figure 16: Analysis of NK cells in PBMCs and tumor samples of HNSCC patients.
(A) Flow cytometric analysis of NK cells and NK cell subpopulations (regulatory: CD56^{bright}/CD16$^{+/-}$ and cytotoxic: CD56^{dim}/CD16$^+$ NK cells) of patients' PBMCs and corresponding tumor tissues. Healthy PBMCs served as control. NK cell numbers were calculated and plotted as % of CD45$^+$ lymphocytes (n = 9 patients; n = 4 healthy controls). (B) Corresponding NKG2D expression levels of NK cell subpopulations plotted as MFI over background with mean ± SEM (n = 9 patients; n = 4 healthy controls). Statistical significance was analyzed using one-way ANOVA, ns = non-significant for $p > 0.05$, * $p = 0.01 - 0.05$, ** $p = 0.001 - 0.01$, *** $p < 0.001$ and **** $p < 0.0001$.

Regarding regulatory (CD56^{bright}/CD16$^{+/-}$) and cytotoxic (CD56^{dim}/CD16$^+$) NK cell subpopulations, HNSCC patients showed a slight shift towards regulatory NK cells. Analysis of tumor samples confirmed the histological staining showing that only a minor proportion of TILs were NK cells. Interestingly, the infiltrating NK cells were predominantly from the regulatory subpopulation, whereas cytotoxic NK cells were nearly absent. Moreover, analysis of NKG2D expression levels showed a small increase of 0.7 to 1.4-fold for the CD56^{bright} cells and one-

fold for the CD56^{dim} population compared to healthy controls (Figure 16B). Taken together, immunohistochemical and flow cytometry analysis revealed an impaired immune response of NK cells and partly T cell subpopulations in the tumor tissue of HNSCC patients.

3.2 Tumor Spheroids as *in vivo*-like Model System

3.2.1 Characterization of Tumor Spheroids to study NK Cell Functions

In order to further elucidate NKG2D-dependent tumor immune escape, 3D multicellular tumor spheroids, which resemble many features of *in vivo* tumors and allow for systematic studies of molecular parameters in a highly controlled microenvironment, were used [387]. Tumor spheroid cultures possess a complex network of cell-cell contacts as well as pH, oxygen, metabolic and proliferative gradients analogous to the conditions found in poorly vascularized and avascular regions of solid tumors and micrometastases (Figure 17A) [407-410].

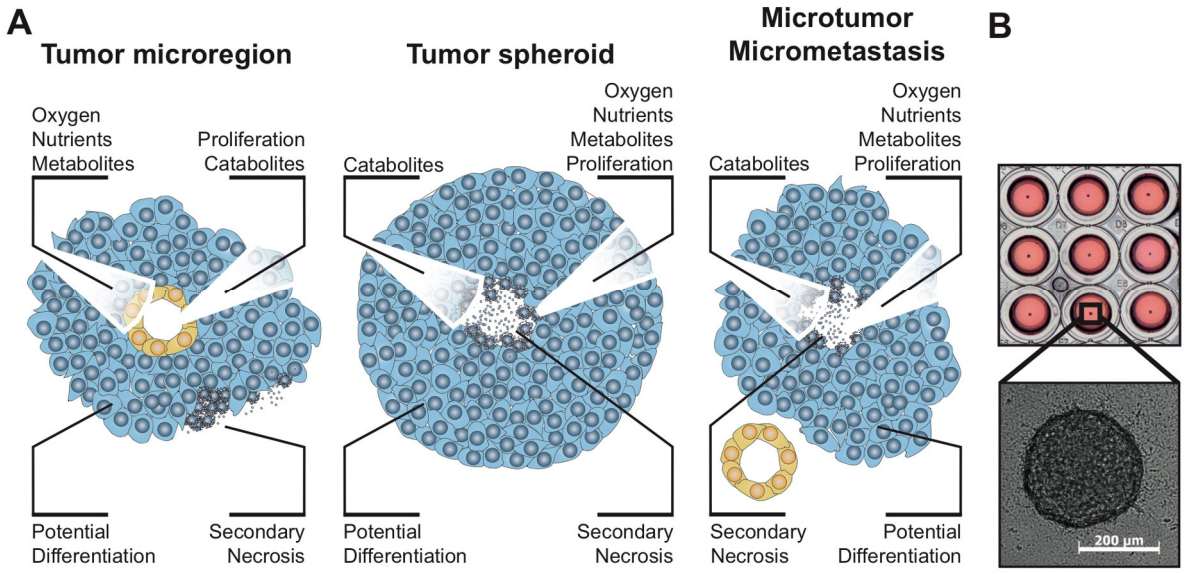

Figure 17: Establishment of tumor spheroids.
(A) Schematic representation of the microarchitecture of tumor spheroids, avascular tumor microregions and developing micrometastases (based on Friedrich *et al.* [411]) highlighting the pathophysiological similarities and differences. (B) Representative tumor spheroids derived from 2x10^3 cells are shown in an agarose-coated 96-well plate and by transmission microscopy at 50x magnification.

Single tumor spheroids are formed by aggregation of several thousand cells [407, 409] on agarose-coated 96-well plates (Figure 17B) and are consequently comprised of an outer re-

gion of proliferating cells around a layer of quiescent cells and, if the tumor spheroid is large enough, a necrotic core [410].

Tumor spheroids were grown from the primary tumor-derived HNSCC cell lines FaDu, CAL27 and Detroit562 of different epithelial origins and the cervical carcinoma cell line SiHa. NK cell killing showed a large degree of NKG2D-dependency as shown in cytotoxicity assays with primary human NK cells at different effector-to-target (E:T) ratios in the absence and presence of NKG2D-specific blocking antibodies. NKG2D blocking led to 50.4% and 41.9% inhibition of NK cells' cytotoxicity towards FaDu and Detroit562 cells, respectively (Figure 18). In contrast, NKG2D-mediated killing of CAL27 cells only accounts for 24.7%, whereas the cervical carcinoma cell line SiHa showed 71.2% NKG2D-dependency.

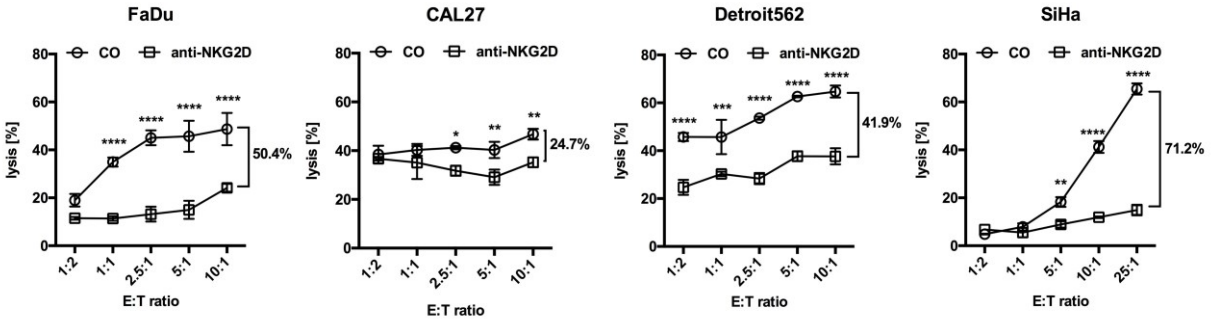

Figure 18: NKG2D-dependent NK cell cytotoxicity of tumor cell lines.
CFSE-labeled FaDu, CAL27, Detroit562 or SiHa cells were co-cultured with primary human NK cells overnight (4 h for SiHa cells) in different E:T ratios and analyzed by flow cytometry. To analyze NKG2D-dependent killing, NK cells were pre-incubated with anti-NKG2D blocking antibodies. Target cell lysis was calculated by gating on dead $CFSE^{+}/SytoxBlue^{+}$ or viable $CFSE^{+}/SytoxBlue^{-}$ cells. Data are shown as mean ± SEM of triplicates of a representative experiment. Statistical significance was analyzed using one-way ANOVA with: * $p < 0.05$, ** $p = 0.005$, *** $p = 0.0001$ and **** $p < 0.0001$.

Mature tumor spheroids formed within 24 - 48 h (d0) after seeding into agarose-coated 96-well plates. Microscopic analyses revealed that tumor spheroids retained a spherical shape in solid state and were stable for roughly two to four days with minor compaction due to cellular rearrangement (Figure 19). Below a radius of 200 µm, the critical distance of free diffusion of nutrients, oxygen and metabolic waste products, tumor spheroids remained solid without signs of unwanted central necrosis. Thus, tumor spheroids are not loose or unsystematic cell aggregates, but preserve a complex and structured cellular network. To establish cytotoxicity assays with primary human NK cells, tumor cells were stained with CFSE prior to tumor spheroid formation for easy detection with flow cytometric-based assays. Moreover, the use

of a 96-well plate format allowed for screening of individual tumor spheroids and was applicable for high throughput screening.

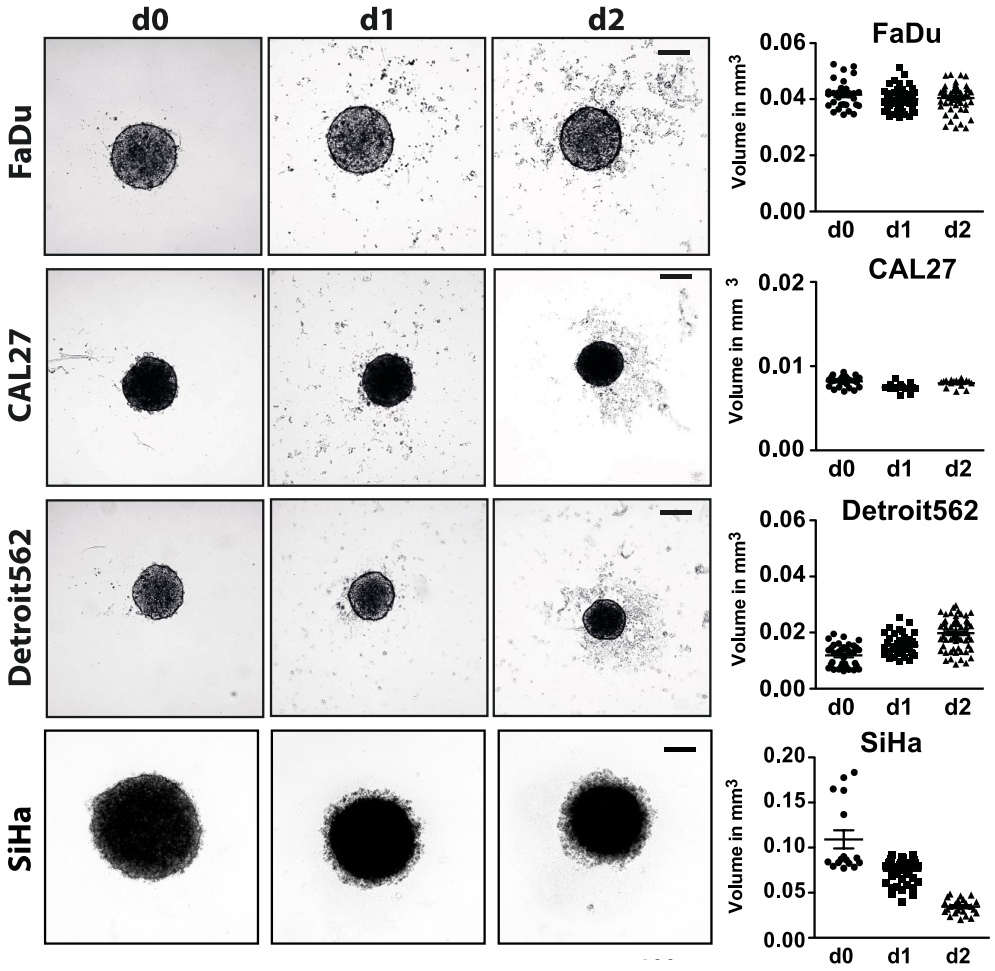

Figure 19: Growth kinetics of tumor spheroids.
FaDu, CAL27, Detroit562 and SiHa tumor spheroids were monitored for three days after reaching the solid spheroidical state by phase contrast microscopy at 50x magnification. Representative phase contrast pictures are shown. Size bar corresponds to 100 µm. Tumor spheroid volume (in mm^3) was calculated based on area determination using Fiji software of individual spheroids from six independent experiments.

Tumor spheroid destruction was studied during co-culture with primary human NK cells at different E:T ratios for 48 h. The quantification by flow cytometry based on the loss of CFSE-labeled target cells revealed that 69% of FaDu, 64% of CAL27, 69% of Detroit562 and 79% of SiHa cells were efficiently killed at an E:T ratio of 20:1 (Figure 20). Thereby, tumor sphe-

roids showed an E:T dependent destruction by NK cells. Notably, they are more resistant to NK cell cytotoxicity due to their 3D architecture than corresponding monolayer cultures. Therefore, tumor spheroids resemble a versatile *in vivo*-like 3D model to study the antitumor functions of cytotoxic lymphocytes in high throughput screening and were further used to determine the influence of NKG2D-dependent tumor immune escape.

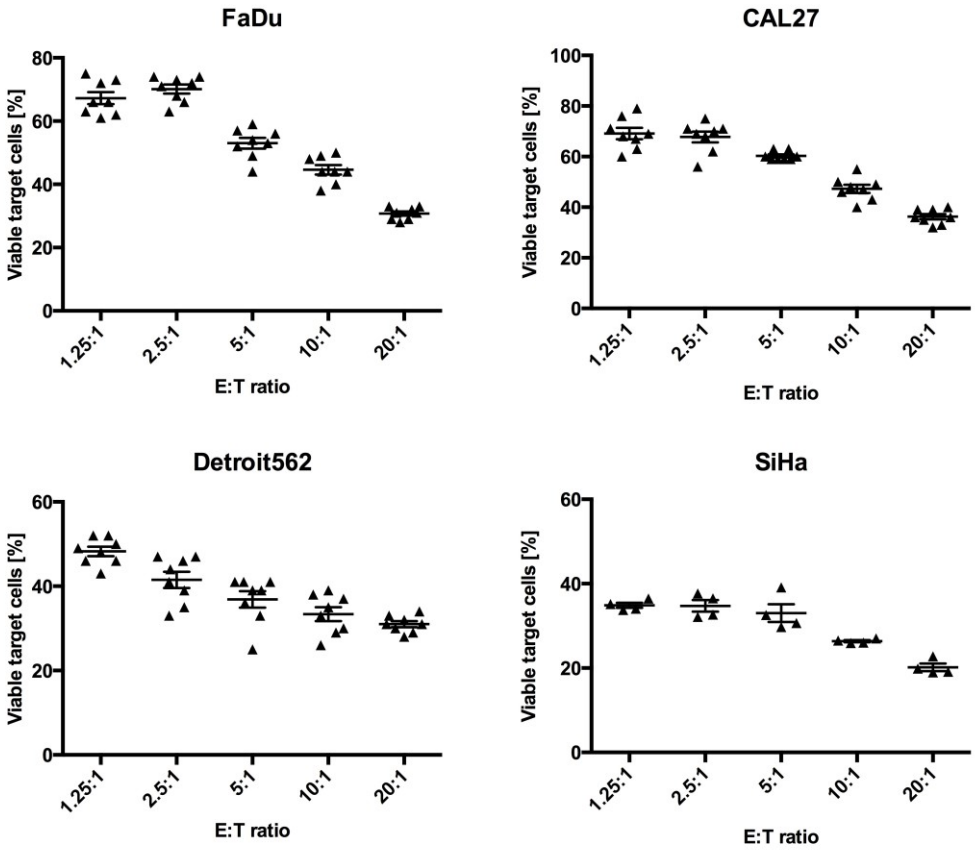

Figure 20: NK cell cytotoxicity against tumor spheroids.
CFSE-labeled FaDu, CAL27, Detroit562 and SiHa tumor spheroids were co-cultured with NK cells at different E:T ratios for 48 h. Tumor spheroid destruction was quantified by flow cytometry and evaluation of viable ($CFSE^+/SytoxBlue^-$) and dead target ($CFSE^+/SytoxBlue^+$) cells. Data are presented as percentage viable target cells with mean ± SEM of 8 individual tumor spheroids of a representative experiment.

3.2.2 HNSCC Tumor Spheroids show a characteristic Signature of shed NKG2D Ligands

HNSCC and SiHa cell lines showed a defined surface expression pattern of the NKG2D ligands MICA, MICB and ULBP2/3 (Figure 21 and Table 11). Moreover, HNSCC cell lines

generated from primary tumors are usually low for ULBP1 due to loss of ULBP1 expression during cell line generation [412]. The differences of NKG2D ligand expression of primary tumor cells and cell lines can be explained by differential transcriptional regulation of the individual ligands mediated by environmental factors.

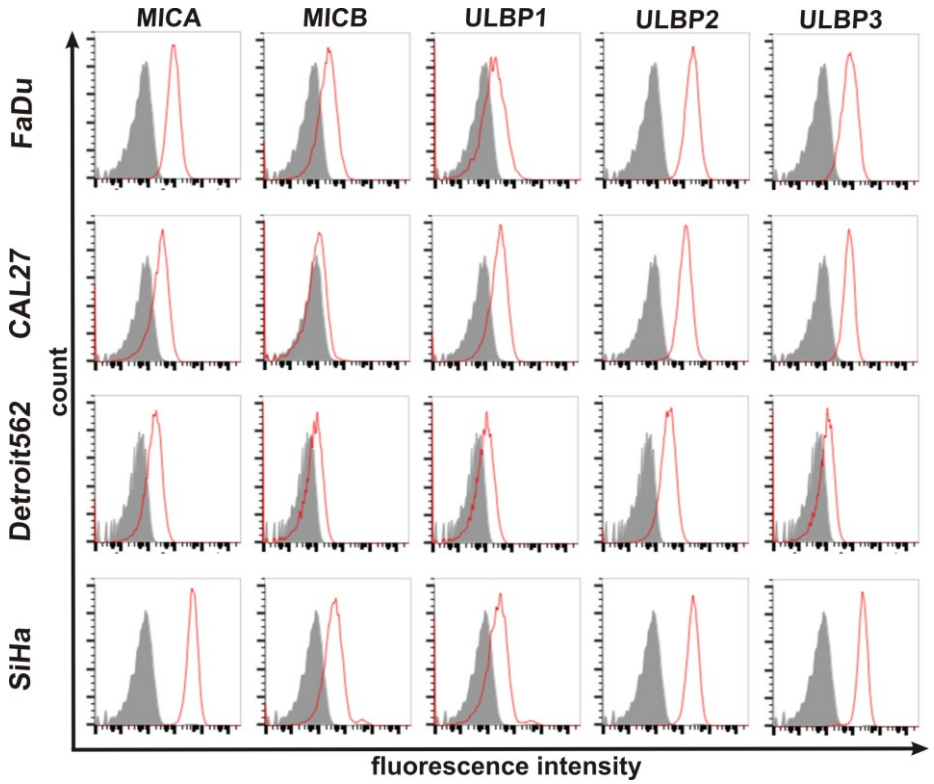

Figure 21: NKG2D ligand surface expression on tumor cell lines.
Surface expression of NKG2D ligands (MICA, MICB, ULBP1-3) on FaDu, CAL27, Detroit562 and SiHa tumor cells analyzed by flow cytometry. Grey = isotype control, red = NKG2DL antibody. One representative experiment of four is shown.

The expression of the individual NKG2D ligands were compared and summarized as expression patterns for each cell line in Table 11.

Table 11: NKG2D ligand expression patterns on cell lines.
Expression calculated from median fluorescence intensities (MFI) presented as +/- = no/weak, + = weak, ++ = moderate and +++ = high expression (n = 8).

Cell line	MICA	MICB	ULBP1	ULBP2	ULBP3
FaDu	+++	++	+/-	++	+
CAL27	++	+	+	+++	+/-
Detroit562	++	+	+/-	++	+
SiHa	+++	+	+	+++	+++

In order to investigate NKG2D ligand shedding in HNSCC tumor spheroids, supernatants were probed for the levels of sMICA, sMICB, sULBP1, sULBP2 and sULBP3 over three days (d0, d1, d2) by respective ELISAs. Due to continuous shedding, soluble NKG2D ligands accumulated in the supernatant of FaDu, CAL27, Detroit562 and SiHa tumor spheroids reaching saturation after three days of culture (Figure 22).

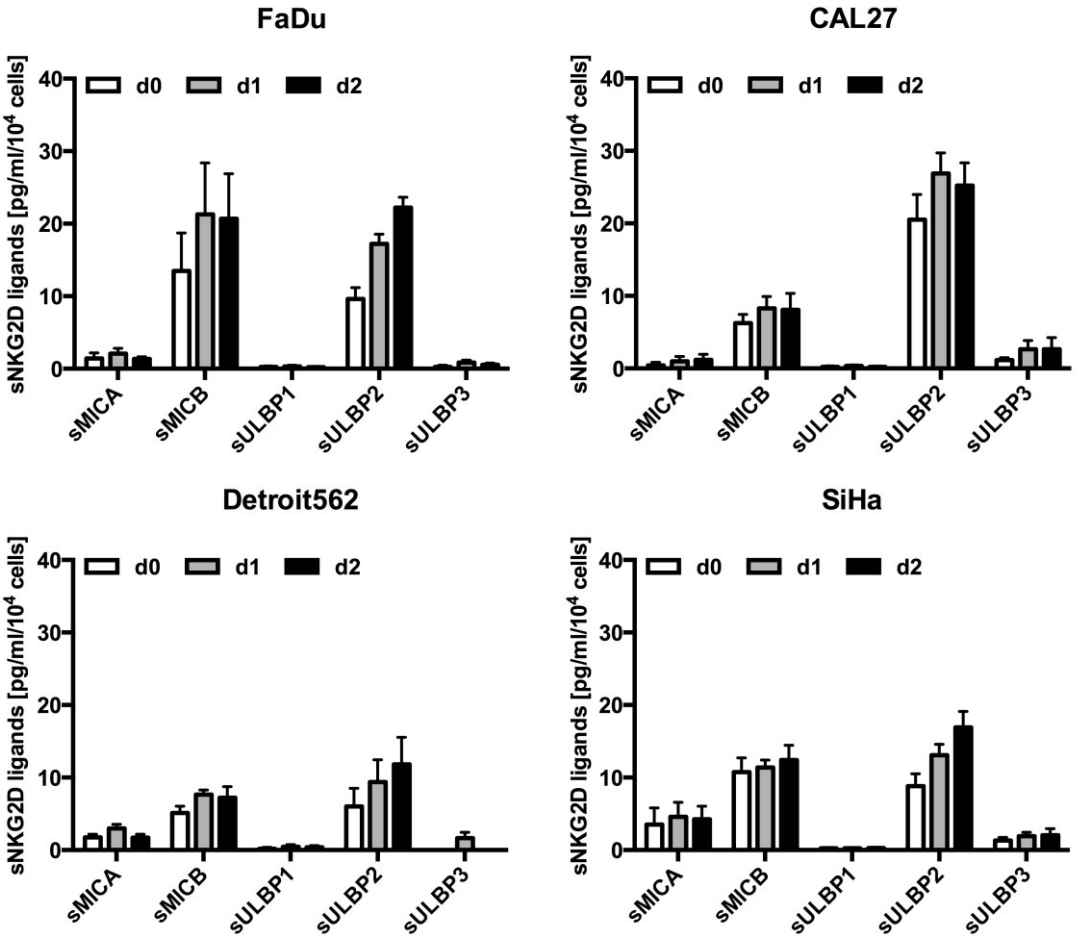

Figure 22: Tumor spheroids continuously shed NKG2D ligands.
Kinetics of sNKG2D ligand release analyzed in FaDu, CAL27, Detroit562 and SiHa tumor spheroids. Supernatants of tumor spheroids were collected on three consecutive days (d0-d2) and concentrated 10-fold. sMICA, sMICB and sULBP1-3 concentrations were analyzed by respective ELISAs and data are shown as mean ± SEM in pg/ml/10^4 cells of three independent experiments, measured in duplicates.

The predominant ligands shed into the supernatant of tumor spheroids grown from these cell lines within two days were sMICA (FaDu: 1.3 ± 0.3 pg/ml per 10^4 cells; CAL27: 1.2 ± 0.8 pg/ml per 10^4 cells; Detroit562: 1.7 ± 0.4 pg/ml per 10^4 cells; SiHa: 4.3 ± 1.8 pg/ml per 10^4 cells), sMICB (FaDu: 20.7 ± 6.2 pg/ml per 10^4 cells; CAL27: 8.1 ± 2.2 pg/ml

per 10^4 cells; Detroit562: 7.7 ± 0.5 pg/ml per 10^4 cells; SiHa: 4.3 ± 1.8 pg/ml per 10^4 cells) and sULBP2 (FaDu: 22.2 ± 1.4 pg/ml per 10^4 cells; CAL27: 25.2 ± 3.1 pg/ml per 10^4 cells; Detroit562: 11.8 ± 3.7 pg/ml per 10^4 cells; SiHa: 16.9 ± 0.4 pg/ml per 10^4 cells). Notably, sULBP3 and sULBP1 were low or close to the detection limit of the assay with sULBP3 mainly found in supernatants of CAL27 and SiHa tumor spheroids (CAL27: 2.7 ± 1.6 pg/ml per 10^4 cells; SiHa: 2.0 ± 0.9 pg/ml per 10^4 cells). Interestingly, the kinetics of soluble NKG2D ligand release into the supernatant parallels the expression level and loss of MICA/B, and ULBP2/3 from the cell surface. Moreover, sNKG2D ligands accumulate in the supernatant after 48 h. Theses data demonstrate a continuous ligand shedding by tumor cells itself with a rapid reproduction and accumulation of sNKG2D ligands as it is seen in cancer patients.

3.2.3 sNKG2D Ligands diminish NK Cell Cytotoxicity towards Tumor Spheroids

To investigate the impact of sNKG2D ligands on NK cell cytotoxicity towards tumor spheroids, solid tumor spheroids were co-cultured with primary human NK cells pre-incubated with CAL27 cell culture supernatant (CAL27 SN) containing high sNKG2D ligand levels (27.63 ng/ml), or sNKG2D ligand-depleted CAL27 supernatant (sNKG2D ligands: 2.66 ng/ml; Figure 23B). NK cells pre-incubated in basal culture medium served as controls. NK cell cytotoxicity towards individual tumor spheroids was analyzed after 48 h co-incubation by flow cytometry based on the loss of CFSE-labeled target cells. In the absence of sNKG2D ligands (kill CO), NK cells efficiently destroyed tumor spheroids with 59%, 58% and 43% lysis of FaDu, CAL27 and SiHa tumor spheroids, respectively (Figure 23A). By contrast, in the presence of shed NKG2D ligands (CAL27-SN), NK cell killing was strongly inhibited by 25% for FaDu and 46% for SiHa tumor spheroids demonstrating the large degree of NKG2D-dependency on NK cell killing as shown earlier with blocking antibodies in single cell cytotoxicity experiments. Moreover, 19% NKG2D ligand-dependent inhibition of tumor spheroid destruction could be seen for CAL27 cells, which are less susceptible to NKG2D-dependent killing. Importantly, impaired tumor spheroid destruction could be restored by specific depletion of sNKG2D ligands (SN depleted) from cell culture supernatant (Figure 23A/B). Again, sNKG2D ligand-dependent inhibition of NK cells' cytotoxic function was

correlated with NKG2D inhibition and downregulation (Figure 23C). Thus, the inhibitory potential of sNKG2D ligands in HNSCC plasma and their role in tumor recognition and elimination could be verified under *in vivo*-like conditions in the tumor spheroid model.

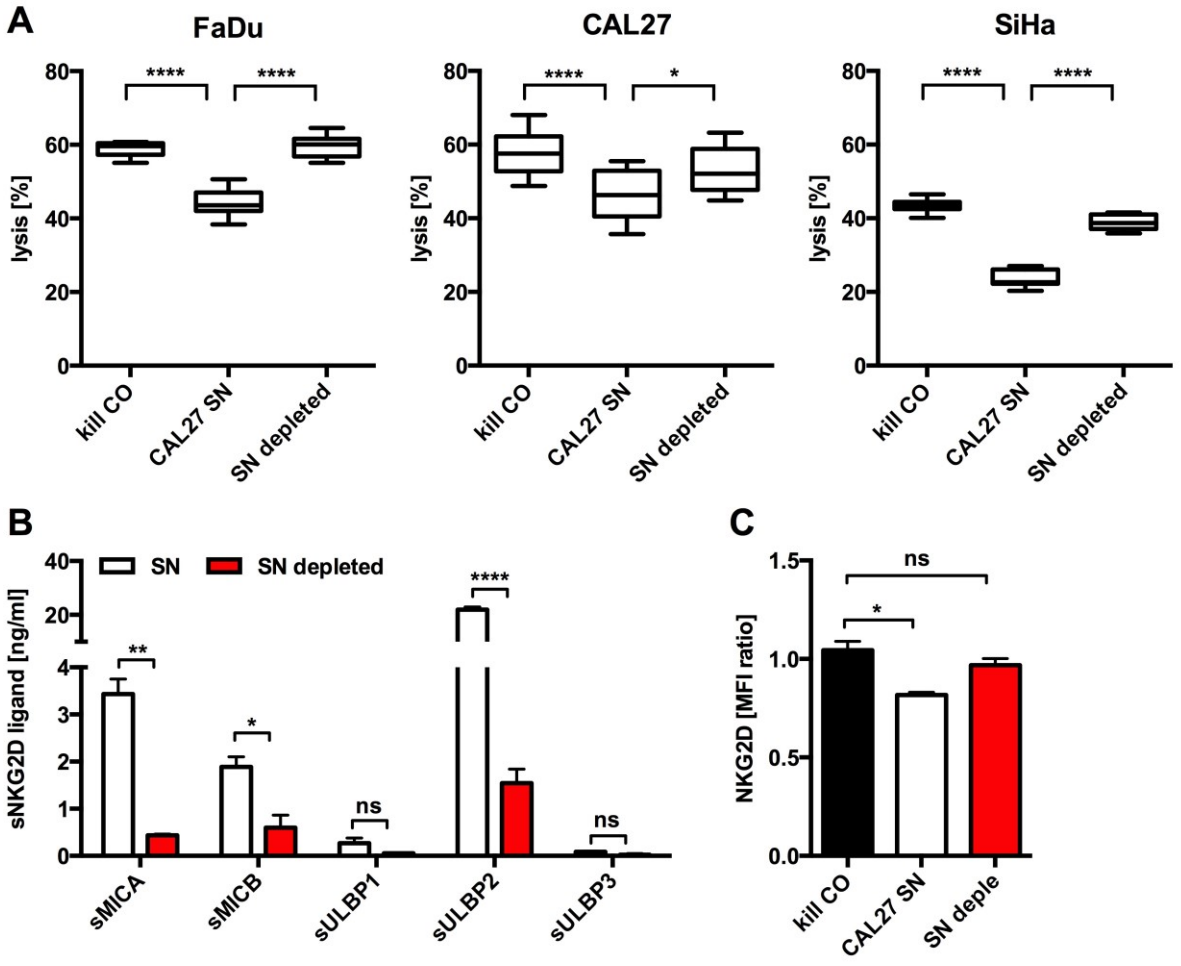

Figure 23: NK cell cytotoxicity towards tumor spheroids is inhibited by sNKG2D ligands.
(A) Primary human NK cells pre-incubated overnight with CAL27 SN, NKG2D ligand-depleted SN or medium (kill CO) prior to co-incubation with CFSE-labeled tumor spheroids for 48 h. FaDu, CAL27 or SiHa tumor spheroid lysis measured by flow cytometric analysis of live ($CFSE^+/SytoxBlue^-$) and dead ($CFSE^+/SytoxBlue^+$) tumor cells (see also Figure S3). Bars correspond to mean ± SEM of 8 tumor spheroids of a representative experiment. (B) sNKG2D ligand levels of non-/ and sNKG2D ligand-depleted CAL27 supernatant analyzed by ELISAs. Data are shown as mean ± SEM of duplicates of a representative experiment. Statistical significance was analyzed using one-way ANOVA with: ns = non-significant for $p > 0.05$, * $p < 0.05$, ** $p = 0.005$, *** $p = 0.0001$ and **** $p < 0.0001$. (C) Flow cytometric analysis of NKG2D surface expression on primary human NK cells after incubation with CAL27 SN or sNKG2D ligand-depleted SN. Data are represented as MFI ratio normalized to kill CO as mean ± SEM of duplicates of a representative experiment. Statistical significance was analyzed by Student's t-test for $p < 0.05$.

3.2.4 sNKG2D Ligands impair NK Cell Infiltration in Tumor Spheroids

NK cell infiltration is a prerequisite for NK cell function and tumor immunosurveillance [413]. Strikingly, NK cell infiltration into primary HNSCC tumor tissues was nearly absent as shown by imunohistochemical stainings for $CD56^+$ cells. Up to now, many studies extensively investigated NK cell cytotoxicity in well-established functional assays, whereas little is known about NK cell infiltration due to the lack of appropriate model systems for solid tumors. In this study, *in vivo*-like tumor spheroids were used as 3D model system for the long-term analysis of tumor immunosurveillance and immune cell infiltration. For infiltration studies, primary human NK cells were mixed with tumor cells at a low E:T ratio of 1:1, to reduce tumor spheroid destruction and allow for the analysis of infiltrated NK cells, and seeded into 1.5% agarose-coated 96-well plates. NKG2D-dependent cytotoxicity was inhibited by NK cell pre-incubation overnight with a cocktail of shed NKG2D ligands (CAL27 SN) or purified sMICA (20 ng/ml). Tumor spheroid integrity was monitored by light microscopy for 48 h. During co-incubation, NK cells proliferated and accumulated in the periphery of the tumor spheroids as seen in phase contrast pictures. At endpoint of analyses, cryosections of tumor spheroids were stained with CD45-specific antibodies for the detection of infiltrated NK cells (Figure 24A and Figure S4A/B). In the absence of sNKG2D ligands (Kill CO), NK cell killing was accompanied by massive infiltration into HNSCC and SiHa spheroids. Roughly 66%, 38% and 65% of the cells comprising the FaDu, CAL27 or SiHa tumor spheroids, respectively, were NK cells (Figure 24C). In contrast, NK cell infiltration was strongly inhibited in the presence of a cocktail of different sNKG2D ligands or sMICA. Here, only 38%, 21% and 29% of the cells comprising the FaDu, CAL27 or SiHa tumor spheroids, respectively, were NK cells (Figure 24B). Interestingly, the same amount of sMICA alone was sufficient for NK cell inhibition when compared to the cocktail of all shed ligands in the CAL27 supernatant. These data support the finding, that the total burden of sNKG2D ligands is crucial for NK cell dysfunction in cancer patients. Furthermore, staining of tumor spheroid cryosections for apoptosis induction (anti-cleaved caspase-3 antibodies) demonstrated the degree of tumor cell lysis and moreover, that infiltrated, pre-treated NK cells were often double positive for CD45 and cleaved caspase-3 compared to untreated NK cells. Thus, NK cells might show an exhausted phenotype and therefore proliferate less and become apoptotic under inhibitory conditions.

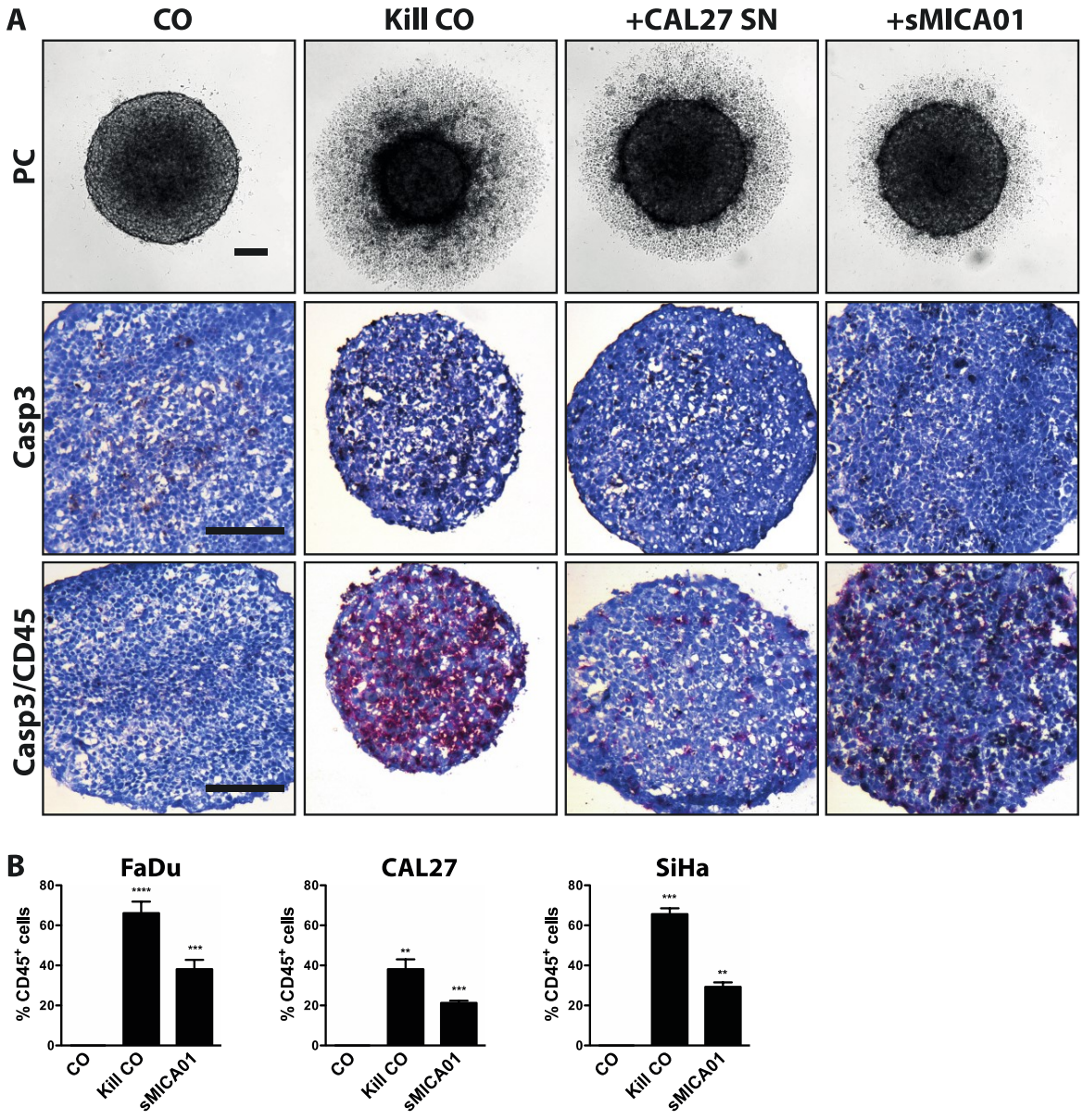

Figure 24: NK cell infiltration into tumor spheroids is inhibited by sNKG2D ligands.
NK cells pre-treated overnight with CAL27 SN, sMICA01 or untreated (kill CO) prior to co-culturing with FaDu, CAL27 or SiHa cells for 48 h (see also Figure S4). (A) Representative phase contrast pictures of FaDu tumor spheroids at 50x magnification after 48 h are shown. Cryosections of spheroids were stained for NK cells (anti-CD45 antibody, red) and apoptosis (anti-active caspase-3 antibody, brown). Representative histology pictures are shown at 200x magnification. Size bar corresponds to 200 µm. (B) Percentage of infiltrated NK cells in FaDu, CAL27 or SiHa tumor spheroids quantified in 10 vision fields of cryosections under 200x magnification with ImageJ. Bars correspond to mean ± SEM of 10 vision fields counted individually and significance compared to CO was determined by Student's t-test. ** $p = 0.005$, *** $p = 0.0001$ and **** $p < 0.0001$.

NK cells can be divided into two major sub-populations based on the relative expression of the markers CD16 and CD56. Whereas the $CD56^{dim}/CD16^{+}$ population is the pre-dominant population in peripheral blood and is characterized by its cytotoxic function, $CD56^{bright}/CD16^{dim/-}$ NK cells are abundant cytokine producers and have an immunoregulatory role [414]. To further identify the infiltrated NK cells, expanded primary human NK cells were sorted for the cytotoxic ($CD56^{dim}/CD16^{+}$) and regulatory ($CD56^{bright}/CD16^{dim/-}$) populations. FaDu tumor spheroids were incubated for 48 h with either NK cell population at an E:T ratio of 1:1 for infiltration studies. Cryosections stained with CD45-specific antibodies revealed, that both populations infiltrated tumor spheroids to the same extend (Figure 25). Thus, indicating that not only cytotoxic NK cells play a role in tumor elimination, but also regulatory NK cells are needed for effective tumor immunosurveillance.

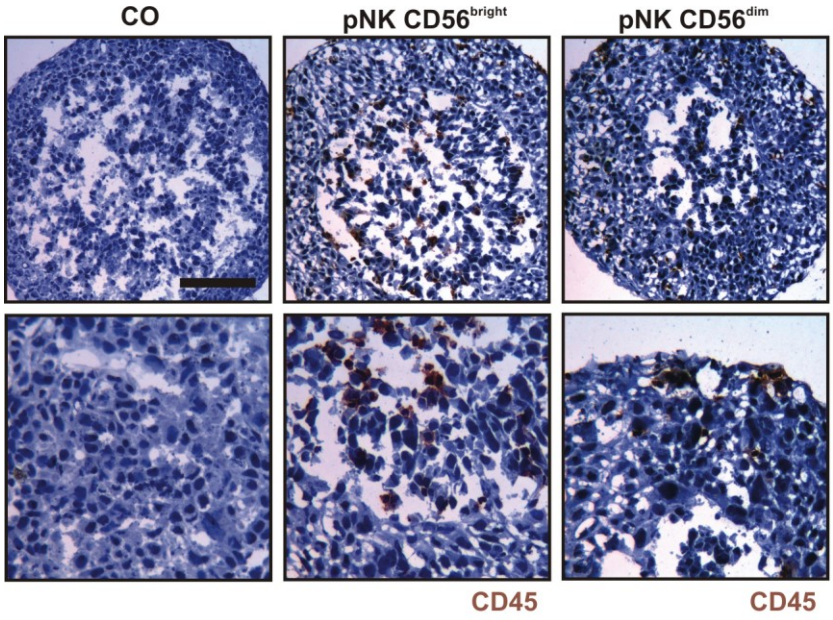

Figure 25: Cytotoxic and regulatory NK cells infiltrate tumor spheroids.
FaDu tumor spheroids were co-cultured with sorted pNK cells (cytotoxic $CD56^{dim}/CD16^{+}$ and regulatory $CD56^{bright}/CD16^{dim/-}$). Cryosections of tumor spheroids were stained for NK cell infiltration (anti-CD45 antibody, red) and representative pictures are shown under 200x (top row) and 400x (bottom row) magnification. Size bar correspond to 200 µm and 100 µm, respectively.

The presented infiltration studies demonstrated a direct correlation of NK cell cytotoxicity and infiltration for successful elimination of *in vivo*-like solid tumor spheroids. Moreover, tumor spheroid assays revealed for the first time an NKG2D-dependent inhibition of NK cell infiltration capacity. Thus, sNKG2D ligands impair NK cell functions not only on the cytotox-

ic level, but also facilitate tumor escape due to the failure to infiltrate tumors. Further studies are needed to characterize phenotypic differences of infiltrating and non-infiltrating peripheral NK cell sub-populations. In this context, a MACS-based (magnetic activated cell sorting) protocol for the isolation and quantification of tumor spheroid infiltrated NK cells was established, which allows for phenotypic analysis of the different NK cell subpopulations in future studies (see 5.1.4, Figure S5) [387].

3.3 Adsorption Apheresis to deplete sNKG2D Ligands

The analysis of HNSCC plasma suggests that the cumulative plasma level of all sNKG2D ligands is indicative for the extent of NKG2D-dependent tumor immune escape in HNSCC. Importantly, the specific depletion of sNKG2D ligands from HNSCC patients' plasma or cell culture supernatant could efficiently restore NK cell functions. Consequently, plasma depletion of sNKG2D ligands might be a clinical intervention strategy to significantly boost anti-tumor efficacy of $NKG2D^+$ cytotoxic lymphocytes. Moreover, combining cellular therapies with adsorption apheresis of sNKG2D ligands could not only be beneficial for autologous, but also for adoptively transferred immune cells after haploidentical stem cell transplantation. For this purpose, an adsorption apheresis procedure based on a bioreactive surface was developed for a new collaborative medical approach prior to cell-based therapies to improve the clinical outcome for cancer patients.

3.3.1 Monoclonal Antibodies to deplete sMICA

For a proof of concept study, monoclonal anti-MICA antibodies, raised by immunizing BALB/c mice with a mixture of MICA*01 and MICA*04 [296], were screened for their suitability to generate a biofunctionalized surface for the depletion of sMICA from human plasma. The MICA-specific antibody clone AMO1 and the MICA/B-specific antibody clone BAMO3, which were used in sandwich ELISA for sMICA detection, were further characterized. The antibody epitopes were determined using MICA peptide spot arrays (Figure 26B/D; see 5.1.6). The AMO1 antibody specifically recognizes an epitope (NKTWDRET) in the α1-helical domain of MICA (Figure 26A/B), which is conserved throughout different allelic variants (see 5.1.9.1). In contrast, the BAMO3 antibody binds to an epitope (RICQGEEQRF) in

the α3-helical domain of MICA (Figure 26C/D), which is also present in the α3-helical domain of MICB (see 5.1.9.2).

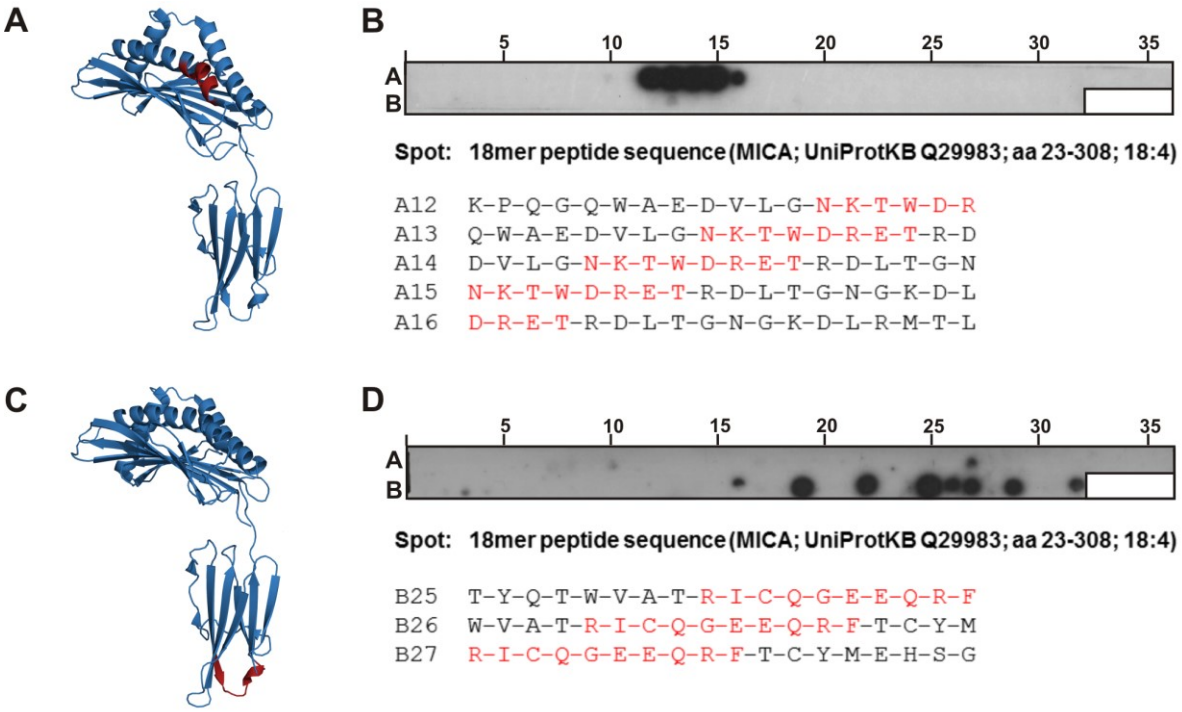

Figure 26: Epitope mapping of anti-MICA monoclonal antibodies.
(A/C) Crystal structure of the unbound sMICA ectodomain (blue) containing the amino acids 23 - 297 and the epitope of the (A) anti-MICA antibody (AMO1) in the α1-helical domain (NKTWDRET; red) and (C) the anti-MICA antibody (BAMO3) in the α3-helical domain (RICQGEEQRF; red); PDB 1HYR. (B/D) Peptide spot arrays (18mer peptides; off-set of 4 amino acids) of the human MICA were incubated with the anti-MICA antibodies and detected with an anti-mouse IgG HRP-conjugated antibody. The signals of spots (B) A11-A16 mark the epitope region in the α1-helical domain and (D) B25-B27 the epitope region in the α3-helical domain. Corresponding sequences of the spots are depicted; overlapping amino acids are marked in red. Complete spot sequences are depicted in 5.1.6, antibody control in Figure S10.

To test the depletion capacity of the monoclonal antibodies, either cell culture supernatant containing recombinant soluble MICA*01 and MICA*04 allelic variants or human plasma supplemented with sMICA*01/04 (production and purification of sMICA variants Figure S7) were incubated with antibody-coupled sepharose beads over night. Analysis of sMICA levels pre- and post-depletion showed efficient removal of sMICA from cell culture supernatant for both anti-MICA antibodies, whereas beads coupled to a mouse IgG antibody control had no effect (Figure 27). Unexpectedly, efficient depletion of sMICA from human plasma could only be achieved for the antibody with the epitope in the α1-helical domain (Figure 27A). In contrast, the antibody directed against the α3-helical domain could not mediate sMICA deple-

tion. This failure was also seen for monoclonal antibodies raised against a specific peptide within the α3-helical domain of MICA (data not shown). Thus, the α3-helical domain of sMICA might possess a binding site for an additional factor in human plasma leading to the blocking of the antibody epitope. This hypothesis is supported by the existence of an interaction site of the disulphide isomerase ERp5 needed for MICA proteolysis, which is also located in the α3-helical domain between the two cysteins (C225 and C282) [299]. Since plasma is a highly complex protein mixture, the identification of an interfering factor was not further addressed in this study.

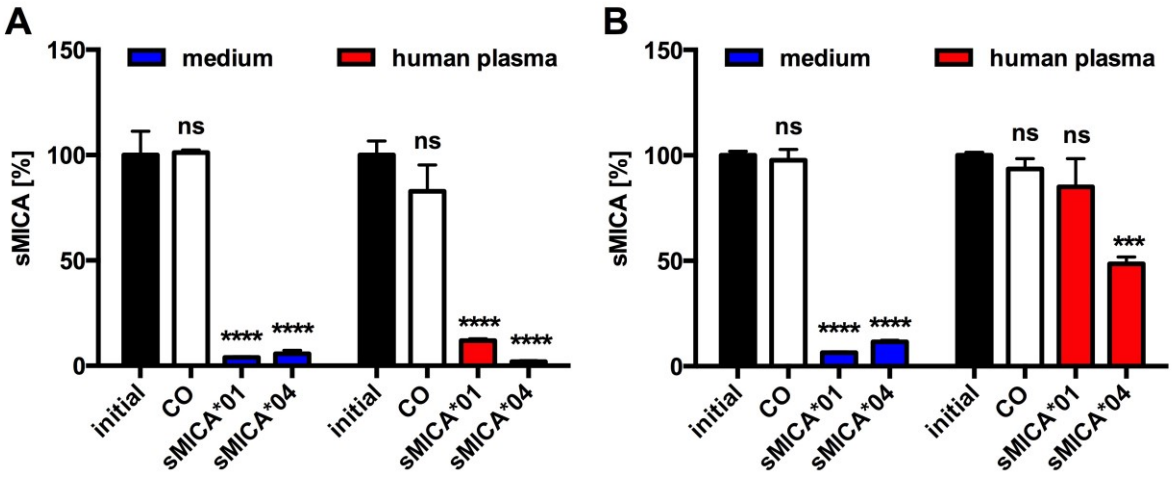

Figure 27: Depletion capacity of anti-MICA monoclonal antibodies.
Human plasma or cell culture medium supplemented with recombinant sMICA*01 or sMICA*04 (20 ng/ml) was incubated overnight with beads coupled to anti-MICA antibodies binding in the (A) α1-helical domain (AMO1) or (B) α3-helical domain (BAMO3). Beads with mouse IgG_1 antibody served as control (CO). sMICA levels were measured by ELISA and normalized to the initial sMICA concentration. Data are represented as mean ± SEM of duplicates of a representative experiment. Statistical significance compared to CO was determined by Student's t-test. ns = non-significant for $p > 0.05$, *** $p < 0.001$ and **** $p < 0.0001$.

For further evaluation, the monoclonal antibody against sMICA with the epitope in the α1-helical domain was covalently coupled to magnetic beads. To test the depletion efficacy of the anti-MICA antibody beads, human plasma of 20 different healthy donors was supplemented with recombinant sMICA*04. *In vitro* depletion experiments with the antibody-coupled beads showed a depletion efficiency of 97% for sMICA from human plasma independent of the donor immune status or plasma contents (Figure 28A). Since MICA is a highly polymorphic NKG2D ligand with over 70 known allelic variants and the allelic identity of sMICA in patients' serum is unknown, next the recognition and depletion capacity of the anti-MICA anti-

body against sMICA allelic variants frequently found in the Caucasian population [249] was determined. Therefor, C1R cells transfected with the single MICA allelic variants MICA*01, MICA*04, MICA*07 and MICA*08 (see 5.1.9.1 alignment of MICA allelic variants) were used and MICA shedding/release was induced by serum starvation.

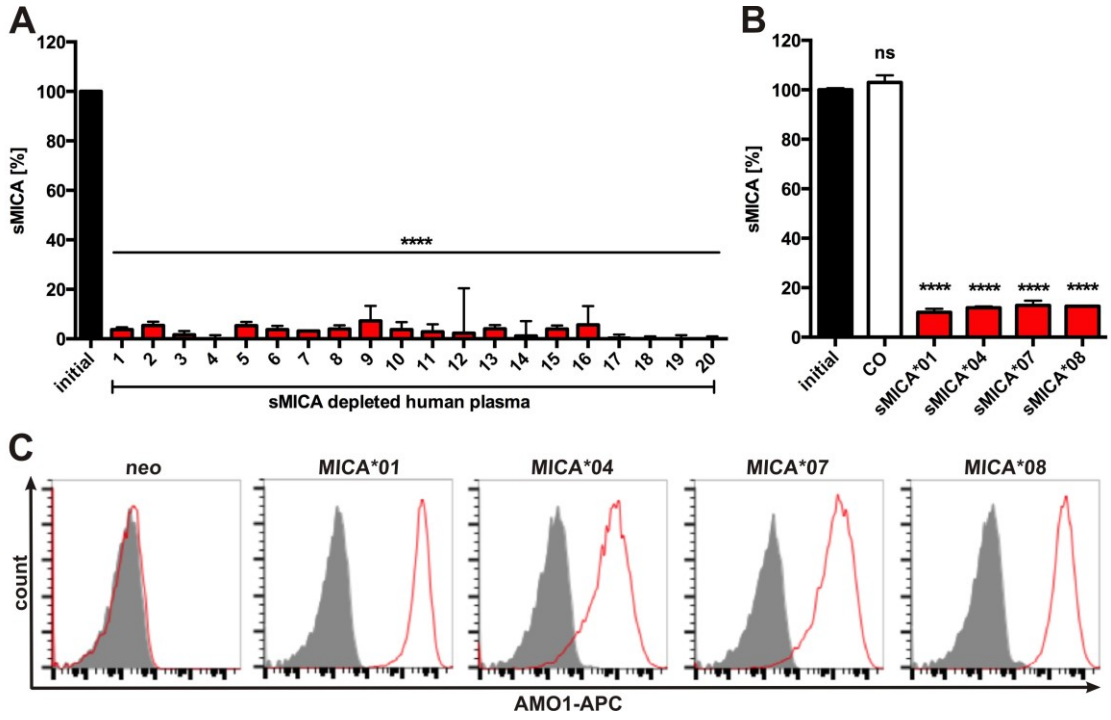

Figure 28: sMICA depletion by adsorption apheresis using an anti-MICA antibody.
(A) Depletion of sMICA*04 (20 ng/ml) from human plasma (20 healthy donors) with AMO1 antibody-coupled beads overnight. Soluble MICA*04 plasma levels pre- (initial) and post-depletion (1 - 20) were measured by ELISA and normalized to the initial sMICA*04 level. Data represented as mean ± SEM of duplicates of a representative experiment. (B) Depletion of sMICA allelic variants (sMICA*01, sMICA*04, sMICA*07 and sMICA*08) from C1R supernatants with AMO1 antibody-coupled beads overnight. Beads with mouse IgG_1 antibody served as control (CO). sMICA levels were measured by ELISA and normalized to the initial sMICA levels. Data are represented as mean ± SEM of two experiments measured in duplicates. Statistical significance compared to CO was determined by Student's t-test; **** $p < 0.0001$. (C) Flow cytometric analyses of AMO1 antibody binding to C1R cell transfectants expressing sMICA allelic variants (sMICA*01, sMICA*04, sMICA*07 and sMICA*08) or C1R mock transfected (neo) cells. The antibody was directly conjugated to APC. Grey = isotype control; red = AMO1 antibody.

Staining of the different C1R cell clones with the antibody showed comparable surface expression of the MICA allelic variants (Figure 28C). The *in vitro* depletion of the cell supernatants containing the distinct sMICA allelic variants demonstrated a high depletion capacity of 89% for all sMICAs tested (Figure 28B). Moreover, these data show, that beside soluble

NKG2D ligands also exosomes containing NKG2D ligands (MICA*08) could be efficiently removed.

In a next step, the anti-MICA antibody was covalently coupled to a sepharose matrix to generate an adsorber cartridge for sMICA apheresis. In an *ex vivo* apheresis-like experiment the cartridge containing the antibody-functionalized sepharose was coupled to a pumping-system (Äkta Prime System) and depletion efficacy was evaluated using a 200 ml human plasma reservoir supplemented with sMICA*04 (Figure 29A). The residual sMICA*04 plasma levels were determined by ELISA after each plasma volume exchange through the adsorber cartridge with a flow rate of 25 ml/min. Efficient removal of sMICA from human plasma could be achieved after one volume exchange with 50% residual sMICA compared to the initial plasma level (Figure 29B). Moreover, after several rounds of plasma exchange 90% of sMICA*04 could be removed.

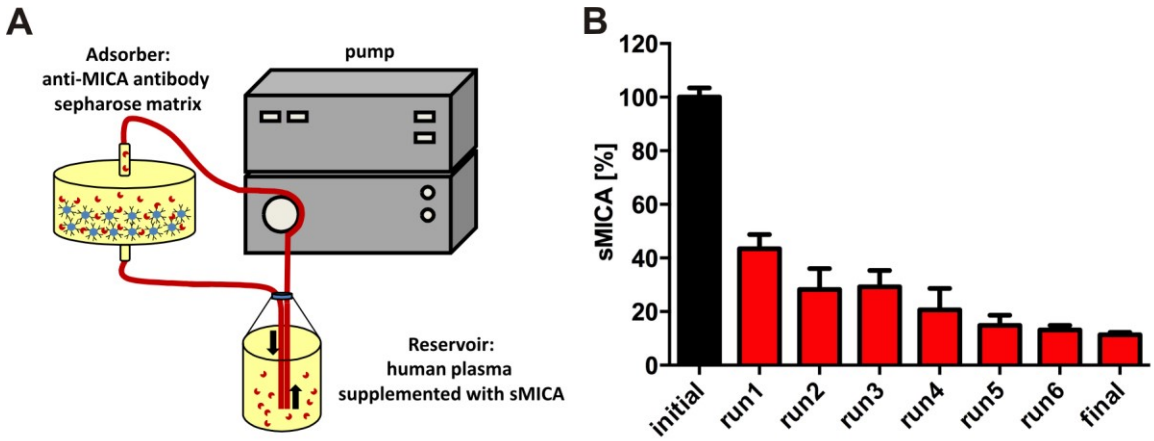

Figure 29: *Ex vivo* depletion of sMICA*04 from human plasma using an adsorber cartridge.
(A) Schematic overview of the *ex vivo* sMICA depletion from human plasma under apheresis-like conditions using an Äkta Prime System with an adsorber cartridge containing the anti-MICA antibody covalently coupled to a sepharose matrix. (B) Human plasma (200 ml from a healthy volunteer) was supplemented with sMICA*04 (20 ng/ml) and the plasma was run through the adsorber cartridge with a flow rate of 25 ml/min. After each plasma exchange (run 1 - 6) sMICA*04 concentrations were measured by ELISA and normalized to the initial sMICA*04 plasma concentration. Data are represented as mean ± SEM of two independent experiments measured in duplicates.

The characterization and *in vitro* depletion experiments using the functionalized sepharose matrix clearly demonstrated that the anti-MICA monoclonal antibody directed against a conserved epitope in the α1-helical domain is a promising candidate for an adsorption apheresis of sMICA from plasma of cancer patients.

3.3.2 Pan-specific Depletion of sNKG2D Ligands using NKG2D Proteins

Analyses of HNSCC patients' plasma revealed an individual pattern for NKG2D ligand release. Moreover, it could be shown that the cumulative level of sNKG2D ligands is important for the extent of NKG2D-dependent inhibition of cytotoxic lymphocytes. Regarding different cancer entities, the individual impact of NKG2D ligands to tumor immune escape can vary. Therefore, the simultaneous removal of all sNKG2D ligands might be important for a clinical intervention strategy aiming at a broad patient cohort independent on the individual clinical situation. For this purpose, different recombinant NKG2D proteins were generated and characterized for their suitability as a pan-specific tool to generate a biofunctionalized surface for the simultaneous adsorption apheresis of all sNKG2D ligands from human plasma.

3.3.2.1 NKG2D Proteins expressed in E. coli

NKG2D is a homodimeric type II transmembrane protein with an extracellular C-type lectin-like domain [243]. The production of high amounts of functional homodimeric recombinant protein is challenging with regard to correct protein folding and formation of disulfide bonds. The most popular and well-established expression host for the fast and efficient generation of recombinant proteins in high amounts at low costs is *Escherichia coli* [415]. Most *E. coli* strains have disadvantages such as lack of posttranslational modifications (i.e. glycosylation) or are incapable of disulfide bond formation, and therefore overexpression of recombinant proteins often results in protein aggregation and formation of intracellular inclusion bodies [416, 417]. Inclusion body formation might be favored to yield high amounts of proteins, which are protected from proteolytical degradation. These proteins allow for the generation of native-folded proteins due to *in vitro* refolding strategies [418]. In this thesis, the NKG2D extracellular domain was produced in the BL21 (DE3) *E. coli* strain using an optimized IMAC purification and refolding protocol adapted from Steinle *et al.* [249]. Two rNKG2D variants were produced containing different affinity-tags for immobilization to generate a biofunctionalized matrix. The rNKG2D-Biotin protein containing a C-terminal His-tag for affinity purification and an additional N-terminal Avi-tag, which allows for *in vitro* biotinylation of the protein, was purified from inclusion bodies and refolded (Figure 30). Analysis of the elution fractions after affinity purification from inclusion bodies revealed high amounts of pure unfolded rNKG2D protein with a molecular mass of about 17 kDa which accounts for mono-

meric proteins (Figure 30A). Moreover, protein aggregates or dimeric protein forms with a molecular mass of 35 kDa could be detected. After refolding, to ensure formation of intramolecular disulfide bonds and thus correct protein folding, the protein was *in vitro* biotinylated to generate the actual rNKG2D-Biotin and further purified by SEC (Figure 30B/C). Although highly pure biotinylated dimeric rNKG2D could be produced as shown by SDS-PAGE and immunoblot analyses, most of the protein purified from inclusion bodies precipitated during the refolding procedure and formed aggregates as seen in the SEC chromatogram (fraction *). Only around 2-5% of protein isolated from inclusion bodies (0.3 mg protein per litre of *E. coli* culture) showed the correct folding and could be used for further functional assays.

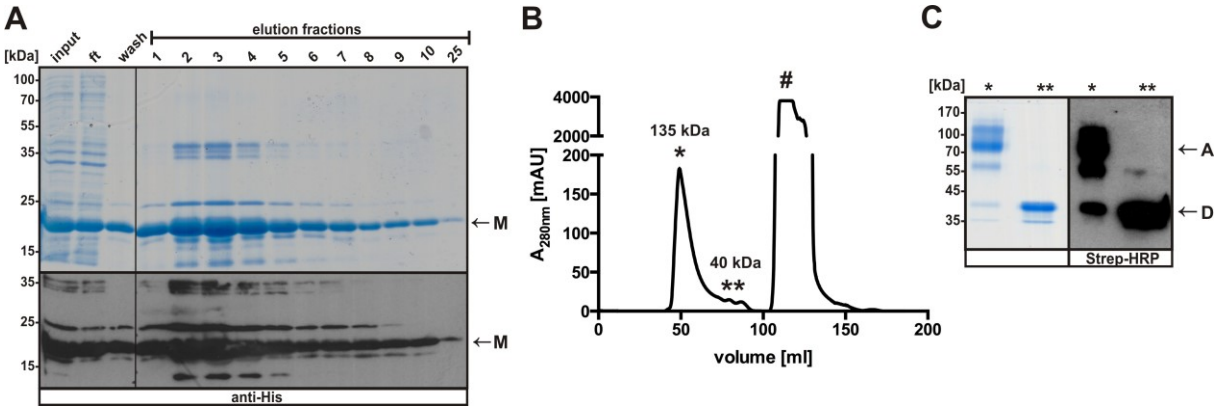

Figure 30: Affinity purification and biotinylation of NKG2D produced in *E. coli*.
(A) Reducing SDS-PAGE (Coomassie-stained) and immunoblot (anti-His HRP-conjugated antibody) of aliquots (input, flow-through (ft), wash and eluate fractions) after affinity purification via Ni-NTA agarose from *E. coli* inclusion bodies. M = monomeric rNKG2D. (B) Size exclusion chromatography (SEC) of refolded and *in vitro* biotinylated rNKG2D on a HiLoad 16/600 Superdex 200 pg column. Peaks correspond to * = aggregated protein (~135 kDa), ** = biotinylated NKG2D dimers (~40 kDa), # = unbound biotin. (C) Pooled peak fractions (*; **) of SEC were analyzed by non-reducing (- DTT) Coomassie-stained SDS-PAGE and immunoblot (streptavidin HRP-conjugate). A = aggregates; D = dimers.

The high amounts of aggregated proteins during refolding and *in vitro* biotinylation of rNKG2D-Biotin substantially decreased the protein yield of dimeric rNKG2D. To improve the production of rNKG2D and to analyze the impact of the affinity-tags on protein folding, in a second approach rNKG2D-His was produced containing a C- or N-terminal His-tag only. Compared to the biotinylated rNKG2D, IMAC purification of rNKG2D-His from inclusion bodies showed higher protein yield and reduced aggregate formation (shown exemplarely for rNKG2D with N-terminal His-tag, Figure 31A). Moreover, CD spectrometric analysis of rNKG2D with the N-teminal His-tag after refolding showed that the protein had a homogene-

ous fold consisting of predominantly β-sheet secondary structures (Figure 31B) which is in accordance with the crystal structure of NKG2D published by Li *et al.* [243]. SDS-PAGE analysis under non-reducing conditions showed a highly pure rNKG2D-His protein comprising the monomeric and dimeric form (Figure 31C). Around 1 mg of rNKG2D-His could be obtained per litre of *E. coli* culture. In contrast, although the rNKG2D with the C-terminal His-tag resembled the N-terminal tagged protein in SDS-PAGE, this protein showed a more α-helical secondary structure after refolding in CD spectroscopy and was not functional in binding studies on NKG2D ligand expressing cells as shown by J. Havenstein (group of J. Koch, Georg-Speyer-Haus, Frankfurt am Main [419]). Thus, the positively charged His-tag positioned at the C-terminus impaired the folding of the protein, whereas positioning at the truncated N-terminus of rNKG2D was favorable. The N-terminal tagged protein was further used in functional studies in comparison with the rNKG2D-Biotin.

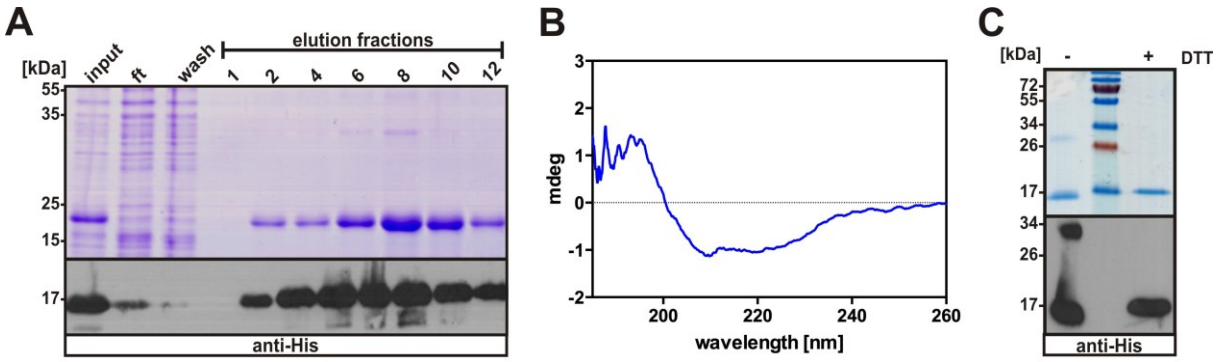

Figure 31: Characterization of *E. coli* derived rNKG2D-His.
(A) Reducing SDS-PAGE (Coomassie-stained) and immunoblot (anti-His HRP-conjugated antibody) of aliquots (input, flow-through (ft), wash and eluate fractions) after affinity purification via Ni-NTA agarose from *E. coli* inclusion bodies. (B) CD-spectroscopy of refolded rNKG2D-His (N-terminal His-tag) showing homogeneous protein folding with a prominent β-sheet structure. (C) Pooled peak fractions of SEC were analyzed by non-reducing (- DTT) and reducing (+ DTT) Coomassie-stained SDS-PAGE and immunoblot (anti-His HRP-conjugated).

Functional analyses of rNKG2D-Biotin and rNKG2D-His showed binding of cell surface NKG2D ligands expressed on HEK293T cells (Figure 32A/C; NKG2D ligand expression pattern see Figure S12). Moreover, in ELSA measurements, both proteins bound the sNKG2D ligands sMICA/B and the sULBP1-3. As indicated by different adsorption units, rNKG2D showed different affinities for the individual ligands (Figure 32B/D). This is in accordance with binding studies for human and mouse NKG2D showing binding affinities between

0.3 µM and 1 µM for the corresponding ligands [243, 248, 252]. Moreover, binding of glycosylated sNKG2D ligands expressed in mammalian cells was independent on glycosylation status of rNKG2D as described earlier [249].

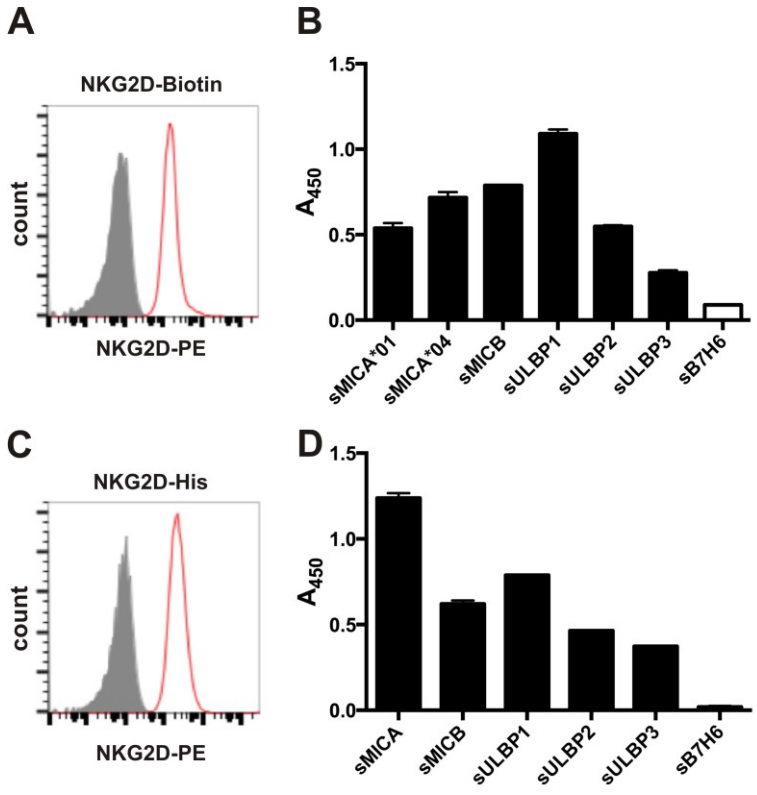

Figure 32: NKG2D ligand recognition and depletion with rNKG2D proteins.
Binding of rNKG2D-Biotin (A) and rNKG2D-His (C) to HEK293T cells expressing NKG2D ligands (NKG2D ligand expression pattern of HEK293T see Figure S12) was analyzed by flow cytometry with an anti-NKG2D PE-conjugated antibody. Grey = antibody control, red = NKG2D binding. Binding of rNKG2D-Biotin (B) and rNKG2D-His (D) to individual recombinant NKG2D ligands analyzed by ELISA. B7H6::hIgG1-Fc served as control. Data are represented as mean ± SEM of one representative experiment out of three.

To validate the sNKG2D ligand depletion capability of rNKG2D, the proteins were immobilized on streptavidin magnetic beads via Biotin or anti-His beads, respectively. Supernatants supplemented with recombinant sMICA/B and sULBP1-3 were incubated with respective rNKG2D-Biotin or rNKG2D-His beads (Figure 33). The sNKG2D ligands bound specifically to rNKG2D-Biotin coupled beads as shown by immunoblot analysis of bead eluates, whereas no binding could be observed for biotin-coupled control beads or soluble B7H6 fusion proteins, an activating ligand for NKp30 (Figure 33A). Moreover, analysis of the supernatants

after depletion with rNKG2D-His coupled beads clearly demonstrated a reduction in sNKG2D ligand levels with an overall depletion efficacy of 74.7 ± 8.2% (Figure 33B). The *in vitro* depletion experiments clearly demonstrated the suitability of rNKG2D proteins for the pan-specific sNKG2D ligand depletion.

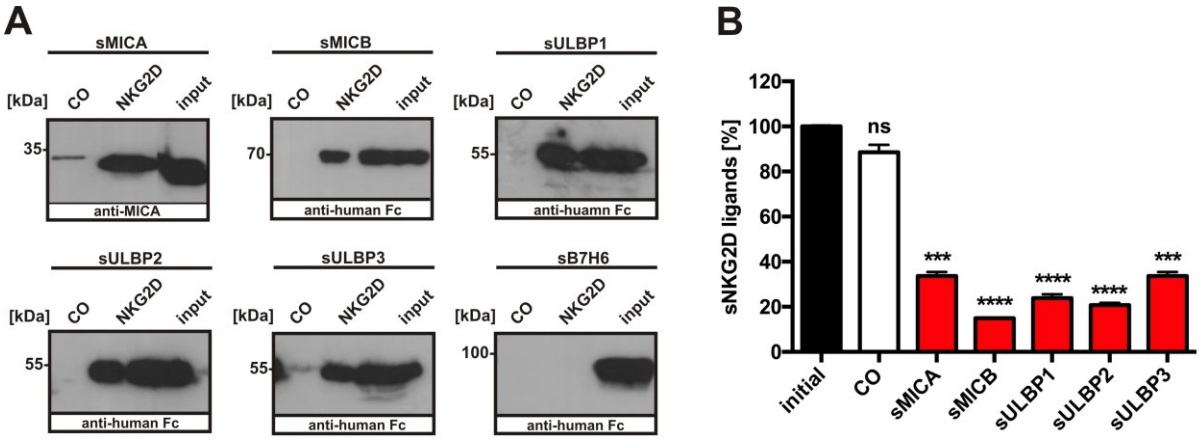

Figure 33: Depletion of sNKG2D ligands using rNKG2D coupled beads.
Depletion of recombinant NKG2D ligands from supernatants with rNKG2D-Biotin coupled magnetic Streptaividin-beads (A) or rNKG2D-His magnetic beads (B). Immunoblot analyses of NKG2D ligands in the supernatant (input) before depletion and in bead eluates (NKG2D) (anti-MICA antibodies in combination with anti-mouse HRP-conjugated antibodies or anti-human Fc-HRP). Biotin-loaded Streptavidin beads served as controls (CO). (B) NKG2D ligand levels in supernatants pre- (initial) and post-depletion determined by respective ELISAs. BAG6-His coupled beads served as control (CO). Ligand levels were normalized to the initial levels and are shown as mean ± SEM measured in dublicates of a representative experiment. Statistical significance was determined by Student's t-test; *** $p < 0.001$; **** $p < 0.0001$.

Since the expression and purification strategy for the rNKG2D-His protein showed higher amounts of correctly folded protein at high purity compared to the rNKG2D-Biotin, the His-tagged protein was produced for the generation of a biofunctionalized sepharose matrix for the use in adsorption apheresis. Unexpectedly, the amine-reactive coupling methods used failed to stabley immobilize functional rNKG2D proteins to the sepharose. One possible explanation is the disruption of the NKG2D structure at the binding interface comprising lysine residues with primary amine groups, which might be addressed by the coupling reaction. Additionally, a further aspect was taken into account. Proteins produced in *E. coli* have the disadvantage of high endotoxin (lipopolysaccharide, LPS) contaminants, which might negatively influence protein immobilization and moreover can cause side effects in human organisms and are therefore not applicable for clinical use. Consequently, a new strategy for the production of a NKG2D recombinant protein for the use in adsorption apheresis was developed.

3.3.2.2 NKG2D::hIgG1-Fc Fusion Proteins

Soluble Fc-based fusion proteins are suitable tools for the *in vitro* study of receptor-ligand interactions, as shown for NCR receptors [154, 377], and are of interest as therapeutic agents in immunotherapies addressing various diseases [420]. Usually, the proteinaceous molecule of interest is directly linked to the flexible hinge region of a human IgG1 Fc-part. The advantages of fusion to the Fc-part are (i) expression of high amount of soluble proteins in conventional mammalian producer cell lines, (ii) improved protein stability, (iii) the formation of stable homodimers mediated by the Fc-part and (iv) cost-effective purification and immobilization via Protein A/G matrices [421]. In this thesis, the fusion of the NKG2D extracellular domain to the N-terminus of the human Fc-part did not lead to the expression of functional proteins (data not shown). Since NKG2D is a type II transmembrane protein it can be hypothesized that the Fc-part induced dimerization of the fusion proteins leads to sterical hindrances and might cause an inverse homodimer formation of the extracellular NKG2D domain, when the protein was fused with its C-terminus to the N-terminal Fc-hinge region. Consequently, new fusion protein constructs were generated with the NKG2D extracellular domain fused to the C-terminus of the Fc-part. The resulting NKG2D::hIgG1-Fc proteins were transiently expressed in HEK293T cells, secreted into the culture supernatant and affinity purified via Protein A (see Figure S9A). In functional assays the NKG2D fusion protein efficiently bound to NKG2D ligands expressed on cell lines as shown by flow cytometry (see Figure S9B). Unexpectedly, Fc-directed immobilization to different bead matrices (i.e. anti-human IgG-Fc or Protein A magnetic beads) for depletion experiments resulted in partial loss of NKG2D functionality (see Figure S9C). This might be attributed to steric disturbances in the NKG2D extracellular domain located at the C-terminal end of the Fc-part upon immobilization. Additionally, insertion of a longer flexible glycine-serine linker between NKG2D and the Fc-part could not improve immobilization of functional fusion proteins (see Figure S9C). To ensure immobilization directed to the N-terminus of the Fc-part, an additional Avi-tag was fused to the IgG-Fc hinge region. Co-transfection of mammalian cells with plasmids encoding for BirA ligase with an *endoplasmatic reticulum* or secretion signal sequence allowed for direct *in vivo* biotinylation of Avi-tagged proteins. *In vivo* biotinylated NKG2D::hIgG1-Fc proteins and BirA ligase were transiently expressed in HEK293T cells and the fusion protein was affinity purified from cell culture supernatant via Protein A (Figure 34). Out of 250 ml culture supernatant (corresponding to $1x10^8$ cells) 0.5 - 1 mg biotinylated NKG2D fusion proteins could be

purified with high homogeneity and purity with a molecular mass of around 100 kDa as shown by SEC analysis (Figure 34B). As expected, NKG2D fusion proteins formed stable homodimers due to the intermolecular disulfide bonds in the IgG1-Fc hinge region as shown by reducing and non-reducing SDS-PAGE (Figure 34C).

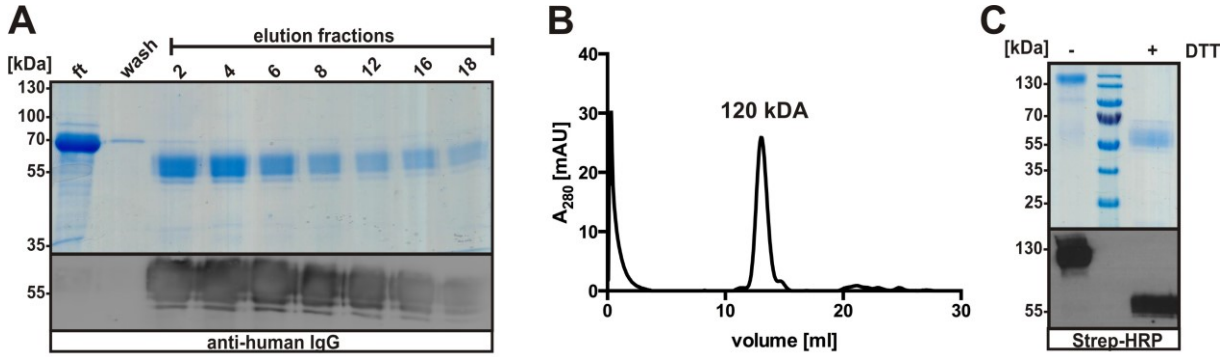

Figure 34: Biotinylated NKG2D::hIgG1-Fc proteins assemble as homodimers.
NKG2D::hIgG1-Fc proteins were expressed and *in vivo* biotinylated in 293T cells after transient transfection. (A) Reducing SDS-PAGE (Coomassie-stained) and immunoblot (anti-human IgG-Fc HRP-conjugated antibody) of aliquots (flow-through (ft), wash and eluate fractions) after affinity purification via ProteinA sepharose from cell culture supernatants. (B) Size exclusion chromatography (SEC) of purified NKG2D::IgG1-Fc on a Superdex 200 10/300 GL column. (C) Pooled peak fractions were analyzed by non-reducing (- DTT) or reducing (+ DTT) Coomassie-stained SDS-PAGE and immunoblot (streptavidin HRP-conjugate). Under reducing conditions, the disulfide-linked IgG homodimeric NKG2D::hIgG1-Fc proteins disassemble to their monomeric forms.

In flow cytometric analyses, biotinylated NKG2D::hIgG1-Fc proteins bound efficiently to the different NKG2D ligands expressed on C1R cell transfectants (Figure 35), whereas no Fc-mediated background binding to NKG2D ligand negative C1R wildtype cells could be observed. Moreover, the different fluorescence intensities indicated different binding affinities for the respective ligands, especially for the MICA allelic variants when compared to the expression profiles shown by anti-MICA antibody staining (see Figure S11). For further analysis of the binding properties, the approximate equilibrium binding constants (K_D values) were determined by ELISA using immobilized recombinant sNKG2D ligands with graded amounts of NKG2D fusion proteins. Biotinylated NKG2D::hIgG1-Fc specifically bound with high affinity to the different NKG2D ligands in a dose dependent manner. The determined K_D values corresponded to the flow cytometric results with C1R cells showing comparable binding affinities for the ligands sMICA*01, sMICB and sULBP1-3 with K_D values ranging between 19 - 75 nM (Table 12). All experiments were performed from the same NKG2D::hIgG1-Fc

protein dilution series and showed preserved B_{max} values for sMICA*01, sMICB and sULBP1-3 as an indicator for the total amount of binding sites in the protein solution.

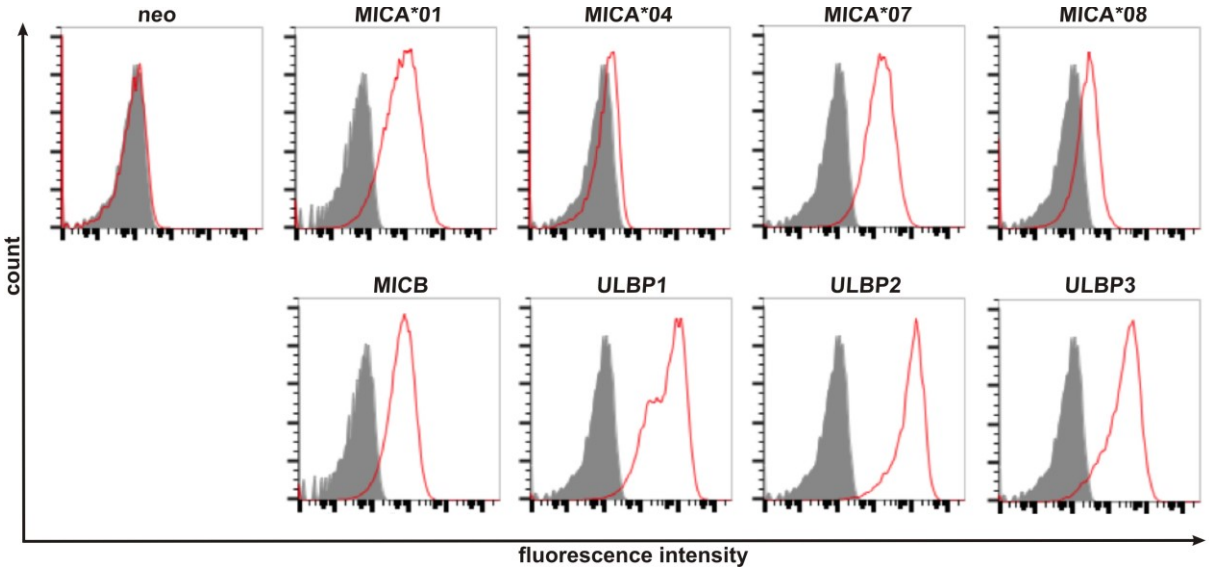

Figure 35: Binding of biotinylated NKG2D::hIgG1-Fc on C1R transfectants.
Binding of biotinylated NKG2D fusion proteins to C1R cell transfectants expressing individual NKG2D ligands (MICA allelic variants, MICB or ULBP1-3, see also Figure S11) were analyzed by flow cytometry. C1R mock transfected cells (neo) served as control. Grey = anti-human IgG-Fc antibody control, red = NKG2D::hIgG1-Fc.

In contrast, the NKG2D::hIgG1-Fc binding affinity to sMICA*04 was 10-fold lower compared to sMICA*01. The different affinities are related to the amino acid residue at position 152 in the α2-helical domain of MICA, where methionine accounts for high affinity alleles such as MICA*01 and MICA*07 whereas the substitution to valine in MICA*04 and MICA*08 led to low affinity binding [249] (see 5.1.9.1; M152/V152 corresponds to M129/V129 (amino acid position without 23 aa signal sequence) in Steinle *et al.*). The slight differences in B_{max} for the binding to sMICA*04 resulted from the 10-fold lower binding affinity and are attributed to the method of analysis. Thus, the equilibrium binding constants are regarded as approximate values. Importantly, binding affinities of NKG2D::hIgG1-Fc fusion proteins were 10- to 50-fold higher than for the rNKG2D variants produced in *E. coli*. The improved binding affinities of NKG2D fusion proteins might favor also the apheresis of sNKG2D ligands.

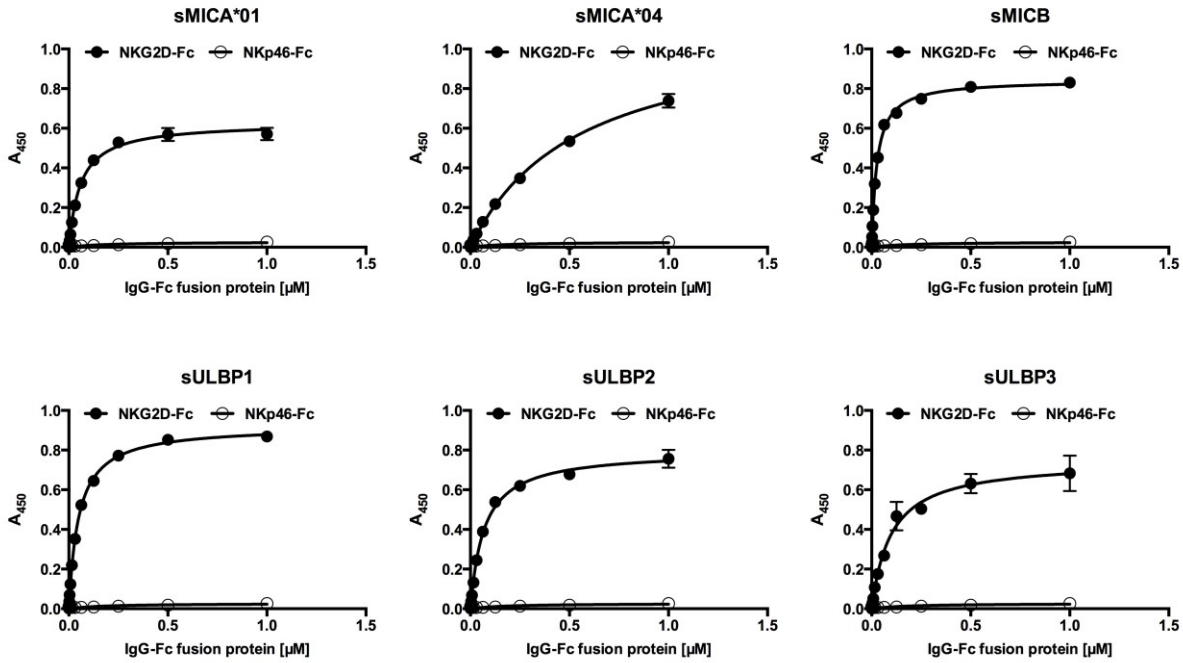

Figure 36: Binding kinetics of biotinylated NKG2D-Fc to NKG2D ligands.
Binding of graded amounts of NKG2D-Fc (black circles) or NKp46-Fc (open circles) proteins to recombinant NKG2D ligands analyzed by ELISA. Data were fitted to a 1:1 Langmuir binding model to determine K_D and B_{max} values. A representative of three independent experiments is shown.

Table 12: Equilibrium binding constants of biotinylated NKG2D::hIgG1-Fc
Equilibrium binding constants (K_D) and B_{max} values of biotinylated NKG2D::hIgG1-Fc to its ligands as determined by ELISA (see Figure 36).

NKG2D ligand	K_D [nM]	B_{max}
sMICA*01	43 ± 6	0.521 ± 0.018
sMICA*04	456 ± 59	0.928 ± 0.057
sMICB	19 ± 3	0.693 ± 0.024
sULBP1	36 ± 6	0.737 ± 0.032
sULBP2	51 ± 6	0.670 ± 0.021
sULBP3	75 ± 7	0.678 ± 0.018

For *in vitro* depletion assays, the biotinylated NKG2D::hIgG1-Fc proteins were covalently coupled to streptavidin magnetic beads. Depletion capacity was evaluated using healthy human plasma supplemented with individual recombinant sNKG2D ligands (Figure 37A/B).

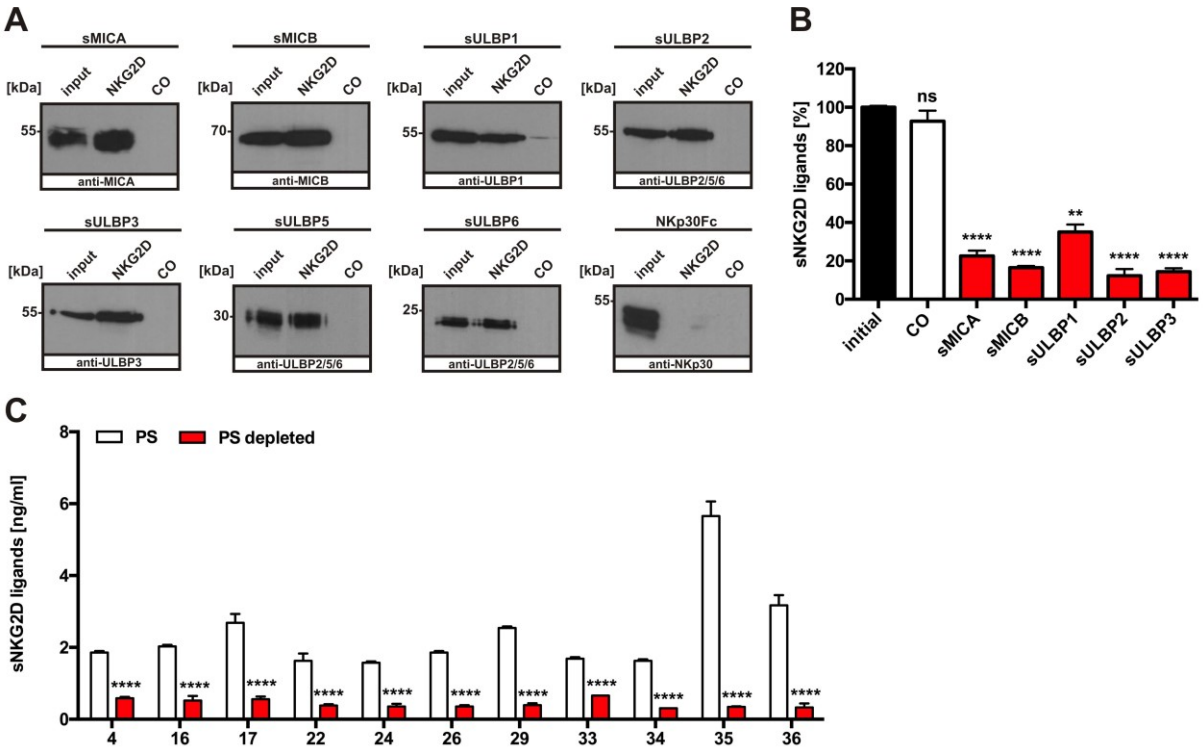

Figure 37: Biotinylated NKG2D::hIgG1-Fc proteins deplete sNKG2D ligands.
(A/B) Depletion of recombinant NKG2D ligands supplemented to healthy human plasma (20 ng/ml of NKG2D ligands) with NKG2D::hIgG1-Fc coupled magnetic Streptaividin-beads. (A) Immunoblot analyses of recombinant sNKG2D ligands or NKp30-Fc control protein in the plasma before depletion (input) and in bead eluates (NKG2D) with respective anti-NKG2D ligand antibodies in combination with anti-mouse HRP-conjugated antibodies. Biotin-loaded Streptavidin-beads served as controls (CO). (B) Recombinant NKG2D ligand plasma levels pre- (initial) and post-depletion analyzed by respective ELISAs. Plasma levels were normalized to the initial plasma levels and are shown as mean ± SEM of three independent experiments. (C) Analysis of sNKG2D ligand levels in HNSCC patients' plasma before (PS) and after depletion (PS depleted) with NKG2D::hIgG1-Fc coupled Streptavidin-beads. Plasma levels are shown as mean ± SEM measured in dublicates. Statistical significance compared to CO or PS, respectively, was determined by Student's t-test; ** $p = 0.005$; **** $p < 0.0001$.

The NKG2D-coupled beads specifically removed the recombinant sNKG2D ligands sMICA/B, sULBP1-3 from human plasma as shown by immunoblot analysis of the bead eluates (Figure 37A). Furthermore, depletion of recombinant sULBP5/6 could be shown for the first time due to newly commercially available recombinant proteins. The depletion could be confirmed by determination of the residual sNKG2D ligand levels in the plasma. The depletion efficacies ranged between 82% and 94% for the ligands sMICA/B and sULBP1/2, and 72% for sULBP1 compared to the initial plasma levels (Figure 37B). As control, biotin coupled beads showed no reduction in sNKG2D ligand levels. Moreover, sULBP5/6 plasma levels could not be determined due to missing antibody combinations for the establishment of spe-

cific sandwich ELISAs. To further evaluate the simultaneous depletion capacity for naturally shed sNKG2D ligands, plasma samples of HNSCC patients were incubated with the NKG2D-coupled beads. The analysis of the patients' plasma pre- and post-depletion revealed efficient removal of sNKG2D ligands resulting in a median depletion of 88.8 ± 9.1% of the initial cumulative sNKG2D ligand burden (Figure 37C). The simultaneous depletion of sNKG2D ligands from patients' plasma using biotinylated NKG2D::hIgG1-Fc coupled beads was independent of the patients' individual sNKG2D ligand pattern and cumulative plasma level. Notably, NKG2D removed the ligands with the same efficacy as the bead cocktail of monoclonal anti-NKG2D ligand antibodies (shown in Figure 11A).

In conclusion, in this thesis a functional *in vivo* biotinylated, homodimeric NKG2D::hIgG1-Fc fusion protein could be generated in a mammalian cell system showing high affinity binding to the different NKG2D ligands. Importantly, the NKG2D fusion protein efficiently depleted sNKG2D ligands from patients' plasma comparable to anti-NKG2D ligand monoclonal antibodies. Thus, NKG2D fusion proteins are suitable tools for the generation of a pan-specific adsorber matrix for the simultaneous adsorption apheresis of sNKG2D ligands. Pan-specific adsorption apheresis would allow for the treatment of a broad patient cohort, independent of the individual patients' sNKG2D ligand composition and burden. Moreover, the NKG2D::hIgG1-Fc proteins would even allow for improvement of binding affinities to cognate ligands as shown exemplarily in an affinity maturation study using NKG2D::hIgG1-Fc mutant proteins with single amino acid substitutions bioinformatically calculated for high affinity binding to sMICA (see 5.1.8).

3.4 Preclinical Evaluation of Adsorption Apheresis in Rhesus Macaques

The *in vitro* depletion experiments using an anti-MICA antibody or NKG2D::hIgG1-Fc functionalized matrices demonstrated a successful and efficient removal of sNKG2D ligands from human plasma and could restore NK cells' functions in cytotoxicity experiments. To investigate the applicability of the newly generated adsorber matrix for a clinical therapy, a pre-clinical *in vivo* validation of sNKG2D ligand adsorption was performed. For this purpose, the anti-MICA adsorber matrix was used in a proof of concept study. Due to the fact that the generation of biotinylated NKG2D::hIgG1-Fc for pre-clinical application requires the time-

consuming and expensive establishment for commercially high-scale clinical-grade protein production and protein coupling to the sephaose matrix, which was not feasible during this thesis, the pan-specific adsorber was not validated in the animal model.

3.4.1 Pilot Study

For the pre-clinical validation of adsorption apheresis, a rhesus macaque (*Macaca mulatta*) model was used. Human and rhesus MICA display a sequence identity of 79% (see 5.1.9.3), human and rhesus NKG2D of 94% (see 5.1.9.4). Moreover, the body weight of 7 - 10 kg and a blood volume of roughly 7% of the body weight make rhesus monkeys a suitable model system to validate the efficacy of sNKG2D ligand adsorption apheresis. Since no rhesus macaque cancer disease models exist, only adsorption apheresis was investigated. Therefore, soluble human MICA was infused into the rhesus macaques prior to adsorption apheresis.

In a pilot study, the body distribution and serum stability of human sMICA*04 after intravenous injection was validated. Therefor, two rhesus monkeys were injected with 100 µg sMICA*04 per liter of blood volume (BV) and sMICA plasma levels were analyzed over three hours by ELISA (Figure 38A/B). About 15 - 25% of the initially injected sMICA could be found in monkeys' plasma 15 min after injection reflecting the process of natural body distribution due to sMICA diffusion from the blood into the tissues. The injected sMICA showed an exponential plasma decrease during the first 150 min after injection reaching a stable plasma level with a diffusion equilibrium of about 3 - 5 ng/ml three hours after injection, which resembles the plasma levels found in cancer patients. Moreover, urine samples were analyzed for renal clearance of the administered sMICA (Figure 38C/D). Notably, no sMICA could be detected in the urine of the animals. Additionally, incubation of sMICA in rhesus plasma at 37 °C showed a stable plasma level without signs of sMICA degradation in the plasma (Figure 38G). These data indicate that the decreasing sMICA plasma levels were not caused by renal clearance or proteolytical degradation and are only due to the body distribution resulting in stable sMICA plasma levels, which allow for adsorption apheresis. Notably, these plasma levels were stable for at least 6 h post injection (data not shown).

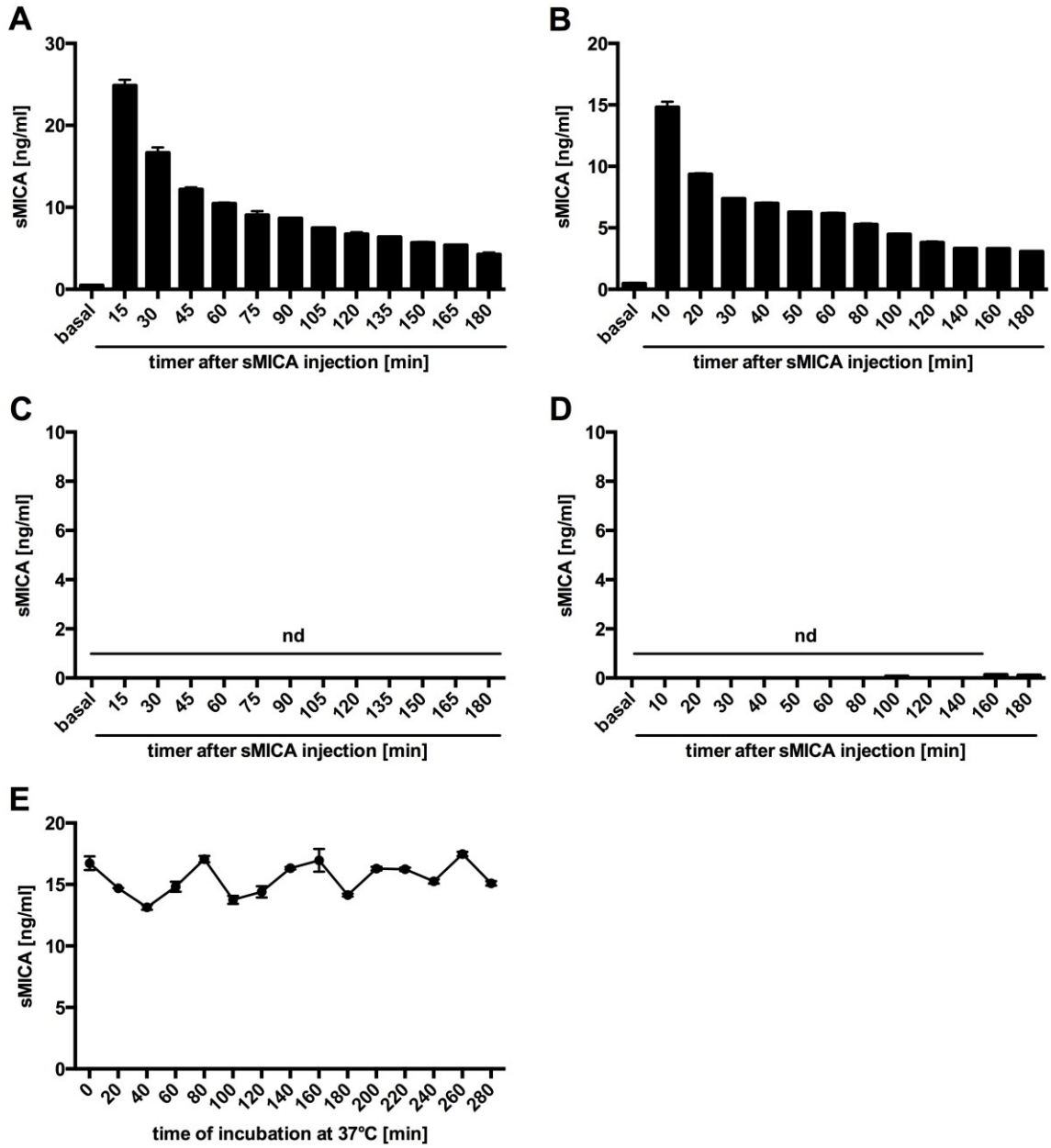

Figure 38: Analysis of sMICA body distribution and plasma stability.
Two animals (left/right) were injected with 100 µg/l blood volume sMICA*04 to evaluate sMICA body distribution. Blood and urine samples were taken before injection (basal) and during three hours after injection. (A/B) Analysis of sMICA*04 plasma levels by ELISA. Data are represented as mean ± SEM of duplicates. (C/D) Analysis of sMICA*04 in urine by ELISA to determine renal clearance of sMICA. Data are represented as mean ± SEM of duplicates; nd = not detectable. (E) Rhesus macaque plasma was supplemented with sMICA*04 and incubated at 37 °C to analyze sMICA plasma stability. Plasma samples were measured every 20 min in duplicates by ELISA. Data are represented as mean ± SEM.

Additionally, analysis of NKG2D expression on $CD3^+$ T cell and $CD3^-$ NK cell subpopulations from rhesus PBMCs revealed that the basal NKG2D expression levels and cell numbers were not affected by human sMICA*04 (Figure 39 A/B).

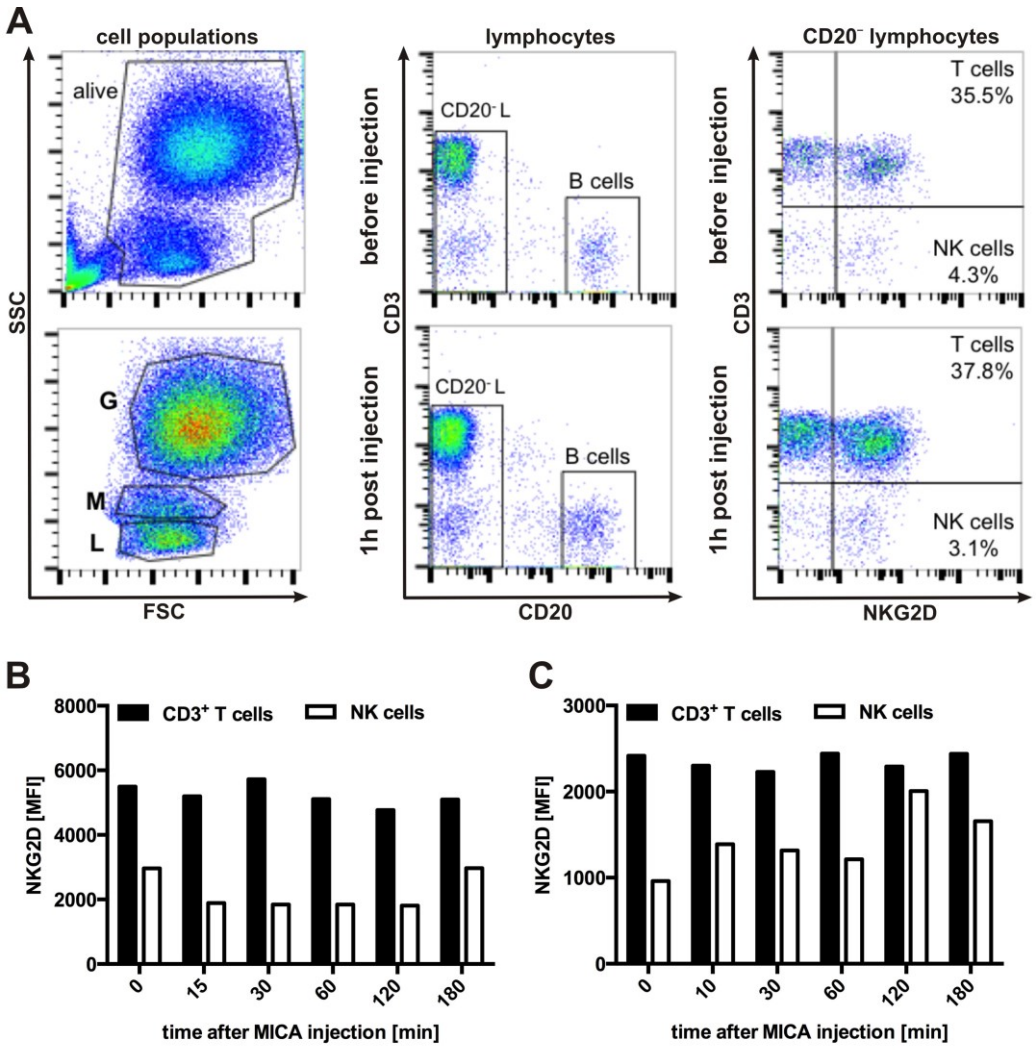

Figure 39: Analysis of rhesus monkey blood cells.
Flow cytometric analysis of primary rhesus PBMCs from whole blood samples. (A) Gating strategy of viable (alive) PBMCs and determination of granulocyte (G), monocyte (M) and lymphocyte (L) populations (left). The lymphocyte fraction was further discriminated in B cells and $CD20^-$ lymphocytes ($CD20^-$ L; middle). $CD3^+/NKG2D^+$ T cell and $CD3^-/NKG2D^+$ NK cell subsets were determined from the CD20- L population (right). Representative dot plots of one animal are shown for blood samples taken directly before sMICA*04 injection and 1 h post injection. (B/C) Flow cytometric analysis of NKG2D surface expression on $CD3^+$ T cells and NK cell over 3 h of two animals.

Three weeks after sMICA injection, the plasma of the animals was probed for anti-MICA IgG and IgM antibody production. No anti-MICA antibodies of the IgG/IgM subclasses could be

detected excluding antigenicity and related destruction of the administered human sMICA protein (Figure 40A/B).

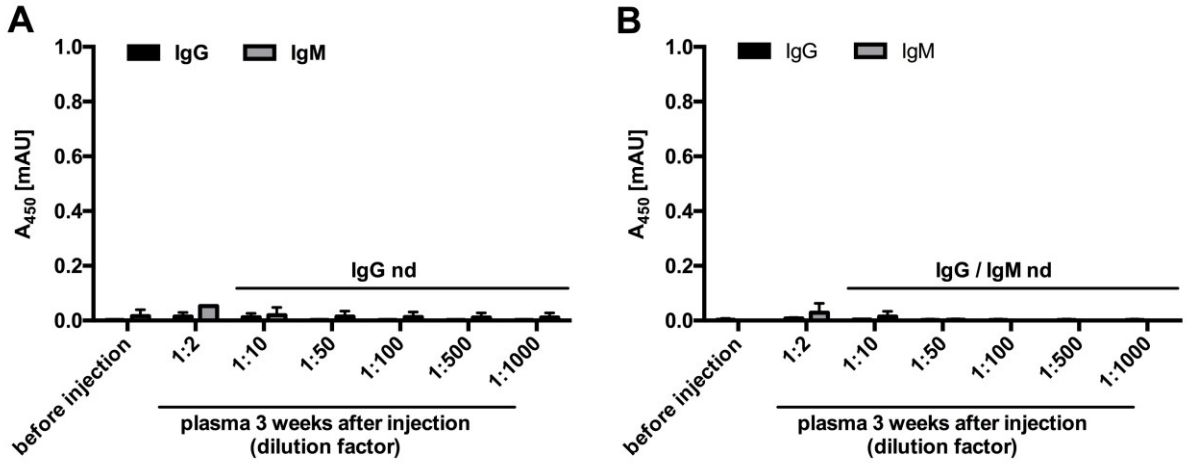

Figure 40: No adaptive immune response towards human sMICA*04 in rhesus macaques.
(A/B) Determination of anti-MICA IgG/IgM antibodies in the plasma of two rhesus macaques three weeks after sMICA*04 injection. Different plasma dilutions of the two animals were probed for anti-MICA IgG (black bars) or IgM (grey bars) antibody subclasses on sMICA*04 coated ELISA plates. Antibodies were detected with monkey IgG- or IgM-specific HRP-conjugated antibodies. Data are represented as mean ± SEM; nd = not detectable.

Collectively, the data of the pilot study demonstrated that rhesus macaques are a suitable *in vivo* model for the pre-clinical validation of adsorption apheresis, which allows for human sMICA injection resulting in a stable plasma level without causing side effects or immune reactions against sMICA.

3.4.2 *In vivo* Adsorption Apheresis

For adsorption apheresis, an adsorber cartridge with the anti-MICA antibody-functionalized sepharose matrix was produced for the use in a Life18™ apheresis unit from Miltenyi Biotec. Two animals were injected with 100 µg/l BV sMICA*04 and the apheresis was started 15 min post-injection. The apheresis was run until three complete exchanges of the animals' plasma volume were reached. The analysis of sMICA plasma levels showed that only three plasma volume exchanges were sufficient for efficient depletion of sMICA with 1.44 ± 0.06% and 3.48 ± 1.79% remaining sMICA*04 in the plasma of the two animals, respectively (Figure 41A/B). Apparently, the decline of sMICA in the plasma during the first 30 minutes of the

apheresis resembled the body distribution seen in the pilot study but the effect of sMICA removal through the adsorber cartridge was detectable after one plasma volume exchange and showed a significant faster decline in the plasma when compared to the sole effects of body distribution with 24.17 ± 0.09% and 27.98 ± 0.46% remaining sMICA*04 in the plasma at the end of the experiment.

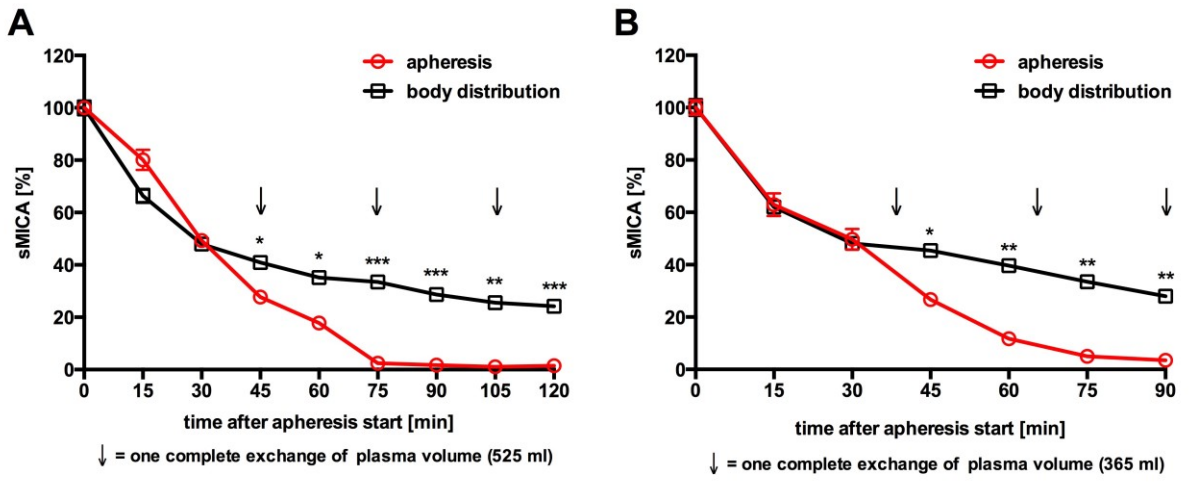

Figure 41: *In vivo* adsorption apheresis of sMICA in two rhesus macaques.
(A/B) Animals were injected with 100 µg/l blood volume sMICA*04. Apheresis was started 15 min post injection using a Life18™ apheresis unit (Miltenyi Biotec). sMICA plasma concentrations were determined by ELISA every 15 min and normalized to the initial sMICA (15 min post injection). Data are represented as mean ± SEM of duplicates. Pilot study (no apheresis) = body distribution: black open squares; apheresis: red open circles. Statistical significance was analyzed using Student's t-test with * $p < 0.05$; ** $p < 0.001$; *** $p < 0.0001$. Arrows indicate the time points of consecutive plasma volume (PV) exchanges ((C) PV= 525 ml; (D) PV= 365 ml).

The pre-clinical validation of the adsorber cartridge clearly demonstrated that adsorption apheresis is an effective therapeutic strategy to remove sNKG2D ligands from plasma in a living organism. Thus, adsorption apheresis prior to immune cell therapies might be a promising combinatorial medical approach for the treatment of cancer patients to augment immune cell functions of autologous and adoptively transferred lymphocytes by interfering with NKG2D-dependent tumor immune escape.

4 Discussion

The human activating receptor NKG2D plays a major role in tumor immunosurveillance. However, the release of soluble ectodomains of NKG2D ligands from the tumor cell surface is a potent strategy mediating tumor evasion from NKG2D-dependent recognition and elimination by cytotoxic lymphocytes [373]. In this respect, NKG2D-dependent tumor immune escape has been described in a variety of cancers, including leukemia, neuroblastoma, cervical carcinoma, and multiple myeloma [422]. Although the NKG2D/NKG2D ligand system is well characterized, the complexity of this system still needs further investigation to improve the efficacy of tumor immunosurveillance and to develop new anti-cancer therapies [152, 201]. This is due to i) the diverse expression patterns of the numerous stress-induced and structurally related NKG2D ligands in many different cancer entities [246, 422], ii) the heterogeneity of the tumors and tumor microenvironment in individual cancer patients, and iii) the expression levels of the NKG2D receptor and its multiple functions in innate and adaptive immune cells [423, 424]. Moreover, most studies on NKG2D-dependent tumor immune escape relied on the investigation of one or two sNKG2D ligands, mainly concentrating on sMICA/B and sULBP2. Therefore, the knowledge of the cumulative sNKG2D ligand levels and their impact is scarce. In this thesis, monitoring of HNSCC patients' plasma revealed elevated sNKG2D ligand levels, which impair NKG2D-dependent NK cell cytotoxicity. Based on tumor spheroids, besides reduced cytotoxicity, also inhibition of NK cell infiltration through sNKG2D ligands could be demonstrated. Furthermore, the specific depletion of sNKG2D ligands could restore NK cells' antitumor functions. Thus, an adsober matrix for the depletion of sNKG2D ligands based on monoclonal antibodies or recombinant NKG2D proteins was established and validated in a proof of concept study in rhesus monkeys.

4.1 sNKG2D Ligands mediate Tumor Immune Escape in HNSCC

HNSCC tumors overexpress the NKG2D ligands MICA and MICB, which renders them susceptible to NK cell lysis [425, 426]. Moreover, impaired NK cell functions in HNSCC implicate an important role of NK cells in HNSCC immunosurveillance [427, 428]. Along this line, increased levels of sMICA could be identified in HNSCC patients' plasma, which diminished NK cell cytotoxicity [304, 320, 321]. In this thesis, the impact of the sNKG2D ligands sMICA/B and sULBP1-3 to NKG2D-dependent tumor escape was evaluated in 44 HNSCC pa-

tients using sandwich ELISAs optimized for stable and reproducible detection in human plasma. It should be noted that sULBP4-6 could not be analyzed due to the lack of appropriate antibody pairs and recombinant proteins for establishing specific ELISAs. Profiling of HNSCC plasma revealed that the cumulative level of sNKG2D ligands is patient specific and correlates with disease progression and tumor load. The soluble ligands accumulated upon the pre-metastatic stage III characterized by locally established tumors without signs of metastases in regional lymph nodes. Thus, defective NKG2D-mediated tumor surveillance rather plays a role in advanced disease than being involved in tumor formation. This is in accordance with studies from different malignancies such as prostate cancer, multiple myeloma and HNSCC showing a correlation of increased sMICA and sMICB plasma levels with disease staging and progression [303, 304, 324, 325, 429]. One explanation for the accumulation of sNKG2D ligands in advanced disease could be due to the upregulation of MMPs, which mediate ligand shedding, in association with increased tumor invasiveness [430-432]. Moreover, individual patients showed different patterns of sNKG2D ligands highlighting the heterogeneous nature of HNSCC. These data suggest a prominent role for sULBPs, especially sULBP1 and sULBP3, in HNSCC when compared to the levels of sMICA and sMICB. The diverse NKG2D ligand expression and release is in accordance with studies of other cancer entities showing distinct ligand patterns, but no tumor expressing all NKG2D ligands at the same time [258, 425]. This can be explained by differential transcriptional regulation of the ligands, which is influenced by many factors of the tumor microenvironment and cancer therapies [246, 412]. Whereas MICA/B expression was shown to be upregulated by heat-shock and oxidative stress [223, 433], upregulation of ULBP expression could be correlated to the induction of the tumor suppressor p53 [434] or inhibition of proteasome activity [412, 435]. Upon cellular stress, NKG2D ligand expression is induced by the ATM/ATR (ataxia telangiectasia mutated/ATM and Rad3-related) DNA damage response, which is constitutively active in advanced tumors and can be induced by DNA-damaging chemotherapeutic drugs or local radiation [274, 436]. Interestingly, palliative chemo- and/or radiotherapy had little effect on sNKG2D ligand levels in HNSCC patients' plasma analyzed. The slight reduction of sNKG2D ligand plasma levels might be due to reduced tumor mass in patients currently under treatment. However, further studies including a larger patient cohort under therapy are needed to further evaluate the effect of chemo- and/or radiotherapy on tumor burden and sNKG2D ligand levels. Moreover, upregulation of NKG2D ligand surface expression on tumor cells

upon chemo- and radiotherapy should be analyzed for a better understanding of the impact of therapeutic strategies on the NKG2D/NKG2D ligand system. Thus, profiling of the sNKG2D ligand status of cancer patients as prognostic and/or diagnostic marker might be crucial for selection of strategies for personalized immunotherapy.

4.2 Immunosuppressive Factors and low Lymphocyte Infiltration in HNSCC Patients

Since HNSCC is characterized by an immunosuppressive tumor microenvironment, major tumor-associated cytokines and chemokines were analyzed in HNSCC patients' plasma. In contrast to previous reports, no significant alterations in TNF-α or IL-10 levels and only a non-significant decrease of IFN-γ when compared to healthy control plasma could be detected [320, 366, 437]. In the present study, RANTES, MIP-1β, MCP-1 and IL-6 were significantly elevated but showed no significant correlation with disease characteristics. The most prominent factor analyzed was TGF-β1, which increased during disease progression. Overall, altered cytokine and chemokine levels found in HNSCC patients are highly heterogeneous and patient specific, but commonly show an immunosuppressive, pro-inflammatory and pro-angiogenic phenotype accounting for the aggressive malignant behavior of HNSCC [438, 439]. Up to now, several studies showed variations in distinct cytokine levels for HNSCC. However, it should be noted that the level of cytokines could vary using different assays such as ELISA or flow cytometry-based cytokine bead arrays (CBA) and depends on the material analyzed, since the complex cytokine network is modulated not only by tumor cells itself but also by immune cells. In the study of Bose *et al.* [366] cytokines were analyzed from PBMC culture supernatants isolated from HNSCC patients rather than from plasma of HNSCC patients. Other studies analyzed cytokine levels in primary tissue or HNSCC cell lines. Consequently, comparison of different studies might be difficult with regard to sample origin, method of analysis and comparison to healthy controls. Therefore, a uniform diagnostic method should be established to evaluate the cytokine status of patients in the clinic.

Immunohistochemistry of primary HNSCC tumors further confirmed the immunosuppressive status of HNSCC patients. In this respect, TAMs of the M2 phenotype were frequently found in primary HNSCC tumors, which are critical modulators of the immunosuppressive (e.g. by secretion of immunosuppressive factors and inhibition of T and NK cell proliferation and ac-

tivation) and pro-tumorigenic (e.g. promoting angiogenesis, invasion and tumor growth) microenvironment [396, 440]. In contrast, low numbers of $CD3^+/CD8^+$ tumor-infiltrating lymphocytes could be found in the tumor core and nearly no infiltration of $CD56^+$ NK cells (and presumably NKT cells) could be detected. This observation is in accordance with a study of Mukhopadhyaya *et al.* [441] reporting that tumor infiltrating lymphocytes in tumor tissues and diseased lymph nodes of HNSCC patients showed a decreased percentage of $CD3^+$ and $CD4^+$ T cells and significantly low numbers of NK cells, which showed highly compromised cytotoxic activity [442]. Analysis of HNSCC patients' PBMCs showed reduced numbers of peripheral cytotoxic $CD56^{dim}/CD16^+$ NK cells, whereas the number and distribution of peripheral $CD4^+/CD8^+$ T cell subsets were unchanged. In contrast to other reports analyzing lymphocytes from whole blood samples or isolated NK cells, no decrease in overall NK cell numbers or circulating regulatory NK cells could be seen in the analyzed isolated PBMCs from HNSCC patients [366, 427]. Interestingly, only a slight increase of NKG2D expression could be detected on the patients' immune cells compared to those of healthy controls, further indicating a low activation status and impaired NKG2D-mediated antitumor functions of these cells. There is accumulating evidence that immune cell invasion into solid tumors is an important factor for survival of patients [443-448], and also for the success of cellular therapies [449]. Thus, low T cell infiltration and especially the absence of infiltrating NK cells, in particular cytotoxic NK cells, are indicative for insufficient immunosurveillance of HNSCC and account for the need of immunotherapies to redirect and activate cytotoxic immune cells to the tumor site to improve HNSCC patients' outcome.

4.3 sNKG2D Ligands and TGF-β1 in Patients' Plasma impair NK Cell Cytotoxicity

The impact of shed NKG2D ligands in patients' plasma on NK cell cytotoxicity was evaluated in *in vitro* cytotoxicity assays using primary IL-2 pre-activated NK cells of healthy donors [385] and a target cell line (SiHa), which is highly susceptible to NKG2D-mediated cytotoxicity. NK cells pre-incubated with plasma of HNSCC patients showed drastically reduced cytotoxicity by NKG2D blocking, and presumably downregulation, when compared to NK cells incubated with plasma of healthy donors. Correlation of plasma levels and tumor cell lysis revealed an additional inhibitory effect on NK cell cytotoxicity when HNSCC plasma con-

tained high levels of both sNKG2D ligands and TGF-β1. Moreover, analysis of the plasma of a patient before and after surgery demonstrated a direct correlation of high sNKG2D ligands and TGF-β1 plasma levels with tumor burden. This is in agreement with a recent study by Kloess *et al.* [320] showing a synergistic effect of high sMICA and TGF-β1 plasma levels in HNSCC patients on NKG2D-dependent NK cell inhibition, and correlation of increased sMICA and TGF-β1 levels with advanced disease stage. In this respect, several studies showed that high plasma levels of individual sNKG2D ligands from different tumor entities correlated with impaired NK and T cell functions via NKG2D blocking and/or internalization [302, 305, 314-317]. However, some reports have failed to confirm receptor downregulation by soluble NKG2D ligands [297, 298]. Several explanations for the conflicting results can be considered. On the one hand, NKG2D downregulation could depend on the nature and affinity of the released ligand. In this respect, it was shown that incubation of NK cells with supernatants containing exosomal MICA*08 or ULBP3 triggered significantly more NKG2D downregulation compared to supernatants with monovalent soluble ULBP2 or soluble MICA*019 indicating that multivalent ligands on exosomes can mediate cross-linking of the receptors, which is necessary to induce receptor internalization [246, 311, 312]. Interestingly, a recent study by Quatrini *et al.* [450] showed that ligand stimulation induced ubiquitylation of DAP10 leading to the endocytosis of NKG2D-DAP10 complexes, which was required for the activation of NK cell functions, such as the secretion of cytotoxic granules and IFN-γ. Thus, NKG2D downregulation upon persistent exposure to NKG2D ligands on the surface of tumor cells might contribute to the functional regulation of NK cell effector functions. Moreover, Deng *et al.* [451] showed that the soluble form of the mouse ligand Mult1 secreted by tumor cells activated mouse NK cells by upregulation of NKG2D surface expression and stimulated tumor rejection *in vivo.* The authors proposed that the high-affinity of soluble Mult1 compared to the lower affinities of sMICA/B might be an explanation for the opposed effects, and that soluble Mult1 mediate NK cell stimulation by a different mechanism. Morover, it could not be excluded that sNKG2D ligands form multivalent proteins in plasma, which can bind and cross-link the receptor despite a low affinity or concentration. In this respect, recombinant monovalent soluble MICA derived from HEK293T cells and *E. coli* failed to downregulate NKG2D and to inhibit NK cell cytotoxicity in functional assays (data not shown). The molecular basis remains unknown, however, it might be attributed to subtle differences in protein folding or posttranslational modification, since sMICA purified from tumor cell lines after shedding

could inhibit NKG2D as shown in cytotoxicity experiments. In addition, the different affinities of the ligands may account for the extent of NKG2D downregulation. Therefore, the effect on NK cell functions might depend on the individual composition of sNKG2D ligands in patients' plasma. On the other hand, reduced receptor staining upon sNKG2D ligand exposure may reflect blockade of the epitope recognized by NKG2D-specific antibodies (most commercially available anti-NKG2D antibodies block NKG2D-dependent NK cell activation) rather than reduced receptor surface expression. In most studies it could not be excluded that other components (e.g. TGF-β1 [293, 295]) in patients' plasma contributed and mediated NKG2D downregulation. Elevated levels of TGF-β1 were found in plasma of lung cancer, colorectal cancer and glioma patients and inversely correlated with NKG2D surface expression on NK cells and CTLs of these patients [293, 401]. It could be shown that TGF-β1-induced NKG2D downregulation was partially dependent on transcriptional regulation of NKG2D and due to repression of DAP10, which leads to retention and lysosomal degradation of NKG2D [149, 452]. Therefore, the exact molecular mechanism of sNKG2D ligand- and TGF-β1-mediated NKG2D inhibition needs further investigation. Importantly, in this thesis it could be shown that NKG2D-dependent NK cell dysfunction was predominantly mediated by sNKG2D ligands in HNSCC patients' plasma, since the specific depletion of sNKG2D ligands from patients' plasma restored NKG2D-dependent killing and thus blocking and/or downregulation of the NKG2D receptor on NK cells. Although the sole depletion of sNKG2D ligands was sufficient to restore NKG2D-depenent cytotoxicity *in vitro*, it should be noted, that the impact of TGF-β1 to NKG2D inhibition *in vivo* might be stronger by not only directly decreasing the expression level on NK cells, but also by acting through the suppressive function of Tregs [294]. Tregs were shown to be increased in HNSCC patients and can further mediate their suppressive functions by downregulation of T cell, NK or NKT cell subtypes as well as by interfering with the antigen-presentation function of dendritic cells [366]. Taken together, this leads to the assumption that NKG2D-dependent tumor immune escape can be mediated by a synergistic effect of sNKG2D ligands and other effector molecules (e.g. TGF-β1) and is dependent on disease progression in a patient specific manner. Therefore, combining therapeutic strategies targeting sNKG2D ligands and TGF-β1 might be considered to further promote and restore antitumor functions of cytotoxic lymphocytes.

4.4 Reduced NK Cell Cytotoxicity correlates with decreased Infiltration in Tumor Spheroids

Tumor spheroids have been widely applied in investigative drug screens for chemo- and radiosensitivity [410], and their metabolic and proliferative profiles have been well determined. However, little work has been done applying spheroids in the context of immunosurveillance of tumor cells by NK cells. Previous studies showed NK cell resistance of Ewing's sarcoma cells that were cultured in a 3D culture model [453] and activity of PBMCs or γδ T cells in tumor spheroids [454, 455]. In this thesis, tumor spheroids were used as a model system for the analysis of NKG2D-dependent tumor immune escape and NK cell functions based on flow cytometry assays and immunohistochemistry. This novel application of tumor spheroids enables the analysis of cytotoxic functions and infiltration of immune cells under *in vivo*-like conditions using commercially available reagents and commonly used cell biological methods. Furthermore, the used 96-well plate format allows for high throughput screening of single spheroid arrays with high reproducibility.

Tumor spheroids grown from HNSCC cell lines of different epithelial origin or of the cervical carcinoma cell line SiHa varied in their susceptibility to NKG2D-dependent killing as shown by blocking experiments. Interestingly, destruction of a three-dimensional tumor spheroid took much longer when compared to the parental monolayer cultures, highlighting their validity for the *in vivo* situation. Characterization of tumor spheroids showed distinct expression patterns of the different NKG2D ligands, with usually low ULBP1 expression. This is in agreement with other studies showing altered ligand expression and a loss of ULBP1 expression during HNSCC cell line generation [412]. Continuous shedding of sMICA/B and sULBPs could be detected in tumor spheroid supernatants reaching saturation after approximately 48 h. This rapid re-production and accumulation of sNKG2D ligands in the supernatants further highlight their role for tumor immune escape. The re-production of sNKG2D ligands by tumor cells, the sNKG2D ligand levels in patients' plasma and the serum half-live of 6 days for sMICA/B [297] indicate that a considerable time frame of several days might exists for depletion of sNKG2D ligands as intervention strategy to boost antitumor functions of NK cells.

Since human plasma is a complex and elusive mixture of soluble factors such as cytokines and chemokines originating from various cell types, the NKG2D-dependent tumor immune

escape was further elucidated in tumor spheroid assays using tumor cell line supernatants containing a cocktail of sNKG2D ligands or purified sMICA (generated by shedding). As expected, sNKG2D ligands in the supernatant of CAL27 cells blocked NKG2D on NK cells and inhibited related NK cell cytotoxicity towards tumor spheroids, as it was seen with single cell suspensions using HNSCC plasma for NK cell pre-incubation. Although tumor spheroids are more complex and showed higher resistance to NK cell cytotoxicity, the inhibition of tumor spheroid destruction was in accordance with the different NKG2D-dependencies of the cell lines used showing the strongest effect for SiHa tumor spheroids compared to FaDu or CAL27 spheroids. Again, depletion of sNKG2D ligands from CAL27 supernatant showed restoration of NKG2D-dependent tumor spheroid destruction as it was seen for patients' plasma. Thus, tumor-like spheroids further confirmed the importance of NKG2D-mediated tumor immune escape in cancer. Moreover, the same amount of sMICA, purified from supernatant of tumor cells after shedding, inhibited NK cell cytotoxicity to the same extent as the cocktail of sNKG2D ligands in cell culture supernatant. This supports the hypothesis, that the extent of NKG2D inhibition is dependent on the composition of sNKG2D ligands in the plasma and the level of high-affinity ligands.

It was shown that tumor infiltration of NK cells coincides with antitumor activity and is associated with a better prognosis in several cancer entities such as colorectal cancer, non-small cell lung cancer, and clear cell renal cell carcinoma [404, 405, 413, 443, 456]. Although NK cells hold promise for anti-cancer therapy, NK cell infiltration into tumors and their phenotype and function within the tumor has not yet been extensively investigated. This is partly due to a lack of appropriate model systems [404, 405, 413, 456-460]. Due to their 3D structure with a complex network of cell-cell contacts, tumor spheroids were used in this thesis for the investigation of NK cell infiltration. As demonstrated by co-staining of tumor spheroid cryosections with antibodies specific for CD45 and active capsase-3, it became evident that NK cell cytotoxicity was accompanied by a massive NK cell infiltration. However, in the presence of sNKG2D ligands or sMICA, NK cell numbers in tumor spheroids as well as NK cell killing were reduced. These data demonstrate a direct correlation between inhibition of NK cell cytotoxicity via NKG2D-dependent immune escape and decreased NK cell infiltration into tumor spheroids. The reduced infiltration into tumor spheroids also reflects the low or absent NK cell infiltration observed in primary tumor tissue of HNSCC patients. However, the molecular details of NKG2D-dependent inhibition of immune cell infiltration need further

analysis in primary tumor samples. Interestingly, sNKG2D ligand pre-treated NK cells in tumor spheroids were often double positive for CD45 and cleaved caspase-3 compared to untreated NK cells. Therefore, it might be speculated that under inhibitory conditions NK cells might proliferate less and become apoptotic. Diminished NK cell stability was also obsereved in peripheral IL-2 activated NK cells from HNSCC patients and healthy controls treated with patients' plasma [320]. The decreased infiltration of sNKG2D ligand pre-treated NK cells indicate that sNKG2D ligands might also mediate suppressive mechanisms affecting the migratory capability and tumor chemoattraction of NK cells. Therefore, it is expected that HNSCC patients could benefit from immunotherapies interfering with NKG2D-dependent immune escape by boosting cytotoxic functions and redirect immune cells to infiltrate tumors.

Moreover, data using sorted NK cell populations (cytotoxic $CD3^{-}CD16^{+}CD56^{dim}$ and regulatory $CD3^{-}CD16^{-}CD56^{bright}$) indicate that both subtypes are capable to infiltrate into tumor spheroids to the same extend. However, the majority of NK cells accumulated and proliferated in the periphery of the tumor spheroids. These NK cell subpopulations could phenotypically differ from infiltrated NK cells. In this respect, a study of Horowitz *et al*. [461] could show the existence of more than 6,000 - 30,000 phenotypically distinct NK cell subsets in the blood of a single human [462]. Moreover, Bhat *et al*. [66] could show that NK cells were not equally active in forming contacts and killing targets but few 'hyperactive' NK cells were observed in cytotoxicity assays. Therefore, further characterization of these isolated subpopulations will be instrumental to decipher which factors determine infiltration and will help to improve cellular therapies of solid cancers. In this respect, the newly established MACS-based isolation protocol (see 5.1.4) allows for the discrimination of infiltrating and peripheral subpopulations by isolation and enrichment of infiltrated NK cells from tumor spheroids and represents a versatile tool for further studies addressing the phenotypic analyses and influence of soluble factors on different immune cell subtypes. The contribution of the NKG2D/NKG2D ligand system to chemotaxis of NK cells, as shown in tumor spheroids, indicated other than yet anticipated functions of NKG2D in tumor immunosuveillance. The determination of the molecular mechanisms by which sNKG2D ligands and TGF-β1 impair NKG2D-mediated NK cell cytotoxicity, migration and tumor chemoattraction is thereby of particular intrest for a better understanding of NKG2D-dependent tumor immune escape in solid cancers.

4.5 Cancer Therapies targeting NKG2D/NKG2D Ligands

In the recent years, the NKG2D/NKG2D ligand system came into focus as target for new anti-cancer therapies to overcome tumor immune escape and improve NKG2D-dependent immunosurveillance. On the one hand, NKG2D ligands are highly expressed on a broad variety of tumor cells of different origin, whereas expression on healthy tissues is observed only poorly [226, 463]. On the other hand, the NKG2D receptor is monomorphic and expressed on all NK cells and several T cell subsets, providing multiple effector cells mediating NKG2D-dependent antitumor functions [201, 246]. Thus, NKG2D and/or NKG2D ligand-targeting therapeutic measures hold promise for anti-cancer therapies applicable to a broad patient cohort suffering from different types of cancer. One considerable access point is the modulation of NKG2D ligand expression on tumor cells, which were selected for low NKG2D ligand profiles due to immunoediting. In this respect, conventional therapies such as local radiation and chemotherapy [274, 436], or administration of proteasome and HDAC inhibitors [464-467] were shown to upregulate NKG2D ligand expression on tumor cells as a consequence of induction of cellular stress pathways (e.g. DNA damage response) enhancing their susceptibility to NKG2D-dependent elimination. However, the use and therapeutic regimen of these agents must be carefully considered regarding pleiotropic effects such as inhibition of NK cell activity by the drugs themself [468], NKG2D downregulation due to persistent NKG2D ligand exposure [287, 288], or the possibility of induction of ligand expression on healthy tissues. Therapeutic approaches to enhance recognition of less immunogenic tumors can also be based on the administration of monoclonal antibodies or bi-specific proteins. Experimental studies showed substantial antitumor effects by improving NKG2D-dependent cytotoxicity when applying chimeric proteins of NKG2D ligands fused to a single-chain antibody fragment or protein specific for a certain tumor antigen expressed on lymphoma and multiple myeloma cells (e.g. ULBP2-BB4 [333], anti-CD20-MICA [335] or anti-CEA-MICA [469]). A chimeric protein of the NKG2D receptor and a CD3ζ-specific single-chain fragment could retarget T cells to NKG2D ligand expressing tumors in mice [334]. Furthermore, Kellner *et al.* [470] showed a synergistic effect of ADCC- and NKG2D-mediated killing of lymphoma cells by combining therapeutic antibodies (e.g. rituximab) with an anti-CD20-ULBP2 chimeric protein [335]. Up to now, several monoclonal antibodies were approved for cancer treatment by the US Food and Drug Administration (FDA) as first or second line treatment of several hematological malignancies and some solid tumors [471]. Antibody-based therapies can

act through several mechanisms to increase the hosts' antitumor effects and enhance innate and adaptive immunity. These include checkpoint blockade antibodies (e.g anti-CTLA-4 or anti-PD1) targeting suppression of T cells, or antibodies against tumor-associated antigens (e.g. anti-HER2, anti-EGFR and anti-CD20) inhibiting signaling pathways, which are important for tumor cell proliferation, angiogenesis and metastasis, as well as inducing ADCC or complement-dependent cytotoxicity (CDC) [471, 472]. An example for successful antibody therapy is the anti-EGFR human-mouse chimeric monoclonal antibody cetuximab, which was approved by the FDA for the treatment of patients with advanced HNSCC. Cetuximab treatment resulted in improved survival of patients in clinical trials when given in combination with radiotherapy or cisplatin chemotherapy [473]. However, administration of antibodies can result in adverse side effects (e.g. allergic reactions, hypertension or diarrhea) and toxicity caused by on- and/or off-target effects due to the choice of antigens or antibody construct [474]. In case of cetuximab skin toxicity could be observed due to the expression of EGFR in the basal layer of the epidermis. Moreover, some patients were less responsive to cetuximab treatment due to the expression of the mutant EGFRvIII variant on tumor cells and polymorphisms in the FcγRIIIa (CD16a) receptor, that impact binding of cetuximab to cytotoxic lymphocytes [473, 475]. A critical aspect for efficacy and applicability of antibody therapy is therefore the targeted tumor antigen. Most antigens are either not exclusively expressed by tumor cells, show a high degree of mutations in tumor entities or can be downregulated during tumor progression.

In this respect, *Salih* and coworkers [476] introduced a recombinant fusion protein of the NKG2D ectodomain and a human IgG-Fc part as therapeutic option for the treatment of leukemia and breast cancer, especially HER2/neu negative breast cancer cells, which were not susceptible to trastuzumab (monoclonal anti-HER2/neu antibody) treatment. They could show the induction of ADCC-mediated antitumor/-leukemia NK cell reactivity against NKG2D ligand expressing tumor cells *in vitro* by the NKG2D fusion protein with an ADCC-optimized Fc part [476, 477]. However, binding of the NKG2D fusion protein to NKG2D ligands on tumor cells blocked NKG2D-mediated activation and cytolytic function of NK cells. Moreover, the efficacy against tumors and the emergence of possible side effects (e.g on NKG2D ligand expressing healthy tissues) must be further addressed in *in vivo* studies. The development of therapeutic anticancer agents is therefore dependent on the extensive and critical

evaluation of their pharmacodynamics, pharmacokinetics, immunogenicity and effector functions in laboratory and clinical trials.

Besides, cellular therapies based on adoptive transfer of NKG2D$^+$ cytotoxic lymphocytes (i.e. NK cells) showed promising therapeutic potential in patients suffering from leukemia and some solid tumors [478]. Several clinical trials showed a beneficial effect of *ex vivo* IL-2 expanded and activated allogeneic NK cell transfusion or NK cell transfer in combination with IL-2 treatment in cancer patients without causing severe GvHD [479-482]. Moreover, redirecting genetically engineered T cells expressing an NKG2D-targeting CAR could induce tumor elimination of NKG2D ligand expressing cells in a TCR-independent manner and even activated the hosts' antitumor immunity in mice [346-348, 483]. However, a recent study by vanSeggelen *et al.* [484] reported severe off-tumor toxicity of T cells expressing different NKG2D-CAR constructs in multiple mouse strains. The authors concluded that the high expression levels of highly active NKG2D-CARs led to the recognition of NKG2D ligands expressed on healthy tissues. The combination of CAR T cells and chemotherapy thereby enhanced toxicity by upregulation of NKG2D ligands in the lung of the mice. Moreover, they could show, that NKG2D-CAR expressing T cells secreted high levels of inflammatory cytokines, which might contribute to severe toxicity, similar to those observed in several clinical trials with T cell therapies [485]. Due to the severe toxicity of NKG2D-CAR T cells in mice, the use of NKG2D-CAR T cells for therapeutic applications in humans should be carfully considered. Regarding the safety of cytokine-activated allogeneic NK cells in clinical trials and the enhanced antitumor efficacy of NKG2D-CAR transduced NK cells in mice [353], NK cell-based cellular therapies might be a promising alternative approach in cancer therapy.

The efficacies of cellular therapies or the different NKG2D-targeting immunotherapeutic strategies, however, depend on a robust expression of the ligands on the tumor cell surface and the NKG2D receptor on cytotoxic immune cells, which can both be impaired by the release of NKG2D ligands. This could be demonstrated in a clinical phase I/II trial in which patients suffering from high-risk neuroblastoma were treated with allogeneic IL-2 stimulated NK cells after HSCT in order to improve the clinical outcome [305]. In this study, elevated levels of sMICA in patients' plasma correlated significantly with impaired NKG2D-dependent cytotoxicity of the donor NK cells *in vivo*. This effect could only be temporarily reversed by infusion of large numbers of *ex vivo* stimulated NK cells expressing high NKG2D levels, which could retain cytotoxicity via non-occupied NKG2D receptors after sMICA scavenging.

Therefore, cellular immunotherapies should be combined with NKG2D-dependent tumor immune escape intervention strategies to improve their antitumor efficacy. In this respect, neutralizing monoclonal antibodies against the soluble NKG2D ligands might be considered. Jinushi *et al.* [486] could show that patients treated with anti-CTLA-4 antibodies or vaccinated with autologous, irradiated tumor cells had high titers of anti-MICA antibodies, which correlated with decreased sMICA levels and opsonized tumor cells for DC cross-presentation. However, the numerous NKG2D ligands would require the clinical administration of a cocktail of ligand-specific antibodies or the use of recombinant NKG2D proteins, which could both bind to membrane associated NKG2D ligands on tumor cells and therefor block the NKG2D-dependent tumor clearance by cytotoxic lymphocytes. Since NKG2D ligand shedding is mediated by MMPs, targeting MMP activity might be a possibility for intervention. Due to the contribution of MMPs to aggressive tumor growth, metastases, angiogeneis and poor patients prognosis, several MMP inhibitors were studied in clinical cancer trials to inhibit tumor progression and angiogenesis [487]. MMPs are involved in many other processes such as tissue morphogenesis and tissue repair, therefore most of these trials failed due to severe side effects of the early broad-range MMP inhibitors [488, 489]. However, the therapeutic use of MMP inhibitors for intervention of NKG2D ligand shedding was not assessed in these trials. Combining MMP inhibitors for short-term treatment of cancer patients prior to cellular therapies could be a possible therapeutic strategy to enhance antitumor functions of immune cells. The re-production kinetics of sNKG2D ligands implicate that a short-term application of MMP inhibitors might be sufficient to inhibit NKG2D ligand release and render tumor cells more susceptibile to NKG2D-dependent recognition. Thus, changing the therapeutic regimen of MMP inhibitors might reduce systemic effects of the drugs.

4.6 Adsorption Apheresis of sNKG2D Ligands as new therapeutic Concept to improve Lymphocyte Functions

Within this thesis, it could be shown that the depletion of sNKG2D ligands from patients' plasma or cell culture supernatants was sufficient to restore NK cell cytotoxicity *in vitro*. Therefore, adsorption apheresis of sNKG2D ligands was considered as therapeutic strategy to overcome NKG2D-dependent tumor immune escape and to improve the efficacy of cytotoxic lymphocytes. As proof of concept, the monoclonal antibody AMO1 with an epitope in the α1-

helical domain of the representative ligand MICA coupled to different matrices proofed useful to efficiently remove sMICA from human plasma at apheresis-like conditions *in vitro*. Moreover, the antibody epitope, which is located in a highly conserved region of MICA, ensured the recognition and depletion of different allelic variants and even MICA released on exosomes (MICA*08). This is of importance regarding the high polymorphism and the variable MICA allelic frequencies in a number of human populations as well as the lack of allele and haplotype profiles of most cancer patients [220, 490]. Interestingly, no antibody with an epitope in the α3-helical domain could efficiently deplete sMICA from plasma as shown for the BAMO3 antibody. This might be due to masking of the recognition site by soluble factors interacting with sMICA in the plasma, conformational changes in the flexible terminus after shedding, or the proteolytical cleavage of sMICA variants with staggered termini lacking parts of the epitope [296, 298]. Interestingly, binding of the BAMO3 antibody to sMICA from human plasma was not altered when BAMO3 was used as capture antibody in ELISA measurements. In addition, the BAMO3 antibody could not inhibit shedding of sMICA (data not shown) although its binding region overlapped in parts with the binding site of the disulfide-isomerase ERp5, which is needed for MICA cleavage and was proposed as target for MICA shedding intervention [299, 491]. Thus, antibodies for an intracorporeal intervention of MICA shedding or sMICA neutralization must be carefully analyzed with respect to toxicity, their epitope and binding properties as well as blocking NKG2D recognition of membrane-bound MICA on tumor cells. Adsorption apheresis is an extracorporeal application and the choice and development of antibody constructs or recombinant proteins might not be as critical, since the immunogenic side effects and toxicity mediated by therapeutic antibodies and proteins are due to the *in vivo* application. Moreover, choosing an antibody with an epitope in the NKG2D binding site does not interfere with NKG2D recognition of tumor cells *in vivo*.

Although monoclonal antibodies are commonly used as therapeutic agents in several clinical settings and the bioprocessing technology for the large-scale production of clinical grade antibodies advanced [492], generating an adsorber cartridge using multiple monoclonal antibodies for the different NKG2D ligands might not be applicable for the clinics due to unreasonable manufacturing efforts. The patient specific composition of the individual sNKG2D ligands in the plasma would further necessitate the generation of individualized adsorber matrices with different combinations and amounts of the respective anti-NKG2D ligand antibodies to ensure efficient removal of all ligands leading to NKG2D inhibition. The generation of an adsorber

containing six different antibodies or the use of six different adsorber cartridges in an apheresis setup is technically demanding, uncommercialy, and the combination of numerous antibodies might not be compatible with guidelines for FDA approval. Morover, the high polymorphism of the NKG2D ligands is critical for the selection of each individual antibody regarding specificity to the ligands and the capability to recognize distinct allelic variants. In this respect, the biotinylated NKG2D::IgG1-Fc fusion protein developed in this thesis was validated for the efficient and simultaneous depletion of sNKG2D ligands from human plasma. In contrast to the recombinant NKG2D proteins produced in *E. coli*, the fusion of the NKG2D ectodomain to the human Fc part containing a biotinylation sequence enhanced protein stability, improved the production and purification steps using a mammalian cell line and ensured the Fc-directed immobilization of functional proteins due to the biotin-tag. *In vitro* depletion experiments further demonstrated that the NKG2D fusion protein removed the sNKG2D ligands from human plasma with comparable efficacy as the cocktail of monoclonal antibodies used for the depletion prior to cytotoxicity assays. The NKG2D-functionalized matrix for adsorption apheresis would have several advantages: i) the production process of the NKG2D fusion proteins is comparable to that of recombinant monoclonal antibodies with regard to cell lines used and purification strategies [493], but would need the industrial clinical-grade production of only one protein component, ii) the recombinant NKG2D proteins can bind to all different ligands and their allelic variants comparable to the NKG2D receptor on cytotoxic lymphocytes and antagonizes the key player of tumor immune escape, and iii) the pan-specific adsorber would therefore be applicable to a broad patient cohort independent of the sNKG2D ligand composition in the plasma. However, since the NKG2D protein was developed for the laboratory use, industrial high-scale production processes and coupling procedures must be specially optimized from the currently used protocols and further characterized and validated for a pre-clinical study and future clinical application.

To proof the feasibility of adsorption apheresis of sNKG2D ligands in a living organism, a pre-clinical study using the anti-MICA (AMO1) antibody-functionalized adsorber was conducted in rhesus monkeys. Although murine models are a powerful tool to address immunological questions in cancer research, several genetical and functional differences in NK cell subpopulations, the different expression and function of inhibitory and activating receptors, especially of the NKG2D receptor and its diverse ligands [451, 494, 495], limit their use for analysis of NKG2D-dependent NK cell functions. Moreover, the small body size and related

blood volume of mice accounts for technical constraints for adsorption apheresis. In contrast, due to the high phylogenetic relatedness of humans and non-human primates, NK cell subtypes and the NKG2D/NKG2D ligand system display a high degree of homology [496]. Moreover, the body size and blood volume of rhesus monkeys allowed for the validation of adsorption apheresis using the Life18^{TM} apheresis unit, which is currently used for apheresis applications in the clinics. The proof of concept study in rhesus monkeys demonstrated that the quantitative removal of sMICA could be achieved after only three plasma volume exchanges and therefore proofed technically feasible and might be a supportive therapy for HNSCC patients in order to restore cytotoxicity of NKD2D^{+} immune cells. However, the non-disease animal model could not reveal the re-production kinetics of sNKG2D ligands by tumor cells *in vivo*. Since no inhibitory effect of human sMICA could be observed on basal NKG2D expression levels of non-activated NK cells during the experiment, the impact of sMICA depletion on the cytotoxic capacity of the animals' immune cells could not be determined. These questions must be addressed in future clinical trials with cancer patients. However, based on the results from *in vitro* cytotoxicity experiments adsorption apheresis of sNKG2D ligands might help to maintain and prolong the cytotoxic activity of endogenous NKG2D^{+} NK cells and, if combined prior to administration of cellular therapies, of adoptively transferred immune cells after haploidentical stem cell transplantation. Besides healthy donor derived cell products this will also include T cells and NK cells which have been functionalized with CARs, especially NKG2D-CARs. Several studies showed that NKG2D is upregulated on activated CD8^{+} T cells and enhanced T cell proliferation, Ca^{2+}-mobilization as well as mediate TCR-independent killing of NKG2D ligand expressing tumor cells by CD8^{+} and γδ T cells [195, 215, 216, 266, 497, 498]. Moreover, sNKG2D ligands and TGF-β1 lead to impaired NKG2D expression levels and activation of T cells [315, 319, 401, 499]. Thus, although NKG2D functions as co-stimulatory receptor in CD8^{+} T cells and γδ T cells it is supposed that sNKG2D ligand apheresis might also improve the antitumor functions of these immune cells.

Compared to NKG2D-dependent tumor immune escape interfering immunotherapies, which rely on the administration of therapeutic compounds, adsorption apheresis represents a minimal invasive procedure similar to plasmapheresis in autoimmune diseases and hemodialysis of diabetic patients, which can be repeated several times to scavenge reappearing sNKG2D ligands from patients' plasma without causing severe side effects [500, 501]. Therefore, ad-

sorption apheresis represents an ideal supportive therapeutic concept, which can be combined with several immunotherapies such as adoptive immune cell transfer or antibody therapy to improve antitumor immunity.

4.7 Concluding Remarks and Perspectives

During the last years, the number of therapeutic strategies for cancer treatment increased due to advances in our understanding of tumor immunology. The development of new immunotherapies substantially increased the clinical outcome of cancer patients. However, a large number of patients fail to respond and succumb to progressive disease. A central goal in oncology is therefore the identification of new biomarkers and the use of combinatorial cancer therapies to individualize therapeutic regimens and to overcome tumor immune escape mechanisms.

The results of this thesis demonstrated the impact of sNKG2D ligands in HNSCC. The patterns of soluble immunosuppressive factors were shown to be patient specific and to depend on the individual clinical situation. Thus, profiling of sNKG2D ligands in patients' plasma together with immunosuppressive cytokines, especially TGF-β1, should be considered in the clinics as diagnostic and/or prognostic marker combination. To ensure a stable diagnostic procedure, diverse NKG2D ligand ELISAs could be optimized for clinical use. Furthermore, the development of cytometric bead arrays for the multiple NKG2D ligands would allow for the rapid detection of multiple parameters from small plasma sample volumes. Regarding the numerous therapies targeting the NKG2D/NKG2D ligand system and the broad expression pattern of sNKG2D ligands in multiple cancer entities, including sNKG2D ligands in the diagnostics of cancer patients would help to stratify patient cohorts and select for individualized strategies to improve patients' outcome.

Along this line, adsorption apheresis of sNKG2D ligands might substantially increase the efficacy of tumor immunotherapy and might thus be a versatile supportive module in a variety of settings. The clinical-grade production of the NKG2D fusion proteins will allow for the evaluation of the pan-specific adsorber in a clinical study with a patient cohort selected for high sNKG2D ligand plasma levels. The clinical study will decipher the therapeutic potential of adsorption apheresis on the restoration of innate and adaptive immune cell functions as well as the reproduction kinetics of sNKG2D ligands by the tumor. Furthermore, adsorption

apheresis can be conducted in combination with subsequent cellular immunotherapy with allogeneic NK or T cells.

Several lines of argumentation indicate that adsorption apheresis of sNKG2D ligands might be a powerful supportive strategy in cancer therapy. First, the overall sNKG2D ligand level correlates with tumor burden as shown by studies with patients pre- and post-surgery. Thus, the tumor load determines the maximum level of sNKG2D ligands in the plasma. Second, adsorption apheresis will increase the fraction of $NKG2D^+$ immune cells that are capable of attacking $NKG2DL^+$ tumor cells. In turn, the tumor mass and its capacity to reproduce sNKG2D ligands will be reduced. Third, adsorption apheresis is an extracorporeal application and does not interfere with antitumor NKG2D-dependent immune cell functions. Along this line, it is a minimal invasive strategy that can be repeated several times after cellular therapy in order to scavenge reappearing sNKG2D ligands from patients' plasma. Moreover, previous results indicated that plasma levels of sNKG2D ligands (i.e. sMICA) remained low for more than 72 h after scavenging in neuroblastoma patients [305]. Therefore, a considerable time frame between two adsorption apheresis cycles might exists for improved antitumor activity of cytotoxic lymphocytes. Thus, the periodic boosting of the $NKG2D^+$ immune cells by adsorption apheresis will lead to constant shrinking of the tumor mass, sustained reduction of sNKG2D ligand plasma levels, and extended antitumor activity of $NKG2D^+$ immune cells. Notably, the intervals between two cycles of adsorption apheresis might increase with tumor mass reduction. Furthermore, the apheresis concept could be easily expanded combining two adsorber cartridges to deplete further soluble immunosuppressive factors in particular TGF-β1, which was shown to have an additive effect on NKG2D-dependent NK cell inhibition.

Whereas hematological malignancies are highly susceptible to immunotherapies, the development of successful treatments for solid cancers is still challenging and often limited by low infiltration capacities of cytotoxic lymphocytes as seen in primary tumors of HNSCC patients. Different factors such as immunoediting, immunoevasion and the cellular crosstalk with other immune cells within the complex tumor microenvironment influence the antitumor activity of T and NK cells [281, 502-505]. Within this thesis, infiltration studies using tumor spheroids further indicated a potential role of sNKG2D ligands on inhibition of NK cell infiltration. However, the molecular mechanism how sNKG2D ligands reduce infiltration frequencies of NK cells in primary tumors must be further elucidated. Furthermore, the determination of the phenotype and functionality of infiltrating immune cells vs. immune cells in the tumor pe-

riphery might be of importance to establish and optimize protocols for the generation of efficacious effectors for the use in cellular cancer therapies. Up to now, the majority of data about human NK cell subtypes were based on studies with peripheral blood lymphocytes and little is known about NK cells in human tissues due to their limited accessibility. Moreover, the use of syngeneic mouse models is limited due to phenotypical and functional differences of murine and human NK cell subsets [506]. The tumor spheroid model and the presented MACS-based NK cell isolation protocol (see 5.1.4) offers the possibility to separate NK cell subpopulations of the tumor periphery from infiltrated NK cells and allows for the quantitative recovery of viable infiltrated NK cells. In order to decipher phenotypic differences, which account for the ability to infiltrate tumor spheroids, these isolated and enriched NK cell subpopulations could be further used in comparative microarray analyses to determine mRNA expression profiles of inhibitory and activating receptors, cytokines/chemokines and integrins. In addition, proteomic and gene expression profiles of NK cell subpopulations could be assessed using mass cytometry (CyTOF) or single cell PCR. Using NK cells pre-incubated with human plasma or cell culture supernatant will thereby help to decipher the modulatory potential of sNKG2D ligands and other soluble immunoregulatory factors on immune cell activity. The 3D spheroid model and MACS-based isolation protocol could be further adapted to different cytotoxic lymphocyte populations, such as NKT cells, $CD8^+$ and γδ T cells. Furthermore, other cell types that might affect the tumor micromilieu can be included into the tumor spheroid assays to introduce further complexity of the tumor microenvironment and allow the analysis of the cellular cross-talk between different immune cells. Besides, tissue-derived tumor spheres and organotypic multicellular spheroids could be directly generated by dissection of primary tumor tissues from cancer patients [507]. The phenotypic and transcriptional profiling data could not only increase the understanding of the diverse functions of NK cell subpopulations but could also be used for stratification of patient- or donor-derived immune cells to improve and personalize cellular immunotherapy.

5 Appendix

5.1 Supplemental Data

5.1.1 sNKG2D Ligand Patterns in HNSCC Patients' Plasma

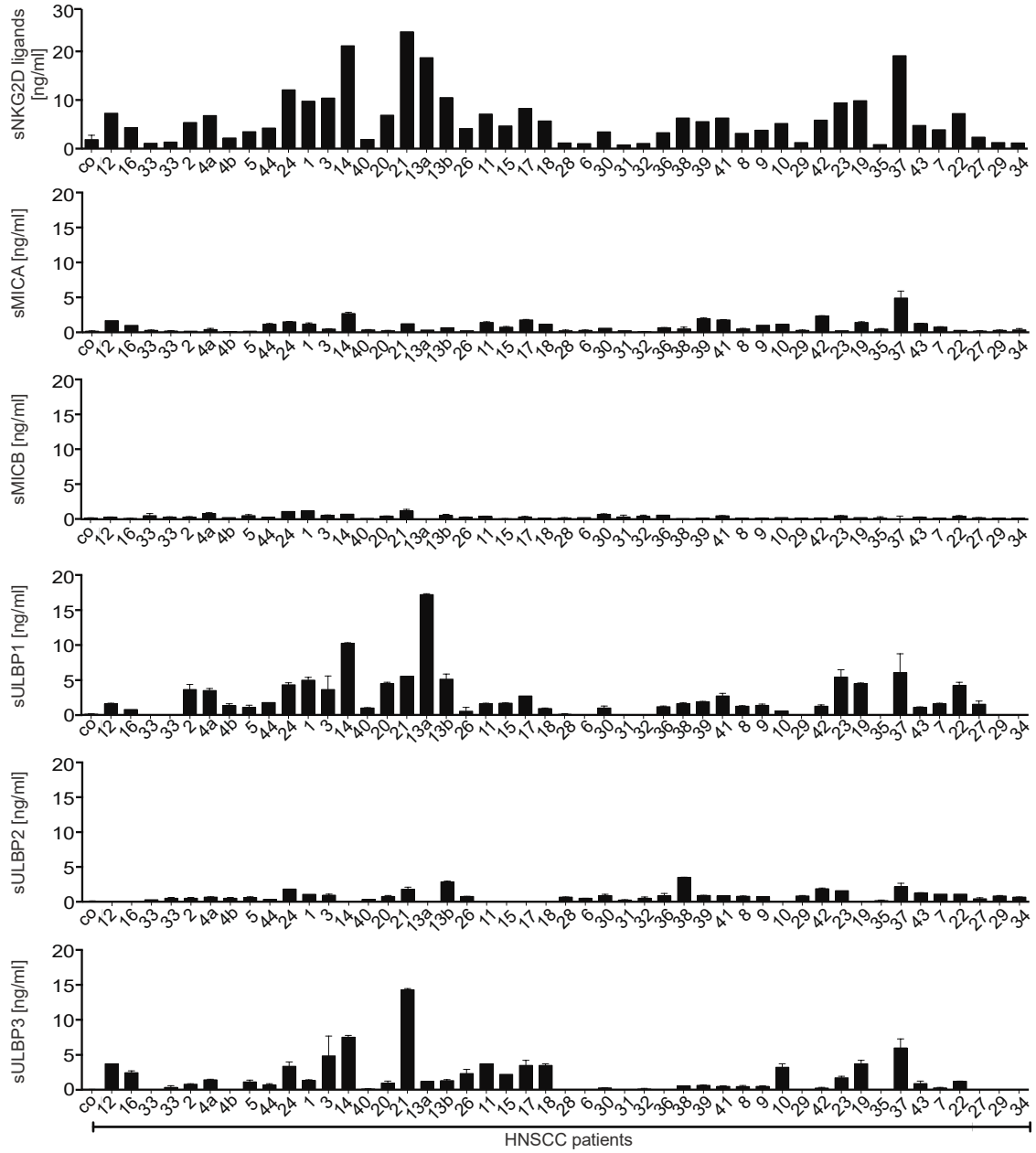

Figure S1: sNKG2D ligand plasma levels of individual HNSCC patients.
Patients' plasma samples were analyzed for their sNKG2D ligand levels by respective ELISAs (see also Figure 5). HNSCC patients are indicated by number and are presented with increasing disease stage (I - IVC). The mean plasma levels of 12 age-matched healthy controls were used as controls (CO). Bars correspond to mean ± SEM of duplicates or the sum of sNKG2D ligands for each patient.

5.1.2 Gating Strategies of Cytotoxicity Assays

Gating strategies of cytotoxicity assays for evaluation of tumor cell lysis in cell suspension (Figure S2; according to 3.1.4) and tumor spheroids (Figure S3; according to 3.2.3). Tumor ($CFSE^+$) and NK ($CD45\text{-}APC^+$) cell populations were separated. Tumor cell killing was calculated based on live/dead cell discrimination according to SytoxBlue staining. The ratio and total cell count of live ($CFSE^+/SytoxBlue^-$) and dead ($CFSE^+/SytoxBlue^+$) cells was determined. Dot plots of representative experiments are shown for human plasma or CAL27 supernatant pre-treated NK cells.

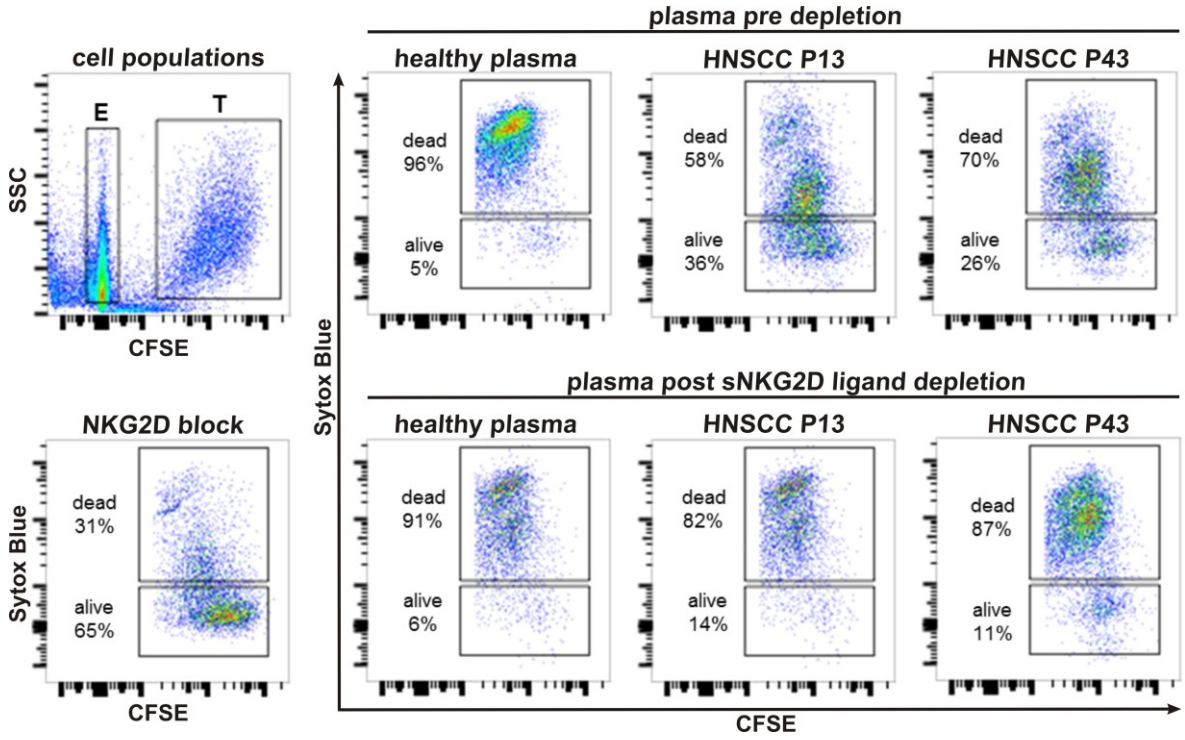

Figure S2: Cytotoxicity assays with plasma-treated primary human NK cells.
Flow cytometric analysis of cytotoxicity assay with human plasma pre-treated primary NK cells towards SiHa target cells (see also Figure 11). Gating strategy on CFSE-labeled SiHa target (T) and anti-CD45-APC stained effector (E) NK cells and analysis of live ($CFSE^+/SytoxBlue^-$) and dead ($CFSE^+/SytoxBlue^+$) cells in the target cell population (T). Dot plots of a representative experiment are shown for non-depleted and sNKG2D ligand-depleted healthy plasma and two HNSCC patients' plasma (patient 13 and 43). NK cells pre-incubated with anti-NKG2D blocking antibodies served as control.

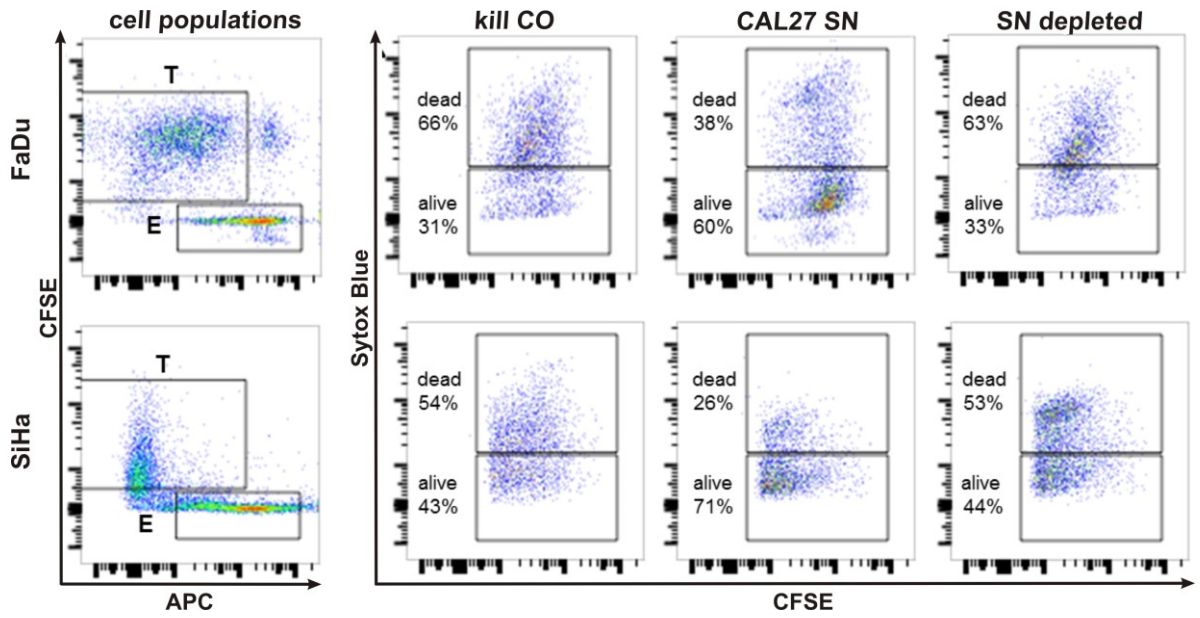

Figure S3: Cytotoxicity assay of FaDu and SiHa tumor spheroids.
Flow cytometric analysis of tumor spheroids cytotoxicity assays with CAL27 SN and NKG2D-ligand depleted SN pre-treated primary human NK cells (see also Figure 23). Gating strategy on CFSE-labeled target (T) and analysis of live ($CFSE^+/SytoxBlue^-$) and dead ($CFSE^+/SytoxBlue^+$) target cells. Dot plots of one representative experiment are shown for FaDu and SiHa spheroids.

5.1.3 Infiltration of Tumor Spheroids

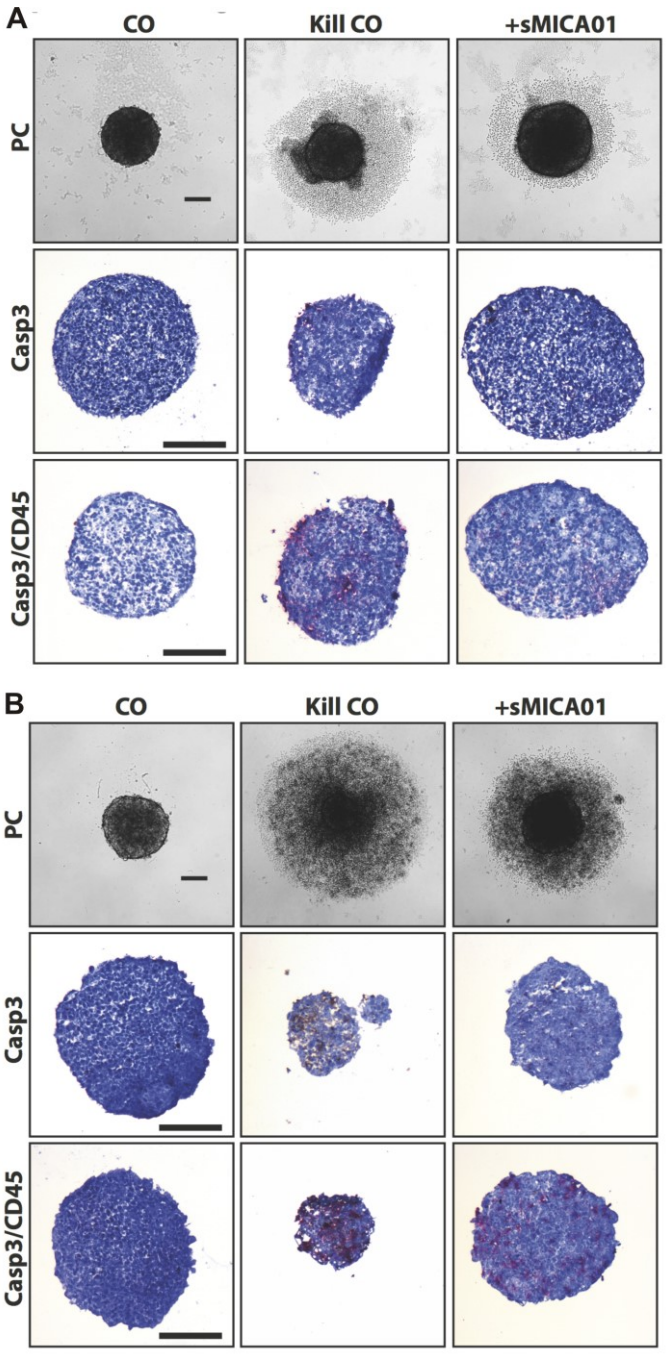

Figure S4: NK cell infiltration into tumor spheroids.
NK cells were pre-treated overnight with sMICA01 or were left untreated (kill CO) prior to co-culturing with CAL27 (A) or SiHa cells (B) (see also Figure 24). Tumor spheroid formation was monitored by light microscopy for 48 h. Cryosections of spheroids after 48 h were stained for NK cells (anti-CD45 antibody, red) and apoptosis (anti-active caspase-3 antibody, brown). Representative histology pictures are shown at 200x magnification. Size bar corresponds to 200 µm.

5.1.4 MACS-based Protocol for the Isolation of Tumor Spheroid infiltrating NK Cells

Solid SiHa tumor spheroids were co-cultured with primary human NK cells at a low E:T ratio of 3:1 for 24 h. Peripheral NK cells were removed from the spheroid fraction and disintegrated tumor spheroids were subjected to MACS isolation for the recovery of infiltrated $CD45^+$ NK cells. The resulting three fractions were generated i) peripheral non-infiltrating NK cells in the tumor spheroid supernatant (P), ii) tumor cells in the flow through of the MACS column (F), and iii) infiltrated NK cells recovered after elution from the MACS column (E) (Figure S5A). Flow cytometric analysis of the individual cell fractions showed that the majority of NK cells were detected in the periphery as seen earlier in microscopic analyses. A total count of $30.5 \pm 4.8 \times 10^4$ peripheral and $3.5 \pm 1.3 \times 10^4$ (16.2% of total NK cells) infiltrated NK cells could be recovered from SiHa tumor spheroids (Figure S5B). Regarding cell viability, 80.5 ± 0.5 % of the peripheral NK cells were viable (P fraction: 1.0 ± 0.0 % dead NK cells) compared to 74.3 ± 6.9 % viable infiltrated NK cells (E fraction: 12.7 ± 7.1 % dead NK cells; Figure S5C). Most importantly, infiltrated NK cells could be isolated with a high purity, with only 22.7 ± 2.7 % tumor cells (Figure S5C/D). Moreover, analysis of tumor cell viability demonstrated efficient tumor cell killing after 24 h co-incubation with 51.7 ± 1.4 % residual viable and 29.0 ± 3.2 % dead tumor cells in the flow through (F fraction) and only 7.0 ± 0.0 % viable and 11.5 ± 1.5 % dead tumor cells in the periphery (P fraction). Notably, tumor spheroid destruction was incomplete due to the low E:T ratio used in these experiments focused on NK cell infiltration. Thus, the presented tumor spheroid assay proofed useful to investigate immunosurveillance and associated immune escape by soluble mediators as well as tumor spheroid infiltration. Furthermore, the MACS-based isolation protocol offers new possibilities to investigate and characterize infiltrated NK cell subpopulations in future studies.

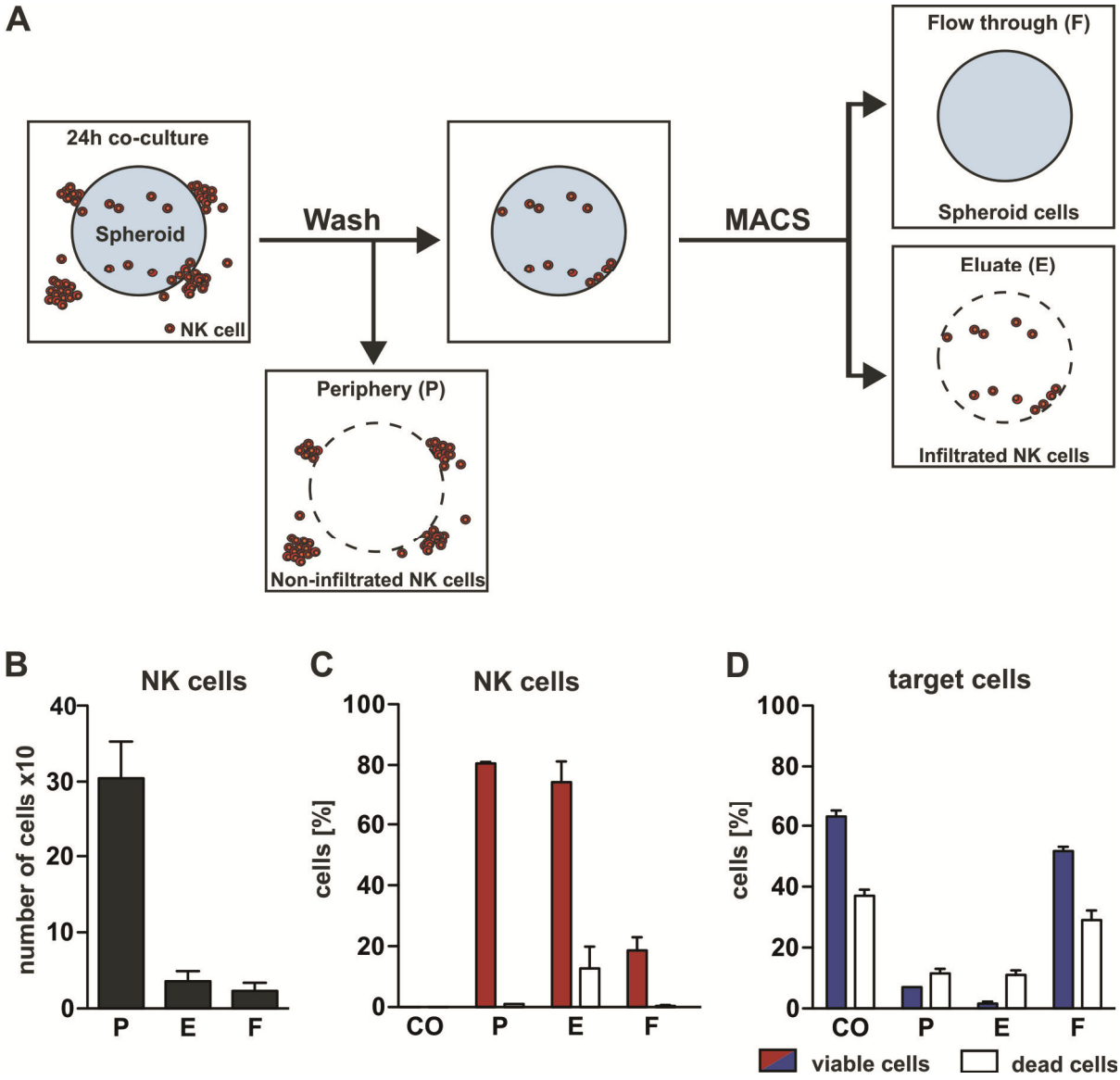

Figure S5: Isolation and enrichment of infiltrated NK cells from tumor spheroids.
(A) Work flow of MACS-based cell fractionation. Tumor spheroid co-cultures (E:T=3:1; 24 h) of a 96-well plate were pooled, washed to remove peripheral NK cells (P) and residual spheroids were disintegrated and subjected to CD45 MACS-bead isolation leading to the flow through (F) containing tumor cells and the column eluate (E) containing infiltrated NK cells. Cells from all fractions were quantified by flow cytometry after SytoxBlue staining (live/dead discrimination). Tumor spheroids cultured without NK cells served as controls. (B) Total number of viable $CD45^+$ NK cells per fraction. Quantification of cell viability for NK cells (C) and tumor cells (D). Data is represented as mean ± SEM of three individual experiments.

5.1.5 Production of recombinant Proteins

Soluble MICA variants for ELISA (rMICA*01/04; sMICA*01/04), depletion (sMICA*01/04; MICA*01/04::hIgG1-Fc) or adsorption apheresis (sMICA*04) studies.

*5.1.5.1 E. coli derived rMICA*01/04*

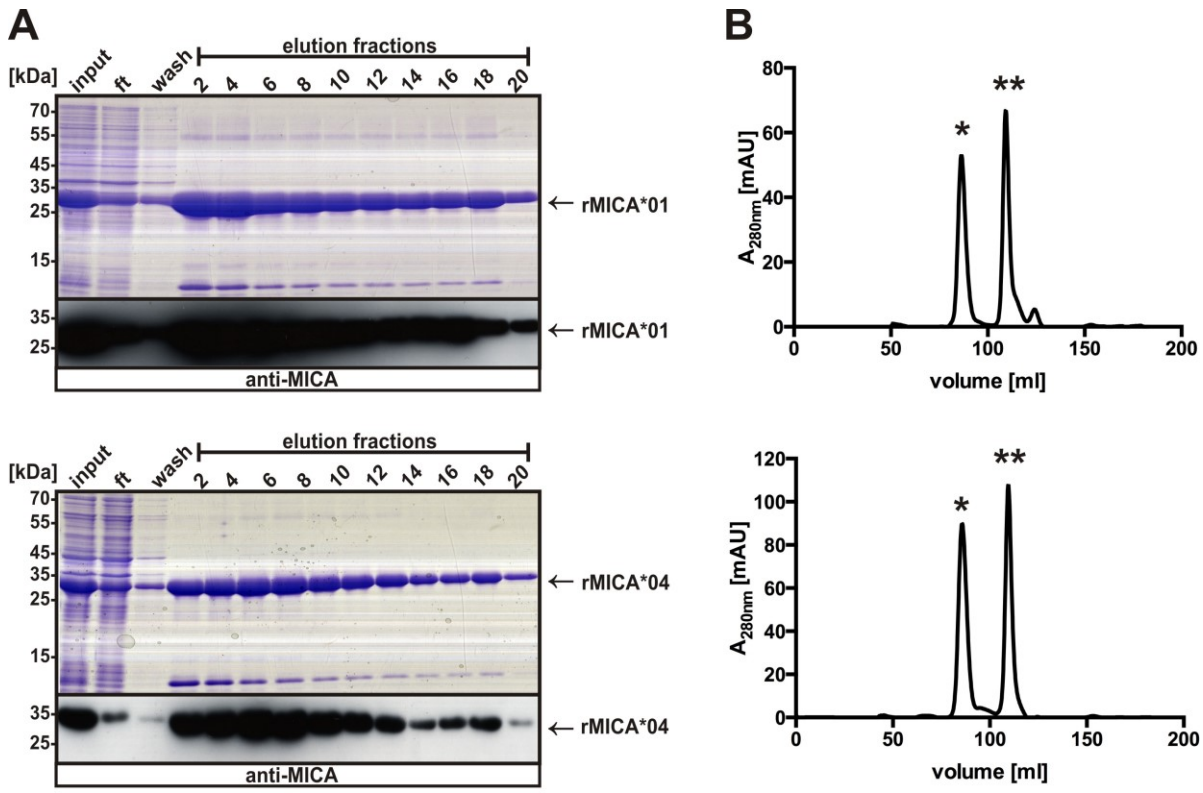

Figure S6: Production and purification of rMICA*01/04 from *E. coli*.
Recombinant proteins rMICA*01 (upper panel) and rMICA*04 (lower panel) were expressed in *E. Coli* and purified from inclusion bodies. (A) Reducing SDS-PAGE (Coomassie-stained) and immunoblot (polyclonal anti-MICA antibody in combination with an anti-goat HRP-conjugated antibody) of aliquots (input, flow-through (ft), wash and eluate fractions) of rMICA*01/04 (ectodomain containing a C-terminal His-tag) after affinity purification via Ni-NTA agarose from solubilized inclusion bodies. (B) Size exclusion chromatography (SEC) of purified and refolded rMICA*01/04 on a HiLoad 16/600 Superdex 200 pg column. * = MICA ~33 kDA; ** = degradation products ~5 kDA

*5.1.5.2 sMICA*01/04 produced in HEK293T Cells*

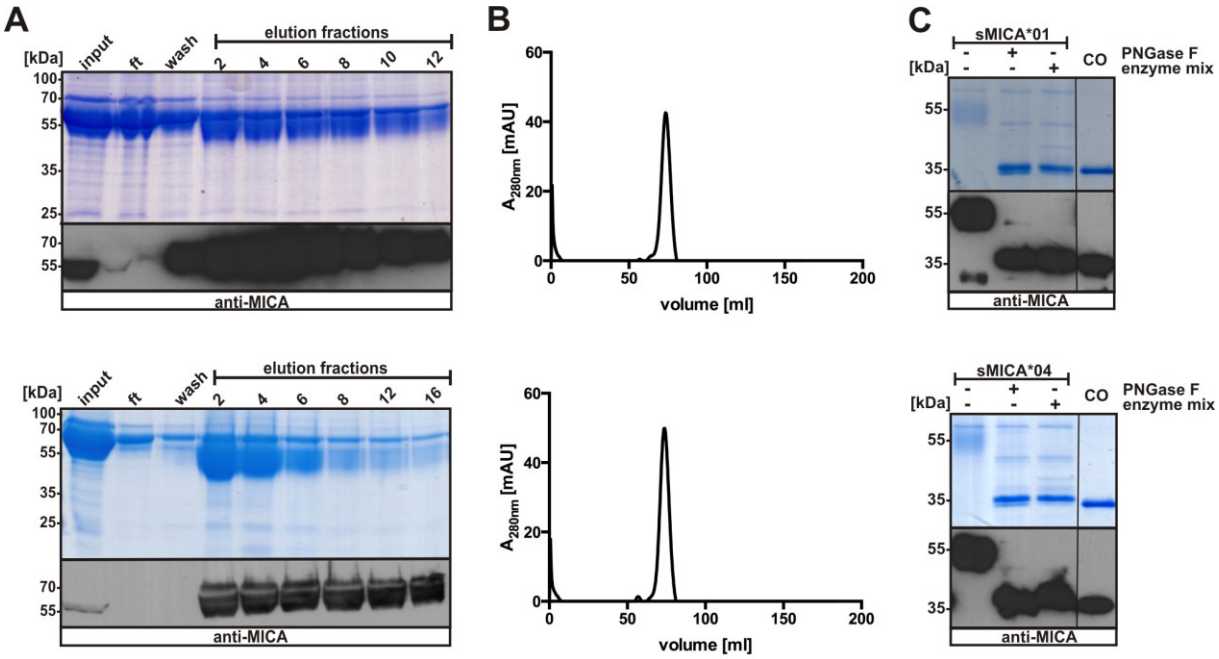

Figure S7: Characterization of recombinant sMICA proteins.
Recombinant proteins sMICA*01 (upper panel) and sMICA*04 (lower panel) were expressed in HEK293T cells after transient transfection. (A) Reducing SDS-PAGE (Coomassie-stained) and immunoblot (polyclonal anti-MICA antibody in combination with an anti-goat HRP-conjugated antibody) of aliquots (input, flow-through (ft), wash and eluate fractions) of sMICA*01/04 (ectodomain containing a C-terminal His-tag) after affinity purification via Ni-NTA agarose from HEK293T cell culture supernatants. (B) Size exclusion chromatography (SEC) of purified sMICA*01/04 on a Superdex 200 column. Peaks correspond to MICA proteins with a molecular mass of ~65 kDa. (C) Deglycosylation of purified sMICA*01/04 proteins. Reducing SDS-PAGE (Coomassie-stained) and immunoblot (polyclonal anti-MICA antibody in combination with an anti-goat HRP conjugated antibody) of untreated (glycosylated; lane 1), PNGaseF treated (removal of N-linked glycans; lane 2) or enzyme mix treated (removal of N- and O-linked glycans; lane 3) sMICA*01/04. The equivalent non-glycosylated sMICA variants produced in *E. coli* served as control (CO; lane 4).

*5.1.5.3 MICA*01/04::hIgG1-FcEQ produced in HEK293T Cells*

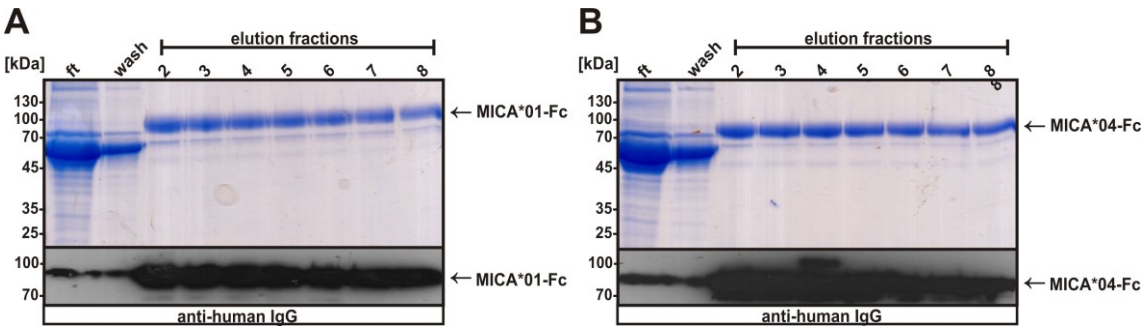

Figure S8: Production and purification of MIA*01/04::hIgG1-Fc proteins.
MICA*01(A) and sMICA*04 (B) Fc fusion proteins were expressed in HEK293T cells. Non-reducing SDS-PAGE (Coomassie-stained) and immunoblot (anti-human IgG HRP-conjugated antibody) of aliquots (flow-through (ft), wash and eluates) from Protein A purification of culture supernatants.

5.1.5.4 NKG2D::hIgG1-Fc produced in HEK293T Cells

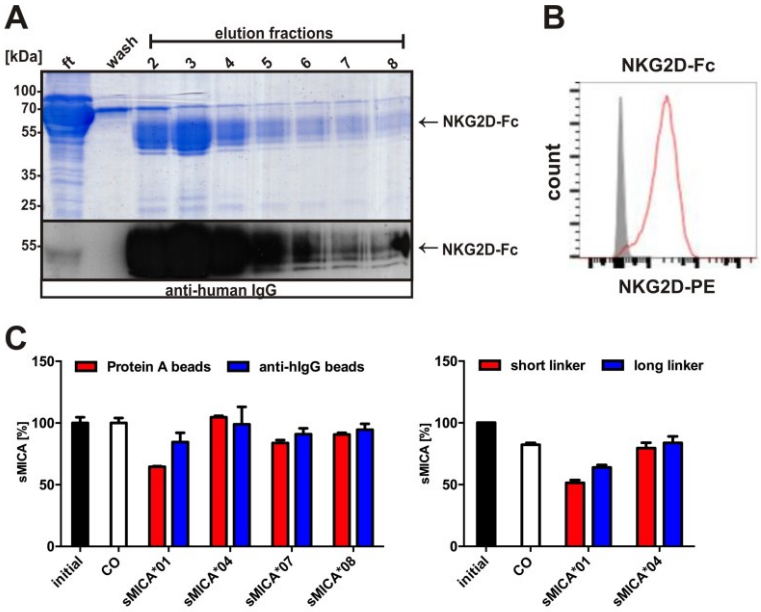

Figure S9: Characterization of NKG2D::hIgG1-FcEQ produced in HEK293T cells.
(A) NKG2D::hIgG1-Fc expressed in HEK293T cells. Non-reducing SDS-PAGE (Coomassie-stained) and immunoblot (anti-human IgG HRP-conjugated antibody) of aliquots (flow-through (ft), wash and eluates) after purification via Protein A from culture supernatants. (B) Binding analysis of NKG2D::hIgG1-Fc to HEK293T cells by flow cytometry with an anti-human IgG-Dylight649 antibody. Grey = antibody control, red = NKG2D. (C) Depletion of sMICA allelic variants using NKG2D::hIgG1 coupled to Protein A- or anti-human IgG magnetic beads (left) or fusion proteins containing a short (GSSG) or long ($(GGGS)_3$) flexible linker. Beads coupled with NKp30::hIgG1-Fc served as controls. MICA levels before and post depletion were determined by ELSIA and normalized to the initial sMICA levels. Data are represented as mean ± SEM of a representative experiment out of three.

5.1.6 Peptide Spot Sequences

MICA amino acid sequence (Q29983; aa 23 - 308); spots of 18mer peptides, off-set of 4 amino acids:

A1 AEPHSLRYNLTVLSWDGS	A24 EIRVCEIHEDNSTRSSQH	B11 PMVNVTRSEASEGNITVT
A2 SLRYNLTVLSWDGSVQSG	A25 CEIHEDNSTRSSQHFYYD	B12 VTRSEASEGNITVTCRAS
A3 NLTVLSWDGSVQSGFLTE	A26 EDNSTRSSQHFYYDGELF	B13 EASEGNITVTCRASGFYP
A4 LSWDGSVQSGFLTEVHLD	A27 TRSSQHFYYDGELFLSQN	B14 GNITVTCRASGFYPWNIT
A5 GSVQSGFLTEVHLDGQPF	A28 QHFYYDGELFLSQNLETK	B15 VTCRASGFYPWNITLSWR
A6 SGFLTEVHLDGQPFLRCD	A29 YDGELFLSQNLETKEWTM	B16 ASGFYPWNITLSWRQDGV
A7 TEVHLDGQPFLRCDRQKC	A30 LFLSQNLETKEWTMPQSS	B17 YPWNITLSWRQDGVSLSH
A8 LDGQPFLRCDRQKCRAKP	A31 QNLETKEWTMPQSSRAQT	B18 ITLSWRQDGVSLSHDTQQ
A9 PFLRCDRQKCRAKPQGQW	A32 TKEWTMPQSSRAQTLAMN	B19 WRQDGVSLSHDTQQWGDV
A10 CDRQKCRAKPQGQWAEDV	A33 TMPQSSRAQTLAMNVRNF	B20 GVSLSHDTQQWGDVLPDG
A11 KCRAKPQGQWAEDVLGNK	A34 SSRAQTLAMNVRNFLKED	B21 SHDTQQWGDVLPDGNGTY
A12 KPQGQWAEDVLGNKTWDR	A35 QTLAMNVRNFLKEDAMKT	B22 QQWGDVLPDGNGTYQTWV
A13 QWAEDVLGNKTWDRETRD	A36 MNVRNFLKEDAMKTKTHY	B23 DVLPDGNGTYQTWVATRI
A14 DVLGNKTWDRETRDLTGN	B1 NFLKEDAMKTKTHYHAMH	B24 DGNGTYQTWVATRICQGE
A15 NKTWDRETRDLTGNGKDL	B2 EDAMKTKTHYHAMHADCL	B25 TYQTWVATRICQGEEQRF
A16 DRETRDLTGNGKDLRMTL	B3 KTKTHYHAMHADCLQELR	B26 WVATRICQGEEQRFTCYM
A17 RDLTGNGKDLRMTLAHIK	B4 HYHAMHADCLQELRRYLK	B27 RICQGEEQRFTCYMEHSG
A18 GNGKDLRMTLAHIKDQKE	B5 MHADCLQELRRYLKSGVV	B28 GEEQRFTCYMEHSGNHST
A19 DLRMTLAHIKDQKEGLHS	B6 CLQELRRYLKSGVVLRRT	B29 RFTCYMEHSGNHSTHPVP
A20 TLAHIKDQKEGLHSLQEI	B7 LRRYLKSGVVLRRTVPPM	B30 YMEHSGNHSTHPVPSGKV
A21 IKDQKEGLHSLQEIRVCE	B8 LKSGVVLRRTVPPMVNVT	B31 SGNHSTHPVPSGKVLVLQ
A22 KEGLHSLQEIRVCEIHED	B9 VVLRRTVPPMVNVTRSEA	B32 STHPVPSGKVLVLQSHWQ
A23 HSLQEIRVCEIHEDNSTR	B10 RTVPPMVNVTRSEASEGN	

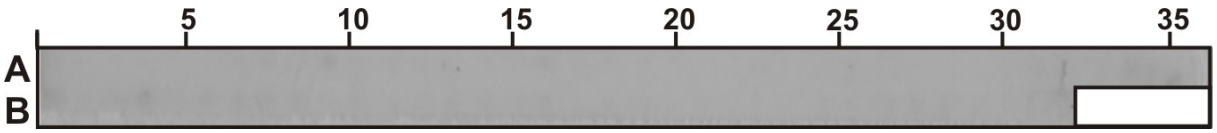

Figure S10: Peptide spot array control corresponding to Figure 26.
Peptide spot arrays (18mer peptides; off-set of 4 amino acids) of the human MICA were incubated with anti-mouse IgG HRP-conjugated antibody.

5.1.7 Expression of NKG2D Ligands on C1R and HEK293T Cells

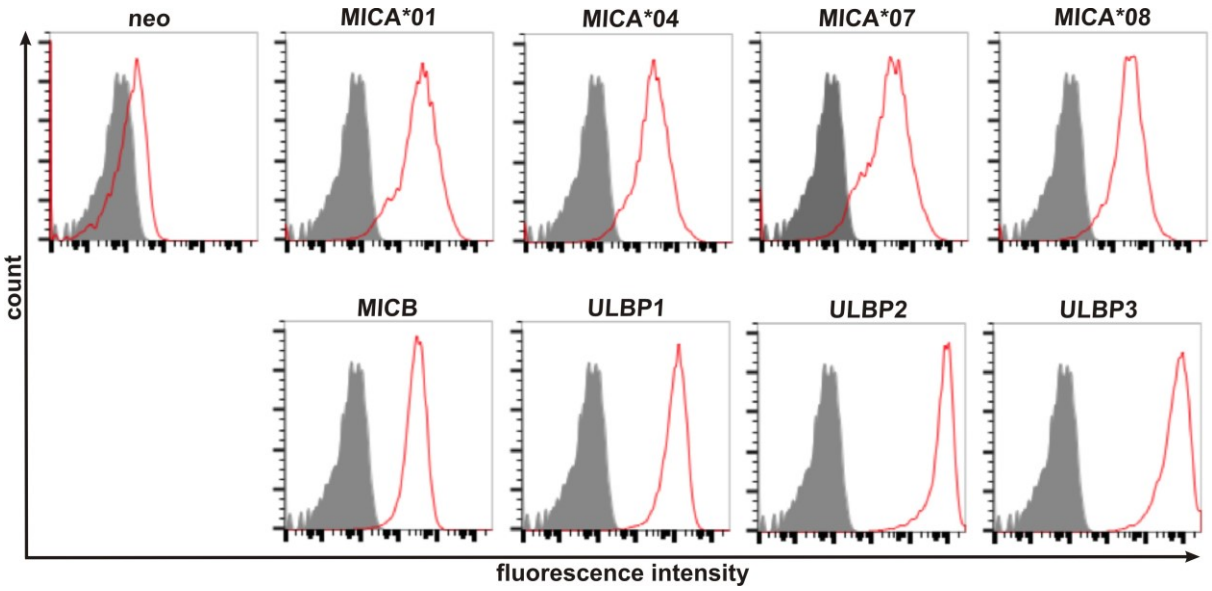

Figure S11: Surface expression of NKG2D ligands on NKG2D ligand transfected C1R cells.
Flow cytometric analyses of NKG2D ligand surface expression on C1R cell transfectants expressing sMICA allelic variants (sMICA*01, sMICA*04, sMICA*07 and sMICA*08), MICB, ULBP1-3 or C1R mock transfected (neo) cells. Respective cell clones were stained with monoclonal mouse anti-NKG2D ligand antibodies (all R&D systems) and anti-mouse IgG1 or anti-mouse $IgG2_{a/b}$ APC-conjugated secondary antibodies. Grey = secondary antibody control; red = NKG2D ligand antibodies.

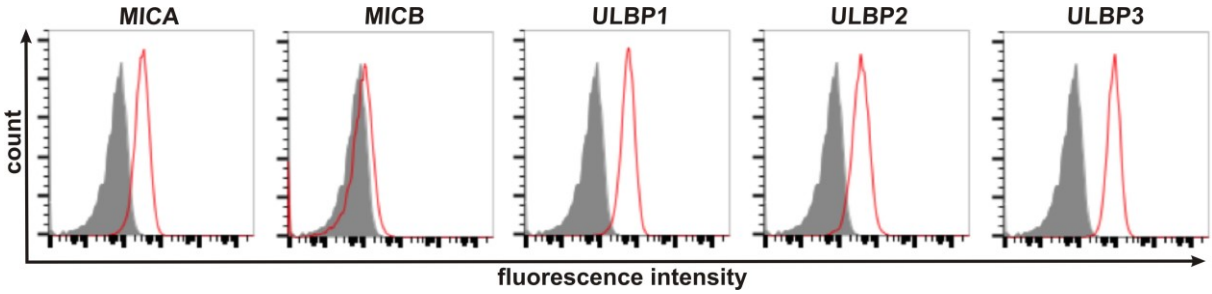

Figure S12: Surface expression of NKG2D ligand on HEK293T cells.
Flow cytometric analyses of NKG2D ligand surface expression on HEK293T cells. Cells were stained with monoclonal mouse anti-NKG2D ligand antibodies (all R&D systems) and anti-mouse IgG1 or anti-mouse $IgG2_{a/b}$ APC-conjugated secondary antibodies. Grey = secondary antibody control; red = NKG2D ligand antibodies.

5.1.8 Affinity Maturation of NKG2D Proteins

The binding affinity of protein-protein interactions determines the effect of biosensors, antibodies, small molecules or chemical compounds. Consequently, manipulation of binding affinities is an important point for the design and development of therapeutics. In this thesis, recombinant NKG2D proteins proofed to be a promising tool for the pan-specific adsorption of sNKG2D ligands from patients' plasma. Although NKG2D's binding affinities to the different ligands varied, successful depletion could be achieved for all ligands tested. Nevertheless, it was of interest, if the binding properties of NKG2D could be further improved. Therefor, a structure-based method for the rational prediction of single point mutations in the receptor-ligand binding interface that enhance binding affinities was used [508]. As proof of concept, point mutations for the enhanced binding to MICA were predicted depending on the crystal structure of the NKG2D-MICA complex (PDB; 1HYR) [243]. Single point mutations were bioinformatically calculated using the molecular modeling program Rosetta [509] by A. Metz (group of H. Gohlke, Computational Pharmaceutical Chemistry and Molecular Bioinformatics, Heinrich-Heine University, Düsseldorf, Germany).

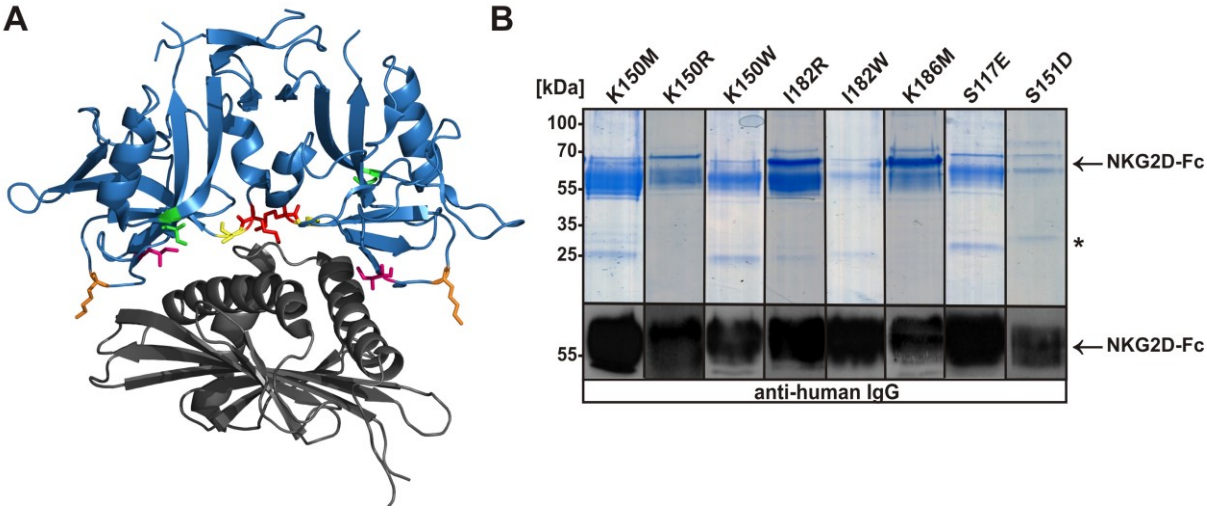

Figure S13: Production of NKG2D::hIgG1-Fc MICA-affinity mutants.
(A) Crystal structure of the NKG2D homodimer (blue) bound to the sMICA α1/2-helical domain (grey); PDB 1HYR. Amino acids in the NKG2D binding interface for mutation analyses are highlighted. Green = S117; red = K150; yellow = S151; purple = I182; orange = K186. (B) Reducing SDS-PAGE (Coomassie-stained) and immunoblot analyses (anti-human IgG-Fc HRP conjugated antibody) of affinity-purified NKG2D-Fc proteins containing the mutations K150M; K150R; K150W; I182R; I182W; K186M; S117E and S151D.

Based on the bioinformatical data, eight single mutations in the NKG2D's binding interface (Figure S13A) were chosen for laboratory characterization. The mutations comprise the amino acid substitutions of the lysine at position 150 to methionine (K150M), arginine (K150R) or tryptophan (K150W), the lysine at position 186 to methionine (K186M), the isoleucine at position 182 to arginine (I182R) or tryptophan (I182W), the serine at position 117 to glutamic acid (S117E) as well as the serine at position 151 to aspartic acid (S151D). Since changing the hydrophobic surface area can influence protein folding, NKG2D mutants produced in *E. coli* resulted in refolding problems for some mutants (data not shown). Therefor, the single mutations were introduced into the NKG2D::hIgG1-Fc protein and all eight mutants could be successfully expressed in HEK293T cells (Figure S13B).

Functional studies showed efficient binding of the mutants to HEK293T cells expressing different NKG2D ligands (Figure S14A). Interestingly, only slight differences in binding of the mutants compared to the wildtype NKG2D fusion protein could be observed. Further evaluation of the binding affinities to sMICA*01 by ELISA measurement revealed that the amino acid substitution K150R had no effect on binding affinity, whereas substitutions K150M, K150W, I182W and S151D led to the loss of sMICA*01 binding and the substitutions I182R and K186M had lower binding affinities compared to wildtype NKG2D::hIgG1-Fc. Interestingly, only the mutant with the S117E substitution showed a highly improved affinity to sMICA*01, which was 10-fold stronger than the binding of the wildtype NKG2D fusion protein (Figure S14B). The ELISA results are in accordance with the results from flow cytometry experiments indicating that the slight differences of cell surface binding are caused by the altered MICA recognition, whereas binding to the other ligands expressed on HEK293T cells seems to be unchanged. One explanation for the difference of the laboratory results and the *in situ* calculations could be the failure of the program to calculate the single point mutations simultaneously for both monomeric NKG2D binding sites. Thus, the impact on the structure and binding interface of the dimeric fusion proteins might be stronger than predicted. Nevertheless, the structure-based prediction of high affinity point mutations led to the generation of a NKG2D::hIgG1-Fc protein containing the amino acid substitution S117E with high affinity for MICA. In principal, these data show the possibility to further improve the binding properties of NKG2D. However, the use of the mutant protein as therapeutic agent might be critical, since changes in the binding interface could also affect the specificity of the NKG2D protein.

Therefore, further studies are needed for the detailed characterization of the mutant protein regarding binding affinity for cognate ligands and allelic variants as well as its specificity.

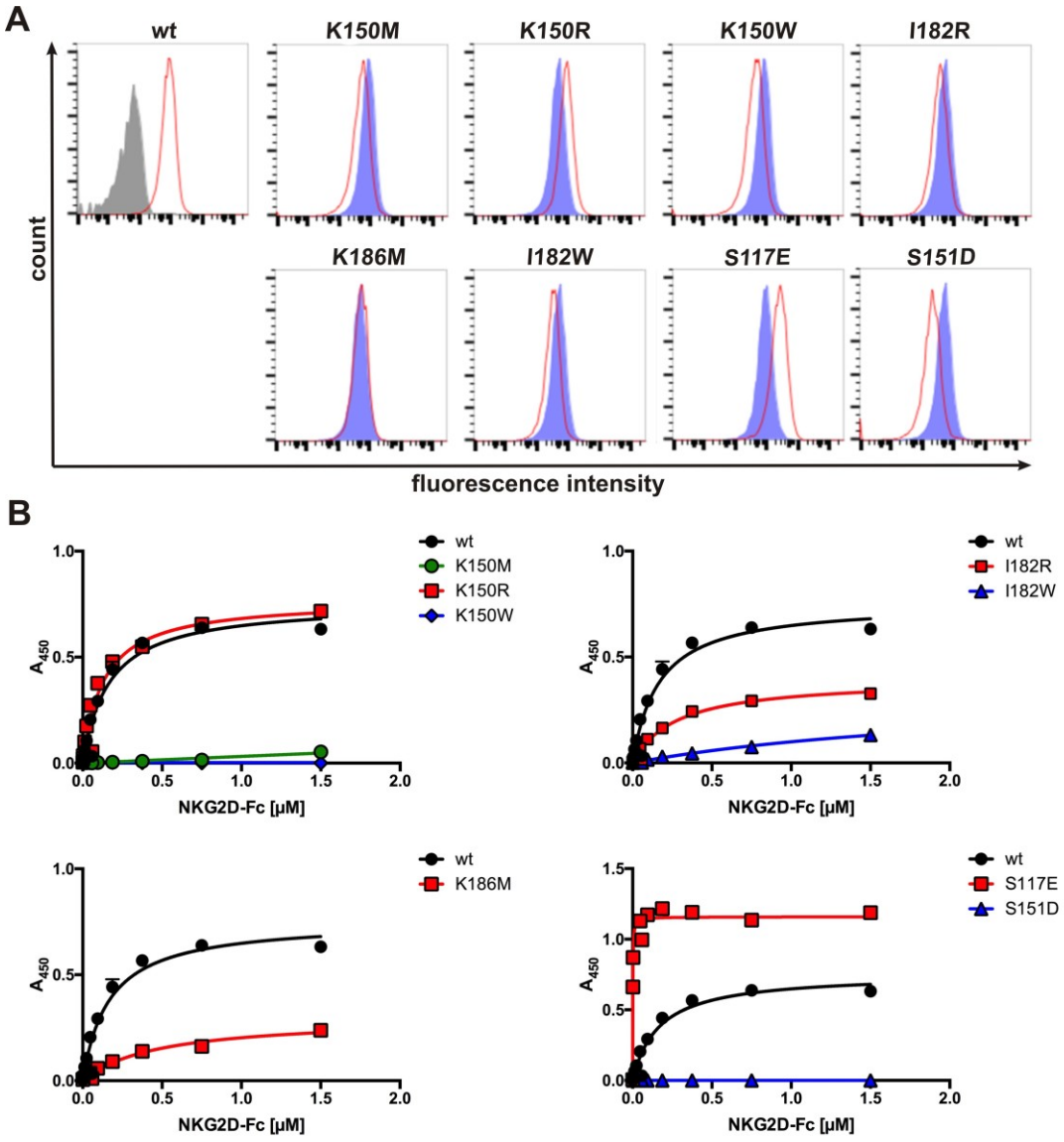

Figure S14: Binding characteristics of NKG2D::hIgG1-Fc mutant proteins.
(A) Flow cytometric analyses of NKG2D::hIgG1-Fc mutant proteins binding to HEK293T cells. Grey = antibody control; blue = wildtype NKG2D-Fc; red = NKG2D-Fc mutants. (B) Binding kinetics of graded amounts of NKG2D-Fc fusion proteins to sMICA analyzed by ELISA. Wildtype NKG2D-Fc protein served as control (black). Respective mutant proteins are highlighted in red, blue and green. Data are represented as mean ± SEM of a representative experiment of three independent experiments.

5.1.9 Protein Sequence Alignments

5.1.9.1 Human MICA allelic Variants

Sequences of MICA*01 (UniProtKB Q29983), MICA*04, MICA*07 (G9FRT9) and MICA*08 (L0L8F7). Identical amino acids (dash), signal peptide sequence (grey, underlined), N-linked glycosylation sites (blue), M152/V152 (red), the AMO1 antibody epitope (red box) and the BAMO3 antibody epitope (grey box).

```
MICA*01    1 MGLGPVFLLLAGIFPFAPPGAAAEPHSLRYNLTVLSWDGSVQSGFLTEVHLDGQPFLRCD
MICA*04      ----------------------------------------------A-----------Y-
MICA*07      ----------------------------------------------A-----------
MICA*08      ----------------------------------------------A-----------Y-

MICA*01   61 RQKCRAKPQGQWAEDVLGNKTWDRETRDLTGNGKDLRMTLAHIKDQKEGLHSLQEIRVCE
MICA*04      ----------------------------------------------------------
MICA*07      ----------------------------------------------------------
MICA*08     P----------------------------------------------------------

MICA*01  121 IHEDNSTRSSQHFYYDGELFLSQNLETKEWTMPQSSRAQTLAMNVRNFLKEDAMKTKTHY
MICA*04      ------------------------V--E---V----------------------------
MICA*07      -------------------------E----------------------------------
MICA*08      -------------------------E---V----------------------------

MICA*01  181 HAMHADCLQELRRYLKSGVVLRRTVPPMVNVTRSEASEGNITVTCRASGFYPWNITLSWR
MICA*04      ---------------E-S-----R-----------------------S---R----T--
MICA*07      ----------------------------------------------------------
MICA*08      ---------------E-----------------------------S---R--I-T--

MICA*01  241 QDGVSLSHDTQQWGDVLPDGNGTYQTWVATRICQGEEQRFTCYMEHSGNHSTHPVPSGKV
MICA*04      ----------------------------------------------------------
MICA*07      ----------------------------------------------------------
MICA*08      --------------------------------R-------------------------

MICA*01  301 LVLQSHWQTFHVSAVAAAA  IFVIIIFYVR CCKKKTSAAEGPELVSLQVLDQHPVGTS
MICA*04      -------------------AA---------- ----------------------------
MICA*07      -------------------  ---------- ----------------------------
MICA*08      -----------------GC  CY FCYY-FLL

MICA*01  361 DHRDATQLGFQPLMSDLGSTGSTEGA
MICA*04      -------------------------
MICA*07      -------------------------
```

5.1.9.2 Human MICA and Human MICB

Sequence alignment of human MICA (UniProtKB Q29983) and human MICB (Q29980). Identical amino acids (dash), signal peptide sequence (grey, underlined), N-linked glycosylation sites (blue), the AMO1 antibody epitope (red box) and the BAMO3 antibody epitope (grey box).

```
MICA_HUMAN   1 MGLGPVFLLLAGIFPFAPPGAAAEPHSLRYNLTVLSWDGSVQSGFLTEVHLDGQPFLRCD
MICB_HUMAN     ----R-L-F--VA------A----------M---Q-E-------A-G---------Y-

MICA_HUMAN  61 RQKCRAKPQGQWAEDVLGNKTWDRETRDLTGNGKDLRMTLAHIKDQKEGLHSLQEIRVCE
MICB_HUMAN     ---R--------------A----T--E---E--Q---R--T------G-----------

MICA_HUMAN 121 IHEDNSTRSSQHFYYDGELFLSQNLETKEWTMPQSSRAQTLAMNVRNFLKEDAMKTKTHY
MICB_HUMAN     ----S---G-R----------------Q-S-V-------------T--W----------

MICA_HUMAN 181 HAMHADCLQELRRYLKSGVVLRRTVPPMVNVTRSEASEGNITVTCRASGFYPWNITLSWR
MICB_HUAMN     R--Q-----K-Q-------AI-----------C--V------------S---R----T--

MICA_HUMAN 241 QDGVSLSHDTQQWGDVLPDGNGTYQTWVATRICQGEEQRFTCYMEHSGNHSTHPVPSGKV
MICB_HUMAN     --------N----------------------R----------------G---------

MICA_HUMAN 301 LVLQSHWQTFHVSAVAAAAIFVIIIFYVRCCKKKTSAAEGPELVSLQVLDQHPVGTSDHR
MICB_HUMAN     -----QRTD-PYVSA-MPCFVI---LC-P--------------------------G---

MICA_HUMAN 361 DATQLGFQPLMSDLGSTGSTEGA
MICB_HUMAN     --A---------AT---------
```

5.1.9.3 Human MICA and M. mulatta MIC homologs

Sequence alignment of the human MICA protein (UniProtKB Q29983, MICA_HUMAN) and the *Macaca mulatta* MIC homologs MIC1 and MIC3 (UniProtKB O98268, MIC1_MACMU; Q9XS20, MIC3_MACMU). Identical amino acids (dash), the MICA signal peptide sequence (grey, underlined), N-linked glycosylation sites (blue) and the AMO1 antibody epitope (red box).

```
MICA_HUMAN   1 MGLGPVFLLLAGIFPFAPPGAAAEPHSLRYNLTVLSWDGSVQSGFLTEVHLDGQPFLRCD
MIC1_MACMU             F--S-----R------L------V----R---------A-G-----L--LY-
MIC3_MACMU                           -L------V----R------E--G-G---S-L-V-Y-

MICA_HUMAN  61 RQKCRAKPQGQWAEDVLGNKTWDRETRDLTGNGKDLRMTLAHIKDQKEGLHSLQEIRVCE
MIC1_MACMU     ------R---E-S-----A----T--G---E------------G--G--------K---
MIC3_MACMU     -ETR--R-------A---A----T--G---E------R--T--EG--G------D-QN--

MICA_HUMAN 121 IHEDNSTRSSQHFYYDGELFLSQNLETKEWTMPQSSRAQTLAMNVRNFLKEDAMKTKTHY
MIC1_MACMU     -------GGLR----------------Q---EL---------L-I---W---T-------
MIC3_MACMU     -Y--G--GG-R-------R---L--A-Q---VA-----------   -W---T---N---

MICA_HUMAN 181 HAMHADCLQELRRYLKSGVVLRRTVPPMVNVTRSEASEGNITVTCRASGFYPWNITLSWR
MIC1_MACMU     RTVQ----KK-QQ--E-R-AV---A-------H-------------------R--A-T--
MIC3_MACMU     ---Q----KK----Q--R-AV---A-------H-------------------R--A-T--

MICA_HUMAN 241 QDGVSLSHDTQQWGDVLPDGNGTYQTWVATRICQGEEQRFTCYMEHSGNHSTHPVPSGKV
MIC1_MACMU     ------N-NA----GI---Q------------R-------A------------------
MIC3_MACMU     ------N--A----GI---Q------------R-------A------------------

MICA_HUMAN 301 LVLQSHWQTFHV      SAVAAAAIFVIIIFYVRCCKKKTSAAEGPELVSLQVLDQHPV
MIC1_MACMU     --F--Q-LDIPYVLAVAAA  V---AIFV--L--L-----------------RT------
MIC3_MACMU     --F--Q-LDIPYVLGVAAA------AIFV--L--L------------

MICA_HUMAN 361 GTSDHRDATQLGFQPLMSDLGSTGSTEGA
MIC1_MACMU   --G------
```

5.1.9.4 Human NKG2D and M. mulatta homolog

Sequence alignment of the human NKG2D protein (UniProtKB P26718, NKG2D_HUMAN) and the *Macaca mulatta* homolog (UniProtKB Q9MZJ7, NKG2D_MACMU). Identical amino acids are indicated as dash.

```
NKG2D_HUMAN  MGWIRGRRSRHSWEMSEFHNYNLDLKKSDFSTRWQKQRCPVVKSKCRENASPFFFCCFIA
NKG2D_MACMU  --------P--NL--------K-G-A-------C-------I----------L-------

NKG2D_HUMAN  VAMGIRFIIMVAIWSAVFLNSLFNQEVQIPLTESYCGPCPKNWICYKNNCYQFFDESKNW
NKG2D_MACMU  -----------T----------------------------------------N-----

NKG2D_HUMAN  YESQASCMSQNASLLKVYSKEDQDLLKLVKSYHWMGLVHIPTNGSWQWEDGSILSPNLLT
NKG2D_MACMU  ------------------------------------------------------------

NKG2D_HUMAN  IIEMQKGDCALYASSFKGYIENCSTPNTYICMQRTV
NKG2D_MACMU  ------------------------I-----------
```

5.2 Protein Sequences

Unless otherwise denoted, nucleotide sequences originate from commercial plasmid vectors or can be found at the NCBI database (www.ncbi.nlm.nih.gov). Respective accession numbers and used base pairs are indicated for each fragment. Respective plasmid numbers of the intralaboratory database are depicted. Amino acids depicted in black result from the cloning strategy. Signal sequences are depicted in grey and are underlined, the different affinity tags (N-/C-terminal fusion indicated by subscripted characters) are shown in red, IgG1-FcEQ in green and the respective NKG2D and NKG2D ligand protein sequences in blue. Amino acids for single point mutations are in bold and underlined.

5.2.1 NKG2D Proteins

- **NKG2D protein:** UniProtKB P26718; Ref.Seq. NM_007360

The different protein domains are separated by dashes, amino acid color scheme: orange = cytoplasmic domain (CYD aa 1 - 51); purple = transmembrane domain (TMD aa 52 -

72); blue = extracellular domain (ECD aa 73 - 216). For the following constructs, only the NKG2D ECD (bp 217 - 651) was used.

MGWIRGRRSRHSWEMSEFHNYNLDLKKSDFSTRWQKQRCPVVKSKCRENAS|PFFFCCFIAVAMGIRF
IIMVAIWSAVFL|NSLFNQEVQIPLTESYCGPCPKNWICYKNNCYQFFDESKNWYESQASCMSQNASL
LKVYSKEDQDLLKLVKSYHWMGLVHIPTNGSWQWEDGSILSPNLLTIIEMQKGDCALYASSFKGYIEN
CSTPNTYICMQRTV

- **His_N-NKG2D:** plasmid no. 1901

HHHHHHHHHHSSGHIEGRHMNSLFNQEVQIPLTESYCGPCPKNWICYKNNCYQFFDESKNWYESQASC
MSQNASLLKVYSKEDQDLLKLVKSYHWMGLVHIPTNGSWQWEDGSILSPNLLTIIEMQKGDCALYASS
FKGYIENCSTPNTYICMQRTV

- **Avi_N-NKG2D-Flag/His_C:** plasmid no. 5802

MDYKDDDDKGMV|HHHHHHSAEGSGNSLFNQEVQIPLTESYCGPCPKNWICYKNNCYQFFDESKNWYE
SQASCMSQNASLLKVYSKEDQDLLKLVKSYHWMGLVHIPTNGSWQWEDGSILSPNLLTIIEMQKGDCA
LYASSFKGYIENCSTPNTYICMQRTVLNDIFEAQKIEWHE

- **IL2ss-IgG1-FcEQ::NKG2D:** plasmid no. 6837

The ECD sequence of wildtype NKG2D is shown in blue. Amino acids exchanged by single point mutations for the generation of mutant NKG2D fusion proteins for affinity maturation (see 5.1.8; plasmid no. 6838 - 6845) are depicted in bold and are underlined.

MYRMQLLSCIALSLALVTNSISAMVRSDKTHTCPPCPAPEL**E**GGPSVFLFPPKPKDTLMISRTPEVTC
VVVDVSHEDPEVKFNWYVDGVEVHNAKTKPREEQY**Q**STYRVVSVLTVLHQDWLNGKEYKCKVSNKALP
APIEKTISKAKGQPREPQVYTLPPSREEMTKNQVSLTCLVKGFYPSDIAVEWESNGQPENNYKTTPPV
LDSDGSFFLYSKLTVDKSRWQQGNVFSCSVMHEALHNHYTQKSLSLSPGKGSSGNSLFNQEVQIPLTE
SYCGPCPKNWICYKNNCYQFFDE**S**KNWYESQASCMSQNASLLKVYSKEDQDLLKLV**KS**YHWMGLVHIP
TNGSWQWEDGSILSPNLLTI**I**EMQ**K**GDCALYASSFKGYIENCSTPNTYICMQRTV

- **IL2ss-Avi-IgG1-FcEQ::NKG2D:** plasmid no. 6846

MYRMQLLSCIALSLALVTNSISAMSGLNDIFEAQKIEWHEVRSDKTHTCPPCPAPELEGGPSVFLFPP
KPKDTLMISRTPEVTCVVVDVSHEDPEVKFNWYVDGVEVHNAKTKPREEQYQSTYRVVSVLTVLHQDW
LNGKEYKCKVSNKALPAPIEKTISKAKGQPREPQVYTLPPSREEMTKNQVSLTCLVKGFYPSDIAVEW
ESNGQPENNYKTTPPVLDSDGSFFLYSKLTVDKSRWQQGNVFSCSVMHEALHNHYTQKSLSLSPGKGS
SGNSLFNQEVQIPLTESYCGPCPKNWICYKNNCYQFFDESKNWYESQASCMSQNASLLKVYSKEDQDL
LKLVKSYHWMGLVHIPTNGSWQWEDGSILSPNLLTIIEMQKGDCALYASSFKGYIENCSTPNTYICMQ
RTV

5.2.2 MICA Proteins

- **MICA*01 protein:** UniProtKB Q29983; Ref.Seq. NM_001177519 (L14848, EMBL)

The different protein domains are separated by dash, amino acid color scheme: grey, underlined = signal peptide; blue = extracellular domain (ECD, aa 24 - 307); purple = transmembrane domain (TMD, aa 308 - 328); orange = cytoplasmic domain (CYD, aa 329 - 383). For MICA*01 constructs only the ECD (aa 24 - 299; bp 70 - 879) was used.

MGLGPVFLLLAGIFPFAPPGAAA|EPHSLRYNLTVLSWDGSVQSGFLTEVHLDGQPFLRCDRQKCRAK
PQGQWAEDVLGNKTWDRETRDLTGNGKDLRMTLAHIKDQKEGLHSLQEIRVCEIHEDNSTRSSQHFYY
DGELFLSQNLETKEWTMPQSSRAQTLAMNVRNFLKEDAMKTKTHYHAMHADCLQELRRYLKSGVVLRR
TVPPMVNVTRSEASEGNITVTCRASGFYPWNITLSWRQDGVSLSHDTQQWGDVLPDGNGTYQTWVATR
ICQGEEQRFTCYMEHSGNHSTHPVPSGKVLVLQSHW|QTFHVSAVAAAAIFVIIIFYVR|CCKKKTSA
AEGPELVSLQVLDQHPVGTSDHRDATQLGFQPLMSDLGSTGSTEGA

- **MICA*01-His$_C$:** plasmid no. 5701

MEPHSLRYNLTVLSWDGSVQSGFLTEVHLDGQPFLRCDRQKCRAKPQGQWAEDVLGNKTWDRETRDLT
GNGKDLRMTLAHIKDQKEGLHSLQEIRVCEIHEDNSTRSSQHFYYDGELFLSQNLETKEWTMPQSSRA
QTLAMNVRNFLKEDAMKTKTHYHAMHADCLQELRRYLKSGVVLRRTVPPMVNVTRSEASEGNITVTCR
ASGFYPWNITLSWRQDGVSLSHDTQQWGDVLPDGNGTYQTWVATRICQGEEQRFTCYMEHSGNHSTHP
VPSGKHHHHHH

- **MICA*04-His$_C$:** Ref.Seq. U56943 (bp 1 - 828); plasmid no. 5801

Amino acid differences to MICA*01 are marked in yellow.

MEPHSLRYNLTVLSWDGSVQSGFLAEVHLDGQPFLRYDRQKCRAKPQGQWAEDVLGNKTWDRETRDLT
GNGKDLRMTLAHIKDQKEGLHSLQEIRVCEIHEDNSTRSSQHFYYDGELFLSQNVETEEWTVPQSSRA
QTLAMNVRNFLKEDAMKTKTHYHAMHADCLQELRRYLESSVVLRRRVPPMVNVTRSEASEGNITVTCR
ASSFYPRNITLTWRQDGVSLSHDTQQWGDVLPDGNGTYQTWVATRICQGEEQRFTCYMEHSGNHSTHP
VPSGKHHHHHH

- **IL2ss-sMICA*01-His$_C$:** plasmid no. 8502

MYRMQLLSCIALSLALVTNSMEPHSLRYNLTVLSWDGSVQSGFLTEVHLDGQPFLRCDRQKCRAKPQG
QWAEDVLGNKTWDRETRDLTGNGKDLRMTLAHIKDQKEGLHSLQEIRVCEIHEDNSTRSSQHFYYDGE
LFLSQNLETKEWTMPQSSRAQTLAMNVRNFLKEDAMKTKTHYHAMHADCLQELRRYLKSGVVLRRTVP
PMVNVTRSEASEGNITVTCRASGFYPWNITLSWRQDGVSLSHDTQQWGDVLPDGNGTYQTWVATRICQ
GEEQRFTCYMEHSGNHSTHPVPSGKHHHHHH

- **IL2ss-MICA*04-His$_C$:** Ref.Seq. U56943 (bp 1 - 828); plasmid no. 8504

MYRMQLLSCIALSLALVTNSMEPHSLRYNLTVLSWDGSVQSGFLAEVHLDGQPFLRYDRQKCRAKPQG
QWAEDVLGNKTWDRETRDLTGNGKDLRMTLAHIKDQKEGLHSLQEIRVCEIHEDNSTRSSQHFYYDGE
LFLSQNVETEEWTVPQSSRAQTLAMNVRNFLKEDAMKTKTHYHAMHADCLQELRRYLESSVVLRRRVP
PMVNVTRSEASEGNITVTCRASSFYPRNITLTWRQDGVSLSHDTQQWGDVLPDGNGTYQTWVATRICQ
GEEQRFTCYMEHSGNHSTHPVPSGKHHHHHH

- **IL2ss-MICA*01::IgG1-FcEQ:** plasmid no. 6834

MYRMQLLSCIALSLALVTNSMEPHSLRYNLTVLSWDGSVQSGFLTEVHLDGQPFLRCDRQKCRAKPQG
QWAEDVLGNKTWDRETRDLTGNGKDLRMTLAHIKDQKEGLHSLQEIRVCEIHEDNSTRSSQHFYYDGE
LFLSQNLETKEWTMPQSSRAQTLAMNVRNFLKEDAMKTKTHYHAMHADCLQELRRYLKSGVVLRRTVP
PMVNVTRSEASEGNITVTCRASGFYPWNITLSWRQDGVSLSHDTQQWGDVLPDGNGTYQTWVATRICQ
GEEQRFTCYMEHSGNHSTHPVPSGKRSDKTHTCPPCPAPELEGGPSVFLFPPKPKDTLMISRTPEVTC
VVVDVSHEDPEVKFNWYVDGVEVHNAKTKPREEQYQSTYRVVSVLTVLHQDWLNGKEYKCKVSNKALP
APIEKTISKAKGQPREPQVYTLPPSREEMTKNQVSLTCLVKGFYPSDIAVEWESNGQPENNYKTTPPV
LDSDGSFFLYSKLTVDKSRWQQGNVFSCSVMHEALHNHYTQKSLSLSPGK

- **IL2ss-MICA*04::IgG1-FcEQ:** plasmid no. 6835

MYRMQLLSCIALSLALVTNSMEPHSLRYNLTVLSWDGSVQSGFLAEVHLDGQPFLRYDRQKCRAKPQG
QWAEDVLGNKTWDRETRDLTGNGKDLRMTLAHIKDQKEGLHSLQEIRVCEIHEDNSTRSSQHFYYDGE
LFLSQNVETEEWTVPQSSRAQTLAMNVRNFLKEDAMKTKTHYHAMHADCLQELRRYLESSVVLRRRVP
PMVNVTRSEASEGNITVTCRASSFYPRNITLTWRQDGVSLSHDTQQWGDVLPDGNGTYQTWVATRICQ
GEEQRFTCYMEHSGNHSTHPVPSGKRSDKTHTCPPCPAPELEGGPSVFLFPPKPKDTLMISRTPEVTC
VVVDVSHEDPEVKFNWYVDGVEVHNAKTKPREEQYQSTYRVVSVLTVLHQDWLNGKEYKCKVSNKALP
APIEKTISKAKGQPREPQVYTLPPSREEMTKNQVSLTCLVKGFYPSDIAVEWESNGQPENNYKTTPPV
LDSDGSFFLYSKLTVDKSRWQQGNVFSCSVMHEALHNHYTQKSLSLSPGK

5.2.3 NKG2D Ligands

The NKG2D ligands MICA (allelic variants 001, 004, 007 and 008), MICB and ULBP1-3 were expressed as full-length constructs in C1R cells (inducible MICA*01 in UKF-NB3). All constructs were fused to the MICA signal peptide (ss; bp 1 - 69; grey, underlined).

- **ss-His$_N$-MICA*01:** Ref.Seq. L14848 (bp 70 - 1152); plasmid no. 9102

MGLGPVLLFLAGIFHFAPPGAAADHHHHHHEPHSLRYNLTVLSWDGSVQSGFLTEVHLDGQPFLRCDR
QKCRAKPQGQWAEDVLGNKTWDRETRDLTGNGKDLRMTLAHIKDQKEGLHSLQEIRVCEIHEDNSTRS
SQHFYYDGELFLSQNLETKEWTMPQSSRAQTLAMNVRNFLKEDAMKTKTHYHAMHADCLQELRRYLKS
GVVLRRTVPPMVNVTRSEASEGNITVTCRASGFYPWNITLSWRQDGVSLSHDTQQWGDVLPDGNGTYQ
TWVATRICQGEEQRFTCYMEHSGNHSTHPVPSGKVLVLQSHWQTFHVSAVAAAAIFVIIIFYVRCCKK
KTSAAEGPELVSLQVLDQHPVGTSDHRDATQLGFQPLMSDLGSTGSTEGA

- **ss-His$_N$-MICA*04:** Ref.Seq. U56943 (bp 1 - 822); plasmid no. 9104

MGLGPVLLFLAGIFHFAPPGAAADHHHHHHEPHSLRYNLTVLSWDGSVQSGFLAEVHLDGQPFLRYDR
QKCRAKPQGQWAEDVLGNKTWDRETRDLTGNGKDLRMTLAHIKDQKEGLHSLQEIRVCEIHEDNSTRS
SQHFYYDGELFLSQNVETEEWTVPQSSRAQTLAMNVRNFLKEDAMKTKTHYHAMHADCLQELRRYLES
SVVLRRRVPPMVNVTRSEASEGNITVTCRASSFYPRNITLTWRQDGVSLSHDTQQWGDVLPDGNGTYQ
TWVATRICQGEEQRFTCYMEHSGNHSTHPVPSGKVLVLQSHWQTFHVSAVAAAAAAIFVIIIFYVRCC
KKKTSAAEGPELVSLQVLDQHPVGTSDHRDATQLGFQPLMSALGSTGSTEGA

- **ss-His$_N$-MICA*07:** Ref.Seq. U56946 (bp 1 - 822); plasmid no. 9106

MGLGPVLLFLAGIFHFAPPGAAADHHHHHHEPHSLRYNLTVLSWDGSVQSGFLAEVHLDGQPFLRCDR
QKCRAKPQGQWAEDVLGNKTWDRETRDLTGNGKDLRMTLAHIKDQKEGLHSLQEIRVCEIHEDNSTRS
SQHFYYDGELFLSQNLETEEWTMPQSSRAQTLAMNVRNFLKEDAMKTKTHYHAMHADCLQELRRYLKS
GVVLRRTVPPMVNVTRSEASEGNITVTCRASGFYPWNITLSWRQDGVSLSHDTQQWGDVLPDGNGTYQ
TWVATRICQGEEQRFTCYMEHSGNHSTHPVPSGKVLVLQSHWQTFHVSAVAAAAIFVIIIFYVRCCKK
KTSAAEGPELVSLQVLDQHPVGTSDHRDATQLGFQPLMSDLGSTGSTEGA

- **ss-His$_N$-MICA*08:** Ref.Seq. U56947 (bp 1 - 822); plasmid no. 9108

MGLGPVLLFLAGIFHFAPPGAAADHHHHHHEPHSLRYNLTVLSWDGSVQSGFLAEVHLDGQPFLRYDR
QKCRAKPQGQWAEDVLGNKTWDRETRDLTGNGKDLRMTLAHIKDQKEGLHSLQEIRVCEIHEDNSTRS
SQHFYYDGELFLSQNLETEEWTVPQSSRAQTLAMNVRNFLKEDAMKTKTHYHAMHADCLQELRRYLES
GVVLRRTVPPMVNVTRSEASEGNITVTCRASSFYPRNIILTWRQDGVSLSHDTQQWGDVLPDGNGTYQ
TWVATRICRGEEQRFTCYMEHSGNHSTHPVPSGKVLVLQSHWQTFHVSAVAAGCCYFCYYYFLCPLL

- **ss-His$_N$-MICB:** UniProtKB Q29980; Ref.Seq. NM_005931.4 (bp 69 - 1152); plasmid no. 9110

MGLGPVLLFLAGIFHFAPPGAAADHHHHHHEPHSLRYNLMVLSQDESVQSGFLAEGHLDGQPFLRYDR
QKRRAKPQGQWAEDVLGAKTWDTETEDLTENGQDLRRTLTHIKDQKGGLHSLQEIRVCEIHEDSSTRG
SRHFYYDGELFLSQNLETQESTVPQSSRAQTLAMNVTNFWKEDAMKTKTHYRAMQADCLQKLQRYLKS
GVAIRRTVPPMVNVTCSEVSEGNITVTCRASSFYPRNITLTWRQDGVSLSHNTQQWGDVLPDGNGTYQ
TWVATRIRQGEEQRFTCYMEHSGNHGTHPVPSGKVLVLQSQRTDFPYVSAAMPCFVIIIILCVPCCKK
KTSAAEGPELVSLQVLDQHPVGTGDHRDAAQLGFQPLMSATGSTGSTEGA

- **ss-His$_N$-ULBP1:** UniProtKB Q9BZM6; Ref.Seq. AF304377 (bp 85 - 735); plasmid no. 9112

MGLGPVLLFLAGIFHFAPPGAAADHHHHHHTHCLCYDFIITPKSRPEPQWCEVQGLVDERPFLHYDCV
NHKAKAFASLGKKVNVTKTWEEQTETLRDVVDFLKGQLLDIQVENLIPIEPLTLQARMSCEHEAHGHG
RGSWQFLFNGQKFLLFDSNNRKWTALHPGAKKMTEKWEKNRDVTMFFQKISLGDCKMWLEEFLMYWEQ
MLDPTKPPSLAPGTTQPKAMATTLSPWSLLIIFLCFILAGR

- **ss-His$_N$-ULBP2:** UniProtKB Q9BZM5; Ref.Seq. AF304378 (bp 88 - 741);

plasmid no. 9114

MGLGPVLLFLAGIFHFAPPGAAADHHHHHHPHSLCYDITVIPKFRPGPRWCAVQGQVDEKTFLHYDCG
NKTVTPVSPLGKKLNVTTAWKAQNPVLREVVDILTEQLRDIQLENYTPKEPLTLQARMSCEQKAEGHS
SGSWQFSFDGQIFLLFDSEKRMWTTVHPGARKMKEKWENDKVVAMSFHYFSMGDCIGWLEDFLMGMDS
TLEPSAGAPLAMSSGTTQLRATATTLILCCLLIILPCFILPGI

- **ss-His$_N$-ULBP3:** UniProtKB Q9BZM4; Ref.Seq. AF349596 (bp 91 - 735);

plasmid no. 9116

MGLGPVLLFLAGIFHFAPPGAAADHHHHHHAHSLWYNFTIIHLPRHGQQWCEVQSQVDQKNFLSYDCG
SDKVLSMGHLEEQLYATDAWGKQLEMLREVGQRLRLELADTELEDFTPSGPLTLQVRMSCECEADGYI
RGSWQFSFDGRKFLLFDSNNRKWTVVHAGARRMKEKWEKDSGLTTFFKMVSMRDCKSWLRDFLMHRKK
RLEPTAPPTMAPGLAQPKAIATTLSPWSFLIILCFILPGI

6 References

1. Janeway, C.A., Travers, P., Walport, M., and and Shlomchik, M., *Immunobiology : the immune system in health and disease*. 6th ed. 2005, New York: Garland Science.
2. Chaplin, D.D., *1. Overview of the human immune response.* J Allergy Clin Immunol, 2006. **117**(2 Suppl Mini-Primer): p. S430-5.
3. Cooper, M.D. and Alder, M.N., *The evolution of adaptive immune systems.* Cell, 2006. **124**(4): p. 815-22.
4. Parkin, J. and Cohen, B., *An overview of the immune system.* Lancet, 2001. **357**(9270): p. 1777-89.
5. Morgan, B.P., Marchbank, K.J., Longhi, M.P., Harris, C.L., and Gallimore, A.M., *Complement: central to innate immunity and bridging to adaptive responses.* Immunol Lett, 2005. **97**(2): p. 171-9.
6. Beutler, B., Hoebe, K., Du, X., and Ulevitch, R.J., *How we detect microbes and respond to them: the Toll-like receptors and their transducers.* J Leukoc Biol, 2003. **74**(4): p. 479-85.
7. Lacy, P. and Stow, J.L., *Cytokine release from innate immune cells: association with diverse membrane trafficking pathways.* Blood, 2011. **118**(1): p. 9-18.
8. Mackay, C.R., *Chemokines: immunology's high impact factors.* Nat Immunol, 2001. **2**(2): p. 95-101.
9. Nemazee, D., *Receptor editing in lymphocyte development and central tolerance.* Nat Rev Immunol, 2006. **6**(10): p. 728-40.
10. Zhu, J., Yamane, H., and Paul, W.E., *Differentiation of effector CD4 T cell populations (*).* Annu Rev Immunol, 2010. **28**: p. 445-89.
11. Zhang, N. and Bevan, M.J., *CD8(+) T cells: foot soldiers of the immune system.* Immunity, 2011. **35**(2): p. 161-8.
12. Schwartz, R.H., *T cell anergy.* Annu Rev Immunol, 2003. **21**: p. 305-34.
13. Vivier, E., Tomasello, E., Baratin, M., Walzer, T., and Ugolini, S., *Functions of natural killer cells.* Nat Immunol, 2008. **9**(5): p. 503-10.
14. Waldhauer, I. and Steinle, A., *NK cells and cancer immunosurveillance.* Oncogene, 2008. **27**(45): p. 5932-43.
15. Jost, S. and Altfeld, M., *Control of human viral infections by natural killer cells.* Annu Rev Immunol, 2013. **31**: p. 163-94.
16. Moretta, A., Marcenaro, E., Parolini, S., Ferlazzo, G., and Moretta, L., *NK cells at the interface between innate and adaptive immunity.* Cell Death Differ, 2008. **15**(2): p. 226-33.
17. Sun, J.C., Beilke, J.N., and Lanier, L.L., *Adaptive immune features of natural killer cells.* Nature, 2009. **457**(7229): p. 557-61.
18. Sun, J.C. and Lanier, L.L., *NK cell development, homeostasis and function: parallels with CD8(+) T cells.* Nat Rev Immunol, 2011. **11**(10): p. 645-57.
19. Farag, S.S. and Caligiuri, M.A., *Human natural killer cell development and biology.* Blood Rev, 2006. **20**(3): p. 123-37.
20. Moretta, L., Bottino, C., Pende, D., Castriconi, R., Mingari, M.C., and Moretta, A., *Surface NK receptors and their ligands on tumor cells.* Semin Immunol, 2006. **18**(3): p. 151-8.
21. Kiessling, R., Klein, E., and Wigzell, H., *"Natural" killer cells in the mouse. I. Cytotoxic cells with specificity for mouse Moloney leukemia cells. Specificity and distribution according to genotype.* Eur J Immunol, 1975. **5**(2): p. 112-7.
22. Kiessling, R., Klein, E., Pross, H., and Wigzell, H., *"Natural" killer cells in the mouse. II. Cytotoxic cells with specificity for mouse Moloney leukemia cells. Characteristics of the killer cell.* Eur J Immunol, 1975. **5**(2): p. 117-21.
23. Freud, A.G. and Caligiuri, M.A., *Human natural killer cell development.* Immunol Rev, 2006. **214**: p. 56-72.
24. Di Santo, J.P., *Natural killer cell developmental pathways: a question of balance.* Annu Rev Immunol, 2006. **24**: p. 257-86.
25. Yokota, Y., Mansouri, A., Mori, S., Sugawara, S., Adachi, S., Nishikawa, S., and Gruss, P., *Development of peripheral lymphoid organs and natural killer cells depends on the helix-loop-helix inhibitor Id2.* Nature, 1999. **397**(6721): p. 702-6.
26. Hazenberg, M.D. and Spits, H., *Human innate lymphoid cells.* Blood, 2014. **124**(5): p. 700-9.
27. Cella, M., Fuchs, A., Vermi, W., Facchetti, F., Otero, K., Lennerz, J.K., Doherty, J.M., Mills, J.C., and Colonna, M., *A human natural killer cell subset provides an innate source of IL-22 for mucosal immunity.* Nature, 2009. **457**(7230): p. 722-5.
28. Sonnenberg, G.F. and Artis, D., *Innate lymphoid cells in the initiation, regulation and resolution of inflammation.* Nat Med, 2015. **21**(7): p. 698-708.
29. Westermann, J. and Pabst, R., *Distribution of lymphocyte subsets and natural killer cells in the human body.* Clin Investig, 1992. **70**(7): p. 539-44.
30. Zhang, Y., Wallace, D.L., de Lara, C.M., Ghattas, H., Asquith, B., Worth, A., Griffin, G.E., Taylor, G.P., Tough, D.F., Beverley, P.C., and Macallan, D.C., *In vivo kinetics of human natural killer cells: the effects of ageing and acute and chronic viral infection.* Immunology, 2007. **121**(2): p. 258-65.
31. Cooper, M.A., Fehniger, T.A., and Caligiuri, M.A., *The biology of human natural killer-cell subsets.* Trends Immunol, 2001. **22**(11): p. 633-40.
32. Cooper, M.A., Fehniger, T.A., Turner, S.C., Chen, K.S., Ghaheri, B.A., Ghayur, T., Carson, W.E., and Caligiuri, M.A., *Human natural killer cells: a unique innate immunoregulatory role for the CD56(bright) subset.* Blood, 2001. **97**(10): p. 3146-51.
33. Mandelboim, O., Malik, P., Davis, D.M., Jo, C.H., Boyson, J.E., and Strominger, J.L., *Human CD16 as a lysis receptor mediating direct natural killer cell cytotoxicity.* Proc Natl Acad Sci U S A, 1999. **96**(10): p. 5640-4.
34. Vitale, M., Della Chiesa, M., Carlomagno, S., Pende, D., Arico, M., Moretta, L., and Moretta, A., *NK-dependent DC maturation is mediated by TNFalpha and IFNgamma released upon engagement of the NKp30 triggering receptor.* Blood, 2005. **106**(2): p. 566-71.
35. Moretta, L., Bottino, C., Pende, D., Mingari, M.C., Biassoni, R., and Moretta, A., *Human natural killer cells: their origin, receptors and function.* Eur J Immunol, 2002. **32**(5): p. 1205-11.
36. Moretta, A., *Natural killer cells and dendritic cells: rendezvous in abused tissues.* Nat Rev Immunol, 2002. **2**(12): p. 957-64.
37. Mocikat, R., Braumuller, H., Gumy, A., Egeter, O., Ziegler, H., Reusch, U., Bubeck, A., Louis, J., Mailhammer, R., Riethmuller, G., Koszinowski, U., and Rocken, M., *Natural killer cells activated by MHC class I(low) targets prime dendritic cells to induce protective CD8 T cell responses.* Immunity, 2003. **19**(4): p. 561-9.
38. Martin-Fontecha, A., Thomsen, L.L., Brett, S., Gerard, C., Lipp, M., Lanzavecchia, A., and Sallusto, F., *Induced recruitment of NK cells to lymph nodes provides IFN-gamma for T(H)1 priming.* Nat Immunol, 2004. **5**(12): p. 1260-5.
39. Barreira da Silva, R. and Munz, C., *Natural killer cell activation by dendritic cells: balancing inhibitory and activating signals.* Cell Mol Life Sci, 2011. **68**(21): p. 3505-18.

40. Piccioli, D., Sbrana, S., Melandri, E., and Valiante, N.M., *Contact-dependent stimulation and inhibition of dendritic cells by natural killer cells.* J Exp Med, 2002. **195**(3): p. 335-41.
41. Ferlazzo, G., Morandi, B., D'Agostino, A., Meazza, R., Melioli, G., Moretta, A., and Moretta, L., *The interaction between NK cells and dendritic cells in bacterial infections results in rapid induction of NK cell activation and in the lysis of uninfected dendritic cells.* Eur J Immunol, 2003. **33**(2): p. 306-13.
42. Ferlazzo, G., Semino, C., and Melioli, G., *HLA class I molecule expression is up-regulated during maturation of dendritic cells, protecting them from natural killer cell-mediated lysis.* Immunol Lett, 2001. **76**(1): p. 37-41.
43. Nguyen, K.B., Salazar-Mather, T.P., Dalod, M.Y., Van Deusen, J.B., Wei, X.Q., Liew, F.Y., Caligiuri, M.A., Durbin, J.E., and Biron, C.A., *Coordinated and distinct roles for IFN-alpha beta, IL-12, and IL-15 regulation of NK cell responses to viral infection.* J Immunol, 2002. **169**(8): p. 4279-87.
44. Orange, J.S. and Biron, C.A., *Characterization of early IL-12, IFN-alphabeta, and TNF effects on antiviral state and NK cell responses during murine cytomegalovirus infection.* J Immunol, 1996. **156**(12): p. 4746-56.
45. Andrews, D.M., Andoniou, C.E., Scalzo, A.A., van Dommelen, S.L., Wallace, M.E., Smyth, M.J., and Degli-Esposti, M.A., *Cross-talk between dendritic cells and natural killer cells in viral infection.* Mol Immunol, 2005. **42**(4): p. 547-55.
46. Ferlazzo, G., Pack, M., Thomas, D., Paludan, C., Schmid, D., Strowig, T., Bougras, G., Muller, W.A., Moretta, L., and Munz, C., *Distinct roles of IL-12 and IL-15 in human natural killer cell activation by dendritic cells from secondary lymphoid organs.* Proc Natl Acad Sci U S A, 2004. **101**(47): p. 16606-11.
47. Nagler, A., Lanier, L.L., Cwirla, S., and Phillips, J.H., *Comparative studies of human FcRIII-positive and negative natural killer cells.* J Immunol, 1989. **143**(10): p. 3183-91.
48. Ferlazzo, G., Thomas, D., Lin, S.L., Goodman, K., Morandi, B., Muller, W.A., Moretta, A., and Munz, C., *The abundant NK cells in human secondary lymphoid tissues require activation to express killer cell Ig-like receptors and become cytolytic.* J Immunol, 2004. **172**(3): p. 1455-62.
49. Vivier, E., Raulet, D.H., Moretta, A., Caligiuri, M.A., Zitvogel, L., Lanier, L.L., Yokoyama, W.M., and Ugolini, S., *Innate or adaptive immunity? The example of natural killer cells.* Science, 2011. **331**(6013): p. 44-9.
50. Lanier, L.L., *NK cell recognition.* Annu Rev Immunol, 2005. **23**: p. 225-74.
51. Vivier, E., Ugolini, S., Blaise, D., Chabannon, C., and Brossay, L., *Targeting natural killer cells and natural killer T cells in cancer.* Nat Rev Immunol, 2012. **12**(4): p. 239-52.
52. Karre, K., *NK cells, MHC class I molecules and the missing self.* Scand J Immunol, 2002. **55**(3): p. 221-8.
53. Bryceson, Y.T., March, M.E., Ljunggren, H.G., and Long, E.O., *Activation, coactivation, and costimulation of resting human natural killer cells.* Immunol Rev, 2006. **214**: p. 73-91.
54. Biassoni, R., Cantoni, C., Pende, D., Sivori, S., Parolini, S., Vitale, M., Bottino, C., and Moretta, A., *Human natural killer cell receptors and co-receptors.* Immunol Rev, 2001. **181**: p. 203-14.
55. Ljunggren, H.G. and Karre, K., *In search of the 'missing self': MHC molecules and NK cell recognition.* Immunol Today, 1990. **11**(7): p. 237-44.
56. Tortorella, D., Gewurz, B.E., Furman, M.H., Schust, D.J., and Ploegh, H.L., *Viral subversion of the immune system.* Annu Rev Immunol, 2000. **18**: p. 861-926.
57. Hewitt, E.W., *The MHC class I antigen presentation pathway: strategies for viral immune evasion.* Immunology, 2003. **110**(2): p. 163-9.
58. Karre, K., Ljunggren, H.G., Piontek, G., and Kiessling, R., *Selective rejection of H-2-deficient lymphoma variants suggests alternative immune defence strategy.* Nature, 1986. **319**(6055): p. 675-8.
59. Brown, A.C., Oddos, S., Dobbie, I.M., Alakoskela, J.M., Parton, R.M., Eissmann, P., Neil, M.A., Dunsby, C., French, P.M., Davis, I., and Davis, D.M., *Remodelling of cortical actin where lytic granules dock at natural killer cell immune synapses revealed by super-resolution microscopy.* PLoS Biol, 2011. **9**(9): p. e1001152.
60. Rak, G.D., Mace, E.M., Banerjee, P.P., Svitkina, T., and Orange, J.S., *Natural killer cell lytic granule secretion occurs through a pervasive actin network at the immune synapse.* PLoS Biol, 2011. **9**(9): p. e1001151.
61. Orange, J.S., *Formation and function of the lytic NK-cell immunological synapse.* Nat Rev Immunol, 2008. **8**(9): p. 713-25.
62. van den Broek, M.F., Kagi, D., Zinkernagel, R.M., and Hengartner, H., *Perforin dependence of natural killer cell-mediated tumor control in vivo.* Eur J Immunol, 1995. **25**(12): p. 3514-6.
63. Lieberman, J., *The ABCs of granule-mediated cytotoxicity: new weapons in the arsenal.* Nat Rev Immunol, 2003. **3**(5): p. 361-70.
64. Zamai, L., Ahmad, M., Bennett, I.M., Azzoni, L., Alnemri, E.S., and Perussia, B., *Natural killer (NK) cell-mediated cytotoxicity: differential use of TRAIL and Fas ligand by immature and mature primary human NK cells.* J Exp Med, 1998. **188**(12): p. 2375-80.
65. Morvan, M.G. and Lanier, L.L., *NK cells and cancer: you can teach innate cells new tricks.* Nat Rev Cancer, 2016. **16**(1): p. 7-19.
66. Bhat, R. and Watzl, C., *Serial killing of tumor cells by human natural killer cells--enhancement by therapeutic antibodies.* PLoS One, 2007. **2**(3): p. e326.
67. Choi, P.J. and Mitchison, T.J., *Imaging burst kinetics and spatial coordination during serial killing by single natural killer cells.* Proc Natl Acad Sci U S A, 2013. **110**(16): p. 6488-93.
68. Cooper, M.A., Elliott, J.M., Keyel, P.A., Yang, L., Carrero, J.A., and Yokoyama, W.M., *Cytokine-induced memory-like natural killer cells.* Proc Natl Acad Sci U S A, 2009. **106**(6): p. 1915-9.
69. Paust, S., Senman, B., and von Andrian, U.H., *Adaptive immune responses mediated by natural killer cells.* Immunol Rev, 2010. **235**(1): p. 286-96.
70. O'Leary, J.G., Goodarzi, M., Drayton, D.L., and von Andrian, U.H., *T cell- and B cell-independent adaptive immunity mediated by natural killer cells.* Nat Immunol, 2006. **7**(5): p. 507-16.
71. Kuijpers, T.W., Baars, P.A., Dantin, C., van den Burg, M., van Lier, R.A., and Roosnek, E., *Human NK cells can control CMV infection in the absence of T cells.* Blood, 2008. **112**(3): p. 914-5.
72. Sirianni, M.C., Vincenzi, L., Topino, S., Giovannetti, A., Mazzetta, F., Libi, F., Scaramuzzi, D., Andreoni, M., Pinter, E., Baccarini, S., Rezza, G., Monini, P., and Ensoli, B., *NK cell activity controls human herpesvirus 8 latent infection and is restored upon*

highly active antiretroviral therapy in AIDS patients with regressing Kaposi's sarcoma. Eur J Immunol, 2002. **32**(10): p. 2711-20.
73. Alter, G. and Altfeld, M., *NK cells in HIV-1 infection: evidence for their role in the control of HIV-1 infection.* J Intern Med, 2009. **265**(1): p. 29-42.
74. Verhoeven, D.H., de Hooge, A.S., Mooiman, E.C., Santos, S.J., ten Dam, M.M., Gelderblom, H., Melief, C.J., Hogendoorn, P.C., Egeler, R.M., van Tol, M.J., Schilham, M.W., and Lankester, A.C., *NK cells recognize and lyse Ewing sarcoma cells through NKG2D and DNAM-1 receptor dependent pathways.* Mol Immunol, 2008. **45**(15): p. 3917-25.
75. Hsia, J.Y., Chen, J.T., Chen, C.Y., Hsu, C.P., Miaw, J., Huang, Y.S., and Yang, C.Y., *Prognostic significance of intratumoral natural killer cells in primary resected esophageal squamous cell carcinoma.* Chang Gung Med J, 2005. **28**(5): p. 335-40.
76. Smyth, M.J., Thia, K.Y., Street, S.E., MacGregor, D., Godfrey, D.I., and Trapani, J.A., *Perforin-mediated cytotoxicity is critical for surveillance of spontaneous lymphoma.* J Exp Med, 2000. **192**(5): p. 755-60.
77. Imai, K., Matsuyama, S., Miyake, S., Suga, K., and Nakachi, K., *Natural cytotoxic activity of peripheral-blood lymphocytes and cancer incidence: an 11-year follow-up study of a general population.* Lancet, 2000. **356**(9244): p. 1795-9.
78. Coca, S., Perez-Piqueras, J., Martinez, D., Colmenarejo, A., Saez, M.A., Vallejo, C., Martos, J.A., and Moreno, M., *The prognostic significance of intratumoral natural killer cells in patients with colorectal carcinoma.* Cancer, 1997. **79**(12): p. 2320-8.
79. Villegas, F.R., Coca, S., Villarrubia, V.G., Jimenez, R., Chillon, M.J., Jareno, J., Zuil, M., and Callol, L., *Prognostic significance of tumor infiltrating natural killer cells subset CD57 in patients with squamous cell lung cancer.* Lung Cancer, 2002. **35**(1): p. 23-8.
80. Ishigami, S., Natsugoe, S., Tokuda, K., Nakajo, A., Che, X., Iwashige, H., Aridome, K., Hokita, S., and Aikou, T., *Prognostic value of intratumoral natural killer cells in gastric carcinoma.* Cancer, 2000. **88**(3): p. 577-83.
81. Orange, J.S., *Human natural killer cell deficiencies.* Curr Opin Allergy Clin Immunol, 2006. **6**(6): p. 399-409.
82. Biron, C.A., Byron, K.S., and Sullivan, J.L., *Severe herpesvirus infections in an adolescent without natural killer cells.* N Engl J Med, 1989. **320**(26): p. 1731-5.
83. Lopez, C., Kirkpatrick, D., Read, S.E., Fitzgerald, P.A., Pitt, J., Pahwa, S., Ching, C.Y., and Smithwick, E.M., *Correlation between low natural killing of fibroblasts infected with herpes simplex virus type 1 and susceptibility to herpesvirus infections.* J Infect Dis, 1983. **147**(6): p. 1030-5.
84. Roder, J.C., Haliotis, T., Klein, M., Korec, S., Jett, J.R., Ortaldo, J., Heberman, R.B., Katz, P., and Fauci, A.S., *A new immunodeficiency disorder in humans involving NK cells.* Nature, 1980. **284**(5756): p. 553-5.
85. Sullivan, J.L., Byron, K.S., Brewster, F.E., and Purtilo, D.T., *Deficient natural killer cell activity in x-linked lymphoproliferative syndrome.* Science, 1980. **210**(4469): p. 543-5.
86. Nakajima, T., Mizushima, N., Nakamura, J., and Kanai, K., *Surface markers of NK cells in peripheral blood of patients with cirrhosis and hepatocellular carcinoma.* Immunol Lett, 1986. **13**(1-2): p. 7-10.
87. Pross, H.F. and Lotzova, E., *Role of natural killer cells in cancer.* Nat Immun, 1993. **12**(4-5): p. 279-92.
88. Schantz, S.P., Shillitoe, E.J., Brown, B., and Campbell, B., *Natural killer cell activity and head and neck cancer: a clinical assessment.* J Natl Cancer Inst, 1986. **77**(4): p. 869-75.
89. Funke, J., Durr, R., Dietrich, U., and Koch, J., *Natural killer cells in HIV-1 infection: a double-edged sword.* AIDS Reviews, 2011. **13**(2): p. 67-76.
90. Groth, A., Kloss, S., von Strandmann, E.P., Koehl, U., and Koch, J., *Mechanisms of tumor and viral immune escape from natural killer cell-mediated surveillance.* Journal of Innate Immunity, 2011. **3**(4): p. 344-54.
91. Koch, J., Steinle, A., Watzl, C., and Mandelboim, O., *Activating natural cytotoxicity receptors of natural killer cells in cancer and infection.* Trends Immunol, 2013. **34**(4): p. 182-91.
92. Seidel, E., Glasner, A., and Mandelboim, O., *Virus-mediated inhibition of natural cytotoxicity receptor recognition.* Cell Mol Life Sci, 2012. **69**(23): p. 3911-20.
93. Trambas, C.M. and Griffiths, G.M., *Delivering the kiss of death.* Nat Immunol, 2003. **4**(5): p. 399-403.
94. Bryceson, Y.T., March, M.E., Ljunggren, H.G., and Long, E.O., *Synergy among receptors on resting NK cells for the activation of natural cytotoxicity and cytokine secretion.* Blood, 2006. **107**(1): p. 159-66.
95. Pegram, H.J., Andrews, D.M., Smyth, M.J., Darcy, P.K., and Kershaw, M.H., *Activating and inhibitory receptors of natural killer cells.* Immunol Cell Biol, 2011. **89**(2): p. 216-24.
96. McQueen, K.L. and Parham, P., *Variable receptors controlling activation and inhibition of NK cells.* Curr Opin Immunol, 2002. **14**(5): p. 615-21.
97. Renedo, M., Arce, I., Rodriguez, A., Carretero, M., Lanier, L.L., Lopez-Botet, M., and Fernandez-Ruiz, E., *The human natural killer gene complex is located on chromosome 12p12-p13.* Immunogenetics, 1997. **46**(4): p. 307-11.
98. Wende, H., Colonna, M., Ziegler, A., and Volz, A., *Organization of the leukocyte receptor cluster (LRC) on human chromosome 19q13.4.* Mamm Genome, 1999. **10**(2): p. 154-60.
99. Kelley, J., Walter, L., and Trowsdale, J., *Comparative genomics of natural killer cell receptor gene clusters.* PLoS Genet, 2005. **1**(2): p. 129-39.
100. Kumar, V. and McNerney, M.E., *A new self: MHC-class-I-independent natural-killer-cell self-tolerance.* Nat Rev Immunol, 2005. **5**(5): p. 363-74.
101. Gasser, S. and Raulet, D.H., *Activation and self-tolerance of natural killer cells.* Immunol Rev, 2006. **214**: p. 130-42.
102. Kim, S., Poursine-Laurent, J., Truscott, S.M., Lybarger, L., Song, Y.J., Yang, L., French, A.R., Sunwoo, J.B., Lemieux, S., Hansen, T.H., and Yokoyama, W.M., *Licensing of natural killer cells by host major histocompatibility complex class I molecules.* Nature, 2005. **436**(7051): p. 709-13.
103. Held, W., Kijima, M., Angelov, G., and Bessoles, S., *The function of natural killer cells: education, reminders and some good memories.* Curr Opin Immunol, 2011. **23**(2): p. 228-33.
104. Wagtmann, N., Rajagopalan, S., Winter, C.C., Peruzzi, M., and Long, E.O., *Killer cell inhibitory receptors specific for HLA-C and HLA-B identified by direct binding and by functional transfer.* Immunity, 1995. **3**(6): p. 801-9.
105. Colonna, M. and Samaridis, J., *Cloning of immunoglobulin-superfamily members associated with HLA-C and HLA-B recognition by human natural killer cells.* Science, 1995. **268**(5209): p. 405-8.
106. Vilches, C. and Parham, P., *KIR: diverse, rapidly evolving receptors of innate and adaptive immunity.* Annu Rev Immunol, 2002. **20**: p. 217-51.

107. Moretta, L. and Moretta, A., *Unravelling natural killer cell function: triggering and inhibitory human NK receptors.* EMBO J, 2004. **23**(2): p. 255-9.
108. Carretero, M., Cantoni, C., Bellon, T., Bottino, C., Biassoni, R., Rodriguez, A., Perez-Villar, J.J., Moretta, L., Moretta, A., and Lopez-Botet, M., *The CD94 and NKG2-A C-type lectins covalently assemble to form a natural killer cell inhibitory receptor for HLA class I molecules.* Eur J Immunol, 1997. **27**(2): p. 563-7.
109. Posch, P.E., Borrego, F., Brooks, A.G., and Coligan, J.E., *HLA-E is the ligand for the natural killer cell CD94/NKG2 receptors.* J Biomed Sci, 1998. **5**(5): p. 321-31.
110. Borrego, F., Ulbrecht, M., Weiss, E.H., Coligan, J.E., and Brooks, A.G., *Recognition of human histocompatibility leukocyte antigen (HLA)-E complexed with HLA class I signal sequence-derived peptides by CD94/NKG2 confers protection from natural killer cell-mediated lysis.* J Exp Med, 1998. **187**(5): p. 813-8.
111. Campbell, K.S. and Purdy, A.K., *Structure/function of human killer cell immunoglobulin-like receptors: lessons from polymorphisms, evolution, crystal structures and mutations.* Immunology, 2011. **132**(3): p. 315-25.
112. Uhrberg, M., Valiante, N.M., Shum, B.P., Shilling, H.G., Lienert-Weidenbach, K., Corliss, B., Tyan, D., Lanier, L.L., and Parham, P., *Human diversity in killer cell inhibitory receptor genes.* Immunity, 1997. **7**(6): p. 753-63.
113. Parham, P., *Influence of KIR diversity on human immunity.* Adv Exp Med Biol, 2005. **560**: p. 47-50.
114. Valiante, N.M., Lienert, K., Shilling, H.G., Smits, B.J., and Parham, P., *Killer cell receptors: keeping pace with MHC class I evolution.* Immunol Rev, 1997. **155**: p. 155-64.
115. Gardiner, C.M., *Killer cell immunoglobulin-like receptors on NK cells: the how, where and why.* Int J Immunogenet, 2008. **35**(1): p. 1-8.
116. Vance, R.E., Kraft, J.R., Altman, J.D., Jensen, P.E., and Raulet, D.H., *Mouse CD94/NKG2A is a natural killer cell receptor for the nonclassical major histocompatibility complex (MHC) class I molecule Qa-1(b).* J Exp Med, 1998. **188**(10): p. 1841-8.
117. Takei, F., Brennan, J., and Mager, D.L., *The Ly-49 family: genes, proteins and recognition of class I MHC.* Immunol Rev, 1997. **155**: p. 67-77.
118. Kubota, A., Kubota, S., Lohwasser, S., Mager, D.L., and Takei, F., *Diversity of NK cell receptor repertoire in adult and neonatal mice.* J Immunol, 1999. **163**(1): p. 212-6.
119. Barten, R., Torkar, M., Haude, A., Trowsdale, J., and Wilson, M.J., *Divergent and convergent evolution of NK-cell receptors.* Trends Immunol, 2001. **22**(1): p. 52-7.
120. Long, E.O., *Negative signaling by inhibitory receptors: the NK cell paradigm.* Immunol Rev, 2008. **224**: p. 70-84.
121. Watzl, C. and Long, E.O., *Signal transduction during activation and inhibition of natural killer cells.* Curr Protoc Immunol, 2010. **Chapter 11**: p. Unit 11 9B.
122. Ravetch, J.V. and Lanier, L.L., *Immune inhibitory receptors.* Science, 2000. **290**(5489): p. 84-9.
123. Bryceson, Y.T., Ljunggren, H.G., and Long, E.O., *Minimal requirement for induction of natural cytotoxicity and intersection of activation signals by inhibitory receptors.* Blood, 2009. **114**(13): p. 2657-66.
124. Lanier, L.L., Corliss, B., Wu, J., and Phillips, J.H., *Association of DAP12 with activating CD94/NKG2C NK cell receptors.* Immunity, 1998. **8**(6): p. 693-701.
125. Braud, V.M., Allan, D.S., O'Callaghan, C.A., Soderstrom, K., D'Andrea, A., Ogg, G.S., Lazetic, S., Young, N.T., Bell, J.I., Phillips, J.H., Lanier, L.L., and McMichael, A.J., *HLA-E binds to natural killer cell receptors CD94/NKG2A, B and C.* Nature, 1998. **391**(6669): p. 795-9.
126. Veillette, A., *SLAM-family receptors: immune regulators with or without SAP-family adaptors.* Cold Spring Harb Perspect Biol, 2010. **2**(3): p. a002469.
127. Iguchi-Manaka, A., Kai, H., Yamashita, Y., Shibata, K., Tahara-Hanaoka, S., Honda, S., Yasui, T., Kikutani, H., Shibuya, K., and Shibuya, A., *Accelerated tumor growth in mice deficient in DNAM-1 receptor.* J Exp Med, 2008. **205**(13): p. 2959-64.
128. Vitale, M., Falco, M., Castriconi, R., Parolini, S., Zambello, R., Semenzato, G., Biassoni, R., Bottino, C., Moretta, L., and Moretta, A., *Identification of NKp80, a novel triggering molecule expressed by human NK cells.* Eur J Immunol, 2001. **31**(1): p. 233-42.
129. Spreu, J., Kuttruff, S., Stejfova, V., Dennehy, K.M., Schittek, B., and Steinle, A., *Interaction of C-type lectin-like receptors NKp65 and KACL facilitates dedicated immune recognition of human keratinocytes.* Proc Natl Acad Sci U S A, 2010. **107**(11): p. 5100-5.
130. Hartmann, J., *Influence of the stalk domain and the glycosylation status of the human activating natural killer cell receptor NKp30 on ligand binding.* 2012, Goethe-University Frankfurt am Main.
131. Vivier, E., Nunes, J.A., and Vely, F., *Natural killer cell signaling pathways.* Science, 2004. **306**(5701): p. 1517-9.
132. Pende, D., Parolini, S., Pessino, A., Sivori, S., Augugliaro, R., Morelli, L., Marcenaro, E., Accame, L., Malaspina, A., Biassoni, R., Bottino, C., Moretta, L., and Moretta, A., *Identification and molecular characterization of NKp30, a novel triggering receptor involved in natural cytotoxicity mediated by human natural killer cells.* J Exp Med, 1999. **190**(10): p. 1505-16.
133. Vitale, M., Bottino, C., Sivori, S., Sanseverino, L., Castriconi, R., Marcenaro, E., Augugliaro, R., Moretta, L., and Moretta, A., *NKp44, a novel triggering surface molecule specifically expressed by activated natural killer cells, is involved in non-major histocompatibility complex-restricted tumor cell lysis.* J Exp Med, 1998. **187**(12): p. 2065-72.
134. Cantoni, C., Bottino, C., Vitale, M., Pessino, A., Augugliaro, R., Malaspina, A., Parolini, S., Moretta, L., Moretta, A., and Biassoni, R., *NKp44, a triggering receptor involved in tumor cell lysis by activated human natural killer cells, is a novel member of the immunoglobulin superfamily.* J Exp Med, 1999. **189**(5): p. 787-96.
135. Sivori, S., Vitale, M., Morelli, L., Sanseverino, L., Augugliaro, R., Bottino, C., Moretta, L., and Moretta, A., *p46, a novel natural killer cell-specific surface molecule that mediates cell activation.* J Exp Med, 1997. **186**(7): p. 1129-36.
136. Pessino, A., Sivori, S., Bottino, C., Malaspina, A., Morelli, L., Moretta, L., Biassoni, R., and Moretta, A., *Molecular cloning of NKp46: a novel member of the immunoglobulin superfamily involved in triggering of natural cytotoxicity.* J Exp Med, 1998. **188**(5): p. 953-60.
137. Tang, Q., Grzywacz, B., Wang, H., Kataria, N., Cao, Q., Wagner, J.E., Blazar, B.R., Miller, J.S., and Verneris, M.R., *Umbilical cord blood T cells express multiple natural cytotoxicity receptors after IL-15 stimulation, but only NKp30 is functional.* J Immunol, 2008. **181**(7): p. 4507-15.
138. Juelke, K. and Romagnani, C., *Differentiation of human innate lymphoid cells (ILCs).* Curr Opin Immunol, 2016. **38**: p. 75-85.

139. Spits, H., Artis, D., Colonna, M., Diefenbach, A., Di Santo, J.P., Eberl, G., Koyasu, S., Locksley, R.M., McKenzie, A.N., Mebius, R.E., Powrie, F., and Vivier, E., *Innate lymphoid cells--a proposal for uniform nomenclature.* Nat Rev Immunol, 2013. **13**(2): p. 145-9.
140. Hudspeth, K., Silva-Santos, B., and Mavilio, D., *Natural cytotoxicity receptors: broader expression patterns and functions in innate and adaptive immune cells.* Front Immunol, 2013. **4**: p. 69.
141. Correia, D.V., Fogli, M., Hudspeth, K., da Silva, M.G., Mavilio, D., and Silva-Santos, B., *Differentiation of human peripheral blood Vdelta1+ T cells expressing the natural cytotoxicity receptor NKp30 for recognition of lymphoid leukemia cells.* Blood, 2011. **118**(4): p. 992-1001.
142. Srivastava, B.I. and Srivastava, M.D., *Expression of natural cytotoxicity receptors NKp30, NKp44, and NKp46 mRNAs and proteins by human hematopoietic and non-hematopoietic cells.* Leuk Res, 2006. **30**(1): p. 37-46.
143. Montaldo, E., Del Zotto, G., Della Chiesa, M., Mingari, M.C., Moretta, A., De Maria, A., and Moretta, L., *Human NK cell receptors/markers: a tool to analyze NK cell development, subsets and function.* Cytometry A, 2013. **83**(8): p. 702-13.
144. Biassoni, R., Pessino, A., Bottino, C., Pende, D., Moretta, L., and Moretta, A., *The murine homologue of the human NKp46, a triggering receptor involved in the induction of natural cytotoxicity.* Eur J Immunol, 1999. **29**(3): p. 1014-20.
145. Gazit, R., Gruda, R., Elboim, M., Arnon, T.I., Katz, G., Achdout, H., Hanna, J., Qimron, U., Landau, G., Greenbaum, E., Zakay-Rones, Z., Porgador, A., and Mandelboim, O., *Lethal influenza infection in the absence of the natural killer cell receptor gene Ncr1.* Nat Immunol, 2006. **7**(5): p. 517-23.
146. Anderson, P., Caligiuri, M., Ritz, J., and Schlossman, S.F., *CD3-negative natural killer cells express zeta TCR as part of a novel molecular complex.* Nature, 1989. **341**(6238): p. 159-62.
147. Wu, J., Cherwinski, H., Spies, T., Phillips, J.H., and Lanier, L.L., *DAP10 and DAP12 form distinct, but functionally cooperative, receptor complexes in natural killer cells.* J Exp Med, 2000. **192**(7): p. 1059-68.
148. Lanier, L.L., *Up on the tightrope: natural killer cell activation and inhibition.* Nat Immunol, 2008. **9**(5): p. 495-502.
149. Wu, J., Song, Y., Bakker, A.B., Bauer, S., Spies, T., Lanier, L.L., and Phillips, J.H., *An activating immunoreceptor complex formed by NKG2D and DAP10.* Science, 1999. **285**(5428): p. 730-2.
150. Billadeau, D.D., Upshaw, J.L., Schoon, R.A., Dick, C.J., and Leibson, P.J., *NKG2D-DAP10 triggers human NK cell-mediated killing via a Syk-independent regulatory pathway.* Nat Immunol, 2003. **4**(6): p. 557-64.
151. Lanier, L.L., *Natural killer cell receptor signaling.* Curr Opin Immunol, 2003. **15**(3): p. 308-14.
152. Raulet, D.H., *Roles of the NKG2D immunoreceptor and its ligands.* Nat Rev Immunol, 2003. **3**(10): p. 781-90.
153. Mandelboim, O., Lieberman, N., Lev, M., Paul, L., Arnon, T.I., Bushkin, Y., Davis, D.M., Strominger, J.L., Yewdell, J.W., and Porgador, A., *Recognition of haemagglutinins on virus-infected cells by NKp46 activates lysis by human NK cells.* Nature, 2001. **409**(6823): p. 1055-60.
154. Arnon, T.I., Lev, M., Katz, G., Chernobrov, Y., Porgador, A., and Mandelboim, O., *Recognition of viral hemagglutinins by NKp44 but not by NKp30.* Eur J Immunol, 2001. **31**(9): p. 2680-9.
155. Jarahian, M., Fiedler, M., Cohnen, A., Djandji, D., Hammerling, G.J., Gati, C., Cerwenka, A., Turner, P.C., Moyer, R.W., Watzl, C., Hengel, H., and Momburg, F., *Modulation of NKp30- and NKp46-mediated natural killer cell responses by poxviral hemagglutinin.* PLoS Pathog, 2011. **7**(8): p. e1002195.
156. Chaushu, S., Wilensky, A., Gur, C., Shapira, L., Elboim, M., Halftek, G., Polak, D., Achdout, H., Bachrach, G., and Mandelboim, O., *Direct recognition of Fusobacterium nucleatum by the NK cell natural cytotoxicity receptor NKp46 aggravates periodontal disease.* PLoS Pathog, 2012. **8**(3): p. e1002601.
157. Esin, S., Batoni, G., Counoupas, C., Stringaro, A., Brancatisano, F.L., Colone, M., Maisetta, G., Florio, W., Arancia, G., and Campa, M., *Direct binding of human NK cell natural cytotoxicity receptor NKp44 to the surfaces of mycobacteria and other bacteria.* Infect Immun, 2008. **76**(4): p. 1719-27.
158. Li, S.S., Kyei, S.K., Timm-McCann, M., Ogbomo, H., Jones, G.J., Shi, M., Xiang, R.F., Oykhman, P., Huston, S.M., Islam, A., Gill, M.J., Robbins, S.M., and Mody, C.H., *The NK receptor NKp30 mediates direct fungal recognition and killing and is diminished in NK cells from HIV-infected patients.* Cell Host Microbe, 2013. **14**(4): p. 387-97.
159. Mavoungou, E., Held, J., Mewono, L., and Kremsner, P.G., *A Duffy binding-like domain is involved in the NKp30-mediated recognition of Plasmodium falciparum-parasitized erythrocytes by natural killer cells.* J Infect Dis, 2007. **195**(10): p. 1521-31.
160. Arnon, T.I., Achdout, H., Levi, O., Markel, G., Saleh, N., Katz, G., Gazit, R., Gonen-Gross, T., Hanna, J., Nahari, E., Porgador, A., Honigman, A., Plachter, B., Mevorach, D., Wolf, D.G., and Mandelboim, O., *Inhibition of the NKp30 activating receptor by pp65 of human cytomegalovirus.* Nat Immunol, 2005. **6**(5): p. 515-23.
161. Sivori, S., Parolini, S., Marcenaro, E., Castriconi, R., Pende, D., Millo, R., and Moretta, A., *Involvement of natural cytotoxicity receptors in human natural killer cell-mediated lysis of neuroblastoma and glioblastoma cell lines.* J Neuroimmunol, 2000. **107**(2): p. 220-5.
162. Castriconi, R., Dondero, A., Corrias, M.V., Lanino, E., Pende, D., Moretta, L., Bottino, C., and Moretta, A., *Natural killer cell-mediated killing of freshly isolated neuroblastoma cells: critical role of DNAX accessory molecule-1-poliovirus receptor interaction.* Cancer Res, 2004. **64**(24): p. 9180-4.
163. Byrd, A., Hoffmann, S.C., Jarahian, M., Momburg, F., and Watzl, C., *Expression analysis of the ligands for the Natural Killer cell receptors NKp30 and NKp44.* PLoS One, 2007. **2**(12): p. e1339.
164. Bloushtain, N., Qimron, U., Bar-Ilan, A., Hershkovitz, O., Gazit, R., Fima, E., Korc, M., Vlodavsky, I., Bovin, N.V., and Porgador, A., *Membrane-associated heparan sulfate proteoglycans are involved in the recognition of cellular targets by NKp30 and NKp46.* J Immunol, 2004. **173**(4): p. 2392-401.
165. Hershkovitz, O., Jivov, S., Bloushtain, N., Zilka, A., Landau, G., Bar-Ilan, A., Lichtenstein, R.G., Campbell, K.S., van Kuppevelt, T.H., and Porgador, A., *Characterization of the recognition of tumor cells by the natural cytotoxicity receptor, NKp44.* Biochemistry, 2007. **46**(25): p. 7426-36.
166. Zilka, A., Landau, G., Hershkovitz, O., Bloushtain, N., Bar-Ilan, A., Benchetrit, F., Fima, E., van Kuppevelt, T.H., Gallagher, J.T., Elgavish, S., and Porgador, A., *Characterization of the heparin/heparan sulfate binding site of the natural cytotoxicity receptor NKp46.* Biochemistry, 2005. **44**(44): p. 14477-85.
167. Hershkovitz, O., Jarahian, M., Zilka, A., Bar-Ilan, A., Landau, G., Jivov, S., Tekoah, Y., Glicklis, R., Gallagher, J.T., Hoffmann, S.C., Zer, H., Mandelboim, O., Watzl, C., Momburg, F., and Porgador, A., *Altered glycosylation of recombinant NKp30 hampers*

binding to heparan sulfate: a lesson for the use of recombinant immunoreceptors as an immunological tool. Glycobiology, 2008. **18**(1): p. 28-41.
168. Hecht, M.L., Rosental, B., Horlacher, T., Hershkovitz, O., De Paz, J.L., Noti, C., Schauer, S., Porgador, A., and Seeberger, P.H., *Natural cytotoxicity receptors NKp30, NKp44 and NKp46 bind to different heparan sulfate/heparin sequences.* J Proteome Res, 2009. **8**(2): p. 712-20.
169. Brandt, C.S., Baratin, M., Yi, E.C., Kennedy, J., Gao, Z., Fox, B., Haldeman, B., Ostrander, C.D., Kaifu, T., Chabannon, C., Moretta, A., West, R., Xu, W., Vivier, E., and Levin, S.D., *The B7 family member B7-H6 is a tumor cell ligand for the activating natural killer cell receptor NKp30 in humans.* J Exp Med, 2009. **206**(7): p. 1495-503.
170. Li, Y., Wang, Q., and Mariuzza, R.A., *Structure of the human activating natural cytotoxicity receptor NKp30 bound to its tumor cell ligand B7-H6.* J Exp Med, 2011. **208**(4): p. 703-14.
171. Pogge von Strandmann, E., Simhadri, V.R., von Tresckow, B., Sasse, S., Reiners, K.S., Hansen, H.P., Rothe, A., Boll, B., Simhadri, V.L., Borchmann, P., McKinnon, P.J., Hallek, M., and Engert, A., *Human leukocyte antigen-B-associated transcript 3 is released from tumor cells and engages the NKp30 receptor on natural killer cells.* Immunity, 2007. **27**(6): p. 965-74.
172. Simhadri, V.R., Reiners, K.S., Hansen, H.P., Topolar, D., Simhadri, V.L., Nohroudi, K., Kufer, T.A., Engert, A., and Pogge von Strandmann, E., *Dendritic cells release HLA-B-associated transcript-3 positive exosomes to regulate natural killer function.* PLoS One, 2008. **3**(10): p. e3377.
173. Wang, W., Guo, H., Geng, J., Zheng, X., Wei, H., Sun, R., and Tian, Z., *Tumor-released Galectin-3, a soluble inhibitory ligand of human NKp30, plays an important role in tumor escape from NK cell attack.* J Biol Chem, 2014. **289**(48): p. 33311-9.
174. Rosental, B., Brusilovsky, M., Hadad, U., Oz, D., Appel, M.Y., Afergan, F., Yossef, R., Rosenberg, L.A., Aharoni, A., Cerwenka, A., Campbell, K.S., Braiman, A., and Porgador, A., *Proliferating cell nuclear antigen is a novel inhibitory ligand for the natural cytotoxicity receptor NKp44.* J Immunol, 2011. **187**(11): p. 5693-702.
175. Baychelier, F., Sennepin, A., Ermonval, M., Dorgham, K., Debre, P., and Vieillard, V., *Identification of a cellular ligand for the natural cytotoxicity receptor NKp44.* Blood, 2013. **122**(17): p. 2935-42.
176. Garg, A., Barnes, P.F., Porgador, A., Roy, S., Wu, S., Nanda, J.S., Griffith, D.E., Girard, W.M., Rawal, N., Shetty, S., and Vankayalapati, R., *Vimentin expressed on Mycobacterium tuberculosis-infected human monocytes is involved in binding to the NKp46 receptor.* J Immunol, 2006. **177**(9): p. 6192-8.
177. Chong, W.P., Zhou, J., Law, H.K., Tu, W., and Lau, Y.L., *Natural killer cells become tolerogenic after interaction with apoptotic cells.* Eur J Immunol, 2010. **40**(6): p. 1718-27.
178. Arnon, T.I., Achdout, H., Lieberman, N., Gazit, R., Gonen-Gross, T., Katz, G., Bar-Ilan, A., Bloushtain, N., Lev, M., Joseph, A., Kedar, E., Porgador, A., and Mandelboim, O., *The mechanisms controlling the recognition of tumor- and virus-infected cells by NKp46.* Blood, 2004. **103**(2): p. 664-72.
179. Costello, R.T., Sivori, S., Marcenaro, E., Lafage-Pochitaloff, M., Mozziconacci, M.J., Reviron, D., Gastaut, J.A., Pende, D., Olive, D., and Moretta, A., *Defective expression and function of natural killer cell-triggering receptors in patients with acute myeloid leukemia.* Blood, 2002. **99**(10): p. 3661-7.
180. Fauriat, C., Just-Landi, S., Mallet, F., Arnoulet, C., Sainty, D., Olive, D., and Costello, R.T., *Deficient expression of NCR in NK cells from acute myeloid leukemia: Evolution during leukemia treatment and impact of leukemia cells in NCRdull phenotype induction.* Blood, 2007. **109**(1): p. 323-30.
181. Sanchez-Correa, B., Morgado, S., Gayoso, I., Bergua, J.M., Casado, J.G., Arcos, M.J., Bengochea, M.L., Duran, E., Solana, R., and Tarazona, R., *Human NK cells in acute myeloid leukaemia patients: analysis of NK cell-activating receptors and their ligands.* Cancer Immunol Immunother, 2011. **60**(8): p. 1195-205.
182. Garcia-Iglesias, T., Del Toro-Arreola, A., Albarran-Somoza, B., Del Toro-Arreola, S., Sanchez-Hernandez, P.E., Ramirez-Duenas, M.G., Balderas-Pena, L.M., Bravo-Cuellar, A., Ortiz-Lazareno, P.C., and Daneri-Navarro, A., *Low NKp30, NKp46 and NKG2D expression and reduced cytotoxic activity on NK cells in cervical cancer and precursor lesions.* BMC Cancer, 2009. **9**: p. 186.
183. Kovacs, K.A., Steinmann, M., Magistretti, P.J., Halfon, O., and Cardinaux, J.R., *CCAAT/enhancer-binding protein family members recruit the coactivator CREB-binding protein and trigger its phosphorylation.* J Biol Chem, 2003. **278**(38): p. 36959-65.
184. Delahaye, N.F., Rusakiewicz, S., Martins, I., Menard, C., Roux, S., Lyonnet, L., Paul, P., Sarabi, M., Chaput, N., Semeraro, M., Minard-Colin, V., Poirier-Colame, V., Chaba, K., Flament, C., Baud, V., Authier, H., Kerdine-Romer, S., Pallardy, M., Cremer, I., Peaudecerf, L., Rocha, B., Valteau-Couanet, D., Gutierrez, J.C., Nunes, J.A., Commo, F., Bonvalot, S., Ibrahim, N., Terrier, P., Opolon, P., Bottino, C., Moretta, A., Tavernier, J., Rihet, P., Coindre, J.M., Blay, J.Y., Isambert, N., Emile, J.F., Vivier, E., Lecesne, A., Kroemer, G., and Zitvogel, L., *Alternatively spliced NKp30 isoforms affect the prognosis of gastrointestinal stromal tumors.* Nat Med, 2011. **17**(6): p. 700-7.
185. Pietra, G., Manzini, C., Rivara, S., Vitale, M., Cantoni, C., Petretto, A., Balsamo, M., Conte, R., Benelli, R., Minghelli, S., Solari, N., Gualco, M., Queirolo, P., Moretta, L., and Mingari, M.C., *Melanoma cells inhibit natural killer cell function by modulating the expression of activating receptors and cytolytic activity.* Cancer Res, 2012. **72**(6): p. 1407-15.
186. De Maria, A., Fogli, M., Costa, P., Murdaca, G., Puppo, F., Mavilio, D., Moretta, A., and Moretta, L., *The impaired NK cell cytolytic function in viremic HIV-1 infection is associated with a reduced surface expression of natural cytotoxicity receptors (NKp46, NKp30 and NKp44).* Eur J Immunol, 2003. **33**(9): p. 2410-8.
187. Houchins, J.P., Yabe, T., McSherry, C., and Bach, F.H., *DNA sequence analysis of NKG2, a family of related cDNA clones encoding type II integral membrane proteins on human natural killer cells.* J Exp Med, 1991. **173**(4): p. 1017-20.
188. Houchins, J.P., Yabe, T., McSherry, C., Miyokawa, N., and Bach, F.H., *Isolation and characterization of NK cell or NK/T cell-specific cDNA clones.* J Mol Cell Immunol, 1990. **4**(6): p. 295-304; discussion 05-6.
189. Yabe, T., McSherry, C., Bach, F.H., Fisch, P., Schall, R.P., Sondel, P.M., and Houchins, J.P., *A multigene family on human chromosome 12 encodes natural killer-cell lectins.* Immunogenetics, 1993. **37**(6): p. 455-60.
190. Glienke, J., Sobanov, Y., Brostjan, C., Steffens, C., Nguyen, C., Lehrach, H., Hofer, E., and Francis, F., *The genomic organization of NKG2C, E, F, and D receptor genes in the human natural killer gene complex.* Immunogenetics, 1998. **48**(3): p. 163-73.
191. Ho, E.L., Heusel, J.W., Brown, M.G., Matsumoto, K., Scalzo, A.A., and Yokoyama, W.M., *Murine Nkg2d and Cd94 are clustered within the natural killer complex and are expressed independently in natural killer cells.* Proc Natl Acad Sci U S A, 1998. **95**(11): p. 6320-5.

192. Bauer, S., Groh, V., Wu, J., Steinle, A., Phillips, J.H., Lanier, L.L., and Spies, T., *Activation of NK cells and T cells by NKG2D, a receptor for stress-inducible MICA.* Science, 1999. **285**(5428): p. 727-9.
193. Groh, V., Rhinehart, R., Secrist, H., Bauer, S., Grabstein, K.H., and Spies, T., *Broad tumor-associated expression and recognition by tumor-derived gamma delta T cells of MICA and MICB.* Proc Natl Acad Sci U S A, 1999. **96**(12): p. 6879-84.
194. Groh, V., Rhinehart, R., Randolph-Habecker, J., Topp, M.S., Riddell, S.R., and Spies, T., *Costimulation of CD8alphabeta T cells by NKG2D via engagement by MIC induced on virus-infected cells.* Nat Immunol, 2001. **2**(3): p. 255-60.
195. Das, H., Groh, V., Kuijl, C., Sugita, M., Morita, C.T., Spies, T., and Bukowski, J.F., *MICA engagement by human Vgamma2Vdelta2 T cells enhances their antigen-dependent effector function.* Immunity, 2001. **15**(1): p. 83-93.
196. Wang, H., Yang, D., Xu, W., Wang, Y., Ruan, Z., Zhao, T., Han, J., and Wu, Y., *Tumor-derived soluble MICs impair CD3(+)CD56(+) NKT-like cell cytotoxicity in cancer patients.* Immunol Lett, 2008. **120**(1-2): p. 65-71.
197. Jamieson, A.M., Diefenbach, A., McMahon, C.W., Xiong, N., Carlyle, J.R., and Raulet, D.H., *The role of the NKG2D immunoreceptor in immune cell activation and natural killing.* Immunity, 2002. **17**(1): p. 19-29.
198. Diefenbach, A., Jamieson, A.M., Liu, S.D., Shastri, N., and Raulet, D.H., *Ligands for the murine NKG2D receptor: expression by tumor cells and activation of NK cells and macrophages.* Nat Immunol, 2000. **1**(2): p. 119-26.
199. Groh, V., Bruhl, A., El-Gabalawy, H., Nelson, J.L., and Spies, T., *Stimulation of T cell autoreactivity by anomalous expression of NKG2D and its MIC ligands in rheumatoid arthritis.* Proc Natl Acad Sci U S A, 2003. **100**(16): p. 9452-7.
200. Allez, M., Tieng, V., Nakazawa, A., Treton, X., Pacault, V., Dulphy, N., Caillat-Zucman, S., Paul, P., Gornet, J.M., Douay, C., Ravet, S., Tamouza, R., Charron, D., Lemann, M., Mayer, L., and Toubert, A., *CD4+NKG2D+ T cells in Crohn's disease mediate inflammatory and cytotoxic responses through MICA interactions.* Gastroenterology, 2007. **132**(7): p. 2346-58.
201. Coudert, J.D. and Held, W., *The role of the NKG2D receptor for tumor immunity.* Semin Cancer Biol, 2006. **16**(5): p. 333-43.
202. Garrity, D., Call, M.E., Feng, J., and Wucherpfennig, K.W., *The activating NKG2D receptor assembles in the membrane with two signaling dimers into a hexameric structure.* Proc Natl Acad Sci U S A, 2005. **102**(21): p. 7641-6.
203. Upshaw, J.L., Arneson, L.N., Schoon, R.A., Dick, C.J., Billadeau, D.D., and Leibson, P.J., *NKG2D-mediated signaling requires a DAP10-bound Grb2-Vav1 intermediate and phosphatidylinositol-3-kinase in human natural killer cells.* Nat Immunol, 2006. **7**(5): p. 524-32.
204. Colucci, F., Schweighoffer, E., Tomasello, E., Turner, M., Ortaldo, J.R., Vivier, E., Tybulewicz, V.L., and Di Santo, J.P., *Natural cytotoxicity uncoupled from the Syk and ZAP-70 intracellular kinases.* Nat Immunol, 2002. **3**(3): p. 288-94.
205. Diefenbach, A., Tomasello, E., Lucas, M., Jamieson, A.M., Hsia, J.K., Vivier, E., and Raulet, D.H., *Selective associations with signaling proteins determine stimulatory versus costimulatory activity of NKG2D.* Nat Immunol, 2002. **3**(12): p. 1142-9.
206. Rosen, D.B., Araki, M., Hamerman, J.A., Chen, T., Yamamura, T., and Lanier, L.L., *A Structural basis for the association of DAP12 with mouse, but not human, NKG2D.* J Immunol, 2004. **173**(4): p. 2470-8.
207. Rabinovich, B., Li, J., Wolfson, M., Lawrence, W., Beers, C., Chalupny, J., Hurren, R., Greenfield, B., Miller, R., and Cosman, D., *NKG2D splice variants: a reexamination of adaptor molecule associations.* Immunogenetics, 2006. **58**(2-3): p. 81-8.
208. Zompi, S., Hamerman, J.A., Ogasawara, K., Schweighoffer, E., Tybulewicz, V.L., Di Santo, J.P., Lanier, L.L., and Colucci, F., *NKG2D triggers cytotoxicity in mouse NK cells lacking DAP12 or Syk family kinases.* Nat Immunol, 2003. **4**(6): p. 565-72.
209. McVicar, D.W., Taylor, L.S., Gosselin, P., Willette-Brown, J., Mikhael, A.I., Geahlen, R.L., Nakamura, M.C., Linnemeyer, P., Seaman, W.E., Anderson, S.K., Ortaldo, J.R., and Mason, L.H., *DAP12-mediated signal transduction in natural killer cells. A dominant role for the Syk protein-tyrosine kinase.* J Biol Chem, 1998. **273**(49): p. 32934-42.
210. Konjevic, G., Mirjacic Martinovic, K., Vuletic, A., and Radenkovic, S., *Novel aspects of in vitro IL-2 or IFN-alpha enhanced NK cytotoxicity of healthy individuals based on NKG2D and CD161 NK cell receptor induction.* Biomed Pharmacother, 2010. **64**(10): p. 663-71.
211. Wendt, K., Wilk, E., Buyny, S., Schmidt, R.E., and Jacobs, R., *Interleukin-21 differentially affects human natural killer cell subsets.* Immunology, 2007. **122**(4): p. 486-95.
212. Zhu, S., Phatarpekar, P.V., Denman, C.J., Senyukov, V.V., Somanchi, S.S., Nguyen-Jackson, H.T., Mace, E.M., Freeman, A.F., Watowich, S.S., Orange, J.S., Holland, S.M., and Lee, D.A., *Transcription of the activating receptor NKG2D in natural killer cells is regulated by STAT3 tyrosine phosphorylation.* Blood, 2014. **124**(3): p. 403-11.
213. Horng, T., Bezbradica, J.S., and Medzhitov, R., *NKG2D signaling is coupled to the interleukin 15 receptor signaling pathway.* Nat Immunol, 2007. **8**(12): p. 1345-52.
214. Zhang, C., Zhang, J., Niu, J., Zhou, Z., Zhang, J., and Tian, Z., *Interleukin-12 improves cytotoxicity of natural killer cells via upregulated expression of NKG2D.* Hum Immunol, 2008. **69**(8): p. 490-500.
215. Verneris, M.R., Karimi, M., Baker, J., Jayaswal, A., and Negrin, R.S., *Role of NKG2D signaling in the cytotoxicity of activated and expanded CD8+ T cells.* Blood, 2004. **103**(8): p. 3065-72.
216. Maasho, K., Opoku-Anane, J., Marusina, A.I., Coligan, J.E., and Borrego, F., *NKG2D is a costimulatory receptor for human naive CD8+ T cells.* J Immunol, 2005. **174**(8): p. 4480-4.
217. Roberts, A.I., Lee, L., Schwarz, E., Groh, V., Spies, T., Ebert, E.C., and Jabri, B., *NKG2D receptors induced by IL-15 costimulate CD28-negative effector CTL in the tissue microenvironment.* J Immunol, 2001. **167**(10): p. 5527-30.
218. Maccalli, C., Pende, D., Castelli, C., Mingari, M.C., Robbins, P.F., and Parmiani, G., *NKG2D engagement of colorectal cancer-specific T cells strengthens TCR-mediated antigen stimulation and elicits TCR independent anti-tumor activity.* Eur J Immunol, 2003. **33**(7): p. 2033-43.
219. Meresse, B., Chen, Z., Ciszewski, C., Tretiakova, M., Bhagat, G., Krausz, T.N., Raulet, D.H., Lanier, L.L., Groh, V., Spies, T., Ebert, E.C., Green, P.H., and Jabri, B., *Coordinated induction by IL15 of a TCR-independent NKG2D signaling pathway converts CTL into lymphokine-activated killer cells in celiac disease.* Immunity, 2004. **21**(3): p. 357-66.
220. Choy, M.K. and Phipps, M.E., *MICA polymorphism: biology and importance in immunity and disease.* Trends Mol Med, 2010. **16**(3): p. 97-106.
221. Elsner, H.A., Schroeder, M., and Blasczyk, R., *The nucleotide diversity of MICA and MICB suggests the effect of overdominant selection.* Tissue Antigens, 2001. **58**(6): p. 419-21.
222. Bahram, S., Inoko, H., Shiina, T., and Radosavljevic, M., *MIC and other NKG2D ligands: from none to too many.* Curr Opin Immunol, 2005. **17**(5): p. 505-9.

223. Groh, V., Bahram, S., Bauer, S., Herman, A., Beauchamp, M., and Spies, T., *Cell stress-regulated human major histocompatibility complex class I gene expressed in gastrointestinal epithelium.* Proc Natl Acad Sci U S A, 1996. **93**(22): p. 12445-50.
224. Li, P., Willie, S.T., Bauer, S., Morris, D.L., Spies, T., and Strong, R.K., *Crystal structure of the MHC class I homolog MIC-A, a gammadelta T cell ligand.* Immunity, 1999. **10**(5): p. 577-84.
225. Bahram, S., Bresnahan, M., Geraghty, D.E., and Spies, T., *A second lineage of mammalian major histocompatibility complex class I genes.* Proc Natl Acad Sci U S A, 1994. **91**(14): p. 6259-63.
226. Stephens, H.A., *MICA and MICB genes: can the enigma of their polymorphism be resolved?* Trends Immunol, 2001. **22**(7): p. 378-85.
227. Seo, J.W., Walter, L., and Gunther, E., *Genomic analysis of MIC genes in rhesus macaques.* Tissue Antigens, 2001. **58**(3): p. 159-65.
228. Seo, J.W., Bontrop, R., Walter, L., and Gunther, E., *Major histocompatibility complex-linked MIC genes in rhesus macaques and other primates.* Immunogenetics, 1999. **50**(5-6): p. 358-62.
229. Sutherland, C.L., Chalupny, N.J., Schooley, K., VandenBos, T., Kubin, M., and Cosman, D., *UL16-binding proteins, novel MHC class I-related proteins, bind to NKG2D and activate multiple signaling pathways in primary NK cells.* J Immunol, 2002. **168**(2): p. 671-9.
230. Sutherland, C.L., Chalupny, N.J., and Cosman, D., *The UL16-binding proteins, a novel family of MHC class I-related ligands for NKG2D, activate natural killer cell functions.* Immunol Rev, 2001. **181**: p. 185-92.
231. Chalupny, N.J., Sutherland, C.L., Lawrence, W.A., Rein-Weston, A., and Cosman, D., *ULBP4 is a novel ligand for human NKG2D.* Biochem Biophys Res Commun, 2003. **305**(1): p. 129-35.
232. Cosman, D., Mullberg, J., Sutherland, C.L., Chin, W., Armitage, R., Fanslow, W., Kubin, M., and Chalupny, N.J., *ULBPs, novel MHC class I-related molecules, bind to CMV glycoprotein UL16 and stimulate NK cytotoxicity through the NKG2D receptor.* Immunity, 2001. **14**(2): p. 123-33.
233. Kubin, M., Cassiano, L., Chalupny, J., Chin, W., Cosman, D., Fanslow, W., Mullberg, J., Rousseau, A.M., Ulrich, D., and Armitage, R., *ULBP1, 2, 3: novel MHC class I-related molecules that bind to human cytomegalovirus glycoprotein UL16, activate NK cells.* Eur J Immunol, 2001. **31**(5): p. 1428-37.
234. Conejo-Garcia, J.R., Benencia, F., Courreges, M.C., Khang, E., Zhang, L., Mohamed-Hadley, A., Vinocur, J.M., Buckanovich, R.J., Thompson, C.B., Levine, B., and Coukos, G., *Letal, A tumor-associated NKG2D immunoreceptor ligand, induces activation and expansion of effector immune cells.* Cancer Biol Ther, 2003. **2**(4): p. 446-51.
235. Radosavljevic, M., Cuillerier, B., Wilson, M.J., Clement, O., Wicker, S., Gilfillan, S., Beck, S., Trowsdale, J., and Bahram, S., *A cluster of ten novel MHC class I related genes on human chromosome 6q24.2-q25.3.* Genomics, 2002. **79**(1): p. 114-23.
236. Cerwenka, A., Bakker, A.B., McClanahan, T., Wagner, J., Wu, J., Phillips, J.H., and Lanier, L.L., *Retinoic acid early inducible genes define a ligand family for the activating NKG2D receptor in mice.* Immunity, 2000. **12**(6): p. 721-7.
237. Nomura, M., Zou, Z., Joh, T., Takihara, Y., Matsuda, Y., and Shimada, K., *Genomic structures and characterization of Rae1 family members encoding GPI-anchored cell surface proteins and expressed predominantly in embryonic mouse brain.* J Biochem, 1996. **120**(5): p. 987-95.
238. Zou, Z., Nomura, M., Takihara, Y., Yasunaga, T., and Shimada, K., *Isolation and characterization of retinoic acid-inducible cDNA clones in F9 cells: a novel cDNA family encodes cell surface proteins sharing partial homology with MHC class I molecules.* J Biochem, 1996. **119**(2): p. 319-28.
239. Malarkannan, S., Shih, P.P., Eden, P.A., Horng, T., Zuberi, A.R., Christianson, G., Roopenian, D., and Shastri, N., *The molecular and functional characterization of a dominant minor H antigen, H60.* J Immunol, 1998. **161**(7): p. 3501-9.
240. Takada, A., Yoshida, S., Kajikawa, M., Miyatake, Y., Tomaru, U., Sakai, M., Chiba, H., Maenaka, K., Kohda, D., Fugo, K., and Kasahara, M., *Two novel NKG2D ligands of the mouse H60 family with differential expression patterns and binding affinities to NKG2D.* J Immunol, 2008. **180**(3): p. 1678-85.
241. Carayannopoulos, L.N., Naidenko, O.V., Fremont, D.H., and Yokoyama, W.M., *Cutting edge: murine UL16-binding protein-like transcript 1: a newly described transcript encoding a high-affinity ligand for murine NKG2D.* J Immunol, 2002. **169**(8): p. 4079-83.
242. Diefenbach, A., Hsia, J.K., Hsiung, M.Y., and Raulet, D.H., *A novel ligand for the NKG2D receptor activates NK cells and macrophages and induces tumor immunity.* Eur J Immunol, 2003. **33**(2): p. 381-91.
243. Li, P., Morris, D.L., Willcox, B.E., Steinle, A., Spies, T., and Strong, R.K., *Complex structure of the activating immunoreceptor NKG2D and its MHC class I-like ligand MICA.* Nat Immunol, 2001. **2**(5): p. 443-51.
244. Li, P., McDermott, G., and Strong, R.K., *Crystal structures of RAE-1beta and its complex with the activating immunoreceptor NKG2D.* Immunity, 2002. **16**(1): p. 77-86.
245. Fernandez-Messina, L., Ashiru, O., Aguera-Gonzalez, S., Reyburn, H.T., and Vales-Gomez, M., *The human NKG2D ligand ULBP2 can be expressed at the cell surface with or without a GPI anchor and both forms can activate NK cells.* J Cell Sci, 2011. **124**(Pt 3): p. 321-7.
246. Raulet, D.H., Gasser, S., Gowen, B.G., Deng, W., and Jung, H., *Regulation of ligands for the NKG2D activating receptor.* Annu Rev Immunol, 2013. **31**: p. 413-41.
247. Radaev, S., Rostro, B., Brooks, A.G., Colonna, M., and Sun, P.D., *Conformational plasticity revealed by the cocrystal structure of NKG2D and its class I MHC-like ligand ULBP3.* Immunity, 2001. **15**(6): p. 1039-49.
248. McFarland, B.J., Kortemme, T., Yu, S.F., Baker, D., and Strong, R.K., *Symmetry recognizing asymmetry: analysis of the interactions between the C-type lectin-like immunoreceptor NKG2D and MHC class I-like ligands.* Structure, 2003. **11**(4): p. 411-22.
249. Steinle, A., Li, P., Morris, D.L., Groh, V., Lanier, L.L., Strong, R.K., and Spies, T., *Interactions of human NKG2D with its ligands MICA, MICB, and homologs of the mouse RAE-1 protein family.* Immunogenetics, 2001. **53**(4): p. 279-87.
250. Wittenbrink, M., Spreu, J., and Steinle, A., *Differential NKG2D binding to highly related human NKG2D ligands ULBP2 and RAET1G is determined by a single amino acid in the alpha2 domain.* Eur J Immunol, 2009. **39**(6): p. 1642-51.
251. Carayannopoulos, L.N., Naidenko, O.V., Kinder, J., Ho, E.L., Fremont, D.H., and Yokoyama, W., *Ligands for murine NKG2D display heterogeneous binding behavior.* Eur J Immunol, 2002. **32**(3): p. 597-605.

252. O'Callaghan, C.A., Cerwenka, A., Willcox, B.E., Lanier, L.L., and Bjorkman, P.J., *Molecular competition for NKG2D: H60 and RAE1 compete unequally for NKG2D with dominance of H60.* Immunity, 2001. **15**(2): p. 201-11.
253. Champsaur, M. and Lanier, L.L., *Effect of NKG2D ligand expression on host immune responses.* Immunol Rev, 2010. **235**(1): p. 267-85.
254. Kraetzel, K., Stoelcker, B., Eissner, G., Multhoff, G., Pfeifer, M., Holler, E., and Schulz, C., *NKG2D-dependent effector function of bronchial epithelium-activated alloreactive T-cells.* Eur Respir J, 2008. **32**(3): p. 563-70.
255. Caillat-Zucman, S., *How NKG2D ligands trigger autoimmunity?* Hum Immunol, 2006. **67**(3): p. 204-7.
256. Salih, H.R., Antropius, H., Gieseke, F., Lutz, S.Z., Kanz, L., Rammensee, H.G., and Steinle, A., *Functional expression and release of ligands for the activating immunoreceptor NKG2D in leukemia.* Blood, 2003. **102**(4): p. 1389-96.
257. Pende, D., Cantoni, C., Rivera, P., Vitale, M., Castriconi, R., Marcenaro, S., Nanni, M., Biassoni, R., Bottino, C., Moretta, A., and Moretta, L., *Role of NKG2D in tumor cell lysis mediated by human NK cells: cooperation with natural cytotoxicity receptors and capability of recognizing tumors of nonepithelial origin.* Eur J Immunol, 2001. **31**(4): p. 1076-86.
258. Pende, D., Rivera, P., Marcenaro, S., Chang, C.C., Biassoni, R., Conte, R., Kubin, M., Cosman, D., Ferrone, S., Moretta, L., and Moretta, A., *Major histocompatibility complex class I-related chain A and UL16-binding protein expression on tumor cell lines of different histotypes: analysis of tumor susceptibility to NKG2D-dependent natural killer cell cytotoxicity.* Cancer Res, 2002. **62**(21): p. 6178-86.
259. Watson, N.F., Spendlove, I., Madjd, Z., McGilvray, R., Green, A.R., Ellis, I.O., Scholefield, J.H., and Durrant, L.G., *Expression of the stress-related MHC class I chain-related protein MICA is an indicator of good prognosis in colorectal cancer patients.* Int J Cancer, 2006. **118**(6): p. 1445-52.
260. Castriconi, R., Dondero, A., Negri, F., Bellora, F., Nozza, P., Carnemolla, B., Raso, A., Moretta, L., Moretta, A., and Bottino, C., *Both CD133+ and CD133- medulloblastoma cell lines express ligands for triggering NK receptors and are susceptible to NK-mediated cytotoxicity.* Eur J Immunol, 2007. **37**(11): p. 3190-6.
261. Vetter, C.S., Groh, V., thor Straten, P., Spies, T., Brocker, E.B., and Becker, J.C., *Expression of stress-induced MHC class I related chain molecules on human melanoma.* J Invest Dermatol, 2002. **118**(4): p. 600-5.
262. Friese, M.A., Platten, M., Lutz, S.Z., Naumann, U., Aulwurm, S., Bischof, F., Buhring, H.J., Dichgans, J., Rammensee, H.G., Steinle, A., and Weller, M., *MICA/NKG2D-mediated immunogene therapy of experimental gliomas.* Cancer Res, 2003. **63**(24): p. 8996-9006.
263. Siren, J., Sareneva, T., Pirhonen, J., Strengell, M., Veckman, V., Julkunen, I., and Matikainen, S., *Cytokine and contact-dependent activation of natural killer cells by influenza A or Sendai virus-infected macrophages.* J Gen Virol, 2004. **85**(Pt 8): p. 2357-64.
264. Vilarinho, S., Ogasawara, K., Nishimura, S., Lanier, L.L., and Baron, J.L., *Blockade of NKG2D on NKT cells prevents hepatitis and the acute immune response to hepatitis B virus.* Proc Natl Acad Sci U S A, 2007. **104**(46): p. 18187-92.
265. Ward, J., Bonaparte, M., Sacks, J., Guterman, J., Fogli, M., Mavilio, D., and Barker, E., *HIV modulates the expression of ligands important in triggering natural killer cell cytotoxic responses on infected primary T-cell blasts.* Blood, 2007. **110**(4): p. 1207-14.
266. Groh, V., Steinle, A., Bauer, S., and Spies, T., *Recognition of stress-induced MHC molecules by intestinal epithelial gammadelta T cells.* Science, 1998. **279**(5357): p. 1737-40.
267. Diefenbach, A., Jensen, E.R., Jamieson, A.M., and Raulet, D.H., *Rae1 and H60 ligands of the NKG2D receptor stimulate tumour immunity.* Nature, 2001. **413**(6852): p. 165-71.
268. Poggi, A., Venturino, C., Catellani, S., Clavio, M., Miglino, M., Gobbi, M., Steinle, A., Ghia, P., Stella, S., Caligaris-Cappio, F., and Zocchi, M.R., *Vdelta1 T lymphocytes from B-CLL patients recognize ULBP3 expressed on leukemic B cells and up-regulated by trans-retinoic acid.* Cancer Res, 2004. **64**(24): p. 9172-9.
269. Hayakawa, Y., Kelly, J.M., Westwood, J.A., Darcy, P.K., Diefenbach, A., Raulet, D., and Smyth, M.J., *Cutting edge: tumor rejection mediated by NKG2D receptor-ligand interaction is dependent upon perforin.* J Immunol, 2002. **169**(10): p. 5377-81.
270. Guerra, N., Tan, Y.X., Joncker, N.T., Choy, A., Gallardo, F., Xiong, N., Knoblaugh, S., Cado, D., Greenberg, N.M., and Raulet, D.H., *NKG2D-deficient mice are defective in tumor surveillance in models of spontaneous malignancy.* Immunity, 2008. **28**(4): p. 571-80.
271. Smyth, M.J., Swann, J., Cretney, E., Zerafa, N., Yokoyama, W.M., and Hayakawa, Y., *NKG2D function protects the host from tumor initiation.* J Exp Med, 2005. **202**(5): p. 583-8.
272. McGilvray, R.W., Eagle, R.A., Rolland, P., Jafferji, I., Trowsdale, J., and Durrant, L.G., *ULBP2 and RAET1E NKG2D ligands are independent predictors of poor prognosis in ovarian cancer patients.* Int J Cancer, 2010. **127**(6): p. 1412-20.
273. de Kruijf, E.M., Sajet, A., van Nes, J.G., Putter, H., Smit, V.T., Eagle, R.A., Jafferji, I., Trowsdale, J., Liefers, G.J., van de Velde, C.J., and Kuppen, P.J., *NKG2D ligand tumor expression and association with clinical outcome in early breast cancer patients: an observational study.* BMC Cancer, 2012. **12**: p. 24.
274. Gasser, S., Orsulic, S., Brown, E.J., and Raulet, D.H., *The DNA damage pathway regulates innate immune system ligands of the NKG2D receptor*. Nature, 2005. **436**(7054): p. 1186-90.
275. Welte, S.A., Sinzger, C., Lutz, S.Z., Singh-Jasuja, H., Sampaio, K.L., Eknigk, U., Rammensee, H.G., and Steinle, A., *Selective intracellular retention of virally induced NKG2D ligands by the human cytomegalovirus UL16 glycoprotein.* Eur J Immunol, 2003. **33**(1): p. 194-203.
276. Dunn, C., Chalupny, N.J., Sutherland, C.L., Dosch, S., Sivakumar, P.V., Johnson, D.C., and Cosman, D., *Human cytomegalovirus glycoprotein UL16 causes intracellular sequestration of NKG2D ligands, protecting against natural killer cell cytotoxicity.* J Exp Med, 2003. **197**(11): p. 1427-39.
277. Vales-Gomez, M., Browne, H., and Reyburn, H.T., *Expression of the UL16 glycoprotein of Human Cytomegalovirus protects the virus-infected cell from attack by natural killer cells.* BMC Immunol, 2003. **4**: p. 4.
278. Dunn, G.P., Old, L.J., and Schreiber, R.D., *The three Es of cancer immunoediting.* Annu Rev Immunol, 2004. **22**: p. 329-60.
279. Kim, R., Emi, M., and Tanabe, K., *Cancer immunoediting from immune surveillance to immune escape.* Immunology, 2007. **121**(1): p. 1-14.
280. Mittal, D., Gubin, M.M., Schreiber, R.D., and Smyth, M.J., *New insights into cancer immunoediting and its three component phases--elimination, equilibrium and escape.* Curr Opin Immunol, 2014. **27**: p. 16-25.

281. Vitale, M., Cantoni, C., Pietra, G., Mingari, M.C., and Moretta, L., *Effect of tumor cells and tumor microenvironment on NK-cell function.* Eur J Immunol, 2014. **44**(6): p. 1582-92.
282. Rabinovich, G.A., Gabrilovich, D., and Sotomayor, E.M., *Immunosuppressive strategies that are mediated by tumor cells.* Annu Rev Immunol, 2007. **25**: p. 267-96.
283. Zwirner, N.W., Fuertes, M.B., Girart, M.V., Domaica, C.I., and Rossi, L.E., *Cytokine-driven regulation of NK cell functions in tumor immunity: role of the MICA-NKG2D system.* Cytokine Growth Factor Rev, 2007. **18**(1-2): p. 159-70.
284. Vetter, C.S., Lieb, W., Brocker, E.B., and Becker, J.C., *Loss of nonclassical MHC molecules MIC-A/B expression during progression of uveal melanoma.* Br J Cancer, 2004. **91**(8): p. 1495-9.
285. Raffaghello, L., Prigione, I., Airoldi, I., Camoriano, M., Morandi, F., Bocca, P., Gambini, C., Ferrone, S., and Pistoia, V., *Mechanisms of immune evasion of human neuroblastoma.* Cancer Lett, 2005. **228**(1-2): p. 155-61.
286. Le Maux Chansac, B., Moretta, A., Vergnon, I., Opolon, P., Lecluse, Y., Grunenwald, D., Kubin, M., Soria, J.C., Chouaib, S., and Mami-Chouaib, F., *NK cells infiltrating a MHC class I-deficient lung adenocarcinoma display impaired cytotoxic activity toward autologous tumor cells associated with altered NK cell-triggering receptors.* J Immunol, 2005. **175**(9): p. 5790-8.
287. Wiemann, K., Mittrucker, H.W., Feger, U., Welte, S.A., Yokoyama, W.M., Spies, T., Rammensee, H.G., and Steinle, A., *Systemic NKG2D down-regulation impairs NK and CD8 T cell responses in vivo.* J Immunol, 2005. **175**(2): p. 720-9.
288. Oppenheim, D.E., Roberts, S.J., Clarke, S.L., Filler, R., Lewis, J.M., Tigelaar, R.E., Girardi, M., and Hayday, A.C., *Sustained localized expression of ligand for the activating NKG2D receptor impairs natural cytotoxicity in vivo and reduces tumor immunosurveillance.* Nat Immunol, 2005. **6**(9): p. 928-37.
289. Coudert, J.D., Zimmer, J., Tomasello, E., Cebecauer, M., Colonna, M., Vivier, E., and Held, W., *Altered NKG2D function in NK cells induced by chronic exposure to NKG2D ligand-expressing tumor cells.* Blood, 2005. **106**(5): p. 1711-7.
290. Zhang, C., Tian, Z.G., Zhang, J., Feng, J.B., Zhang, J.H., and Xu, X.Q., *[The negative regulatory effect of IFN-gamma on cognitive function of human natural killer cells].* Zhonghua Zhong Liu Za Zhi, 2004. **26**(6): p. 324-7.
291. Zhang, C., Zhang, J., Sun, R., Feng, J., Wei, H., and Tian, Z., *Opposing effect of IFNgamma and IFNalpha on expression of NKG2 receptors: negative regulation of IFNgamma on NK cells.* Int Immunopharmacol, 2005. **5**(6): p. 1057-67.
292. Castriconi, R., Cantoni, C., Della Chiesa, M., Vitale, M., Marcenaro, E., Conte, R., Biassoni, R., Bottino, C., Moretta, L., and Moretta, A., *Transforming growth factor beta 1 inhibits expression of NKp30 and NKG2D receptors: consequences for the NK-mediated killing of dendritic cells.* Proc Natl Acad Sci U S A, 2003. **100**(7): p. 4120-5.
293. Lee, J.C., Lee, K.M., Kim, D.W., and Heo, D.S., *Elevated TGF-beta1 secretion and down-modulation of NKG2D underlies impaired NK cytotoxicity in cancer patients.* J Immunol, 2004. **172**(12): p. 7335-40.
294. Ghiringhelli, F., Menard, C., Terme, M., Flament, C., Taieb, J., Chaput, N., Puig, P.E., Novault, S., Escudier, B., Vivier, E., Lecesne, A., Robert, C., Blay, J.Y., Bernard, J., Caillat-Zucman, S., Freitas, A., Tursz, T., Wagner-Ballon, O., Capron, C., Vainchencker, W., Martin, F., and Zitvogel, L., *CD4+CD25+ regulatory T cells inhibit natural killer cell functions in a transforming growth factor-beta-dependent manner.* J Exp Med, 2005. **202**(8): p. 1075-85.
295. Dasgupta, S., Bhattacharya-Chatterjee, M., O'Malley, B.W., Jr., and Chatterjee, S.K., *Inhibition of NK cell activity through TGF-beta 1 by down-regulation of NKG2D in a murine model of head and neck cancer.* J Immunol, 2005. **175**(8): p. 5541-50.
296. Salih, H.R., Rammensee, H.G., and Steinle, A., *Cutting edge: down-regulation of MICA on human tumors by proteolytic shedding.* J Immunol, 2002. **169**(8): p. 4098-102.
297. Salih, H.R., Goehlsdorf, D., and Steinle, A., *Release of MICB molecules by tumor cells: mechanism and soluble MICB in sera of cancer patients.* Hum Immunol, 2006. **67**(3): p. 188-95.
298. Waldhauer, I. and Steinle, A., *Proteolytic release of soluble UL16-binding protein 2 from tumor cells.* Cancer Res, 2006. **66**(5): p. 2520-6.
299. Kaiser, B.K., Yim, D., Chow, I.T., Gonzalez, S., Dai, Z., Mann, H.H., Strong, R.K., Groh, V., and Spies, T., *Disulphide-isomerase-enabled shedding of tumour-associated NKG2D ligands.* Nature, 2007. **447**(7143): p. 482-6.
300. Boutet, P., Aguera-Gonzalez, S., Atkinson, S., Pennington, C.J., Edwards, D.R., Murphy, G., Reyburn, H.T., and Vales-Gomez, M., *Cutting edge: the metalloproteinase ADAM17/TNF-alpha-converting enzyme regulates proteolytic shedding of the MHC class I-related chain B protein.* J Immunol, 2009. **182**(1): p. 49-53.
301. Liu, G., Atteridge, C.L., Wang, X., Lundgren, A.D., and Wu, J.D., *The membrane type matrix metalloproteinase MMP14 mediates constitutive shedding of MHC class I chain-related molecule A independent of A disintegrin and metalloproteinases.* J Immunol, 2010. **184**(7): p. 3346-50.
302. Song, H., Kim, J., Cosman, D., and Choi, I., *Soluble ULBP suppresses natural killer cell activity via down-regulating NKG2D expression.* Cell Immunol, 2006. **239**(1): p. 22-30.
303. Rebmann, V., Schutt, P., Brandhorst, D., Opalka, B., Moritz, T., Nowrousian, M.R., and Grosse-Wilde, H., *Soluble MICA as an independent prognostic factor for the overall survival and progression-free survival of multiple myeloma patients.* Clin Immunol, 2007. **123**(1): p. 114-20.
304. Tamaki, S., Sanefuzi, N., Kawakami, M., Aoki, K., Imai, Y., Yamanaka, Y., Yamamoto, K., Ishitani, A., Hatake, K., and Kirita, T., *Association between soluble MICA levels and disease stage IV oral squamous cell carcinoma in Japanese patients.* Hum Immunol, 2008. **69**(2): p. 88-93.
305. Kloess, S., Huenecke, S., Piechulek, D., Esser, R., Koch, J., Brehm, C., Soerensen, J., Gardlowski, T., Brinkmann, A., Bader, P., Passweg, J., Klingebiel, T., Schwabe, D., and Koehl, U., *IL-2-activated haploidentical NK cells restore NKG2D-mediated NK-cell cytotoxicity in neuroblastoma patients by scavenging of plasma MICA.* Eur J Immunol, 2010. **40**(11): p. 3255-67.
306. Kumar, V., Yi Lo, P.H., Sawai, H., Kato, N., Takahashi, A., Deng, Z., Urabe, Y., Mbarek, H., Tokunaga, K., Tanaka, Y., Sugiyama, M., Mizokami, M., Muroyama, R., Tateishi, R., Omata, M., Koike, K., Tanikawa, C., Kamatani, N., Kubo, M., Nakamura, Y., and Matsuda, K., *Soluble MICA and a MICA variation as possible prognostic biomarkers for HBV-induced hepatocellular carcinoma.* PLoS One, 2012. **7**(9): p. e44743.
307. Li, J.J., Pan, K., Gu, M.F., Chen, M.S., Zhao, J.J., Wang, H., Liang, X.T., Sun, J.C., and Xia, J.C., *Prognostic value of soluble MICA levels in the serum of patients with advanced hepatocellular carcinoma.* Chin J Cancer, 2013. **32**(3): p. 141-8.
308. Nuckel, H., Switala, M., Sellmann, L., Horn, P.A., Durig, J., Duhrsen, U., Kuppers, R., Grosse-Wilde, H., and Rebmann, V., *The prognostic significance of soluble NKG2D ligands in B-cell chronic lymphocytic leukemia.* Leukemia, 2010. **24**(6): p. 1152-9.

309. Li, K., Mandai, M., Hamanishi, J., Matsumura, N., Suzuki, A., Yagi, H., Yamaguchi, K., Baba, T., Fujii, S., and Konishi, I., *Clinical significance of the NKG2D ligands, MICA/B and ULBP2 in ovarian cancer: high expression of ULBP2 is an indicator of poor prognosis.* Cancer Immunol Immunother, 2009. **58**(5): p. 641-52.
310. Monjazeb, A.M., Zamora, A.E., Grossenbacher, S.K., Mirsoian, A., Sckisel, G.D., and Murphy, W.J., *Immunoediting and antigen loss: overcoming the achilles heel of immunotherapy with antigen non-specific therapies.* Front Oncol, 2013. **3**: p. 197.
311. Fernandez-Messina, L., Ashiru, O., Boutet, P., Aguera-Gonzalez, S., Skepper, J.N., Reyburn, H.T., and Vales-Gomez, M., *Differential mechanisms of shedding of the glycosylphosphatidylinositol (GPI)-anchored NKG2D ligands.* J Biol Chem, 2010. **285**(12): p. 8543-51.
312. Ashiru, O., Boutet, P., Fernandez-Messina, L., Aguera-Gonzalez, S., Skepper, J.N., Vales-Gomez, M., and Reyburn, H.T., *Natural killer cell cytotoxicity is suppressed by exposure to the human NKG2D ligand MICA*008 that is shed by tumor cells in exosomes.* Cancer Res, 2010. **70**(2): p. 481-9.
313. Bacon, L., Eagle, R.A., Meyer, M., Easom, N., Young, N.T., and Trowsdale, J., *Two human ULBP/RAET1 molecules with transmembrane regions are ligands for NKG2D.* J Immunol, 2004. **173**(2): p. 1078-84.
314. Cao, W., Xi, X., Hao, Z., Li, W., Kong, Y., Cui, L., Ma, C., Ba, D., and He, W., *RAET1E2, a soluble isoform of the UL16-binding protein RAET1E produced by tumor cells, inhibits NKG2D-mediated NK cytotoxicity.* J Biol Chem, 2007. **282**(26): p. 18922-8.
315. Groh, V., Wu, J., Yee, C., and Spies, T., *Tumour-derived soluble MIC ligands impair expression of NKG2D and T-cell activation.* Nature, 2002. **419**(6908): p. 734-8.
316. Jinushi, M., Takehara, T., Tatsumi, T., Hiramatsu, N., Sakamori, R., Yamaguchi, S., and Hayashi, N., *Impairment of natural killer cell and dendritic cell functions by the soluble form of MHC class I-related chain A in advanced human hepatocellular carcinomas.* J Hepatol, 2005. **43**(6): p. 1013-20.
317. Salih, H.R., Holdenrieder, S., and Steinle, A., *Soluble NKG2D ligands: prevalence, release, and functional impact.* Front Biosci, 2008. **13**: p. 3448-56.
318. Textor, S., Durst, M., Jansen, L., Accardi, R., Tommasino, M., Trunk, M.J., Porgador, A., Watzl, C., Gissmann, L., and Cerwenka, A., *Activating NK cell receptor ligands are differentially expressed during progression to cervical cancer.* Int J Cancer, 2008. **123**(10): p. 2343-53.
319. Arreygue-Garcia, N.A., Daneri-Navarro, A., del Toro-Arreola, A., Cid-Arregui, A., Gonzalez-Ramella, O., Jave-Suarez, L.F., Aguilar-Lemarroy, A., Troyo-Sanroman, R., Bravo-Cuellar, A., Delgado-Rizo, V., Garcia-Iglesias, T., Hernandez-Flores, G., and Del Toro-Arreola, S., *Augmented serum level of major histocompatibility complex class I-related chain A (MICA) protein and reduced NKG2D expression on NK and T cells in patients with cervical cancer and precursor lesions.* BMC Cancer, 2008. **8**: p. 16.
320. Kloess, S., Chambron, N., Gardlowski, T., Arsenjev, L., Koch, J., Esser, R., Glienke, W., Seitz, O., and Köhl, U., *Increased sMICA and TGF-b1 levels in HNSCC patients impair NKG2D-dependent functionality of activated NK cells.* Oncoimmunology, 2015. **6**(11): p. e1055993.
321. Kloess, S., Chambron, N., Gardlowski, T., Weil, S., Koch, J., Esser, R., Pogge von Strandmann, E., Arseniev, L., Seitz, O., and Köhl, U., *Cetuximab reconstitutes proinflammatory cytokine secretions and tumour-infiltrating capabilities of sMICA-inhibited NK cells in HNSCC tumour spheroids.* Frontiers in Immunology, 2015. **6**: p. 543.
322. Wu, J.D., Atteridge, C.L., Wang, X., Seya, T., and Plymate, S.R., *Obstructing shedding of the immunostimulatory MHC class I chain-related gene B prevents tumor formation.* Clin Cancer Res, 2009. **15**(2): p. 632-40.
323. Holdenrieder, S., Stieber, P., Peterfi, A., Nagel, D., Steinle, A., and Salih, H.R., *Soluble MICA in malignant diseases.* Int J Cancer, 2006. **118**(3): p. 684-7.
324. Holdenrieder, S., Stieber, P., Peterfi, A., Nagel, D., Steinle, A., and Salih, H.R., *Soluble MICB in malignant diseases: analysis of diagnostic significance and correlation with soluble MICA.* Cancer Immunol Immunother, 2006. **55**(12): p. 1584-9.
325. Wu, J.D., Higgins, L.M., Steinle, A., Cosman, D., Haugk, K., and Plymate, S.R., *Prevalent expression of the immunostimulatory MHC class I chain-related molecule is counteracted by shedding in prostate cancer.* J Clin Invest, 2004. **114**(4): p. 560-8.
326. Mottamal, M., Zheng, S., Huang, T.L., and Wang, G., *Histone deacetylase inhibitors in clinical studies as templates for new anticancer agents.* Molecules, 2015. **20**(3): p. 3898-941.
327. Iqbal, N. and Iqbal, N., *Imatinib: a breakthrough of targeted therapy in cancer.* Chemother Res Pract, 2014. **2014**: p. 357027.
328. Blick, S.K. and Scott, L.J., *Cetuximab: a review of its use in squamous cell carcinoma of the head and neck and metastatic colorectal cancer.* Drugs, 2007. **67**(17): p. 2585-607.
329. Dotan, E., Aggarwal, C., and Smith, M.R., *Impact of Rituximab (Rituxan) on the Treatment of B-Cell Non-Hodgkin's Lymphoma.* P T, 2010. **35**(3): p. 148-57.
330. Ruocco, M.G., Pilones, K.A., Kawashima, N., Cammer, M., Huang, J., Babb, J.S., Liu, M., Formenti, S.C., Dustin, M.L., and Demaria, S., *Suppressing T cell motility induced by anti-CTLA-4 monotherapy improves antitumor effects.* J Clin Invest, 2012. **122**(10): p. 3718-30.
331. Pardoll, D.M., *The blockade of immune checkpoints in cancer immunotherapy.* Nat Rev Cancer, 2012. **12**(4): p. 252-64.
332. Chen, L. and Han, X., *Anti-PD-1/PD-L1 therapy of human cancer: past, present, and future.* J Clin Invest, 2015. **125**(9): p. 3384-91.
333. von Strandmann, E.P., Hansen, H.P., Reiners, K.S., Schnell, R., Borchmann, P., Merkert, S., Simhadri, V.R., Draube, A., Reiser, M., Purr, I., Hallek, M., and Engert, A., *A novel bispecific protein (ULBP2-BB4) targeting the NKG2D receptor on natural killer (NK) cells and CD138 activates NK cells and has potent antitumor activity against human multiple myeloma in vitro and in vivo.* Blood, 2006. **107**(5): p. 1955-62.
334. Zhang, T. and Sentman, C.L., *Cancer immunotherapy using a bispecific NK receptor fusion protein that engages both T cells and tumor cells.* Cancer Res, 2011. **71**(6): p. 2066-76.
335. Kellner, C., Hallack, D., Glorius, P., Staudinger, M., Mohseni Nodehi, S., de Weers, M., van de Winkel, J.G., Parren, P.W., Stauch, M., Valerius, T., Repp, R., Humpe, A., Gramatzki, M., and Peipp, M., *Fusion proteins between ligands for NKG2D and CD20-directed single-chain variable fragments sensitize lymphoma cells for natural killer cell-mediated lysis and enhance antibody-dependent cellular cytotoxicity.* Leukemia, 2012. **26**(4): p. 830-4.
336. Kontermann, R.E. and Brinkmann, U., *Bispecific antibodies.* Drug Discov Today, 2015. **20**(7): p. 838-47.

337. Perica, K., Varela, J.C., Oelke, M., and Schneck, J., *Adoptive T cell immunotherapy for cancer.* Rambam Maimonides Med J, 2015. **6**(1): p. e0004.
338. June, C.H., *Adoptive T cell therapy for cancer in the clinic.* J Clin Invest, 2007. **117**(6): p. 1466-76.
339. June, C.H., *Principles of adoptive T cell cancer therapy.* J Clin Invest, 2007. **117**(5): p. 1204-12.
340. Tey, S.K., *Adoptive T-cell therapy: adverse events and safety switches.* Clin Transl Immunology, 2014. **3**(6): p. e17.
341. Cheng, M., Chen, Y., Xiao, W., Sun, R., and Tian, Z., *NK cell-based immunotherapy for malignant diseases.* Cell Mol Immunol, 2013. **10**(3): p. 230-52.
342. Rezvani, K. and Rouce, R.H., *The Application of Natural Killer Cell Immunotherapy for the Treatment of Cancer.* Front Immunol, 2015. **6**: p. 578.
343. Maus, M.V., Grupp, S.A., Porter, D.L., and June, C.H., *Antibody-modified T cells: CARs take the front seat for hematologic malignancies.* Blood, 2014. **123**(17): p. 2625-35.
344. Grupp, S.A., Kalos, M., Barrett, D., Aplenc, R., Porter, D.L., Rheingold, S.R., Teachey, D.T., Chew, A., Hauck, B., Wright, J.F., Milone, M.C., Levine, B.L., and June, C.H., *Chimeric antigen receptor-modified T cells for acute lymphoid leukemia.* N Engl J Med, 2013. **368**(16): p. 1509-18.
345. Corrigan-Curay, J., Kiem, H.P., Baltimore, D., O'Reilly, M., Brentjens, R.J., Cooper, L., Forman, S., Gottschalk, S., Greenberg, P., Junghans, R., Heslop, H., Jensen, M., Mackall, C., June, C., Press, O., Powell, D., Ribas, A., Rosenberg, S., Sadelain, M., Till, B., Patterson, A.P., Jambou, R.C., Rosenthal, E., Gargiulo, L., Montgomery, M., and Kohn, D.B., *T-cell immunotherapy: looking forward.* Mol Ther, 2014. **22**(9): p. 1564-74.
346. Zhang, T., Barber, A., and Sentman, C.L., *Generation of antitumor responses by genetic modification of primary human T cells with a chimeric NKG2D receptor.* Cancer Res, 2006. **66**(11): p. 5927-33.
347. Barber, A., Zhang, T., and Sentman, C.L., *Immunotherapy with chimeric NKG2D receptors leads to long-term tumor-free survival and development of host antitumor immunity in murine ovarian cancer.* J Immunol, 2008. **180**(1): p. 72-8.
348. Barber, A., Meehan, K.R., and Sentman, C.L., *Treatment of multiple myeloma with adoptively transferred chimeric NKG2D receptor-expressing T cells.* Gene Ther, 2011. **18**(5): p. 509-16.
349. Imai, C., Iwamoto, S., and Campana, D., *Genetic modification of primary natural killer cells overcomes inhibitory signals and induces specific killing of leukemic cells.* Blood, 2005. **106**(1): p. 376-83.
350. Jiang, H., Zhang, W., Shang, P., Zhang, H., Fu, W., Ye, F., Zeng, T., Huang, H., Zhang, X., Sun, W., Man-Yuen Sze, D., Yi, Q., and Hou, J., *Transfection of chimeric anti-CD138 gene enhances natural killer cell activation and killing of multiple myeloma cells.* Mol Oncol, 2014. **8**(2): p. 297-310.
351. Muller, T., Uherek, C., Maki, G., Chow, K.U., Schimpf, A., Klingemann, H.G., Tonn, T., and Wels, W.S., *Expression of a CD20-specific chimeric antigen receptor enhances cytotoxic activity of NK cells and overcomes NK-resistance of lymphoma and leukemia cells.* Cancer Immunol Immunother, 2008. **57**(3): p. 411-23.
352. Glienke, W., Esser, R., Priesner, C., Suerth, J.D., Schambach, A., Wels, W.S., Grez, M., Kloess, S., Arseniev, L., and Koehl, U., *Advantages and applications of CAR-expressing natural killer cells.* Front Pharmacol, 2015. **6**: p. 21.
353. Chang, Y.H., Connolly, J., Shimasaki, N., Mimura, K., Kono, K., and Campana, D., *A chimeric receptor with NKG2D specificity enhances natural killer cell activation and killing of tumor cells.* Cancer Res, 2013. **73**(6): p. 1777-86.
354. Cancer Genome Atlas, N., *Comprehensive genomic characterization of head and neck squamous cell carcinomas.* Nature, 2015. **517**(7536): p. 576-82.
355. Leemans, C.R., Braakhuis, B.J., and Brakenhoff, R.H., *The molecular biology of head and neck cancer.* Nat Rev Cancer, 2011. **11**(1): p. 9-22.
356. Ragin, C.C., Modugno, F., and Gollin, S.M., *The epidemiology and risk factors of head and neck cancer: a focus on human papillomavirus.* J Dent Res, 2007. **86**(2): p. 104-14.
357. Ang, K.K., Harris, J., Wheeler, R., Weber, R., Rosenthal, D.I., Nguyen-Tan, P.F., Westra, W.H., Chung, C.H., Jordan, R.C., Lu, C., Kim, H., Axelrod, R., Silverman, C.C., Redmond, K.P., and Gillison, M.L., *Human papillomavirus and survival of patients with oropharyngeal cancer.* N Engl J Med, 2010. **363**(1): p. 24-35.
358. Trivedy, C.R., Craig, G., and Warnakulasuriya, S., *The oral health consequences of chewing areca nut.* Addict Biol, 2002. **7**(1): p. 115-25.
359. Ferlay, J., Shin, H.R., Bray, F., Forman, D., Mathers, C., and Parkin, D.M., *Estimates of worldwide burden of cancer in 2008: GLOBOCAN 2008.* Int J Cancer, 2010. **127**(12): p. 2893-917.
360. Shibuya, K., Mathers, C.D., Boschi-Pinto, C., Lopez, A.D., and Murray, C.J., *Global and regional estimates of cancer mortality and incidence by site: II. Results for the global burden of disease 2000.* BMC Cancer, 2002. **2**: p. 37.
361. Hammarstedt, L., Lindquist, D., Dahlstrand, H., Romanitan, M., Dahlgren, L.O., Joneberg, J., Creson, N., Lindholm, J., Ye, W., Dalianis, T., and Munck-Wikland, E., *Human papillomavirus as a risk factor for the increase in incidence of tonsillar cancer.* Int J Cancer, 2006. **119**(11): p. 2620-3.
362. Shiboski, C.H., Schmidt, B.L., and Jordan, R.C., *Tongue and tonsil carcinoma: increasing trends in the U.S. population ages 20-44 years.* Cancer, 2005. **103**(9): p. 1843-9.
363. Howaldt, H.P., Kainz, M., Euler, B., and Vorast, H., *Proposal for modification of the TNM staging classification for cancer of the oral cavity. DOSAK.* J Craniomaxillofac Surg, 1999. **27**(5): p. 275-88.
364. Freiser, M.E., Serafini, P., and Weed, D.T., *The immune system and head and neck squamous cell carcinoma: from carcinogenesis to new therapeutic opportunities.* Immunol Res, 2013. **57**(1-3): p. 52-69.
365. De Costa, A.M. and Young, M.R., *Immunotherapy for head and neck cancer: advances and deficiencies.* Anticancer Drugs, 2011. **22**(7): p. 674-81.
366. Bose, A., Chakraborty, T., Chakraborty, K., Pal, S., and Baral, R., *Dysregulation in immune functions is reflected in tumor cell cytotoxicity by peripheral blood mononuclear cells from head and neck squamous cell carcinoma patients.* Cancer Immun, 2008. **8**: p. 10.
367. Young, M.R., *Protective mechanisms of head and neck squamous cell carcinomas from immune assault.* Head Neck, 2006. **28**(5): p. 462-70.
368. McLarnon, C., Kulloo, P., Mehanna, H., Kelly, C., and Paleri, V., *Quality-of-life considerations in treatment of unresectable, recurrent head and neck cancer.* Expert Rev Anticancer Ther, 2010. **10**(3): p. 345-52.

369. Akst, L.M., Chan, J., Elson, P., Saxton, J., Strome, M., and Adelstein, D., *Functional outcomes following chemoradiotherapy for head and neck cancer.* Otolaryngol Head Neck Surg, 2004. **131**(6): p. 950-7.
370. Jakowlew, S.B., *Transforming growth factor-beta in cancer and metastasis.* Cancer Metastasis Rev, 2006. **25**(3): p. 435-57.
371. Tong, C.C., Kao, J., and Sikora, A.G., *Recognizing and reversing the immunosuppressive tumor microenvironment of head and neck cancer.* Immunol Res, 2012. **54**(1-3): p. 266-74.
372. Mocellin, S., Marincola, F., Rossi, C.R., Nitti, D., and Lise, M., *The multifaceted relationship between IL-10 and adaptive immunity: putting together the pieces of a puzzle.* Cytokine Growth Factor Rev, 2004. **15**(1): p. 61-76.
373. Ullrich, E., Koch, J., Cerwenka, A., and Steinle, A., *New prospects on the NKG2D/NKG2D ligand system for oncology.* Oncoimmunology, 2013. **2**(10): p. e26097.
374. Bertani, G., *Studies on lysogenesis. I. The mode of phage liberation by lysogenic Escherichia coli.* J Bacteriol, 1951. **62**(3): p. 293-300.
375. Lennox, E.S., *Transduction of linked genetic characters of the host by bacteriophage P1.* Virology, 1955. **1**(2): p. 190-206.
376. Cinatl, J., Cinatl, J., Mainke, M., Weissflog, A., Steigmann, G., Rabenau, H., Doerr, H.W., and Kornhuber, B., *Aphidicolin selectively kills neuroblastoma cells in vitro.* Cancer Lett, 1992. **67**(2-3): p. 199-206.
377. Hartmann, J., Tran, T.V., Kaudeer, J., Oberle, K., Herrmann, J., Quagliano, I., Abel, T., Cohnen, A., Gatterdam, V., Jacobs, A., Wollscheid, B., Tampe, R., Watzl, C., Diefenbach, A., and Koch, J., *The stalk domain and the glycosylation status of the activating natural killer cell receptor NKp30 are important for ligand binding.* J Biol Chem, 2012. **287**(37): p. 31527-39.
378. Binici, J., Hartmann, J., Herrmann, J., Schreiber, C., Beyer, S., Guler, G., Vogel, V., Tumulka, F., Abele, R., Mantele, W., and Koch, J., *A soluble fragment of the tumor antigen BCL2-associated athanogene 6 (BAG-6) is essential and sufficient for inhibition of NKp30 receptor-dependent cytotoxicity of natural killer cells.* J Biol Chem, 2013. **288**(48): p. 34295-303.
379. Hanahan, D., Jessee, J., and Bloom, F.R., *Plasmid transformation of Escherichia coli and other bacteria.* Methods Enzymol, 1991. **204**: p. 63-113.
380. Saiki, R.K., Scharf, S., Faloona, F., Mullis, K.B., Horn, G.T., Erlich, H.A., and Arnheim, N., *Enzymatic amplification of beta-globin genomic sequences and restriction site analysis for diagnosis of sickle cell anemia.* Science, 1985. **230**(4732): p. 1350-4.
381. Mullis, K.B. and Faloona, F.A., *Specific synthesis of DNA in vitro via a polymerase-catalyzed chain reaction.* Methods Enzymol, 1987. **155**: p. 335-50.
382. Ho, S.N., Hunt, H.D., Horton, R.M., Pullen, J.K., and Pease, L.R., *Site-directed mutagenesis by overlap extension using the polymerase chain reaction.* Gene, 1989. **77**(1): p. 51-9.
383. Rudolph, C., Lausier, J., Naundorf, S., Muller, R.H., and Rosenecker, J., *In vivo gene delivery to the lung using polyethylenimine and fractured polyamidoamine dendrimers.* J Gene Med, 2000. **2**(4): p. 269-78.
384. Akinc, A., Thomas, M., Klibanov, A.M., and Langer, R., *Exploring polyethylenimine-mediated DNA transfection and the proton sponge hypothesis.* J Gene Med, 2005. **7**(5): p. 657-63.
385. Huenecke, S., Zimmermann, S.Y., Kloess, S., Esser, R., Brinkmann, A., Tramsen, L., Koenig, M., Erben, S., Seidl, C., Tonn, T., Eggert, A., Schramm, A., Bader, P., Klingebiel, T., Lehrnbecher, T., Passweg, J.R., Soerensen, J., Schwabe, D., and Koehl, U., *IL-2-driven regulation of NK cell receptors with regard to the distribution of CD16+ and CD16- subpopulations and in vivo influence after haploidentical NK cell infusion.* J Immunother, 2010. **33**(2): p. 200-10.
386. Schneider, C.A., Rasband, W.S., and Eliceiri, K.W., *NIH Image to ImageJ: 25 years of image analysis.* Nat Methods, 2012. **9**(7): p. 671-5.
387. Giannattasio, A., Weil, S., Kloess, S., Ansari, N., Stelzer, E.H., Cerwenka, A., Steinle, A., Koehl, U., and Koch, J., *Cytotoxicity and infiltration of human NK cells in in vivo-like tumor spheroids.* BMC Cancer, 2015. **15**(1): p. 351.
388. Lathe, G.H. and Ruthven, C.R., *The separation of substances and estimation of their relative molecular sizes by the use of colums of starch in water.* Biochem J, 1956. **62**(4): p. 665-74.
389. Greenfield, N.J., *Using circular dichroism collected as a function of temperature to determine the thermodynamics of protein unfolding and binding interactions.* Nat Protoc, 2006. **1**(6): p. 2527-35.
390. Laemmli, U.K., *Cleavage of structural proteins during the assembly of the head of bacteriophage T4.* Nature, 1970. **227**(5259): p. 680-5.
391. Towbin, H., Staehelin, T., and Gordon, J., *Electrophoretic transfer of proteins from polyacrylamide gels to nitrocellulose sheets: procedure and some applications.* Proc Natl Acad Sci U S A, 1979. **76**(9): p. 4350-4.
392. Hilpert, K., Winkler, D.F., and Hancock, R.E., *Peptide arrays on cellulose support: SPOT synthesis, a time and cost efficient method for synthesis of large numbers of peptides in a parallel and addressable fashion.* Nat Protoc, 2007. **2**(6): p. 1333-49.
393. Plewnia, G., Schulze, K., Hunte, C., Tampe, R., and Koch, J., *Modulation of the antigenic peptide transporter TAP by recombinant antibodies binding to the last five residues of TAP1.* J Mol Biol, 2007. **369**(1): p. 95-107.
394. Hilpert, J., Grosse-Hovest, L., Grunebach, F., Buechele, C., Nuebling, T., Raum, T., Steinle, A., and Salih, H.R., *Comprehensive analysis of NKG2D ligand expression and release in leukemia: implications for NKG2D-mediated NK cell responses.* J Immunol, 2012. **189**(3): p. 1360-71.
395. Fernandez-Messina, L., Reyburn, H.T., and Vales-Gomez, M., *Human NKG2D-ligands: cell biology strategies to ensure immune recognition.* Front Immunol, 2012. **3**: p. 299.
396. Duray, A., Demoulin, S., Hubert, P., Delvenne, P., and Saussez, S., *Immune suppression in head and neck cancers: a review.* Clin Dev Immunol, 2010. **2010**: p. 701657.
397. Curry, J.M., Sprandio, J., Cognetti, D., Luginbuhl, A., Bar-ad, V., Pribitkin, E., and Tuluc, M., *Tumor microenvironment in head and neck squamous cell carcinoma.* Semin Oncol, 2014. **41**(2): p. 217-34.
398. Hanahan, D. and Coussens, L.M., *Accessories to the crime: functions of cells recruited to the tumor microenvironment.* Cancer Cell, 2012. **21**(3): p. 309-22.
399. Poggi, A. and Zocchi, M.R., *Mechanisms of tumor escape: role of tumor microenvironment in inducing apoptosis of cytolytic effector cells.* Arch Immunol Ther Exp (Warsz), 2006. **54**(5): p. 323-33.
400. Raffaghello, L., Prigione, I., Airoldi, I., Camoriano, M., Levreri, I., Gambini, C., Pende, D., Steinle, A., Ferrone, S., and Pistoia, V., *Downregulation and/or release of NKG2D ligands as immune evasion strategy of human neuroblastoma.* Neoplasia, 2004. **6**(5): p. 558-68.

401. Crane, C.A., Han, S.J., Barry, J.J., Ahn, B.J., Lanier, L.L., and Parsa, A.T., *TGF-beta downregulates the activating receptor NKG2D on NK cells and CD8+ T cells in glioma patients.* Neuro Oncol, 2010. **12**(1): p. 7-13.
402. Balkwill, F.R., Capasso, M., and Hagemann, T., *The tumor microenvironment at a glance.* J Cell Sci, 2012. **125**(Pt 23): p. 5591-6.
403. Fridman, W.H., Pages, F., Sautes-Fridman, C., and Galon, J., *The immune contexture in human tumours: impact on clinical outcome.* Nat Rev Cancer, 2012. **12**(4): p. 298-306.
404. Carrega, P., Morandi, B., Costa, R., Frumento, G., Forte, G., Altavilla, G., Ratto, G.B., Mingari, M.C., Moretta, L., and Ferlazzo, G., *Natural killer cells infiltrating human nonsmall-cell lung cancer are enriched in CD56 bright CD16(-) cells and display an impaired capability to kill tumor cells.* Cancer, 2008. **112**(4): p. 863-75.
405. Eckl, J., Buchner, A., Prinz, P.U., Riesenberg, R., Siegert, S.I., Kammerer, R., Nelson, P.J., and Noessner, E., *Transcript signature predicts tissue NK cell content and defines renal cell carcinoma subgroups independent of TNM staging.* J Mol Med (Berl), 2012. **90**(1): p. 55-66.
406. Halama, N., Braun, M., Kahlert, C., Spille, A., Quack, C., Rahbari, N., Koch, M., Weitz, J., Kloor, M., Zoernig, I., Schirmacher, P., Brand, K., Grabe, N., and Falk, C.S., *Natural killer cells are scarce in colorectal carcinoma tissue despite high levels of chemokines and cytokines.* Clin Cancer Res, 2011. **17**(4): p. 678-89.
407. Mueller-Klieser, W., *Multicellular spheroids. A review on cellular aggregates in cancer research.* J Cancer Res Clin Oncol, 1987. **113**(2): p. 101-22.
408. Mueller-Klieser, W., *Three-dimensional cell cultures: from molecular mechanisms to clinical applications.* Am J Physiol, 1997. **273**(4 Pt 1): p. C1109-23.
409. Sutherland, R.M., *Cell and environment interactions in tumor microregions: the multicell spheroid model.* Science, 1988. **240**(4849): p. 177-84.
410. Hirschhaeuser, F., Menne, H., Dittfeld, C., West, J., Mueller-Klieser, W., and Kunz-Schughart, L.A., *Multicellular tumor spheroids: an underestimated tool is catching up again.* J Biotechnol, 2010. **148**(1): p. 3-15.
411. Friedrich, J., Ebner, R., and Kunz-Schughart, L.A., *Experimental anti-tumor therapy in 3-D: spheroids--old hat or new challenge?* Int J Radiat Biol, 2007. **83**(11-12): p. 849-71.
412. Butler, J.E., Moore, M.B., Presnell, S.R., Chan, H.W., Chalupny, N.J., and Lutz, C.T., *Proteasome regulation of ULBP1 transcription.* J Immunol, 2009. **182**(10): p. 6600-9.
413. Bruno, A., Ferlazzo, G., Albini, A., and Noonan, D.M., *A Think Tank of TINK/TANKs: Tumor-Infiltrating/Tumor-Associated Natural Killer Cells in Tumor Progression and Angiogenesis.* J Natl Cancer Inst, 2014. **106**(8).
414. Poli, A., Michel, T., Theresine, M., Andres, E., Hentges, F., and Zimmer, J., *CD56bright natural killer (NK) cells: an important NK cell subset.* Immunology, 2009. **126**(4): p. 458-65.
415. Rosano, G.L. and Ceccarelli, E.A., *Recombinant protein expression in Escherichia coli: advances and challenges.* Front Microbiol, 2014. **5**: p. 172.
416. Derman, A.I., Prinz, W.A., Belin, D., and Beckwith, J., *Mutations that allow disulfide bond formation in the cytoplasm of Escherichia coli.* Science, 1993. **262**(5140): p. 1744-7.
417. Carrio, M.M. and Villaverde, A., *Construction and deconstruction of bacterial inclusion bodies.* J Biotechnol, 2002. **96**(1): p. 3-12.
418. Basu, A., Li, X., and Leong, S.S., *Refolding of proteins from inclusion bodies: rational design and recipes.* Appl Microbiol Biotechnol, 2011. **92**(2): p. 241-51.
419. Havenstein, J., *Herstellung der extrazellulären Domäne des humanen NK Zellrezeptors NKG2D*. 2010, Georg-Speyer-Haus, Frankfurt am Main: Praxissemester Arbeit, Hochschule Lausitz.
420. Czajkowsky, D.M., Hu, J., Shao, Z., and Pleass, R.J., *Fc-fusion proteins: new developments and future perspectives.* EMBO Mol Med, 2012. **4**(10): p. 1015-28.
421. Carter, P.J., *Introduction to current and future protein therapeutics: a protein engineering perspective.* Exp Cell Res, 2011. **317**(9): p. 1261-9.
422. Nausch, N. and Cerwenka, A., *NKG2D ligands in tumor immunity.* Oncogene, 2008. **27**(45): p. 5944-58.
423. Lanier, L.L., *NKG2D Receptor and Its Ligands in Host Defense.* Cancer Immunol Res, 2015. **3**(6): p. 575-82.
424. Zafirova, B., Wensveen, F.M., Gulin, M., and Polic, B., *Regulation of immune cell function and differentiation by the NKG2D receptor.* Cell Mol Life Sci, 2011. **68**(21): p. 3519-29.
425. Liu, C.J., Lui, M.T., Chen, H.L., Lin, S.C., and Chang, K.W., *MICA and MICB overexpression in oral squamous cell carcinoma.* J Oral Pathol Med, 2007. **36**(1): p. 43-7.
426. Reinders, J., Rozemuller, E.H., van der Weide, P., Oka, A., Slootweg, P.J., Inoko, H., and Tilanus, M.G., *Genes in the HLA region indicative for head and neck squamous cell carcinoma.* Mol Immunol, 2007. **44**(5): p. 848-55.
427. Wulff, S., Pries, R., Borngen, K., Trenkle, T., and Wollenberg, B., *Decreased levels of circulating regulatory NK cells in patients with head and neck cancer throughout all tumor stages.* Anticancer Res, 2009. **29**(8): p. 3053-7.
428. Li, D., Ronson, B., Guo, M., Liu, S., Bishop, J.S., Van Echo, D.A., and O'Malley, B.W., Jr., *Interleukin 2 gene transfer prevents NKG2D suppression and enhances antitumor efficacy in combination with cisplatin for head and neck squamous cell cancer.* Cancer Res, 2002. **62**(14): p. 4023-8.
429. Tamaki, S., Kawakami, M., Ishitani, A., Kawashima, W., Kasuda, S., Yamanaka, Y., Shimomura, H., Imai, Y., Nakagawa, Y., Hatake, K., and Kirita, T., *Soluble MICB serum levels correlate with disease stage and survival rate in patients with oral squamous cell carcinoma.* Anticancer Res, 2010. **30**(10): p. 4097-101.
430. Sato, H. and Takino, T., *Coordinate action of membrane-type matrix metalloproteinase-1 (MT1-MMP) and MMP-2 enhances pericellular proteolysis and invasion.* Cancer Sci, 2010. **101**(4): p. 843-7.
431. Stetler-Stevenson, W.G., Aznavoorian, S., and Liotta, L.A., *Tumor cell interactions with the extracellular matrix during invasion and metastasis.* Annu Rev Cell Biol, 1993. **9**: p. 541-73.
432. Franchi, A., Santucci, M., Masini, E., Sardi, I., Paglierani, M., and Gallo, O., *Expression of matrix metalloproteinase 1, matrix metalloproteinase 2, and matrix metalloproteinase 9 in carcinoma of the head and neck.* Cancer, 2002. **95**(9): p. 1902-10.
433. Venkataraman, G.M., Suciu, D., Groh, V., Boss, J.M., and Spies, T., *Promoter region architecture and transcriptional regulation of the genes for the MHC class I-related chain A and B ligands of NKG2D.* J Immunol, 2007. **178**(2): p. 961-9.

434. Textor, S., Fiegler, N., Arnold, A., Porgador, A., Hofmann, T.G., and Cerwenka, A., *Human NK cells are alerted to induction of p53 in cancer cells by upregulation of the NKG2D ligands ULBP1 and ULBP2.* Cancer Res, 2011. **71**(18): p. 5998-6009.
435. Vales-Gomez, M., Chisholm, S.E., Cassady-Cain, R.L., Roda-Navarro, P., and Reyburn, H.T., *Selective induction of expression of a ligand for the NKG2D receptor by proteasome inhibitors.* Cancer Res, 2008. **68**(5): p. 1546-54.
436. Gasser, S. and Raulet, D., *The DNA damage response, immunity and cancer.* Semin Cancer Biol, 2006. **16**(5): p. 344-7.
437. Kaskas, N.M., Moore-Medlin, T., McClure, G.B., Ekshyyan, O., Vanchiere, J.A., and Nathan, C.A., *Serum biomarkers in head and neck squamous cell cancer.* JAMA Otolaryngol Head Neck Surg, 2014. **140**(1): p. 5-11.
438. Lathers, D.M. and Young, M.R., *Increased aberrance of cytokine expression in plasma of patients with more advanced squamous cell carcinoma of the head and neck.* Cytokine, 2004. **25**(5): p. 220-8.
439. Pries, R. and Wollenberg, B., *Cytokines in head and neck cancer.* Cytokine Growth Factor Rev, 2006. **17**(3): p. 141-6.
440. Chanmee, T., Ontong, P., Konno, K., and Itano, N., *Tumor-associated macrophages as major players in the tumor microenvironment.* Cancers (Basel), 2014. **6**(3): p. 1670-90.
441. Mukhopadhyaya, R., Tatake, R.J., Krishnan, N., Rao, R.S., Fakih, A.R., Naik, S.L., and Gangal, S.G., *Immunoreactivity of lymphocytes from draining lymph nodes, peripheral blood and tumor infiltrates from oral cancer patients.* J Clin Lab Immunol, 1989. **30**(1): p. 21-5.
442. Gangal, S.G., Tatake, R.J., Krishnan, N., Mukhopadhyaya, R., Naik, S.L., Fakih, A.R., and Rao, R.S., *Natural killer and lymphokine-activated killer cell-mediated cytotoxicity in patients with oral cancer.* Semin Surg Oncol, 1989. **5**(5): p. 347-50.
443. Ohtani, H., *Focus on TILs: prognostic significance of tumor infiltrating lymphocytes in human colorectal cancer.* Cancer Immun, 2007. **7**: p. 4.
444. Naito, Y., Saito, K., Shiiba, K., Ohuchi, A., Saigenji, K., Nagura, H., and Ohtani, H., *CD8+ T cells infiltrated within cancer cell nests as a prognostic factor in human colorectal cancer.* Cancer Res, 1998. **58**(16): p. 3491-4.
445. Hasselblom, S., Sigurdadottir, M., Hansson, U., Nilsson-Ehle, H., Ridell, B., and Andersson, P.O., *The number of tumour-infiltrating TIA-1+ cytotoxic T cells but not FOXP3+ regulatory T cells predicts outcome in diffuse large B-cell lymphoma.* Br J Haematol, 2007. **137**(4): p. 364-73.
446. Sato, E., Olson, S.H., Ahn, J., Bundy, B., Nishikawa, H., Qian, F., Jungbluth, A.A., Frosina, D., Gnjatic, S., Ambrosone, C., Kepner, J., Odunsi, T., Ritter, G., Lele, S., Chen, Y.T., Ohtani, H., Old, L.J., and Odunsi, K., *Intraepithelial CD8+ tumor-infiltrating lymphocytes and a high CD8+/regulatory T cell ratio are associated with favorable prognosis in ovarian cancer.* Proc Natl Acad Sci U S A, 2005. **102**(51): p. 18538-43.
447. Balermpas, P., Michel, Y., Wagenblast, J., Seitz, O., Weiss, C., Rodel, F., Rodel, C., and Fokas, E., *Tumour-infiltrating lymphocytes predict response to definitive chemoradiotherapy in head and neck cancer.* Br J Cancer, 2014. **110**(2): p. 501-9.
448. Uppaluri, R., Dunn, G.P., and Lewis, J.S., Jr., *Focus on TILs: prognostic significance of tumor infiltrating lymphocytes in head and neck cancers.* Cancer Immun, 2008. **8**: p. 16.
449. Ames, E. and Murphy, W.J., *Advantages and clinical applications of natural killer cells in cancer immunotherapy.* Cancer Immunol Immunother, 2014. **63**(1): p. 21-8.
450. Quatrini, L., Molfetta, R., Zitti, B., Peruzzi, G., Fionda, C., Capuano, C., Galandrini, R., Cippitelli, M., Santoni, A., and Paolini, R., *Ubiquitin-dependent endocytosis of NKG2D-DAP10 receptor complexes activates signaling and functions in human NK cells.* Sci Signal, 2015. **8**(400): p. ra108.
451. Deng, W., Gowen, B.G., Zhang, L., Wang, L., Lau, S., Iannello, A., Xu, J., Rovis, T.L., Xiong, N., and Raulet, D.H., *Antitumor immunity. A shed NKG2D ligand that promotes natural killer cell activation and tumor rejection.* Science, 2015. **348**(6230): p. 136-9.
452. Lee, J.C., Lee, K.M., Ahn, Y.O., Suh, B., and Heo, D.S., *A possible mechanism of impaired NK cytotoxicity in cancer patients: down-regulation of DAP10 by TGF-beta1.* Tumori, 2011. **97**(3): p. 350-7.
453. Holmes, T.D., El-Sherbiny, Y.M., Davison, A., Clough, S.L., Blair, G.E., and Cook, G.P., *A human NK cell activation/inhibition threshold allows small changes in the target cell surface phenotype to dramatically alter susceptibility to NK cells.* J Immunol, 2011. **186**(3): p. 1538-45.
454. Hirschhaeuser, F., Walenta, S., and Mueller-Klieser, W., *Efficacy of catumaxomab in tumor spheroid killing is mediated by its trifunctional mode of action.* Cancer Immunol Immunother, 2010. **59**(11): p. 1675-84.
455. Hoh, A., Dewerth, A., Vogt, F., Wenz, J., Baeuerle, P.A., Warmann, S.W., Fuchs, J., and Armeanu-Ebinger, S., *The activity of gammadelta T cells against paediatric liver tumour cells and spheroids in cell culture.* Liver Int, 2013. **33**(1): p. 127-36.
456. Bruno, A., Focaccetti, C., Pagani, A., Imperatori, A.S., Spagnoletti, M., Rotolo, N., Cantelmo, A.R., Franzi, F., Capella, C., Ferlazzo, G., Mortara, L., Albini, A., and Noonan, D.M., *The proangiogenic phenotype of natural killer cells in patients with non-small cell lung cancer.* Neoplasia, 2013. **15**(2): p. 133-42.
457. Mamessier, E., Sylvain, A., Thibult, M.L., Houvenaeghel, G., Jacquemier, J., Castellano, R., Goncalves, A., Andre, P., Romagne, F., Thibault, G., Viens, P., Birnbaum, D., Bertucci, F., Moretta, A., and Olive, D., *Human breast cancer cells enhance self tolerance by promoting evasion from NK cell antitumor immunity.* J Clin Invest, 2011. **121**(9): p. 3609-22.
458. Rocca, Y.S., Roberti, M.P., Arriaga, J.M., Amat, M., Bruno, L., Pampena, M.B., Huertas, E., Loria, F.S., Pairola, A., Bianchini, M., Mordoh, J., and Levy, E.M., *Altered phenotype in peripheral blood and tumor-associated NK cells from colorectal cancer patients.* Innate Immun, 2013. **19**(1): p. 76-85.
459. Platonova, S., Cherfils-Vicini, J., Damotte, D., Crozet, L., Vieillard, V., Validire, P., Andre, P., Dieu-Nosjean, M.C., Alifano, M., Regnard, J.F., Fridman, W.H., Sautes-Fridman, C., and Cremer, I., *Profound coordinated alterations of intratumoral NK cell phenotype and function in lung carcinoma.* Cancer Res, 2011. **71**(16): p. 5412-22.
460. Carrega, P., Bonaccorsi, I., Di Carlo, E., Morandi, B., Paul, P., Rizzello, V., Cipollone, G., Navarra, G., Mingari, M.C., Moretta, L., and Ferlazzo, G., *CD56(bright)perforin(low) noncytotoxic human NK cells are abundant in both healthy and neoplastic solid tissues and recirculate to secondary lymphoid organs via afferent lymph.* J Immunol, 2014. **192**(8): p. 3805-15.
461. Horowitz, A., Strauss-Albee, D.M., Leipold, M., Kubo, J., Nemat-Gorgani, N., Dogan, O.C., Dekker, C.L., Mackey, S., Maecker, H., Swan, G.E., Davis, M.M., Norman, P.J., Guethlein, L.A., Desai, M., Parham, P., and Blish, C.A., *Genetic and environmental determinants of human NK cell diversity revealed by mass cytometry.* Sci Transl Med, 2013. **5**(208): p. 208ra145.
462. Lanier, L.L., *Of snowflakes and natural killer cell subsets.* Nat Biotechnol, 2014. **32**(2): p. 140-2.
463. Schrambach, S., Ardizzone, M., Leymarie, V., Sibilia, J., and Bahram, S., *In vivo expression pattern of MICA and MICB and its relevance to auto-immunity and cancer.* PLoS One, 2007. **2**(6): p. e518.

464. Armeanu, S., Bitzer, M., Lauer, U.M., Venturelli, S., Pathil, A., Krusch, M., Kaiser, S., Jobst, J., Smirnow, I., Wagner, A., Steinle, A., and Salih, H.R., *Natural killer cell-mediated lysis of hepatoma cells via specific induction of NKG2D ligands by the histone deacetylase inhibitor sodium valproate.* Cancer Res, 2005. **65**(14): p. 6321-9.
465. Armeanu, S., Krusch, M., Baltz, K.M., Weiss, T.S., Smirnow, I., Steinle, A., Lauer, U.M., Bitzer, M., and Salih, H.R., *Direct and natural killer cell-mediated antitumor effects of low-dose bortezomib in hepatocellular carcinoma.* Clin Cancer Res, 2008. **14**(11): p. 3520-8.
466. Sauer, M., Schuldner, M., Hoffmann, N., Cetintas, A., Reiners, K.S., Shatnyeva, O., Hallek, M., Hansen, H.P., Gasser, S., and von Strandmann, E.P., *CBP/p300 acetyltransferases regulate the expression of NKG2D ligands on tumor cells.* Oncogene, 2016.
467. Skov, S., Pedersen, M.T., Andresen, L., Straten, P.T., Woetmann, A., and Odum, N., *Cancer cells become susceptible to natural killer cell killing after exposure to histone deacetylase inhibitors due to glycogen synthase kinase-3-dependent expression of MHC class I-related chain A and B.* Cancer Res, 2005. **65**(23): p. 11136-45.
468. Krieg, S. and Ullrich, E., *Novel immune modulators used in hematology: impact on NK cells.* Front Immunol, 2012. **3**: p. 388.
469. Germain, C., Larbouret, C., Cesson, V., Donda, A., Held, W., Mach, J.P., Pelegrin, A., and Robert, B., *MHC class I-related chain A conjugated to antitumor antibodies can sensitize tumor cells to specific lysis by natural killer cells.* Clin Cancer Res, 2005. **11**(20): p. 7516-22.
470. Kellner, C., Gunther, A., Humpe, A., Repp, R., Klausz, K., Derer, S., Valerius, T., Ritgen, M., Bruggemann, M., van de Winkel, J.G., Parren, P.W., Kneba, M., Gramatzki, M., and Peipp, M., *Enhancing natural killer cell-mediated lysis of lymphoma cells by combining therapeutic antibodies with CD20-specific immunoligands engaging NKG2D or NKp30.* Oncoimmunology, 2016. **5**(1): p. e1058459.
471. Boyiadzis, M. and Foon, K.A., *Approved monoclonal antibodies for cancer therapy.* Expert Opin Biol Ther, 2008. **8**(8): p. 1151-8.
472. Scott, A.M., Wolchok, J.D., and Old, L.J., *Antibody therapy of cancer.* Nat Rev Cancer, 2012. **12**(4): p. 278-87.
473. Mehra, R., Cohen, R.B., and Burtness, B.A., *The role of cetuximab for the treatment of squamous cell carcinoma of the head and neck.* Clin Adv Hematol Oncol, 2008. **6**(10): p. 742-50.
474. Guan, M., Zhou, Y.P., Sun, J.L., and Chen, S.C., *Adverse events of monoclonal antibodies used for cancer therapy.* Biomed Res Int, 2015. **2015**: p. 428169.
475. Taylor, R.J., Chan, S.L., Wood, A., Voskens, C.J., Wolf, J.S., Lin, W., Chapoval, A., Schulze, D.H., Tian, G., and Strome, S.E., *FcgammaRIIIa polymorphisms and cetuximab induced cytotoxicity in squamous cell carcinoma of the head and neck.* Cancer Immunol Immunother, 2009. **58**(7): p. 997-1006.
476. Raab, S., Steinbacher, J., Schmiedel, B.J., Kousis, P.C., Steinle, A., Jung, G., Grosse-Hovest, L., and Salih, H.R., *Fc-optimized NKG2D-Fc constructs induce NK cell antibody-dependent cellular cytotoxicity against breast cancer cells independently of HER2/neu expression status.* J Immunol, 2014. **193**(8): p. 4261-72.
477. Steinbacher, J., Baltz-Ghahremanpour, K., Schmiedel, B.J., Steinle, A., Jung, G., Kubler, A., Andre, M.C., Grosse-Hovest, L., and Salih, H.R., *An Fc-optimized NKG2D-immunoglobulin G fusion protein for induction of natural killer cell reactivity against leukemia.* Int J Cancer, 2015. **136**(5): p. 1073-84.
478. Ljunggren, H.G. and Malmberg, K.J., *Prospects for the use of NK cells in immunotherapy of human cancer.* Nat Rev Immunol, 2007. **7**(5): p. 329-39.
479. Passweg, J.R., Koehl, U., Uharek, L., Meyer-Monard, S., and Tichelli, A., *Natural-killer-cell-based treatment in haematopoietic stem-cell transplantation.* Best Pract Res Clin Haematol, 2006. **19**(4): p. 811-24.
480. Koehl, U., Esser, R., Zimmermann, S., Tonn, T., Kotchetkov, R., Bartling, T., Sorensen, J., Gruttner, H.P., Bader, P., Seifried, E., Martin, H., Lang, P., Passweg, J.R., Klingebiel, T., and Schwabe, D., *Ex vivo expansion of highly purified NK cells for immunotherapy after haploidentical stem cell transplantation in children.* Klin Padiatr, 2005. **217**(6): p. 345-50.
481. Miller, J.S., Soignier, Y., Panoskaltsis-Mortari, A., McNearney, S.A., Yun, G.H., Fautsch, S.K., McKenna, D., Le, C., Defor, T.E., Burns, L.J., Orchard, P.J., Blazar, B.R., Wagner, J.E., Slungaard, A., Weisdorf, D.J., Okazaki, I.J., and McGlave, P.B., *Successful adoptive transfer and in vivo expansion of human haploidentical NK cells in patients with cancer.* Blood, 2005. **105**(8): p. 3051-7.
482. Ruggeri, L., Capanni, M., Urbani, E., Perruccio, K., Shlomchik, W.D., Tosti, A., Posati, S., Rogaia, D., Frassoni, F., Aversa, F., Martelli, M.F., and Velardi, A., *Effectiveness of donor natural killer cell alloreactivity in mismatched hematopoietic transplants.* Science, 2002. **295**(5562): p. 2097-100.
483. Spear, P., Barber, A., Rynda-Apple, A., and Sentman, C.L., *NKG2D CAR T-cell therapy inhibits the growth of NKG2D ligand heterogeneous tumors.* Immunol Cell Biol, 2013. **91**(6): p. 435-40.
484. VanSeggelen, H., Hammill, J.A., Dvorkin-Gheva, A., Tantalo, D.G., Kwiecien, J.M., Denisova, G.F., Rabinovich, B., Wan, Y., and Bramson, J.L., *T Cells Engineered With Chimeric Antigen Receptors Targeting NKG2D Ligands Display Lethal Toxicity in Mice.* Mol Ther, 2015. **23**(10): p. 1600-10.
485. Dai, H., Wang, Y., Lu, X., and Han, W., *Chimeric Antigen Receptors Modified T-Cells for Cancer Therapy.* J Natl Cancer Inst, 2016. **108**(7).
486. Jinushi, M., Hodi, F.S., and Dranoff, G., *Therapy-induced antibodies to MHC class I chain-related protein A antagonize immune suppression and stimulate antitumor cytotoxicity.* Proc Natl Acad Sci U S A, 2006. **103**(24): p. 9190-5.
487. Vihinen, P. and Kahari, V.M., *Matrix metalloproteinases in cancer: prognostic markers and therapeutic targets.* Int J Cancer, 2002. **99**(2): p. 157-66.
488. Cathcart, J., Pulkoski-Gross, A., and Cao, J., *Targeting Matrix Metalloproteinases in Cancer: Bringing New Life to Old Ideas.* Genes Dis, 2015. **2**(`1): p. 26-34.
489. Fingleton, B., *MMPs as therapeutic targets--still a viable option?* Semin Cell Dev Biol, 2008. **19**(1): p. 61-8.
490. Tamaki, S., Kawakami, M., Yamanaka, Y., Shimomura, H., Imai, Y., Ishida, J., Yamamoto, K., Ishitani, A., Hatake, K., and Kirita, T., *Relationship between soluble MICA and the MICA A5.1 homozygous genotype in patients with oral squamous cell carcinoma.* Clin Immunol, 2009. **130**(3): p. 331-7.
491. Wang, X., Lundgren, A.D., Singh, P., Goodlett, D.R., Plymate, S.R., and Wu, J.D., *An six-amino acid motif in the alpha3 domain of MICA is the cancer therapeutic target to inhibit shedding.* Biochem Biophys Res Commun, 2009. **387**(3): p. 476-81.
492. Kelley, B., *Industrialization of mAb production technology: the bioprocessing industry at a crossroads.* MAbs, 2009. **1**(5): p. 443-52.

493. Berraondo, P. *Therapeutic Fc-Fusion Proteins. Edited by Steven?M. Chamow, Thomas Ryll, Henry?B. Lowman, Deborah Farson ChemMedChem Volume 10, Issue 2*. ChemMedChem, 2015. **10**, 419-19.
494. Colucci, F., Di Santo, J.P., and Leibson, P.J., *Natural killer cell activation in mice and men: different triggers for similar weapons?* Nat Immunol, 2002. **3**(9): p. 807-13.
495. Sungur, C.M. and Murphy, W.J., *Utilization of mouse models to decipher natural killer cell biology and potential clinical applications.* Hematology Am Soc Hematol Educ Program, 2013. **2013**: p. 227-33.
496. Hong, H.S., Rajakumar, P.A., Billingsley, J.M., Reeves, R.K., and Johnson, R.P., *No monkey business: why studying NK cells in non-human primates pays off.* Front Immunol, 2013. **4**: p. 32.
497. Karimi, M., Cao, T.M., Baker, J.A., Verneris, M.R., Soares, L., and Negrin, R.S., *Silencing human NKG2D, DAP10, and DAP12 reduces cytotoxicity of activated CD8+ T cells and NK cells.* J Immunol, 2005. **175**(12): p. 7819-28.
498. Nedellec, S., Bonneville, M., and Scotet, E., *Human Vgamma9Vdelta2 T cells: from signals to functions.* Semin Immunol, 2010. **22**(4): p. 199-206.
499. Wu, J., Groh, V., and Spies, T., *T cell antigen receptor engagement and specificity in the recognition of stress-inducible MHC class I-related chains by human epithelial gamma delta T cells.* J Immunol, 2002. **169**(3): p. 1236-40.
500. Mokrzycki, M.H. and Kaplan, A.A., *Therapeutic plasma exchange: complications and management.* Am J Kidney Dis, 1994. **23**(6): p. 817-27.
501. Bramlage, C.P., Schroder, K., Bramlage, P., Ahrens, K., Zapf, A., Muller, G.A., and Koziolek, M.J., *Predictors of complications in therapeutic plasma exchange.* J Clin Apher, 2009. **24**(6): p. 225-31.
502. Langers, I., Renoux, V., Reschner, A., Touze, A., Coursaget, P., Boniver, J., Koch, J., Delvenne, P., and Jacobs, N., *Natural killer and dendritic cells collaborate in the immune response induced by the vaccine against uterine cervical cancer.* Eur J Immunol, 2014. **44**(12): p. 3585-95.
503. Krneta, T., Gillgrass, A., and Ashkar, A.A., *The influence of macrophages and the tumor microenvironment on natural killer cells.* Curr Mol Med, 2013. **13**(1): p. 68-79.
504. Melero, I., Rouzaut, A., Motz, G.T., and Coukos, G., *T-cell and NK-cell infiltration into solid tumors: a key limiting factor for efficacious cancer immunotherapy.* Cancer Discov, 2014. **4**(5): p. 522-6.
505. Gras Navarro, A., Bjorklund, A.T., and Chekenya, M., *Therapeutic potential and challenges of natural killer cells in treatment of solid tumors.* Front Immunol, 2015. **6**: p. 202.
506. Hayakawa, Y., Huntington, N.D., Nutt, S.L., and Smyth, M.J., *Functional subsets of mouse natural killer cells.* Immunol Rev, 2006. **214**: p. 47-55.
507. Weiswald, L.B., Bellet, D., and Dangles-Marie, V., *Spherical cancer models in tumor biology.* Neoplasia, 2015. **17**(1): p. 1-15.
508. Sammond, D.W., Eletr, Z.M., Purbeck, C., Kimple, R.J., Siderovski, D.P., and Kuhlman, B., *Structure-based protocol for identifying mutations that enhance protein-protein binding affinities.* J Mol Biol, 2007. **371**(5): p. 1392-404.
509. Rohl, C.A., Strauss, C.E., Misura, K.M., and Baker, D., *Protein structure prediction using Rosetta.* Methods Enzymol, 2004. **383**: p. 66-93.

Abbreviations

The table of abbreviations does not contain SI (internationally accepted standard) based units or SI derived units, the one and three letter amino acid code or metric prefixes.

Abbreviation	Description
A	adenine
A450	adsorbance at 450 nm
aa	amino acid
ADAM	a disintegrin and metalloprotease
ADCC	antibody dependent cellular cytotoxicity
AKT	anti-apoptotic kinase
AML	acute myeloid leukemia
Amp	ampicillin
AmpR	ampicillin resistance
APC	antigen-presenting cell
APC	allophycocyanin
APS	ammonium persulfate
ATCC	American Type Culture Collection
ATM	*ataxia telangiectasia* mutated
ATP	adenosine triphosphate
ATR	ATM and Rad3-related
BAG-6	Bcl2-associated anthanogene 6
Bcl-2	B-cell lymphoma protein 2
BCR	B cell receptor
B_{max}	maximum number of binding sites
bp	base pare
BSA	bovine serum albumine
C	cytosine
CAR	chimeric antigen receptor
CBA	cytometric bead array
CD	cluster of differentiation

Abbreviation	Description
CD	circular dichroism
CDC	complement-dependent cytotoxicity
CFSE	carboxyfluorescein succinimidyl ester
CMV	cytomegalovirus
CTL	cytotoxic T lymphocyte
CTLA-4	cytotoxic T lymphocyte-associated protein 4
CTx	chemotherpapy
CV	column volume
d	day
DA	dalton
DAMP	danger-associated molecular pattern
DAP	DNAX activation protein
DAPI	4',6-diamidino-2-phenylindole
DC	dendritic cell
DMEM	Dulbecco's modified Eagle medium
DMSO	dimethyl sulfoxide
DNA	deoxyribonucleic acid
DNAM-1	DNAX-accessory molecule 1
dNTP	deoxyribonucleotide triphosphate
DTT	dithiothreitol
ECL	enhanced chemoluminescence
E. coli	*Escherichia coli*
EDTA	ethylendiaminetetraacetic acid
e.g.	for example
EGFR	epidermal growth factor receptor
ELISA	enzyme linked immunosorbent assay
EOMES	eomesodermin
ER	endoplasmic reticulum
ERp5	endoplasmic reticulum protein 5
et al.	*et alii*

Abbreviation	Description
EtBr	ethidium bromide
EtOH	ethyl alcohol
E:T ratio	effector to target ratio
FACS	fluorescence-activated cell sorting
Fas L	Fas ligand
FCS	fetal calf serum
Fc	fragment crystallizable
FDA	US Food and Drug Administration
FITC	fluorescein isothiocyanate
G	guanine
Gln	L-glutamine
Grb-2	growth factor receptor-bound protein 2
GS linker	glycine-serine linker
GSH	glutathion, reduced
GSSG	glutathione, oxidized
GvHD	graft versus host disease
GvL/T	graft versus leukemia/tumor
HA	hemagglutinin
HCMV	human cytomegalovirus
HDAC	histone deacetylase
HEK	human embryonic kidney
HER2	human epidermal growth factor receptor 2
hIgG	human immunoglobulin G
His-tag	histidine-tag
HIV	human immunodeficiency virus
HLA	human leukocyte antigen
HNSCC	head and neck squamous cell carcinoma
HPV	human papillomavirus
HRP	horseradish peroxidase
HSCT	hematopoietic stem cell transplantation

Abbreviation	Description
HTS	high throughput sampler
H60	histocompatibility antigen 60
iDC	immature dentritic cell
IF	immunofluorescence
IFN	interferon
Ig	immunoglobulin
IHC	immunohistochemistry
IL	interleukin
ILC	innate lymphoid cell
IMAC	immobilized-metal affinity chromatography
IMDM	Iscove's modified Dulbecco's medium
IPTG	isopropyl β-D-1-thiogalactopyranoside
ITAM	tyrosine-based activating motif
ITIM	tyrosine-based inhibitory motif
K_D	equilibrium binding constant
kDA	kilo Dalton
KIR	killer cell Ig-like receptor
LB	lysogeny broth
LMW	low molecular weight
LPS	lipopolysaccharide
mAb	monoclonal antibody
MACMU	*Macaca mulatta*
MACS	magnetic activated cell sorting
MAPK	mitogen-activated protein kinases
MCP-1	monocyte chemoattractant protein 1
MEM	modified Eagle medium
MHC	major histocompatibility complex
MICA/B	MHC class I chain-related protein A/B
MIP-1	macrophage inflammatory protein 1
MLL-5	mixed lineage leukemia 5 protein

Abbreviation	Description
MMP	matrix metalloprotease
mRNA	messenger RNA
Mult1	mouse ULBP-like transcript 1
MW	molecular weight
MWCO	molecular weight cut-off
NCAM	neural cell adhesion molecule (CD56)
NCR	natural cytotoxicity receptor
nd	not detectable
n.d.	not defined
NEAA	non-essential amino acid
NK cell	natural killer cell
NKG2A/C/E	natural killer group 2 member A/C/E
NKG2D	natural killer group 2 member D
No.	number
ns	non-significant
NTA	nitrilotriacetat
OD	optical density
OE	overlap extension
p53	p53 tumor suppressor protein
PAMP	pathogen-associated molecular pattern
PBMC	peripheral blood mononuclear cell
PBS	phosphate-buffered saline
PBS-T	phosphate-buffered saline supplemented with Tween20
PCNA	proliferating cell nuclear antigen
PCR	polymerase chain reaction
PDB	protein data bank
PD-1	programmed cell death protein 1
PD-L1	programmed cell death protein ligand 1
PE	phycoerythrin
PEI	polyethylenimine

Abbreviation	Description
PerCP	peridinin chlorophyll
PFA	paraformaldehyde
PI3K	phosphatidylinositol-3-kinase
PLCγ-1/2	phospholipase Cγ 1/2
PNGase F	Peptide-N-Glycosidase F
PRR	pattern-recognition receptor
RAE-1	retinoic acid early inducible-1
RANTES	regulated upon activation, normal T cell expressed and secreted
RCTx	radio-chemotherapy
RNA	ribonucleic acid
RPMI	roswell park memorial institute medium
RT	room temperature
RTx	radiotherapy
scFv	single chain variable fragment
SDS	sodium dodecyl sulfate
SEC	size exclusion chromatography
SEM	standard error of the mean
SH2	Src homology 2
SHP-1/2	Src homology 2 (SH2)-domain containing phosphatase 1/2
SLAM	signaling lymphocytic activation molecule
sNKG2D ligand	soluble NKG2D ligand
sMICA/B	soluble MICA/B
Src	sarcoma
ss	signal sequence
sULBP	soluble ULBP
Syk	spleen tyrosine kinase
T	thymine
TAE	Tris-acetate-EDTA
TAM	tumor-associated macrophage
TBS	tris-buffered saline

Abbreviation	Description
TBS-T	tris-buffered saline supplemented with Tween20
TCR	T cell receptor
TEMED	N,N,N',N-tetramethylethylenediamine
TGF-α/β	transforming growth factor α/β
TH	T helper
TIL	tumor-infiltrating lymphocyte
TM	melting temperature
TMB	3,3',5,5'-tetramethylbenzidine
TME	tumor microenvironment
TNF	tumor necrosis factor
TRAIL	TNF-related apoptosis-inducing ligand
Treg	regulatory T cell
TRIS	tris(hydroxymethyl)aminomethane
U	uracil
UL16	unique-long 16
ULBP	UL16 binding protein
UV	ultraviolet
V_0	void volume
V_r	retention volume
vs.	versus
v/v	volume per volume
WB	Western blot
wt	wild type
w/v	weight per volume
ZAP70	zeta chain-associated protein 70
3D	3 demensional
3’	three prime end
5’	five prime end

Publications and Presentations

Publications

Weil S, Memmer S, Lechner A, Huppert V, Giannattasio A, Becker T, Müller-Runte A, Lampe K, Beutner D, Quaas A, Schubert R, Herrmann E, Steinle A, Koehl U, Walter L, von Bergwelt-Baildon MS, and Koch J. *NKG2D ligand depletion reconstitutes NK cell immunosurveillance of head and neck squamous cell carcinoma.* (submitted Sept 2016)

Memmer S*, **Weil S***, Beyer S, Zöller T, Peters E, Hartmann J, Steinle A, and Koch J. *The stalk domain of NKp30 contributes to ligand binding and signaling of a pre-assembled NKp30/CD3ζ complex.* J Biol Chem. 2016 Dec 2; 291(49): 25427-25438 (* both authors contributed equally)

Rutkowski E, Leibelt S, Born C, Friede ME, Bauer S, **Weil S**, Koch J, and Steinle A. *Clr-a: A novel immune-related C-type lectin-like molecule exclusively expressed by mouse gut epithelium.* J Immunol. 2017 Jan 15; 198(2):916-926

Kloess S, Chambron N, Gardlowski T, **Weil S**, Koch J, Esser R, Pogge von Strandmann E, Morgan MA, Arseniev L, Seitz O, and Köhl U. *Cetuximab Reconstitutes Pro-Inflammatory Cytokine Secretions and Tumor-Infiltrating Capabilities of sMICA-Inhibited NK Cells in HNSCC Tumor Spheroids*. Front Immunol. 2015 Nov 2;6:543

Giannattasio A*, **Weil S***, Kloess S, Ansari N, Stelzer EH, Cerwenka A, Steinle A, Koehl U, and Koch J. *Cytotoxicity and infiltration of human NK cells in in vivo-like tumor spheroids*. BMC Cancer. 2015 May 3;15:351 (* both authors contributed equally)

Hermes M, **Weil S**, Groth A, Dressel R, Koch J, Walter L. *Characterisation of mouse monoclonal antibodies against rhesus macaque killer immunoglobulin-like receptors KIR3D*. Immunogenetics. 2012 Nov;64(11):845-8

Poster Presentations

"*Escape of head and neck squamous cell carcinoma from NKG2D-dependent NK cell immunosurveillance can be restored by NKG2D ligand depletion",* 14th Cancer Immunotherapy Meeting (CIMT; 2016), Mainz, Germany

"Clinical impact of NKG2D-dependent tumor immune escape in head and neck squamous cell carcinoma (HNSCC)", NK Cell Symposium of the German Society for Immunology (2015), Göttingen, Germany

"Scavenging of soluble NKG2D ligands from patients' plasma to overcome NKG2D-dependent tumor-immune-escape from NK cell cytotoxicity", 15th Meeting of the Society for Natural Immunity (2015), Montebello, Canada

"Depletion of soluble NKG2D ligands to overcome tumor-immune-escape from NKG2D-dependent NK cell cytotoxicity", NK Cell Symposium of the German Society for Immunology (2014), Hannover, Germany

"Investigation of tumor immune escape from NKG2D-dependent NK cell cytotoxicity",
14th Meeting of the Society for Natural Immunity (2013), Heidelberg, Germany

"Investigation of tumor immune escape from NKG2D-dependent NK cell cytotoxicity in spheroids", 10th International Conference on Innate Immunity (2013), Kos, Greek

"Investigation and inhibition of an tumor immune escape from NKG2D-dependent NK cell cytotoxicity", 7th International Cellular Therapy Symposium (2013), Erlangen, Germany

"Investigation and Inhibition of tumor immune escape from NKG2D-dependent NK cell cytotoxicity", 10th Cancer Immunotherapy Meeting (CIMT, 2012), Mainz, Germany

"Inhibition of tumor immune escape from NKG2D-dependent NK cell cytotoxicity", 13th Meeting of the Society for Natural Immunity (2012), Asilomar, CA, USA

Poster presentations at the 3th - 6th UCT Scienceday (2011-2014), Frankfurt a.M., Germany

Oral Presentations

"Clinical impact of NKG2D-dependent tumor immune escape in HNSCC", LOEWE-CGT Friday Afternoon Workshop „Cell Therapy of Cancer"(11/2014), Frankfurt a.M., Germany

"Depletion of NKG2D ligands to overcome NKG2D/NKG2D ligand-dependent tumor immune escape", LOEWE-CGT Friday Afternoon Workshop „Immunological Cell Therapy of Malignant Disorders" (11/2013), Frankfurt a.M., Germany

Travel Grants

05/2015	Travel grant for the 15th Meeting of the Society for Natural Immunity in Montebello, Canada (Vereinigung von Freunden und Förderern der Johann Wolfgang Goethe-Universität, Frankfurt a.M.)
06/2013	Travel grant for the 10th International Conference on Innate Immunity in Kos, Greek (UCT-Trx Programm des Klinikums der Goethe-Universität, Frankfurt a.M.)
04/2012	Travel grant for the 13th Meeting of the Society for Natural Immunity in Asilomar, CA, USA (GlaxoSmithKline Stiftung)

Acknowledgement

Danksagung

Ich möchte mich hiermit bei all denjenigen bedanken, die mir auf verschiedenste Weise bei der Anfertigung dieser Arbeit geholfen haben. Mein besonderer Dank gilt:

Professor Dr. Joachim Koch für das spannende und interessante Thema meiner Doktorarbeit, sein stetiges Engagement und seine Diskussionsbereitschaft. Ich danke ihm für sein Vertrauen in meine Arbeit und die Gelegenheit zur Teilnahme an vielen interessanten Fachtagungen, die dazu beitrugen dieses Projekt voranzubringen. Es war eine spannende und sehr lehrreiche Zeit.

Professorin Dr. Beatrix Süß und Professor Dr. Bodo Laube von der TU Darmstadt für die freundliche und unkomplizierte Übernahme der Begutachtung der vorliegenden Arbeit.

all meinen Kooperationspartnern für die stetige Hilfsbereitschaft und tatkräftige Unterstützung bei der Bearbeitung dieses Projektes. Insbesondere bedanke ich mich bei Professor Dr. Alexander Steinle für die wissenschaftlichen Diskussionen und die Bereitstellung der monoklonalen Antikörper, ohne die dieses Projekt nicht durchführbar gewesen wäre. Den Mitarbeitern der Firma Miltenyi Biotec danke ich für die Zusammenarbeit bei der Herstellung der Apheresekartusche sowie für die Bereitstellung der Life18 Aphereseeinheit und der Hilfe bei der Durchführung der Tierexperimente. Ich danke Professor Dr. Michael von Bergwelt-Baildon und Professor Dr. Dirk Beutner für die tatkräftige Unterstützung und Diskussionsbereitschaft von Seiten der Klinik. Insbesondere danke ich Dr. Axel Lechner für seine Hilfe bei der Auswertung der Patientendaten, der immunhistochemischen Färbungen und zytometrischen Analysen von Tumoren und Patienten PBMCs. Ich danke Professor Dr. Lutz Walter, Dr. Tamara Becker und Dr. Karen Lampe für die Expertise und Unterstützung bei der Durchführung der Tierexperimente.

den Mitarbeitern des Georg-Speyer-Hauses für das angenehme Arbeitsklima, die ständige Hilfsbereitschaft sowie für die hilfreichen fachlichen Diskussionen. Ein besonderer Dank geht an Stephan, Stefanie, Nicole, Jasmin, Betty, Josi, Marek, Sarah und Sabrina für die ge-

meinsame Zeit, unsere gemeinsamen Frühstücksaktionen, Grillabende, Trinkhallentouren und die Freundschaft, die uns auch über die Zeit der Doktorarbeit verbindet.

den Mitgliedern der Arbeitsgruppe Koch für die tolle Zeit im Labor und die ständige Hilfsbereitschaft. Ich danke Julia Havenstein, die während ihrer Praxissemesterarbeit das Projekt vorangetrieben hat sowie meinen Praktikanten Angela, David und Tobias, die mich bei der Durchführung der Experimente unterstützt haben. Insbesondere danke ich Dr. Ariane Giannattasio für ihre Hilfe und Unterstützung bei den Sphäroiden und Killassays. Ein besonderer Dank gilt auch Steffen Beyer, der immer da war, wenn es mal eng wurde und an Stefanie Memmer, die mit mir bis zum Ende "die Stellung" gehalten hat. Ariane, Steffen und Stefanie danke ich aber vor allem für ihre Freundschaft, den vielen Spaß im Labor und in unserer Freizeit, unsere kulinarischen Exkursionen und die Unterstützung bei allen Höhen und Tiefen.

all meinen Freunden, die seit meiner Schulzeit für mich da sind. Ich danke besonders Theresa für ihre Freundschaft, die uns seit dem Studium verbindet, ihre aufmunternden Worte und die vielen schönen und amüsanten Abende in Frankfurt und bei unseren Kurztrips.

meinen Eltern und Geschwistern für ihre bedingungslose Unterstützung, nicht nur während des Studiums und der Doktorarbeit. Danke, dass ihr immer an mich glaubt, mich aufmuntert, wenn es mal nicht so gut läuft, und immer für mich da seid!

meinem Freund Ralf, der mich in allen Lebenslagen unterstützt hat und mir Kraft gegeben hat alle Höhen und Tiefen während meiner Doktorarbeit zu überwinden. Danke, dass du immer für mich da bist!

Curriculum vitae

Lebenslauf

Name	Sandra Weil
Geburtstag	08.08.1984
Geburtsort	Freudenstadt
Nationalität	deutsch

Akademischer Werdegang:

2010 - 2016	Promotion am Georg-Speyer-Haus in Frankfurt a.M., Abteilung "Immunobiology of Natural Killer Cells" unter der Leitung von Prof. Dr. J. Koch
seit 05/2016	Am Institut für medizinische Mikrobiologie und Hygiene an der Universitätsmedizin Mainz, Abteilung "Immunobiology of Natural Killer Cells". Thema: "Investigation of a NKG2D-dependent tumor immune escape mechanism of head and neck squamous cell carcinoma and proof of concept of a clinical intervention strategy"
2004 - 2010	Studium der Biochemie an der Goethe-Universität Frankfurt a. M. Anfertigung der Diplomarbeit am Georg-Speyer-Haus in Frankfurt a. M. unter der Leitung von Prof. Dr. J. Koch Thema: "Etablierung eines proteolytischen Fusionsproteins des Natürlichen Killerzellrezeptors NKp30 zur Ligandenidentifizierung" Abschluss: Diplom Biochemikerin; Note: "sehr gut"

Schulische Laufbahn:

2001 - 2004	Lusie-Büchner-Schule, Ernährungswissenschaftliches Gymnasium Freudenstadt Abschluss: Allgemeine Hochschulreife; Note: 1,4
1995 - 2001	Kepler-Gymnasium Freudenstadt
1991 - 1995	Hartranft Grundschule Freudenstadt

Declaration and Affidavit

Eidesstattliche Erklärung

Ich erkläre hiermit ehrenwörtlich, dass ich die vorliegende Arbeit entsprechend den Regeln guter wissenschaftlicher Praxis selbstständig und ohne unzulässige Hilfe Dritter angefertigt habe.

Sämtliche aus fremden Quellen direkt oder indirekt übernommenen Gedanken sowie sämtliche von Anderen direkt oder indirekt übernommenen Daten, Techniken und Materialien sind als solche kenntlich gemacht. Die Arbeit wurde bisher bei keiner anderen Hochschule zu Prüfungszwecken eingereicht.

Darmstadt, den 25.09.2016

Sandra Weil